APRIL–JUNE 2019 VOL. 11 № 2 (41)

ISSN 2075-8251

ActaNaturae

Targeted Drug Delivery in Lipid-like Nanocages and Extracellular Vesicles

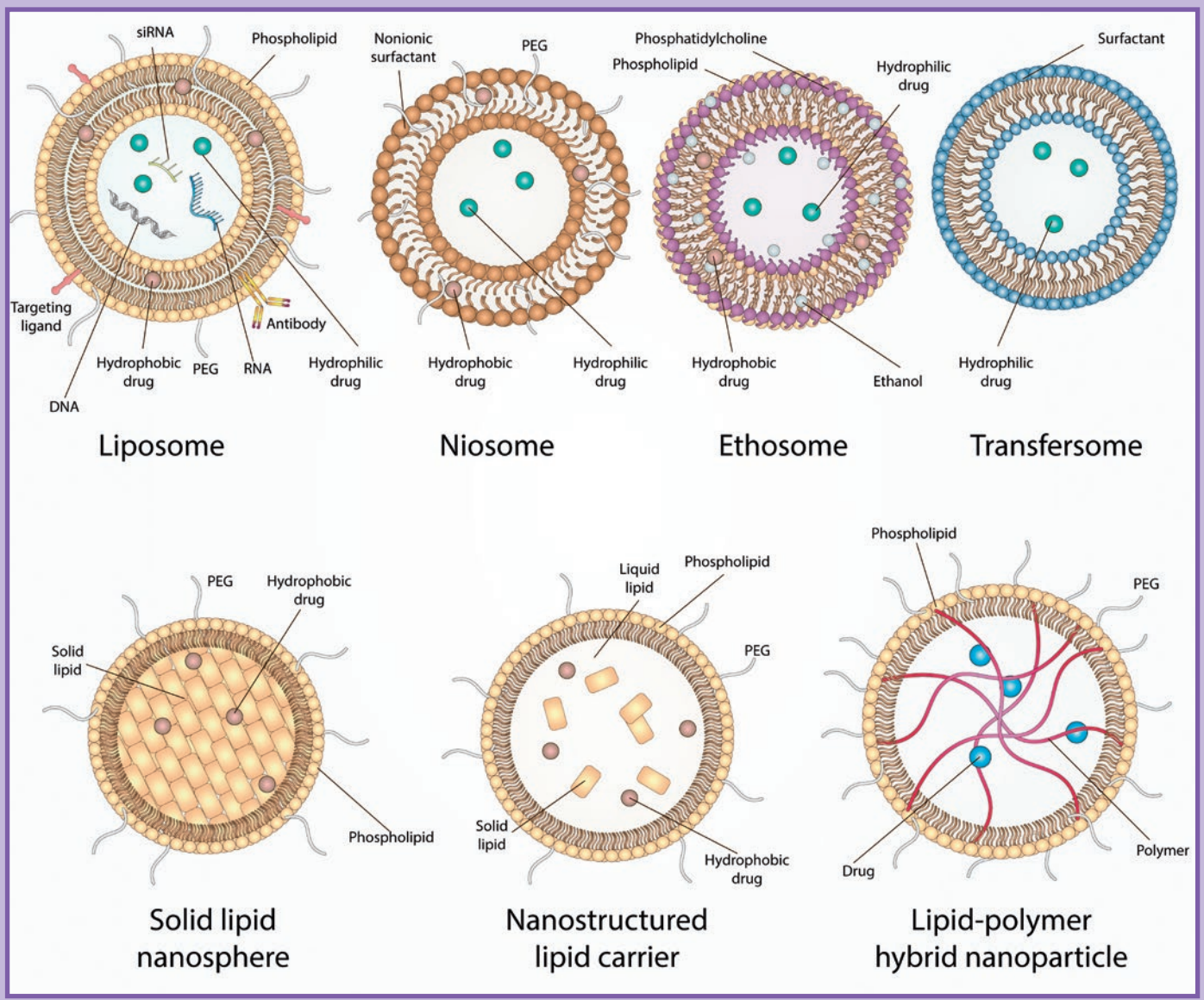

MERCK

Comprehensive solutions for cell analysis

- Cell lines and primary cells
- Traditional and specialized culture media
- Sterilizing filtration
- Biochemical reagents
- Water purification systems
- Cell counting and analysis
- Cryopreservation

An extensive range and top quality of cell lines from our partner, the European Collection of Authenticated Cell Cultures (ECACC):

- 4000 animal and human cell lines;
- Cells of 45 animal species and 50 tissue types;
- 370 B-lymphoblastoid cell lines for which human leukocyte antigen (HLA) typing data are available;
- 480 hybridoma cell lines secreting monoclonal antibodies;
- DNA, RNA, and cDNA extracted from the cell lines from our collection;

SIGMAaldrich.com/ECACC

LLC Merck
Valovaya Str., 35, Moscow, 115054, Russia;
Tel. +7 (495) 937-33-04
E-mail: mm.russia@merckgroup.com, ruorder@sial.com

SIGMAaldrich.com/cellculture
MERCKmillipore.com/cellculture

SIGMA-ALDRICH® is now MERCK

The Profile of Post-translational Modifications of Histone H1 in Chromatin of Mouse Embryonic Stem Cells

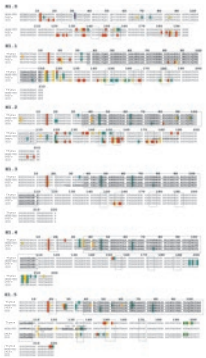

Potential posttranslational modifications of H1 variants from NIH/3T3 cells, MEFs, and ES cells

T. Yu. Starkova, T. O. Artamonova, V. V. Ermakova, E. V. Chikhirzhina, M. A. Khodorkovskii, A. N. Tomilin

Authors compared histone H1 variants from NIH/3T3, mouse embryonic fibroblasts, and mouse embryonic stem cells using matrix-assisted laser desorption/ionization Fourier transform ion cyclotron resonance mass spectrometry (MALDI-FT-ICR-MS). They found significant differences in the nature and positions of the post-translational modifications of H1.3-H1.5 variants in embryonic stem cells compared to differentiated cells.

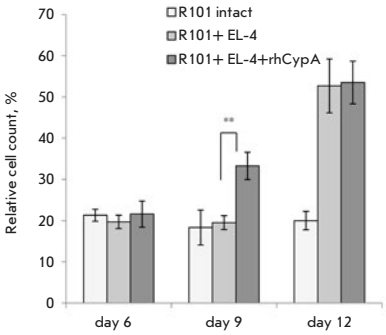

The accumulation dynamics of effector CD8$^+$ T-lymphocytes in the spleen of mice after immunization with lymphoma EL-4 cells

The Role of Recombinant Human Cyclophilin A in the Antitumor Immune Response

A. A. Kalinina, Yu. Yu. Silaeva, D. B. Kazansky, L. M. Khromykh

Cyclophilin A (CypA) is a multifunctional protein that exhibits an isomerase activity and exists in the intracellular and secretory forms. In this work, authors used the model experimental system of lymphoma EL-4 rejection in B10.D2(R101) mice and showed that recombinant human CypA (rhCypA) stimulates the antitumor immune response via early recruitment of granulocytes to the tumor cell localization site and rapid accumulation of effector T-killers.

Septin Polymerization Slows Synaptic Vesicle Recycling in Motor Nerve Endings

P. N. Grigoryev, G. A. Khisamieva, A. L. Zefirov

Septins are GTP-binding proteins recognized as a component of the cytoskeleton. In this study, neurotransmitter release and synaptic vesicle exocytosis and endocytosis were investigated by microelectrode intracellular recording of end-plate potentials and fluorescent confocal microscopy in mouse diaphragm motor nerve endings during septin polymerization induced by forchlorfenuron application. It was concluded that the septin polymerization induced by forchlorfenuron application slows the rate of synaptic vesicle recycling in motor nerve endings due to the impairment of synaptic vesicle transport.

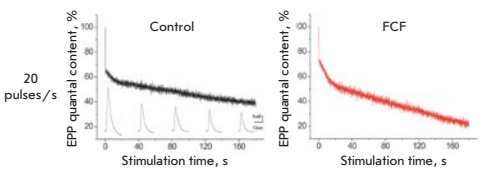

Effect of forchlorfenuron on neurotransmitter release during high-frequency stimulation

ActaNaturae
APRIL-JUNE 2019 VOL. 11 № 2 (41)
since april 2009, 4 times a year

Founders
Acta Naturae, Ltd,
National Research University
Higher School of Economics

Phone/Fax: +7 (495) 727 38 60
E-mail: vera.knorre@gmail.com, actanaturae@gmail.com

Номер подписан в печать 29 июня 2019 г.
Тираж 100 экз. Цена свободная.
Отпечатано в типографии «МИГ ПРИНТ»

Indexed in Pubmed, Web of Science, Scopus, and RISC

CONTENTS

REVIEWS

RESEARCH ARTICLES

SHORT REPORTS

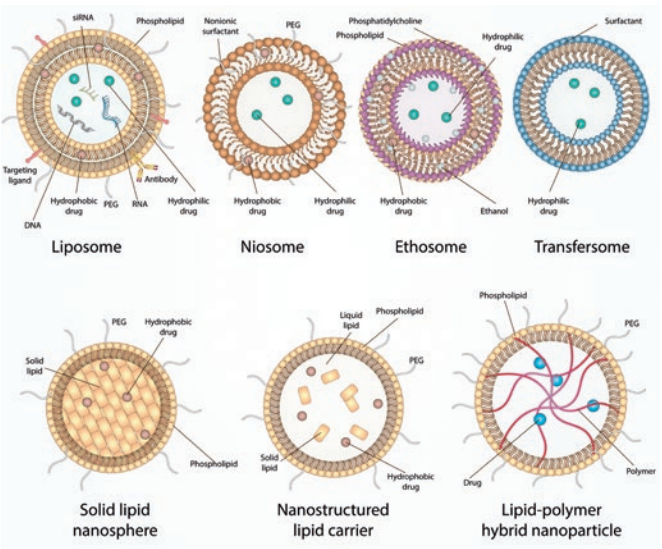

IMAGE ON THE COVER PAGE
(see the article by *A. V. Sokolov et al.*)

Application of Polyhydroxyalkanoates in Medicine and the Biological Activity of Natural Poly(3-Hydroxybutyrate)

A. P. Bonartsev[1,2]*, G. A. Bonartseva[2], I. V. Reshetov[3], M. P. Kirpichnikov[1], K. V. Shaitan[1]
[1]Faculty of Biology, M.V. Lomonosov Moscow State University, Leninskie Gory 1, bldg. 12, Moscow, 119234, Russia
[2]A.N. Bach Institute of Biochemistry, Research Center of Biotechnology of the Russian Academy of Sciences, Leninsky Ave. 33, bldg. 2, Moscow, 119071, Russia
[3]Sechenov First Moscow State University, Trubetskaya Str. 8, bldg. 2, Moscow, 119991, Russia
*E-mail: ant_bonar@mail.ru
Received December 28, 2018; in final form March 28, 2019
DOI: 10.32607/20758251-2019-11-2-4-16

ABSTRACT **Biodegradable and biocompatible polymers, polyhydroxyalkanoates (PHAs), are actively used in medicine to produce a wide range of medical devices and dosage formulations. The medical industry mainly utilizes PHAs obtained by chemical synthesis, but interest in the medical application of natural PHAs obtained biotechnologically is also growing. Synthetic PHAs are the biomimetic analogs of bacterial poly(3-hydroxybutyrate) (PHB) and other natural PHAs. This paper addresses the issue of the presence of biological activity in synthetic and natural PHAs (stimulation of cell proliferation and differentiation, tissue regeneration) and their possible association with various biological functions of PHB in bacteria and eukaryotes, including humans.**
KEYWORDS **polyhydroxyalkanoates, poly(3-hydroxybutyrate), biosynthesis, biomimetics, biodegradation, biocompatibility, regenerative medicine.**
ABBREVIATIONS **PHAs – polyhydroxyalkanoates; sPHAs – chemically synthetized polyhydroxyalkanoates; nPHAs – natural polyhydroxyalkanoates, poly(3-hydroxyalkanoates); PLA – poly(2-hydroxypropanoic) (polylactic) acid, polylactide; PGA – poly(2-hydroxyacetic) (polyglycolic) acid, polyglycolide; PLGA – poly(lactic-co-glycolic) acid (polylactide-co-glycolide); PCL – poly(6-hydroxycaprolactone) (poly(ε-hydroxycaprolactone)); PDS – poly(p-dioxanone); PHB – poly(3-hydroxybutyric) acid (poly(3-hydroxybutyrate)); cPHB – short-chain complexed endogenic PHB; oPHB – medium-chain or oligo-PHB; P4HB – poly(4-hydroxybutyric) acid (poly(4-hydroxybutyrate)); PHV – poly(3-hydroxyvaleric) acid (poly(3-hydroxyvalerate)); PHBV – poly(3-hydroxybutyrate-co-3-hydroxyvalerate); PHHx – poly(3-hydroxyhexanoate); PHBHx – poly(3-hydroxybutyrate-co-3-hydroxyhexanoate); PHBVHx – poly(3-hydroxybutyrate-co-3-hydroxyvalerate-co-3-hydroxyhexanoate); PHBO – poly(3-hydroxybutyrate-co-3-hydroxyoctanoate); PHB4HB – poly(3-hydroxybutyrate-co-4-hydroxybutyrate); 3HB – 3-hydroxybutyrate; FBGCs – foreign body giant cells; NO – nitric oxide; TNF-α – tumor necrosis factor alfa; MSCs – mesenchymal stem cells.**

INTRODUCTION

Polyhydroxyalkanoates (PHAs) are biodegradable polyesters of hydroxycarbonic acids which are produced by either chemical synthesis or bacterial biosynthesis. Since the early 21st century, there has been growing interest in studying these polymers and introducing them in medical practice. Synthetic poly(2-hydroxypropanoic) (polylactic (PLA), polylactides) acid and poly(2-hydroxyacetic) (polyglycolic) acid ((PGA), polyglycolides), poly(6-hydroxycaprolactone) (PCL) and natural poly(3-hydroxybutyric) acid (PHB, poly(3-hydroxybutyrate)); poly(4-hydroxybutyric) acid (P4HB), poly(3-hydroxyvaleric) acid (PHV, poly(3-hydroxyvalerate)), poly(3-hydroxyhexanoate) (PHHx), and their copolymers and polymers with a similar structure, such as poly(*p*-dioxanone) (PDS) (*Fig. 1*), are currently used both in research and clinical practice. These polymers have a similar chemical structure and, therefore, similar physicochemical and biomedical properties: they can be biodegraded in the organism without toxic product formation, are biocompatible with human organs and tissues, exhibit optimal physic-

ochemical properties (thermoplasticity, relatively high hydrophobicity, specific diffusion properties, relatively high strength, and flexibility). Furthermore, they can be produced through efficient technological processes. Such a unique combination of properties by these polymers contributes to their wide use and introduction in medical practice [1–4].

APPLICATION OF POLYHYDROXYALKANOATES IN MEDICINE

PHAs began being widely utilized in medicine as early as in the 1970s. Thus, the first biodegradable Vicryl surgical suture material produced from chemically synthesized polymers appeared on the market of medicinal products back in 1974. Various products made of PHAs are either currently in use or being developed (biodegradable surgical staples, screws, plates, pins and cords, bioresorbable suture material and skin staples, wound and burn dressings, membranes for periodontal guided regeneration, surgical mesh endoprostheses, patches for surgical repair of intestinal and pericardial defects, mesh plugs for coloproctological applications and hernioplasty, vascular prosthetic implants, coronary stents, mesh tubes for nerve regeneration, artificial heart valves, and other medical devices). PHAs are also used in pharmaceutics as components of novel dosage forms and impart such properties as targeted delivery, prolonged activity, reduced toxicity, and enhanced stability to them [1–4] (*Fig. 2*).

All members of the PHA family are characterized by a unique combination of properties. However, synthetic PHAs (sPHAs) such as poly(2-hydroxypropanoic) acid (polylactic acid or polylactide), poly(2-hydroxyacetic) acid (polyglycolic acid or polyglycolide) and their copolymers–poly(lactic-co-glycolic) acids (polylactide-co-glycolides) (PLGAs), poly(6-hydroxycaprolactone), and poly(*p*-dioxanone) – are those most typically used in medicine (*Fig. 1*). The reason behind this is the larger scale application of chemical synthesis in the production of medical polymers and earlier development of a method for the industrial-scale production of sPHAs (PLA, PGA, PCL and their copolymers), earlier certification, conduct of preclinical and clinical trials, and introduction of these polymers in clinical practice (in the 1970s–80s). An important role was also played by the fact that these polymers are very convenient to use (in particular, due to their rapid biodegradation in human tissues) [4–6].

However, PLA, PGA, and their copolymers are synthetic analogs of natural polyhydroxyalkanoates, poly(3-hydroxyalkanoates) (nPHAs). Although synthetic PHAs (including PLA, PGA, PLGA, and PCL) are quite often referred to as biopolymers, as implied by their biodegradability and biocompatibility, it is not fully accurate to use this term, since what are usually referred to as biopolymers are polymeric metabolic by-products of living organisms (bacteria, plants, fungi, and animals); i.e., natural biomacromolecules [7]. Hence, poly(3-hydroxyalkanoates) are reserve polymers in many bacterial species [1], while sPHAs (PLA, PGA, PLGA, PCL, etc.) are not found in nature [4, 8]. Although copolymers of poly(3-hydroxybutyrate) and polylactic acid have been synthesized using genetic engineering techniques employing bacterial strains [9, 10], this only provides additional evidence of their artificial origin. Nevertheless, these polymers also share key properties, although with important distinctions that have been outlined above.

Natural poly(3-hydroxyalkanoates) are polyesters of 3-hydroxyalkanoic acids; therefore, PHB is a linear polyester of (R)-3-hydroxybutyric acid (*Fig. 1*). The distinctions between different nPHAs are a result of the presence of a side radical: poly(3-hydroxybutyrate), poly(3-hydroxyvalerate), poly(3-hydroxyhexanoate), poly(3-hydroxyoctanoate), etc. (*Fig. 1*). All these compounds differ rather significantly in their physicochemical properties, such as crystallinity, the melting point and glass transition temperature, hydrophobicity, plasticity, the Young's modulus, etc. It is important to mention that bacterial biosynthesis typically results in not pure homopolymers of poly(3-hydroxyvalerate), poly(3-hydroxyhexanoate), and other, longer chain PHA monomers but rather in their block copolymers with PHB: poly(3-hydroxybutyrate-co-3-hydroxyvalerate) (PHBV), poly(3-hydroxybutyrate-co-3-hydroxyhexanoate) (PHBHx), poly(3-hydroxybutyrate-co-3-hydroxyvalerate-co-3-hydroxyhexanoate) (PHBVHx), (poly(3-hydroxybutyrate-co-3-hydroxyoctanoate (PHBO), poly(3-hydroxybutyrate-co-4-hydroxybutyrate) (PHB4HB), etc. However, the properties of these copolymers differ significantly from those of PHB and substantially depend on the monomeric composition of the copolymer [11–13].

A technical approach is usually employed to study the biomedical properties (including biological activity) of various PHAs: one of the materials intended for the development of a certain medical device is tested. But what if we analyze the biomedical properties of PHA using PHB as a natural progenitor of almost all the PHAs utilized in medicine in terms of all the functions that this polymer possesses when occurring in nature? In other words, we are going to use biomimetics, an interesting biological discipline [14]. There is all the more reason for this as the biomimetic approach has recently been increasingly in use in the study of various polymers [15].

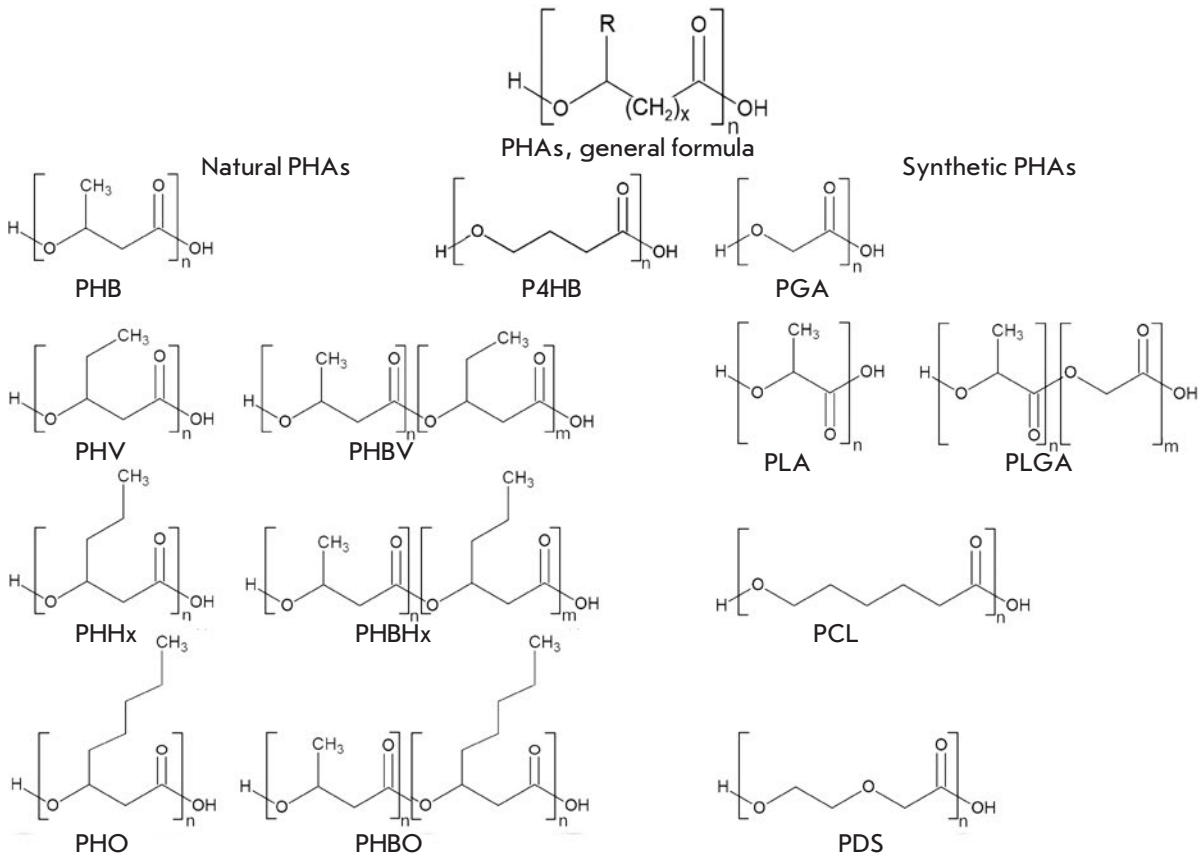

Fig. 1. The general formula for polyhydroxyalkanoates and the structural formulas for a series of natural and synthetic polyhydroxyalkanoates for biomedical applications. Abbreviations: PHB – poly(3-hydroxybutyrate); PHV – poly(3-hydroxyvalerate); PHBV – poly(3-hydroxybutyrate-co-3-hydroxyvalerate); PHHx – poly(3-hydroxyhexanoate); PHBHx – poly(3-hydroxybutyrate-co-3-hydroxyhexanoate); PHO – poly(3-hydroxyoctanoate); PHBO – poly(3-hydroxybutyrate-co-3-hydroxyoctanoate); P4HB – poly(4-hydroxybutyric) acid (poly(4-hydroxybutyrate)); PGA – poly(2-hydroxyacetic) acid (polyclycolic acid, polyglycolide); PLA – poly(2-hydroxypropanoic) acid (polylactic acid, polylactide); PLGA – poly(lactic-co-glycolic) acid (polylactide-co-glycolide); PCL – poly(6-hydroxycaprolactone); PDS – poly(*p*-dioxanone)

THE BIOLOGICAL ACTIVITY OF POLYHYDROXYALKANOATES

Biocompatibility of polyhydroxyalkanoates and their biological activity

Natural biopolymers, such as proteins and peptides, polysaccharides, lipids, nucleic acids, polyprenols, and their copolymers, typically exhibit intense biological activity that is directly related to their specialized functions: enzymatic, regulatory, signaling, defense, transport, etc. Furthermore, even biopolymers such as lipopolysaccharides or pectins playing "neutral" functions (structure-forming or reserve ones) can also exhibit a pronounced biological activity [16]. Therefore, medical products or pharmaceuticals based on some of these biopolymers (collagen, chitosan, and polylysine) may have a biological activity that is sometimes undesirable (e.g., immunotoxicity) [17]. However, despite the intensive research that is currently underway, the question regarding the biological activity of both synthetic and natural PHAs remains rather controversial and insufficiently studied. On the other hand, the wide application of PHAs in medicine is largely a result of the fact that they are highly biocompatible and are either non- or low-toxic, which does not preclude the biological activity in these polymers [17]. Meanwhile, biodegradability is the key reason why PHAs are utilized in medicine. However, the process of polymer biodegradation implies that there is intensive interaction between the polymer and the surrounding living cells and tissues (that often are involved in this process) and that the cells and tissues are affected not

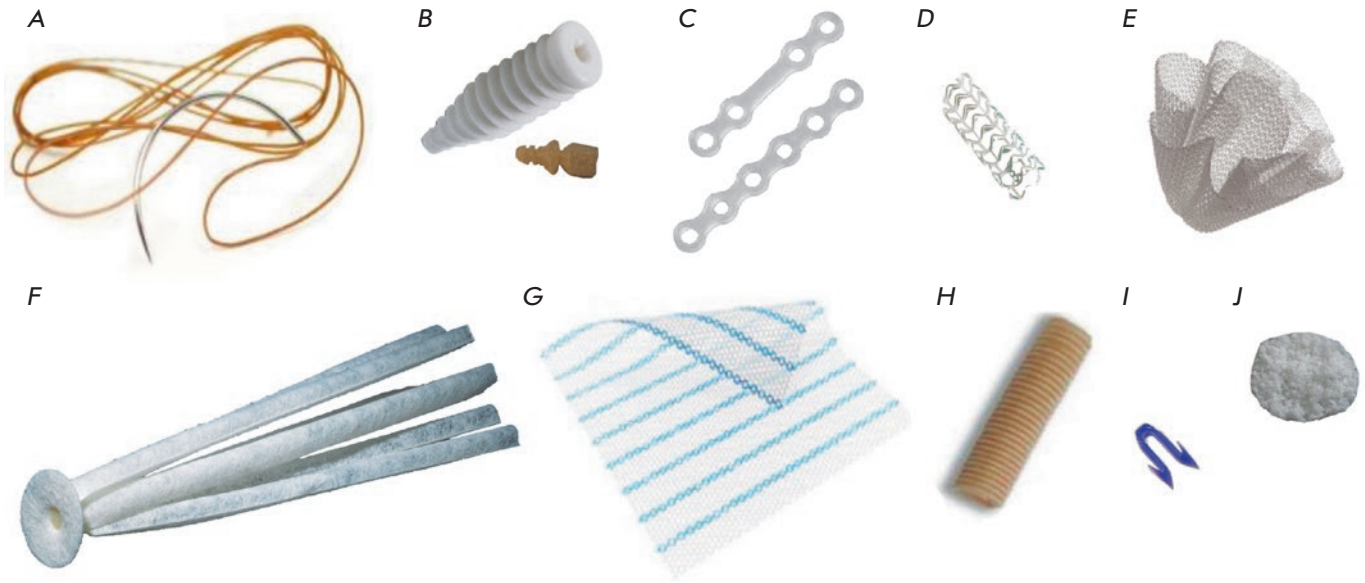

Fig. 2. Medical devices based on synthetic and natural PHAs used in medical practice or currently being developed. *A* – PGA-based bioresorbable sutures (Ethicon, Johnson & Johnson, USA); *B* – Osteotwin™ bioresorbable interference screw for bone fixation based on PLA with a plasticizing agent (Biomatlante, France); *C* – LactoSorb® PLGA-based bioresorbable plates for bone fixation (Biomet, USA); *D* – ABSORB PLA-based bioresorbable coronary stent (Abbott, USA); *E* – Phasix Plug P4HB-based bioresorbable woven plug endoprosthesis for hernioplasty (C.R. Bard Inc., USA); *F* – Gore Bio-A fistula plug PLA-based bioresorbable plug endoprosthesis for coloproctological applications PLA (W. L. Gore & Associates Inc., USA); *G* – Ultrapro Advanced™ partially resorbable mesh endoprosthesis for hernioplasty based on a woven material made of polypropylene monofilaments and PLGA (Ethicon, Johnson & Johnson, USA); *H* – GEM Neurotube mesh tube based on woven PGA material for nerve fusion (Synovis Micro Companies Alliance, USA); *I* – PLA-based bioresorbable staple for an automated skin and soft tissue stapling device (Ethicon, Johnson & Johnson, USA); *J* – ElastoPHB PHBV-based bioresorbable biopolymeric membrane for repairing soft and cartilage tissue defects (BIOMIR Service JSC, Krasnoznamensk, Russia)

only by the polymer, but also by its biodegradation products (oligomers and monomers). In addition, more and more data become available demonstrating that PHAs exhibit an intrinsic biological activity with respect to various cells and tissues in humans and laboratory animals.

All the main PHAs, both the synthetic (PLA, PGA, PLGA and PCL) and natural PHBs (PHBV, PHBHx, P4HB) ones, possess fairly good biocompatibility when compared to many other materials, which is sufficient for utilizing these biodegradable polymers to fabricate implants that come into contact with soft tissues, bones, and blood in compliance with ISO standards 10993 [2, 4, 17, 18]. However, a comparison of the tissue response to PHB and the synthetic polyesters PLA, PGA, or their copolymers, revealed that PHB elicits either a mild or moderate tissue response [2, 3], while PLA, PGA, and PLGA often induce chronic inflammation [18]. In most cases, PHB and its copolymers were characterized by good biocompatibility when used as implanted biomaterials [19–21]. The standard test for tissue reaction to subcutaneous implantation of PHB and its copolymers in film form, which is employed in the protocols of preclinical trials, reveals a mild or moderate response to the foreign material. A thin fibrous capsule (~ 100 μm) is formed during a month and is resorbed once the samples have biodegraded [19–22]. Many studies revealed a low lymphocyte count or virtually no lymphocytes (in particular, T lymphocytes) at the PHB insertion site, indicating that the immune reaction to this polymeric biomaterial is either significantly reduced or absent [23–26]. It was demonstrated that deeply purified PHB and PHBV also exhibit good hemocompatibility, so they can be used to produce blood-contacting medical devices: patches for the pericardial wall, the pulmonary artery, and the right atrium, as well as biodegradable coronary stents [25–30]. However, the biocompatibility of PHB is especially vividly witnessed when using PHB-based devices (e.g., porous scaffolds for bone tissue regeneration). Implantation of PHB-based devices into the area of bone tissue defect is not accompanied by the formation of a connective tissue capsule separating

the polymeric material from the bone tissue, which is observed for many biomedical devices (e.g., those made of PLA). In other words, PHB becomes completely integrated into the bone tissue. Implantation of the PHB-based porous scaffold leads to vigorous vascularization of the scaffold and emergence of islets of the bone tissue newly formed from the granulation tissue in its pores [23, 24, 31]. Evaluation of the expression levels of various cytokines and other markers of inflammation in the implantation site of medical devices based on PHB (and its copolymer PHBV) revealed reduced expression levels of proinflammatory cytokines (interleukins, tumor necrosis factor, monocyte chemoattractant protein, inducible nitric oxide synthase, and C-reactive protein) compared to those for other materials and increased expression of genes encoding various proteins (type I collagen, caveolin-1, cytokeratin, heparan sulfate proteoglycan, thrombomodulin, and prostacycline), which are markers of regenerative processes taking place in cardiac, vascular, intestinal, neural, and osseous tissues [23, 25, 27, 28, 32–35]. However, chronic inflammatory response to the implantation of PHB-based devices (e.g., coronary stent prototypes) was observed in some cases. It should be mentioned that these devices were either fabricated through polymer melting or could have been insufficiently purified [36, 37]. Like during biodegradation, the method used for molding products made of a polymer, especially when applying extrusion or melt molding, may significantly affect the biocompatibility of PHB and its copolymers. Melting causes polymer recrystallization and abruptly slows down water diffusion in the polymer matrix, whereas water is a component that plays a crucial role in the formation of the PHB ultrastructure, which strongly affects its biological properties [38].

Due to its high biocompatibility, PHB is a promising material for use in cell biology and cellular engineering. Various mammalian cells (human and murine fibroblasts, rat, mouse, and human mesenchymal stem cells (MSCs), rabbit bone tissue osteoblasts, human osteogenic sarcoma cells, chondrocytes in rabbit articular cartilage and rabbit smooth muscle cells) exhibit good levels of cell adhesion, proliferation, and viability during *in vitro* cultivation on PHB-based films or porous scaffolds [3]. Nano- and microparticles of PHB and its copolymers have no cytotoxic effect on different cells at concentrations below 1 mg/ml [39, 40]; their endocytosis can be performed not only by macrophages, but also by osteoblasts, fibroblasts, and epithelial tumor cells [41–45]. Meanwhile, the cytotoxicity of PLA and PLGA nanoparticles was not detected only at concentrations below 66–100 μg/ml but was strongly marked at concentrations above 100 μg/ml [41, 46]. Water-soluble PHB oligomers consisting of ~ 25 3-hydroxybutyrate residues conjugated to lipoid acid also had no *in vitro* cytotoxic effect on keratinocytes at concentrations below 9 μg/ml [47].

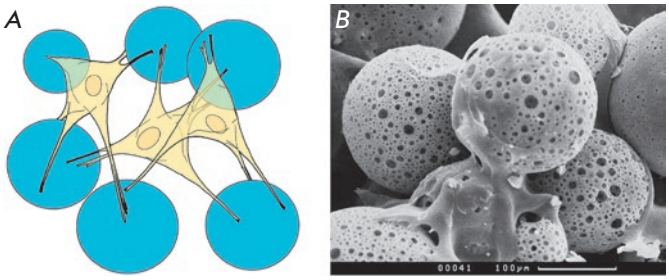

Fig. 3. An *in vitro* experimental model of 3D cultivation of mesenchymal stem cells on PHB-based microspheres: scheme (A) and a SEM image (×300) (*B*) of cell growth on microspheres

Due to their high biocompatibility, PHB and other PHAs can be used to manufacture devices of various structures (porous matrices, microspheres, and scaffolds) for experimental modeling of the 3D growth of various human and mammalian cells (mesenchymal stem cells, fibroblasts, various tumor cell lines) under *in vitro* conditions, which will allow one to create experimental models of various diseases; cancer in particular [48] (*Fig. 3*). Meanwhile, one should bear in mind that characteristics of polymers such as their chemical composition, surface morphology, surface energy and hydrophobicity have a profound impact on cell viability and growth [49]: for example, chemical treatment of the surface of PHB-based items facilitates cell growth on them [3].

Biodegradation of polyhydroxyalkanoates and their biological activity

The biodegradation rate of widely used sPHAs, PLA, and PGA is significantly higher than that of other PHAs, since biodegradation takes place preferentially via hydrolytic destruction. This destruction mechanism of sPHAs is the reason behind the many problems associated with their medical application. Thus, the degradation products of PLA, PGA, and PLGA, which are formed during rapid hydrolysis, have no time to be taken up by the organism and pH decreases drastically near the implant. Chronic tissue irritation caused by reduced pH is considered a serious problem associated with the use of polymer implants based on PLA, PGA, and PLGA; an optimal solution to this problem still needs to be found [18]. Chronic inflammation in response to the destruction of polylactides and polyglycolides can be aggravated by the immune response to release non-stereoregular water-soluble oligomers,

degradation products of polymers belonging to this class [18, 50]. The products of hydrolytic destruction of PLA and PGA were shown to be cytotoxic [18, 41, 46]. Dendritic cells that can be activated by PLGA significantly contribute to the triggering of an inflammatory reaction to this polymer after its implantation [51]. In particular, this inflammatory response is one of the reasons why biodegradation of intraosseous implants made from these polymers is slowed down as they are "preserved" in a connective tissue capsule, which causes various complications, such as implant migration to the bones, fistulization, implant failure, etc. [18]. Various sorts of precautions are used to eliminate chronic inflammation. Hence, anti-inflammatory drugs (dexamethasone or curcumin) [52, 53], antibodies specific to proinflammatory cytokines (interferon-γ) [54] are added to PLGA-based products, or mesenchymal stem cells are used [51].

Natural poly(3-hydroxyalkanoates) are much more resistant to hydrolysis in aqueous media [55], including in the presence of various esterases [55–57]. In living tissues, the biodestruction rate can be manifold higher than that in an aqueous medium under *in vitro* model conditions even in the presence of high concentrations of lipolytic enzymes (e.g., lipase) [22].

Recent data demonstrate that the biodegradation of PHB and its copolymers takes place predominantly through the phagocytic ability of specialized cells (macrophages), as well as foreign body giant cells (FBGCs) and osteoclasts. In other words, specialized biodegradation of these polymers takes place. The insertion of devices based on PHB and its copolymers into the organism results in the recruitment of macrophages in the damaged area, which densely cover the polymeric material as a connective tissue capsule is formed around it and are actively involved in polymer biodegradation. The polymeric biomaterial is exposed to the extracellular fluid and cells, which may lead to cleavage of micro- and nanoparticles, oligomers, and the monomers from it [3, 19, 57–59]. Cells cause superficial erosion of the polymer, without significantly altering its physicochemical properties, which takes place upon bulk hydrolytic destruction of the polymer. It was demonstrated that signs of erosion (erosion pits 20–50 μm in diameter) remained on the polymer surface after macrophages and FBGCs had been removed [25, 26, 60, 61]. The low biodestruction rate reduces the concentrations of degradation products near the implant; for PHB, the predominant degradation product is 3-hydroxybutyric acid, which is much weaker (p*K*α = 4.41) than lactic acid (pKα = 3.73), the main biodegradation product of PLA and PLGA. Therefore, biodegradation of PHB and its copolymers does not cause medium acidification [18–20].

Macrophages are simultaneously activated by the polymeric material, which contributes to their phagocytic activity [36, 40, 62]. Macrophage adhesion on the surface of the polymeric material plays an important role. Biodegradation of polymeric membranes was shown to take place only once macrophages have adhered to their surface. If macrophages are incapable of adhering to the membrane, polymer degradation does not occur [63]. Macrophages and osteoclasts tightly adhere to polymeric PHB films and proliferate on them [62]. The expression of two types of lipases significantly increased after 7- and 14-day contacts between PHB and animal tissues; enhanced expression of the same types of lipases was observed in the liver. Furthermore, increased synthesis of cleaving enzymes such as type 1 and type 2 lipases, amylase, chymotrypsin, and trypsin was observed in the gastric wall immediately at the site where tissues came into contact with a PHB-based patch [34]. Two enzymes cleaving PHB were found in rat tissues: liver serine esterase with maximum activity observed in an alkaline medium (pH 9.5) and kidney esterase active in a neutral medium [64]. Experiments involving low-molecular-weight PHB particles demonstrated that macrophages are involved in the biodegradation of PHB [40]. It was found that macrophages and fibroblasts (although to a lesser extent) can phagocytize PHB particles 1–10 μm in size. At high concentrations of PHB particles (> 10 μg/ml), phagocytosis is accompanied by a toxic effect and changes in the functional status of macrophages but not fibroblasts [40]. Meanwhile, the nanoparticles (15–250 nm in size) of PHB and its copolymers had no significant cytotoxic effect on macrophages even at such a high concentration as 1 mg/ml, unlike PLA nanoparticles [41]. Phagocytosis of PHB microparticles was accompanied by enhanced production of nitric oxide (NO) and tumor necrosis factor-α (TNFα) in the activated macrophages, while phagocytosis of a large amount of microparticles caused microphage death. It was also demonstrated that phagocytosis of PHB particles gradually decreases due to vigorous biodegradation of PHB [40]. It is an interesting fact that not only macrophages, but osteoblasts as well can be involved in *in vitro* endocytosis of microparticles consisting of low-molecular-weight PHB. Upon co-cultivation of these cells, the phagocytic ability of osteoblasts, as well as their osteogenic activity (alkaline phosphatase activity), was stimulated by macrophages phagocytizing polymeric microparticles [40].

Hence, the contact between living cells and polymers even characterized by high biocompatibility can be accompanied by a natural inflammatory response by the organism to the implantation of a foreign body and by the activation of macrophages and osteoclasts as they

cleave the polymer. However, one should differentiate between this biological activity of PHAs and the intrinsic biological activity of polymers as related to their specific properties.

Intrinsic biological activity of polyhydroxyalkanoates

PHB and its copolymers seemingly also exhibit an intrinsic biological activity. As mentioned earlier, they activate immune cells upon implantation, thus inducing secretion of proinflammatory cytokines by these cells [34, 35]. This effect is typical of a regular tissue response to the implantation of almost any materials, especially biodegradable ones. It was demonstrated that PHB-based products (non-woven patches, porous scaffolds) facilitate the regeneration of tissues in different organs: osseous, cardiac and vascular, neural, and intestinal tissues. Application of PHB-based devices causes a high degree of vascularization in the area of tissue defect repair [23–28, 32, 35, 65]. It was shown using the critical (the parietal region of rat skull) and noncritical (rat femur) models of bone defects that PHB-based porous scaffolds facilitate bone tissue regeneration. Minimal tissue response to the implantation related to gradual bioresorption of polymeric material, vigorous vascularization of the matrix, and intergrowth of the newly formed bone tissue into the pores of the PHB-based scaffold were observed at all stages of bone defect regeneration. Expression of osteogenic markers (e.g., type I collagen) is also indicative of bone tissue regeneration in a PHB-based scaffold [23, 24]. We observed a uniform formation of nascent bone tissue over the entire volume of the porous biopolymeric scaffold in the form of islets rather than on the edges; meanwhile, a fibrous capsule did not form around the biopolymeric material, an indication of its complete integration with the bone tissue [24, 65]. All this demonstrates that PHB exhibits excellent biocompatibility with bone tissue and possess an osteoconductive and even osteoinductive potential. The biological activity of PHB and its copolymers produced via bacterial biosynthesis was attributed to the fact that the polymeric material could have been insufficiently purified to remove bacterial lipopolysaccharide or DNA. However, even the highly purified polymer can elicit a cellular response [36].

A biological activity of porous scaffolds based on PHB and its copolymers (PHBV, PHBHx, and PHBVHx) was also demonstrated at a cellular level *in vitro*. Thus, terpolymer PHBVHx stimulated the proliferation of *HaCaT* human kertinocytes grown on polymeric films produced via precipitation from a solution. Investigation of the mechanism of stimulation of cell proliferation using the nanoparticles of this biopolymer demonstrated that the addition of PHBVHx nanoparticles at a concentration of 0.02–0.1 g/l stimulates an

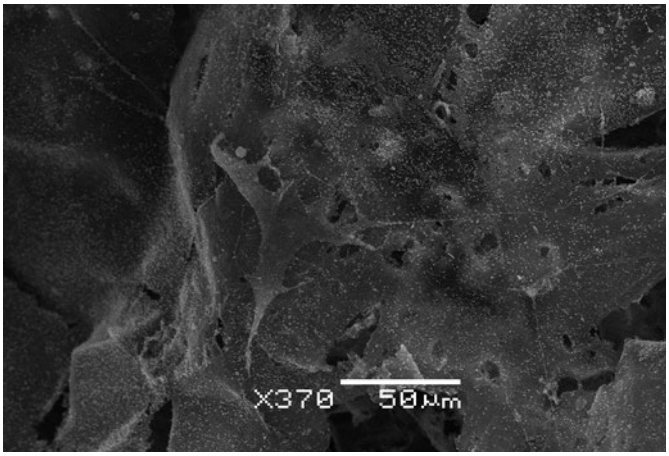

Fig. 4. A mesenchymal stem cell with the osteoblast morphology on the PHB-based polymeric matrix (on the 21st day of cultivation) and calcium salt deposits around it on the matrix. A SEM image (×370)

elevation of the current of calcium ions into the cytoplasm, which is one of the key signaling pathways for the activation of cell division. The degradation product of PHA, monomeric 3-hydroxybutyrate (*D*-3-hydroxybutyric acid, 3HB), also independently induces the activation of *HaCaT* human keratinocytes and *L929* murine fibroblasts when used at concentrations ranging from 0.01 to 0.1 g/l (0.1–1.0 mM), as it increases calcium ion concentration in the cytoplasm, and also suppresses fibroblast apoptosis and necrosis [66–68]. This activity of 3HB is not surprising, since this ketone body is a natural mammalian metabolite that displays a profound biological activity [16]. However, biological activity can be exhibited not only by 3HB, but also by PHA oligomers. Thus, PHB oligomers and their copolymers with 4-hydroxybutyrate and 3-hydroxyhexanoate (with a chain length of 20–25 monomer units) are not cytotoxic when used at concentrations < 20 µg/ml, stimulate proliferation and suppress apoptosis, calcium release into the cytoplasm, and the formation of cell–cell contacts between pancreatic beta cells in mice [69].

It was demonstrated that scaffolds based on PHB and its copolymers (PHBV, PHBHx) promote osteogenic differentiation of osteoblasts and mesenchymal stem cells in humans, rats, and rabbits (isolated both from the adipose tissue and from the bone marrow) when culturing the cells on these materials [23, 24, 39, 63, 70–72]. Differentiation of MSCs cultured on nPHAs-based scaffolds was confirmed by changes in cell morphology (*Fig. 4*), inhibition of their proliferation, increased alkaline phosphatase activity, calcium salt deposition in

the cells [24, 39, 70–72], and expression of markers of osteogenic differentiation, and the formation of osseous tissue (alkaline phosphatase, type 1 collagen, *Runx2*, osteocalcin, and osteopontin) using the immunoenzyme techniques and PCR [23, 24, 70]. However, some studies failed to confirm the induction of osteogenic differentiation upon cultivation of embryonic progenitor populations on the scaffolds [73]. It is worth mentioning here that the growth and differentiation of MSCs can be affected by their physicochemical properties, as well as the microstructure and the topography of the devices made from the polymers used to culture the cells. This effect can even neutralize the influence of the bioactive molecules that stimulate cell growth or differentiation in a particular direction [49, 74, 75]. The impact of PHAs on MSC differentiation can also be related to the bioactivity of their biodegradation product, 3HB. Thus, 3HB at a concentration of 0.005–0.1 g/l (0.05–1 mM) causes osteogenic differentiation of MC3T3-E1 mouse osteoblasts, which was identified based on an elevation of the alkaline phosphatase activity, calcium deposition (Alizarin Red S staining quantification assay), and osteocalcin expression. The osteoinductive activity of 3HB was demonstrated *in vivo* for an osteoporosis model in female rats with their ovaries removed. Nevertheless, 3HB used at lower concentrations did not exhibit such an effect; slow biodegradation of PHAs gives rise to 3HB at concentrations much lower than 0.05 mM [76]. PHBHx also causes chondrogenic differentiation of MSCs, which was observed based on changes in the expression of chondrogenic genes acting as MSC markers (aggrecan, *col2*, *sox9*, *col10*, and *pthrp*) [74]. It was shown in other studies that PHB, PHBHx, PHBVHx, PHBO, and their composites, as well as PLA, stimulate neurogenic differentiation of MSCs, which can be observed based on changes in cell morphology and the expression of the genes coding for lineage-specific proteins (nestin, glial fibrillary acidic protein, and βIII-tubulin) [77, 78]. This theoretically could have been related to the neuroprotective effect of 3HB that was demonstrated earlier if it was not for the fact that the positive impact of 3HB on the nervous system is caused by the nutritional (energy) function of fatty acids, including 3HB, in neurons and manifests itself when these substances are used at extremely high doses [79]. However, it was also demonstrated that 3HB stimulates the formation of neuronal gap junctions for signal transduction, and this fact can be used to explain why this compound improves memory and learning ability [80]. It is interesting that the effects of PHAs on cell proliferation, differentiation, and apoptosis can be realized through integrins, the molecules that mediate cell–cell contacts and are involved in recognition. Differentiation of MSCs and osteoblast apoptosis proceed via the cascade mechanism initiated as PHAs interact with integrins on the cell surface [81, 82].

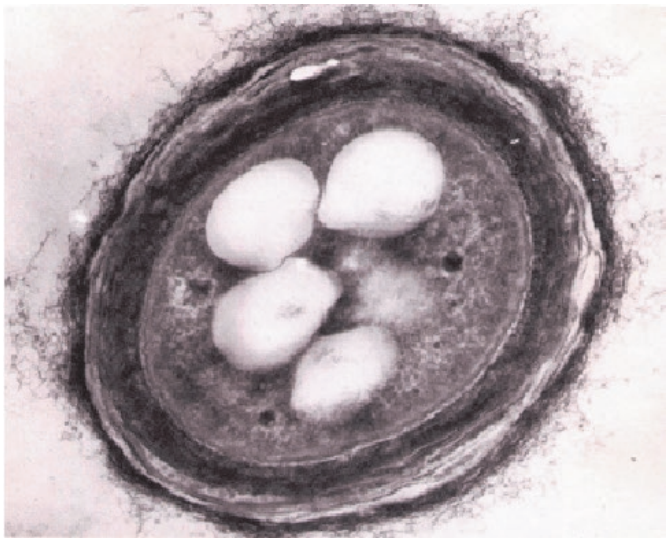

Fig. 5. PHA-producing strain of *Azotobacter chroococcum* 7B with PHB granules in a bacterial cell during polymer biosynthesis (TEM, ×50,000)

BIOLOGICAL ACTIVITY AND NATURAL FUNCTIONS OF POLY(3-HYDROXYBUTYRATE)

Poly(3-hydroxybutyrate) as a reserve polymer in bacteria

Natural poly(3-hydroxyalkanoates) have evolutionarily developed as reserve biopolymers, i.e., polymers that can be biodegraded by enzymatic systems in living organisms to release energy and carbon for cells to remain vitally active and ensure the biosynthesis of other biomolecules. The ability to synthesize reserve nPHAs, and PHB in particular, is commonly observed in prokaryotes; several hundreds of bacterial species utilize this biopolymer as a reserve compound. For most microorganisms, the accumulated nPHAs act as a source of carbon and energy if there is a lack thereof. Bacteria capable of synthesizing nPHAs accumulate the biopolymer in their cytoplasm as discrete inclusions (granules) that typically range between 100 and 800 nm in diameter (*Fig. 5*). The role of nPHAs, and PHB in particular, as a reserve material in bacteria was thoroughly discussed in the review by Anderson and Dawes [83].

Furthermore, human symbiotic and infectious bacteria, such as *Agrobacterium, Clostridium, Ralstonia, Bacillus, Burkholderia, Vibrio, Legionella, Pseudomonas, Mycobacterium, Acinetobacter, Sphin-*

gomonas, Fusobacterium, Neisseria, Streptomyces, Bordetella, and *Rickettsia* either are capable of synthesizing PHB or carry the enzymes (and genes encoding them) involved in its biosynthesis (primarily PHA polymerase). Some of these bacteria (e.g., *Pseudomonas sp.*) can synthesize both PHB and its various copolymers [84]. Many of these bacteria either constitute a significant portion of the normal human gut microbiota, which plays a crucial role in the formation of immunity and other organs (the oral cavity, the lungs, and the skin), or are causative agents of many common infectious diseases. Accordingly, the human immune system recognizes the antigens of these bacteria presumably from the very time the immunity starts to form during infancy. PHB is one of these common antigens familiar to the immunity. This probably is the reason for the high biocompatibility of this biopolymer and those of its synthetic analogs that have a similar structure and physicochemical properties. However, despite the fact that the immune system also comes into contact with lipopolysaccharide at the stage of immunity formation, this biopolymer is a potent immune stimulant. Meanwhile, PHB is also a product of symbiotic and infectious bacteria. It is quite possible that the function of PHB in the human body differs from that of the reserve material in microbiota.

Endogenous poly(3-hydroxybutyrate) in animal tissues and its putative functions

Contrary to the existing opinion that PHB is synthesized solely in prokaryotic cells, this biopolymer was discovered by Reusch [85] in almost all types of organisms. The short-chain complexed PHB (cPHB, ≤ 30 3-hydroxybutyrate monomers), and the medium-chain, or oligo-PHB (oPHB, 100–200 3-hydroxybutyrate monomers) were detected in various organs and tissues of mammals, including humans (as well as cow, sheep, and pig) and birds (chicken and turkey): in blood, brain, heart, liver, kidney, blood vessels, nerves, lipoprotein particles, platelets, etc. The cPHB/oPHB concentration varies from 3–4 μg/g in neural tissues and the brain; to 12 μg/g in blood plasma. The oPHB concentration in human blood plasma can vary in a rather wide range: between 0.6 and 18.2 μg/ml, the average value being 3.5 μg/ml [85]. It should be mentioned that 3HB, the intermediate product of PHB biodegradation, is a so-called ketone body. It is found in mammalian blood and tissues at a normal level of 0.3–1.3 mM and at much higher levels in pathology [86].

Reusch [85] suggested that besides acting as a reserve material and an energy depot in bacteria, PHB also plays different regulatory functions in eukaryotes and prokaryotes. PHB (namely, the short-chain cPHB and oPHB) affects the function of protein receptors and channels, as well as DNA, by forming noncovalent or covalent bonds with them. The researchers attributed the presence of PHB in different human tissues to the existence of some biochemical synthesis mechanisms of this biopolymer. They showed that cPHB and oPHB form noncovalent complexes with inorganic polyphosphates and calcium ions, which can function as nonprotein channels that allow inorganic ions to pass through the cell membrane. These structures also form noncovalent complexes with ion-channel proteins and are their components. They also affect the receptor and channel functions through covalent binding. Thus, PHB oligomers bind covalently to calcium ATPase in the cell membrane of human red blood cells and simultaneously form a complex with inorganic phosphates [86]. Indirect evidence has been obtained showing that PHB–protein conjugates play some physiological role. Thus, conjugation of DP18L antitumor peptides to 3-hydroxydecanoate enhances their activity [87].

Putative functions of poly(3-hydroxybutyrate) in the microbiota of animals

However, PHB can have other functions in the human body that do not require its synthesis. It is fair to assume that PHB is somehow involved in the interplay between gut bacteria, where this biopolymer is synthesized, immune cells, and the intestinal epithelium. This hypothesis is supported by the special role played by PHB in the symbiosis between the gut bacteria and the host organism. For example, the synthesis of PHB contributes to the interaction between *Burkholderia* bacteria and their host, the bean bug *Riptortus pedestris*, making these bacteria more resistant to the immune system of this bug [88]. It was also demonstrated that the biosynthesis of PHB plays a crucial role in the microbiota of sea cucumber *Apostichopus japonicus*. The synthesis of PHB seems to modulate the intestinal microbiota of the sea cucumber, which increases the animal's size manifold [89]. The study focused on the ability of histamine to regulate the synthesis of low-molecular-weight cPHB in *Escherichia coli* deserves close attention. Histamine plays an important role as a means of communication between bacteria and the host organism; it also regulates the intestinal immunity, so that the bacteria are recognized as "self" by the host organism. Therefore, the effect of histamine on the synthesis of cPHB may indicate that this biopolymer is involved in adaptation and coexistence with the host organism [90]. Furthermore, it was demonstrated that PHB is effective in treating infectious diseases: giving PHB as food to brine shrimp *Artemia nauplii* protected them against a disease caused by *Vibrio campbellii*; the effectiveness of PHB was 100-fold higher than that of 3-hydroxybutyric

The biological activity of synthetic and natural PHAs in the human body and the natural functions of poly(3-hydroxybutyrate)

<table>
<tr><th>Biological activity</th><th>Potential causes</th><th>Natural functions</th></tr>
<tr><td>Activation of macrophages and osteoclasts [36, 40, 63].</td><td>The ability to undergo hydrolytic and enzymatic destruction [1–4, 19, 58–60]. Preferentially cellular biodegradation of nPHAs [25, 26, 61, 62].</td><td>The ability of PHB to undergo controlled biodegradation (as an intracellular reserve material in bacteria) [83].</td></tr>
<tr><td>Stimulation of proliferation of cells (keratinocytes, fibroblasts, and beta-cells) [67–70].</td><td>Intrinsic biological activity of nPHAs [69, 81, 82] and 3HB [67, 68].</td><td rowspan="3">The potential signaling function of PHB upon the interplay between gut bacteria synthesizing it and the immune cells and intestinal epithelial cells [88–90, 94]. The potential functionality of endogenous PHB [85]. Various functions of the ketone body 3HB and other 3-hydroxyalkanoates in the mammalian organism [76, 79, 93].</td></tr>
<tr><td>Stimulation of osteogenic, chondrogenic, and neurogenic differentiation of osteoblasts and MSCs [23, 24, 39, 63, 70–72, 77, 78].</td><td rowspan="2">Physicochemical properties of PHAs [24, 49, 71], the microstructure and topography of medical products [74, 75], biodegradability [1–4], intrinsic biological activity of nPHAs [69, 81, 82] and 3HB [77, 80].</td></tr>
<tr><td>Activation of regeneration of various tissues (cardiac and vascular, intestinal, neural, and osseous) [1, 2, 4, 23, 25, 27, 28, 32–35, 36]</td></tr>
<tr><td>Chronic inflammatory response (low [1–4, 19–35], pronounced [18, 36, 37]).</td><td>Acidification of tissues with biodegradation products of PLA [18], immune response to sPHAs with the modified chemical structure [18, 50, 51], insufficient purification, harsh treatment of polymers (e.g., by melting) [38, 49], the microstructure and shape of medical devices [18].</td><td rowspan="2">Low toxicity of PHB as an intracellular reserve material in bacteria [83]; low immunogenicity of PHB due to its presence in mammalian gut microbiota [84] and potential presence of endogenous PHB in mammals [85].</td></tr>
<tr><td>Cytotoxicity (low [1–4, 39–45, 47], pronounced [18, 41, 46]).</td><td>Acidification of tissues with biodegradation products of sPHAs [18, 41, 46].</td></tr>
</table>

acid [91]. Furthermore, PHB can inhibit not only *Vibrio* sp., but also *E. coli* and *Salmonella* sp. [92]. It was also demonstrated that the biodegradation products of some nPHAs (e.g., 3-hydroxyoctanoate) exhibit an antimicrobial activity with respect to a number of Gram-negative and Gram-positive bacteria, as well as inhibit the production of the metabolites associated with the pathogenic activity of these bacteria, while a much higher nPHA concentration is needed for a cytotoxic effect on human fibroblasts [93].

An interesting fact indicating that 3-hydroxybutyrate dimers and trimers are sex pheromones in spiders also indicates that PHB might possess some signaling functions in the organism [94]. It is quite possible that these pheromones can be products of the biosynthesis performed by bacteria in the microbiota of arthropod species. Thus, in *Costelytra zealandica* beetles, sex pheromone is phenol synthesized from tyrosine by symbiotic bacteria *Morganella morganii* in special glands [95]. 3-Hydroxybutyrate dimers and trimers were found in fungus *Hypoxylon truncatum*; however, the mechanism underlying their synthesis is yet to be established [96].

P4HB and PHB4HB are used to manufacture a number of biodegradable medical devices: surgical suture material, woven mesh endoprostheses and plug endoprostheses, as well as scaffolds for soft tissue regeneration. Due to its modified chemical structure, P4HB (as well as PLA and PGA) preferentially undergoes hydrolytic degradation. These polymers do not exist in nature; they are obtained through bioengineering via biosynthesis by the genetically modified *E. coli* strain K12. P4HB monomer, 4-hydroxybutyrate (γ-hydroxybutyric acid), similar to 3-hydroxybutyrate, is a natural metabolite and one of the neurotransmitters used as a potent psychoactive agent and even listed in the controlled drugs register [97].

CONCLUSIONS

Hence, the biological activity of PHAs observed by many researchers (e.g., the ability of these polymers to stimulate the regeneration of bone and cartilage tissues) is related not only to the physicochemical properties of PHAs or to the structure of items based on these polymers, but also to the fact that PHAs exhibit an intrinsic activity, which is in turn caused by the natural functions of PHB, a precursor used to produce these polymers (*Table*). This relationship is also observed between the biodegradability of PHAs used to fabricate medical devices in human tissues and the natural function of PHB as a reserve biopolymer in bacterial cells, since the reserve material must be able to undergo cleavage by cellular enzymes in order to be able to perform its function. This biopolymer possibly has certain signaling functions in our organism through which the gut bacteria interact with the immune cells,

intestinal mucosa, and other tissues by eliciting a certain physiological response in them. It is fair to assume that the structure of PHAs produced by both chemical synthesis and bioengineering is similar to that of PHB, thus making it possible to mimic the biological properties of PHB related to the functions acquired by this biopolymer during the long-term evolution of the organisms in which it is synthesized.

Although the overwhelming majority of devices and pharmaceuticals based on PHAs were produced from synthetic PHAs, several products based on natural PHAs have already been designed and are used in practice: e.g., the ElastoPHB biopolymer membrane system for repairing soft and cartilage tissue defects (BIOMIR Service JSC, Krasnoznamensk, Russia) [98] and Phasix™ Plug TephaFLEX composite mesh endoprosthesis (Tepha Inc., USA) [97] (*Fig. 2*). The bioengineering plant belonging to the Italian company Bio-on (http://www.bio-on.it/index.php) that is currently under construction and is intended for large-scale industrial production of PHB and its copolymers also justifies the never-abating interest in natural PHAs used both in industry (packaging, textile, cosmetics, and household goods) and in medicine.

Hence, the field of science discussed in this review requires further comprehensive and meticulous research, which will allow us to uncover the natural functions of the polymers used in medicine (the biomimetic analogs of natural predecessors) and to design novel, nature-like technologies for producing polymer-based medical items and next-generation drugs. ●

This work was supported by the Russian Foundation for Basic Research (projects Nos. 15-29-04856 ofi-m under section 1 and 18-29-09099 mk under sections 2 and 3).

REFERENCES

1. Mokhtarzadeh A., Alibakhshi A., Hejazi M., Omidi Y., Dolatabadi J.E.N. // Trends Analyt. Chem. 2016. V. 82. P. 367–384.
2. Lim J., You M., Li J., Li Z. // Mater. Sci. Eng. C Mater. Biol. Appl. 2017. V. 79. P. 917–929.
3. Bonartsev A.P., Bonartseva G.A., Shaitan K.V., Kirpichnikov M.P. // Biochemistry (Moscow) Supplement Series B: Biomedical Chemistry. 2011. V. 5. № 1. P. 10–21.
4. Farah S., Anderson D.G., Langer R. // Adv. Drug Deliv. Rev. 2016. V. 107. P. 367–392.
5. Athanasiou K.A., Niederauer G.G., Agrawal C.M. // Biomaterials. 1996. V. 17. № 2. P. 93–102.
6. Middleton J.C., Tipton A.J. // Biomaterials. 2000. V. 21. № 23. P. 2335–2346.
7. Vert M., Doi Y., Hellwich K.H., Hess M., Hodge P., Kubisa P., Rinaudo M., Schue F. // Pure Appl. Chem. 2012. V. 84. № 2. P. 377–410.
8. Biomedical polymers / Ed. Jenkins M. Birmingham, UK: Univ. Birmingham, 2007. 203 p.
9. Park S.J., Kang K.H., Lee H., Park A.R., Yang J.E., Oh Y.H., Song B.K., Jegal J., Lee S.H., Lee S.Y. // J. Biotechnol. 2013. V. 165. № 2. P. 93–98.
10. Jung Y.K., Lee S.Y. // J. Biotechnol. 2011. V. 151. № 1. P. 94–101.
11. Bloembergen S., Holden D.A., Hamer G.K., Bluhm T.L., Marchessault R.H. // Macromolecules. 1986. V. 19. № 11. P. 2865–2871.
12. Barcham P.J. // Novel biosynthetic biodegradable polymers of industrial interest from microorganisms / Ed. Dawes E.A. Dordrecht: Kluwer Acad. Publ., 1990. P. 81–96.
13. Akhtar S., Pouton C.W., Notarianni L.J. // Polymer. 1992. V. 33. № 1. P. 117–126.
14. Vincent J.F., Bogatyreva O.A., Bogatyrev N.R., Bowyer A., Pahl A.K. // J. R. Soc. Interface. 2006. V. 3. № 9. P. 471–482.
15. Kushner A.M., Guan Z. // Angew. Chem. Int. Ed. Engl. 2011. V. 50. № 39. P. 9026–9057.
16. Nelson D.L., Cox M.M. Lehninger Principles of Biochemistry, 5th Edition. New York: W.H. Freeman and Company, 2008. P. 852–860.
17. Sevastianov V.I., Kirpichnikov M.P. (eds.). Biocompatiblematerials: Teaching Tutorial. M: Medical Information Agency, 2011. 540 p.
18. Ramot Y., Haim-Zada M., Domb A.J., Nyska A. // Adv. Drug Deliv. Rev. 2016. V. 107. P. 153–162.
19. Qu X.H., Wu Q., Zhang K.Y., Chen G.Q. // Biomaterials. 2006. V. 27. № 19. P. 3540–3548.
20. Freier T., Kunze C., Nischan C., Kramer S., Sternberg K., Sass M., Hopt U.T., Schmitz K.P. // Biomaterials. 2002. V. 23. № 13. P. 2649–2657.
21. Kawaguchi T., Tsugane A., Higashide K., Endoh H., Hasegawa T., Kanno H., Seki T., Juni K., Fukushima S., Nakano M. // J. Pharm. Sci. 1992. V. 87. № 6. P. 508–512.
22. Boskhomdzhiev A.P., Bonartsev A.P., Makhina T.K., Myshkina V.L., Ivanov E.A., Bagrov D.V., Filatova E.V., Iordanskiĭ A.L., Bonartseva G.A. // Biochemistry (Moscow) Supplement Series B: Biomedical Chemistry. 2010. V. 4. № 2. P. 177–183.
23. Shumilova A.A., Myltygashev M.P., Kirichenko A.K., Nikolaeva E.D., Volova T.G., Shishatskaya E.I. // J. Biomed. Mater. Res. A. 2017. V. 105. № 2. P. 566–577.
24. Zharkova I.I. Scaffolds from biosynthetic copolymer of poly(3-hydroxybutyrate) with poly(ethylene glycol) for bone tissue engineering. M: MSU, 2017.
25. Malm T., Bowald S., Karacagil S., Bylock A., Busch C. // Scand. J. Thorac. Cardiovasc. Surg. 1992. V. 26. № 1. P. 9–14.
26. Malm T., Bowald S., Bylock A., Busch C., Saldeen T. // Eur. Surg. Res. 1994. V. 26. P. 298–308.
27. Malm T., Bowald S., Bylock A., Busch C. // J. Thoracic Cardiovasc. Surgery. 1992. V. 104. P. 600–607.
28. Malm T., Bowald S., Bylock A., Saldeen T., Busch C. // Scandinavian J. Thoracic Cardiovasc. Surgery. 1992. V. 26. № 1. P. 15–21.
29. Sevastianov V.I., Perova N.V., Shishatskaya E.I., Kalacheva G.S., Volova T.G. // J. Biomat. Sci. Polymer Ed. 2003. V. 14. № 10. P. 1029–1042.
30. Unverdorben M., Spielberger A., Schywalsky M., Labahn D., Hartwig S., Schneider M., Lootz D., Behrend D., Schmitz K., Degenhardt R., et al. // Cardiovasc. Intervent. Radiol.

2002. V. 25. № 2. P. 127–132.
31. Kostopoulos L., Karring T. // Clin. Oral. Implants Res. 1994. V. 5. № 2. P. 66–74.
32. Castellano D., Blanes M., Marco B., Cerrada I., Ruiz-Sauri A., Pelacho B., Arana M., Montero J.A., Cambra V., Prosper F., et al. // Stem. Cells Dev. 2014. V. 23. № 13. P. 1479–1490.
33. Pontailler M., Illangakoon E., Williams G.R., Marijon C., Bellamy V., Balvay D., Autret G., Vanneaux V., Larghero J., Planat-Benard V., et al. // Tissue Eng. Part A. 2015. V. 21. № 9–10. P. 1552–1564.
34. Lobler M., Sass M., Kunze C., Schmitz K.P., Hopt U.T. // Biomaterials. 2002. V. 23. № 2. P. 577–583.
35. Lobler M., Sass M., Schmitz K.P., Hopt U.T. // J. Biomed. Mater. Res. 2003. V. 61. P. 165–167.
36. Wu A.C., Grondahl L., Jack K.S., Foo M.X., Trau M., Hume D.A., Cassady A.I. // Biomaterials. 2006. V. 27. № 27. P. 4715–4725.
37. Unverdorben M., Spielberger A., Schywalsky M., Labahn D., Hartwig S., Schneider M., Lootz D., Behrend D., Schmitz K., Degenhardt R., et al. // Cardiovasc. Intervent. Radiol. 2002. V. 25. № 2. P. 127–132.
38. Iordanskii A.L., Ol'khov A.A., Pankova Yu.N., Bonartsev A.P., Bonartseva G.A., Popov V.O. // Macromolecular symposia. 2006. V. 233. P. 108–116.
39. Saad B., Ciardelli G., Matter S., Welti M., Uhlschmid G.K., Neuenschwander P., Suter U.W. // J. Biomed. Mater. Res. 1998. V. 39. № 4. P. 594–602.
40. Saad B., Ciardelli G., Matter S., Welti M., Uhlschmid G. K., Neuenschwander P., Suterl U.W. // J. Biomed. Mater. Res. 1996. V. 30. P. 429–439.
41. Xiong Y.C., Yao Y.C., Zhan X.Y., Chen G.Q. // J. Biomater. Sci. Polymer Ed. 2010. V. 21. № 1. P. 127–140.
42. Bonartsev A.P., Zernov A.L., Yakovlev S.G., Zharkova I.I., Myshkina V.L., Mahina T.K., Bonartseva G.A., Andronova N.V., Smirnova G.B., Borisova J.A., et al. // Anti-Cancer Agents in Med. Chem. 2017. V. 17. № 3. P. 434–441.
43. Ermakova N.P., Bonartsev A.P., Zernov A.L., Konyaeva O.I., Kulbachevskaya N.Y., Merkulova I.B., Abramova T.V., Chaley V.A., Yakovlev S.G., Bonartseva G.A., et al. // Anti-Cancer Agents in Med. Chem. 2017. V. 17. № 15. P. 1661–1668.
44. Lu X.Y., Li M.C., Zhu X.L., Fan F., Wang L.L., Ma J.G. // BMC Biotechnol. 2014. V. 14. P. 4.
45. Penaloza J.P., Marquez-Miranda V., Cabana-Brunod M., Reyes-Ramírez R., Llancalahuen F.M., Vilos C., Maldonado-Biermann F., Velásquez L.A., Fuentes J.A., González-Nilo F.D. // J. Nanobiotechnol. 2017. V. 15. № 1. P. 1.
46. Stevanovic M., Pavlovic V., Petkovic J. // Express. Polymer Lett. 2011. V. 5. № 11. P. 996–1008.
47. Maksymiak M., Debowska R., Jelonek K., Kowalczuk M., Adamus G. // Rapid. Commun. Mass Spectrom. 2013. V. 27. P. 773–783.
48. Solorio L.D., Vieregge E.L., Dhami C.D., Alsberg E. // Tissue Eng. Part B Rev. 2013. V. 19. № 3. P. 209–220.
49. Fischer D., Li Y., Ahlemeyer B., Krieglstein J., Kissel T. // Biomaterials. 2003. V. 24. № 7. P. 1121–1131.
50. Rihova B. // Adv. Drug. Delivery Rev. 1996. V. 21. P. 157–176.
51. Zhu H., Yang F., Tang B., Li X.M., Chu Y.N., Liu Y.L., Wang S.G., Wu D.C., Zhang Y. // Biomaterials. 2015. V. 53. P. 688–698.
52. Vacanti N.M., Cheng H., Hill P.S., Guerreiro J.D., Dang T.T., Ma M., Watson S., Hwang N.S., Langer R., Anderson D.G. // Biomacromolecules. 2012. V. 13. № 10. P. 3031–3038.
53. Su S.H., Nguyen K.T., Satasiya P., Greilich P.E., Tang L., Eberhart R.C. // J. Biomater. Sci. Polymer Ed. 2005. V. 16. № 3. P. 353–370.
54. Khouw I.M., van Wachem P.B., de Leij L.F., van Luyn M.J. // J. Biomed. Mater. Res. 1998. V. 41. P. 202–210.
55. Zhuikov V.A., Bonartsev A.P., Makhina T.K., Myshkina V.L., Voinova V.V., Bonartseva G.A., Shaitan K.V. // Biophysics. 2018. V. 63. №. 2. P. 169–176.
56. Zhuikov V.A., Bonartsev A.P., Bagrov D.V., Yakovlev S.G., Myshkina V.L., Makhina T.K., Bessonov I.V., Kopitsyna M.N., Morozov A.S., Rusakov A.A., et al. // Molecular Crystals Liquid Crystals. 2017. V. 648. № 1. P. 236–243.
57. Abe H., Doi Y. // Biomacromolecules. 2002. V. 3. № 1. P. 133–138.
58. Renstad R., Karlsson S., Albertsson A.C. // Polym. Degrad. Stab. 1999. V. 63. P. 201–211.
59. Kramp B., Bernd H.E., Schumacher W.A., Blynow M., Schmidt W., Kunze C., Behrend D., Schmitz K.P. // Laryngorhinootologie. 2002. V. 81. № 5. P. 351–356.
60. Baptist J.N., Ziegler J.B. // Patent No. 3229766. USA. 1965.
61. Shishatskaya E.I., Volova T.G., Gordeev S.A., Puzyr A.P. // J. Biomater. Sci. Polymer Ed. 2005. V. 16. № 5. P. 643–657.
62. Cool S.M., Kenny B., Wu A., Nurcombe V., Trau M., Cassady A.I., Grøndahl L. // J. Biomed. Mater. Res A. 2007. V. 82. № 3. P. 599–610.
63. Bat E., van Kooten T.G., Feijen J., Grijpma D.W. // Biomaterials. 2009. V. 30. № 22. P. 3652–3661.
64. Saito T., Tomita K., Juni K., Ooba K. // Biomaterials. 1991. V. 12. № 3. P. 309–312.
65. IvanovS.Yu., Bonartsev A.P., GazhvaYu.V., Zharkova I.I., Mukhametshin R.F., Makhina T.K., Myshkina V.L., Bonartseva G.A., Andreeva N.V., Akulina E.A. et al. // Biomedicinskayachimiya. 2015. V. 61. № 6. P. 717–723.
66. Ji Y., Li X.T., Chen G.Q. // Biomaterials. 2008. V. 29. P. 3807–3814.
67. Cheng S., Chen G.Q., Leski M., Zou B., Wang Y., Wu Q. // Biomaterials. 2006. V. 27. P. 3758–3765.
68. Cheng S., Yang F., Xu M., Wu Q., Leski M., Chen G.Q. // Biomacromolecules. 2005. V. 6. P. 593–597.
69. Yang X.D., Zou X.H., Dai Z.W., Luo R.C., Wei C.J., Chen G.Q. // J. Biomater. Sci. Polym. Ed. 2009. V. 20. № 12. P. 1729–1746.
70. de Paula A.C., Zonari A.A., Martins T.M., Novikoff S., da Silva A.R., Correlo V.M., Reis R.L., Gomes D.A., Goes A.M. // Tissue Eng. Part A. 2013. V. 19. № 1–2. P. 277–289.
71. Wang Y.W., Wu Q., Chen G.Q. // Biomaterials. 2004. V. 25. № 4. P. 669–675.
72. Misra S.K., Ansari T., Mohn D., Valappil S.P., Brunner T.J., Stark W.J., Roy I., Knowles J.C., Sibbons P.D., Jones E.V., et al. // J. R. Soc. Interface. 2010. V. 7. № 44. P. 453–465.
73. Zhang S., Prabhakaran M.P., Qin X., Ramakrishna S. // J. Biomater. Appl. 2015. V. 29. № 10. P. 1394–1406.
74. Wang Y., Jiang X.L., Yang S.C., Lin X., He Y., Yan C., Wu L., Chen G.Q., Wang Z.Y., Wu Q. // Biomaterials. 2011. V. 32. № 35. P. 9207–9217.
75. Criscenti G., Vasilevich A., Longoni A., De Maria C., van Blitterswijk C.A., Truckenmuller R., Vozzi G., De Boer J., Moroni L. // Acta Biomater. 2017. V. 55. P. 310–322.
76. Zhao Y., Zou B., Shi Z., Wu Q., Chen G.Q. // Biomaterials. 2007. V. 28. № 20. P. 3063–3073.
77. Wang L., Wang Z.H., Shen C.Y., You M.L., Xiao J.F., Chen G.Q. // Biomaterials. 2010. V. 31. № 7. P. 1691–1698.
78. Lizarraga-Valderrama L.R., Nigmatullin R., Taylor C., Haycock J.W., Claeyssens F., Knowles J.C., Roy I. // Eng. Life Sci. 2015. V. 15. P. 612–621.

79. Zhang J., Cao Q., Li S., Lu X., Zhao Y., Guan J.S., Chen J.C., Wu Q., Chen G.Q. // Biomaterials. 2013. V. 34. № 30. P. 7552–7562.
80. Zou X.H., Li H.M., Wang S., Leski M., Yao Y.C., Yang X.D., Huang Q.J., Chen G.Q. // Biomaterials. 2009. V. 30. № 8. P. 1532–1541.
81. Wang Y., Gao R., Wang P.P., Jian J., Jiang X.L., Yan C., Lin X., Wu L., Chen G.Q, Wu Q. // Biomaterials. 2012. V. 33. № 2. P. 485–493.
82. Wang Y., Jiang X.L., Peng S.W., Guo X.Y., Shang G.G., Chen J.C., Wu Q., Chen G.Q. // Biomaterials. 2013. V. 34. № 15. P. 3737–3746.
83. Anderson A.J., Dawes E.A. // Microbiol. Rev. 1990. V. 54. № 4. P. 450–472.
84. Bonartsev A.P., Voinova V.V., Bonartseva G.A. // Applied Biochemistry and Microbiology. 2018. V. 54. № 6. C. 547–568.
85. Reusch R.N. // Chem. Biodivers. 2012. V. 9. № 11. P. 2343–2366.
86. Larsen T., Nielsen N.I. // J. Dairy Sci. 2005. V. 88. № 6. P. 2004–2009.
87. Szwej E., Devocelle M., Kenny S., Guzik M., O'Connor S., Nikodinovic-Runic J., Radivojevic J., Maslak V., Byrne A.T., Gallagher W.M., el al. // J. Biotechnol. 2015. V. 204. P. 7–12.
88. Kim J.K., Won Y.J., Nikoh N., Nakayama H., Han S.H., Kikuchi Y., Rhee Y.H., Park H.Y., Kwon J.Y., Kurokawa K., et al. // Proc. Natl. Acad. Sci. USA. 2013. V. 110. № 26. P. E2381–E2389.
89. Yamazaki Y., Meirelles P.M., Mino S., Suda W., Oshima K., Hattori M., Thompson F.L., Sakai Y., Sawabe T., Sawabe T. // Sci. Rep. 2016. V. 6. P. 21631.
90. Kyriakidis D.A., Tiligada E. // Amino Acids. 2009. V. 37. № 3. P. 443–458.
91. Defoirdt T., Halet D., Vervaeren H., Boon N., van de Wiele T., Sorgeloos P., Bossier P., Verstraete W. // Environ. Microbiol. 2007. V. 9. № 2. P. 445–452.
92. Defoirdt T., Boon N., Sorgeloos P., Verstraete W., Bossier P. // Biotechnol. Adv. 2009. V. 27. № 6. P. 680–685.
93. Radivojevic J., Skaro S., Senerovic L., Vasiljevic B., Guzik M., Kenny S.T., Maslak V., Nikodinovic-Runic J., O'Connor K.E. // Appl. Microbiol. Biotechnol. 2016. V. 100. № 1. P. 161–172.
94. Schulz S., Toft S. // Science. 1993. V. 260. № 5114. P. 1635–1637.
95. Marshall D.G., Jackson T.A., Unelius C.R., Wee S.L., Young S.D., Townsend R.J., Suckling D.M. // Naturwissenschaften. 2016. V. 103. № 7–8. P. 59.
96. Quang D.N., Hashimoto T., Toyota M., Asakawa Y. // J. Nat. Prod. 2003. V. 66. № 12. P. 1613–1614.
97. Williams S.F., Martin D.P., Moses A.C. // Aesthet. Surg. J. 2016. V. 6 (suppl 2). P. S33–S42.
98. Nemets E.A., Efimov A.E., Egorova V.A., Tonevitsky A.G., Sevastianov V.I. // Bull. Exp. Biol. Med. 2008. V. 145. № 3. P. 371–373.

Molecular Biomarkers of Brain and Spinal Cord Astrocytomas

N. A. Konovalov[1], D. S. Asyutin[1], E. G. Shayhaev[2], S. V. Kaprovoy[1], S. Yu. Timonin[1*]
[1]National Medical Research Center of Neurosurgery, Ministry of Health of the Russian Federation Acad. N.N. Burdenko, 4th Tverskaya-Yamskaya Str. 16, Moscow, 125047, Russia
[2]FGBU Russian Research Center for X-ray Radiology of the Ministry of Health of the Russian Federation Profsouznaya Str. 86, Moscow, 117485, Russia
*E-mail: md.timonin@gmail.com
Received February 1, 2019; in final form April 30, 2019
DOI: 10.32607/20758251-2019-11-2-17-27

ABSTRACT **Spinal cord astrocytomas are rare diseases of the central nervous system. The localization of these tumors and their infiltrative growth complicate their surgical resection, increase the risk of postoperative complications, and require more careful use of radio- and chemotherapy. The information on the genetic mutations associated with the onset and development of astrocytomas provides a more accurate neoplasm diagnosis and classification. In some cases, it also allows one to determine the optimal methods for treating the neoplasm, as well as to predict the treatment outcomes and the risks of relapse. To date, a number of molecular markers that are associated with brain astrocytomas and possess prognostic value have been identified and described. Due to the significantly lower incidence of spinal cord astrocytomas, the data on similar markers are much more sparse and are presented with a lesser degree of systematization. However, due to the retrospective studies of clinical material that have been actively conducted abroad in recent years, the formation of statistically significant genetic landscapes for various types of tumors, including intradural spinal cord tumors, has begun. In this regard, the purpose of this review is to analyze and systematize the information on the most significant genetic mutations associated with various types of astrocytomas, as well as discuss the prospects for using the corresponding molecular markers for diagnostic and prognostic purposes.**
KEYWORDS **spinal cord astrocytoma, glioblastoma, mutations, molecular markers, diagnosis, mechanisms of neoplastic transformation, prognostic value.**
ABBREVIATIONS **CNS – central nervous system; IMSCT – intramedullary spinal cord tumors; PA – pilocytic astrocytoma; SCA – spinal cord astrocytoma; DA – diffuse astrocytoma; AA – anaplastic astrocytoma; GB – glioblastoma; WHO – World Health Organization.**

INTRODUCTION

Primary tumors of the spinal cord are rare diseases; they comprise only 2%–4% of all tumors of the central nervous system (CNS) [1, 2]. Symptoms associated with the development of such tumors can vary greatly depending on the tumor type and localization and include pain, autonomic, motor and sensory impairments, as well as dysfunction of pelvic organs [3]. Without treatment, they can lead to serious CNS dysfunction and patient death.

Historically, there have been three main groups of spinal cord tumors: extradural extramedullary, intradural extramedullary, and intramedullary lesions (*Fig. 1*). The latter group (intramedullary spinal cord tumors, IMSCTs) is the rarest type of CNS neoplasms (5%–10% of all primary spinal cord neoplasms) [4, 5].

The most frequent variants of IMSCTs are ependymomas and astrocytomas, which in total comprise about 90% (60% and 30%, respectively) of all IMSCT cases diagnosed in adults, while the remaining 10% include hemangioblastomas and metastatic tumors [6, 7]. On the contrary, in children under 10 years of age, astrocytomas are usually more common than ependymomas (*Fig. 2*) [8].

Astrocytomas develop from astrocytes, i.e., cells of the glial tissue. Therefore, they belong to the class of glial tumors. According to the WHO classification, there are four types of astrocytomas [9]. Pilocytic astrocytoma (PA, grade I) is a benign, slowly growing tumor separated from healthy tissues, which includes parallel hair-like bundles of glial fibers. It occurs mainly in patients under the age of 20; the 10-year survival rate

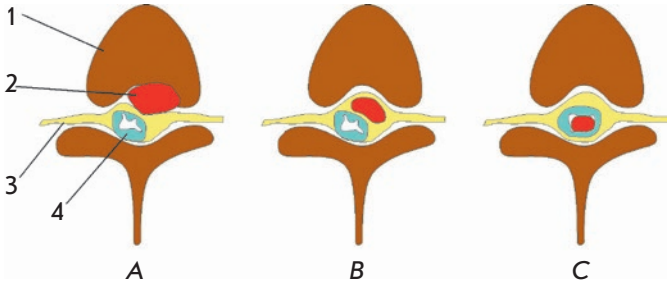

Fig. 1. Types of spinal cord tumors: extradural extramedullary (*A*), intradural extramedullary (*B*), and intradural intramedullary (*C*) tumors. *1* – vertebral body, *2* – tumor, *3* – dura mater, and *4* – spinal cord

exceeds 90% [10, 11]. Diffuse or low-grade astrocytoma (grade II) is an infiltrative tumor with no clear boundaries characterized by slow invasive growth, which gradually progresses to an anaplastic form. Anaplastic astrocytoma (grade III) is an infiltrative malignant tumor of heterogeneous structure which can either arise independently or develop from tumors with a lower grade of malignancy. Anaplastic astrocytoma is characterized by rapid progression and a steady decrease in cell differentiation to atypical glioblastoma. Glioblastoma (grade IV) is a tumor characterized by a high degree of malignancy and rapid infiltrative growth. Glioblastomas can occur *de novo* or develop from tumors of lower grades; they are diagnosed mainly in older patients [12].

In most cases, the detected astrocytomas belong to the grade I or II (85–90%), while the most malignant grades III and IV astrocytomas account for about 10–15% of all cases, with the frequency of a diagnosis of glioblastoma being only 0.2–1.5% [4]. In general, the incidence of primary spinal cord astrocytomas (SCA) is about 2.5 per 100,000 people per year [4]. Clinical manifestations of SCA largely depend on its localization and malignancy degree and most often include pain (~ 70%), sensory disorders (~ 65%), and motor function impairments (~ 50%) [13].

The understanding of the molecular biology of intracranial astrocytomas has significantly expanded over the past 10 years. In particular, some molecular parameters have been included to the WHO classification of CNS tumors (2016) [14]. Meanwhile, the research into the mechanisms of emergence and progression of malignant spinal cord astrocytomas, as well as the development of effective therapy methods, is progressing rather slowly, while the number of publications devoted to this type of tumors is very small compared to the data accumulated on intracranial astrocytomas. The primary reason is the rare incidence of this type of tumors and, therefore, the challenges associated with obtaining a statistically significant number of samples for analysis. In addition, the heterogeneity of the clinical presentation and various treatment strategies make it difficult to conduct a randomized study under standardized conditions [15]. Finally, the small size, localization of these tumors in the parenchyma, and the degree of their infiltration into the surrounding healthy tissues, which significantly increases the risk of complications associated with their surgical resection, make it very difficult to obtain enough tissue material for research. Meanwhile, the data on genetic changes in

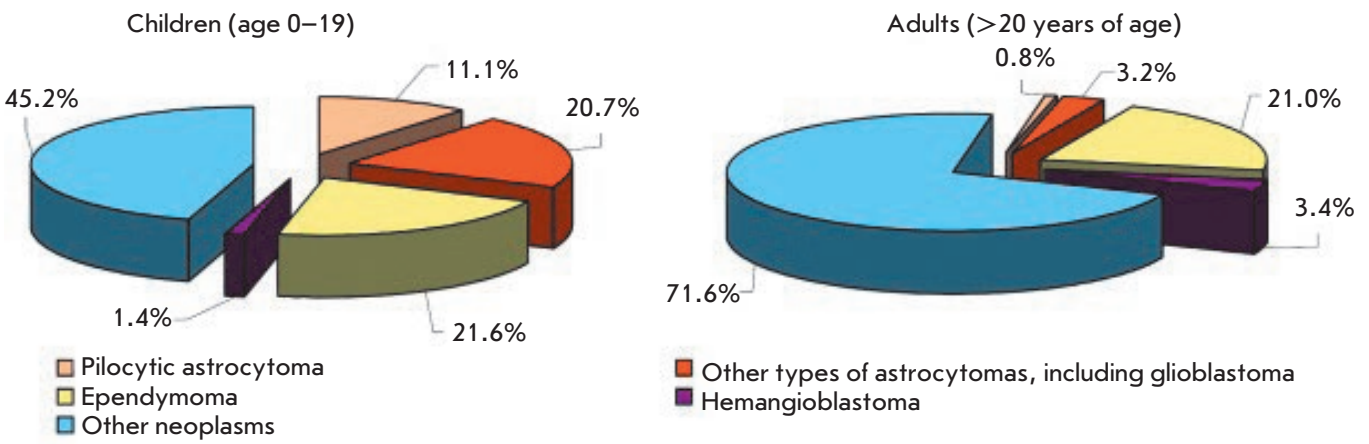

Fig. 2. The incidence of intradural intramedullary primary spinal cord tumors in children under the age of 19 years ($n = 1,238$) and adult patients ($n = 14,822$) according to the U.S. Central Brain Tumor Registry (CBTRUS) data report for 2007–2011. The data are presented according to [15] (with modifications)

SCA cells provide information on the pathophysiological origin of the neoplasm and possible tumor markers; they can also allow one to determine the therapy option, predict the patient's condition and the risk of recurrence [16]. Genetic studies on intracranial astrocytomas have laid the foundation for identifying the candidate genes responsible for the development of SCA, despite the fact that the two types of astrocytomas also present certain differences in their oncogenesis [14].

The aim of this review is to summarize the data on certain genetic mutations associated with the development and progression of astrocytomas and gliomas of various degrees of malignancy, as well as the potential of using them for predicting and diagnosing this type of tumors, including SCA.

Genetic markers associated with astrocytomas

There is abundant evidence of the leading role played by genetic aberrations in the development and progression of primary malignant tumors of the CNS [17–20]. Such aberrations can include complete loss or partial deletion of the chromosome, loss of specific alleles, inactivating mutations, as well as methylation of the gene promoter. Next, we describe in detail some of the most crucial genetic markers associated with astrocytomas, as well as potential marker genes, and consider the prospects of their use for diagnostic and prognostic purposes.

BRAF. The *BRAF* gene, which encodes serine/threonine protein kinase of the RAF protein family, is a proto-oncogene involved in the regulation of cell proliferation and growth [21]. Mutations in this gene can lead to various tumors. For instance, duplication and activation of *BRAF* are found in juvenile PA, which is localized in the cerebellum (80%) and the hypothalamic/chiasmal region (62%) [22]. In some of the PA cases, a hybrid form of the *BRAF* gene has been found, which is formed by fusion with the previously uncharacterized *KIAA1549* gene; this form is distinguished by constitutive activation of BRAF kinase [23, 24]. An activating point mutation, i.e. the substitution of valine to glutamate at position 600 (*BRAF* V600E) [25], as well as several other insertion mutations, are also known [26, 27]. Since this mutation is practically absent in other gliomas and non-glial tumors, it can be used for differential diagnosis and targeted therapy of PA [28]. However, it should be noted that, in some cases, mutations in *BRAF* can be found in diffuse gliomas and malignant astrocytomas, in combination with mutations in other genes, such as *CDKN2A* or *IDH* [29, 30]. According to a number of studies, the point mutation V600 in *BRAF* is more often found in supratentorial PA while hybrid oncogenes are mostly associated with PA located in the basicranial region and the spinal cord [31]. According to the multicenter study on SCA, more than 80% of PAs contain mutations in *BRAF*, with 40% of these cases being presented with a *BRAF*-KIAA1549 mutation and the remaining 60% being presented with *BRAF* duplication variants [32].

CDKN2A. *CDKN2A*, which encodes cyclin-dependent kinase that functions as a tumor suppressor, is another gene crucial to SCA and, in particular, PA [31]. In a cohort of 140 cases of PA, homozygous deletions in this gene were much more common in PAs localized in the brain stem and the spinal cord than in the case of PAs localized in the brain or cerebellum [33]. In addition to PA, deletions in *CDKN2A* are quite often detected in glioblastomas in adult patients. For instance, according to the results of two studies, this mutation was found in about half of the studied glioblastoma cases [34, 35]. In another study, a mutation in this gene was identified in three out of nine patients with high-grade glioblastomas of the spinal cord [36].

IDH1/IDH2. One of the most important discoveries in the study of gliomas (including astrocytomas) was the identification of mutations in the *IDH1* and *IDH2* genes encoding $NADP^+$-dependent homodimers of isocitrate dehydrogenases 1 and 2, which are localized in the cytoplasm and mitochondria, respectively, and catalyze oxidative decarboxylation of isocitrate with the formation of α-ketoglutarate (α-KG) [37]. The *IDH1* mutation is rarely found in primary glioblastomas (< 5%). However, it is diagnosed in 70%–80% of grades II–III astrocytomas and secondary glioblastomas [38, 39]. The *IDH2* mutation is much less common (less than 3% of all gliomas) and never found together with the *IDH1* mutation [39]. In the overwhelming majority of cases (> 90%), the *IDH1* mutation is presented with a substitution of arginine to histidine at position 132 (the enzyme active center). The mutant enzyme variant catalyzes the reduction of α-KG to 2-hydroxyglutarate (2-HG), a competitive inhibitor of α-KG-dependent dioxygenases, thus resulting in genome hypermethylation, which presumably occurs due to inhibition of the TET methylcytosine hydroxylase [40, 41]. In addition, these mutations can alter the histone methylation level by suppressing cell differentiation [42] and also contribute to the accumulation of the hypoxia-induced factor HIF-1α, which affects a number of processes, such as angiogenesis, cell metabolism, growth, differentiation, and apoptosis [43].

Tumors with mutations in *IDH* also typically carry a mutation in the *TP53* gene or 1p/19q codeletion. These additional mutations are mutually exclusive; they are characteristic of astrocytomas (*TP53*) and oligodendro-

gliomas (1p/19q) [44]. The incidence of the *IDH1* mutation in low-grade diffuse astrocytomas and secondary glioblastomas is 88% and 82%, respectively, with the *TP53* mutation being detected in 63% of diffuse astrocytomas [44]. Only a few percents of cases with mutations in *IDH1* or *IDH2* were also characterized by changes in the *PTEN*, *EGFR*, *CDKN2A,* and *CDKN2B* genes. Meanwhile, the incidence of *TP53* mutations was significantly lower (18%) in the samples carrying wild-type *IDH1* and *IDH2*, while mutations in *PTEN*, *EGFR*, *CDKN2A*, and *CDKN2B* were much more frequent (74%). No cases of later occurrence of the *IDH1* mutation after the *TP53* mutation or codeletion were noted, which allows us to conclude that the *IDH1* mutation appears at the earliest stages of oncogenesis and that it is possibly the common early event in the pathogenesis of gliomas of various histological variants.

IDH mutations have never been detected in PAs, which corresponds to the extremely rare transformation of PA into malignant tumors [44]. In addition, *IDH* mutations are very rarely found in primary glioblastomas [38]. This fact allows using *IDH1* and *IDH2* as markers for distinguishing between low-grade diffuse astrocytomas and secondary glioblastomas from PAs and primary glioblastomas.

According to some data, the frequency of *IDH1* and *IDH2* mutations in intracranial astrocytomas and glioblastomas is 68% and 12%, respectively [45]. Yet, there are no accurate data on the frequency of such mutations in SCA, which may be due to the rare incidence of this type of astrocytomas and the small sample size, which does not allow for a statistical analysis [3, 14]. For instance, the study focused on grades II and III SCA ($n = 9$) revealed no *IDH1* R132H mutation, which is the most frequent mutation in intracranial astrocytomas [35]. Another multicenter study on SCA ($n = 17$) also demonstrated the absence of *IDH* mutations in the patients [32]. These results suggest the existence of potential genetic differences between intracranial and spinal tumors at the same histopathological stages.

ATRX. In addition to the accompanying *TP53* and 1p/19q mutations, gliomas with mutations in *IDH* are distinguished by the presence of mutations in the *TERT* and *ATRX* genes, which are involved in telomere elongation. The *TERT* mutation correlates with the 1p/19q codeletion and primary glioblastomas; it is rarely detected in grade II and III astrocytomas and secondary glioblastomas [46]. The *ATRX* mutation is considered a hallmark of astrocytic tumors; it is closely associated with the *IDH* mutation in diffuse astrocytomas and secondary glioblastomas [47]. The *ATRX* mutation is quite rare in the absence of the *IDH* mutation [48]. In addition, *IDH* and *ATRX* mutations are very often associated with the *TP53* mutation, which suggests a cooperative pathogenesis mechanism involving these three proteins [49].

The *ATRX* gene encodes the protein involved in DNA methylation and regulation of the expression of a number of genes. In addition, *ATRX* is associated with the ALT phenotype of tumors, which correlates with the emergence of telomeres of heterogeneous length in the cell; it also regulates the association of histone H3.3 with the telomeric DNA regions and a series of binding sites [50]. Mutations in *ATRX* lead to activity loss by its protein product, which causes typical developmental disorders, such as mental retardation, urogenital abnormalities and alpha-thalassemia. At the cellular level, these impairments manifest themselves by an altered DNA methylation pattern, failure of chromosome disjunction, and telomere dysfunction [51].

The incidence of the *ATRX* mutation in children diagnosed with glioma reaches 30% [52]. In adult patients, this mutation is noted in 71% of grade II–III astrocytomas and 57% of secondary glioblastomas, while in primary glioblastomas its incidence is only 4% of cases [48]. The *ATRX* mutation is found in pilocytic astrocytomas with anaplasia signs [53]. It should be noted that this mutation is more typical of young patients and can serve as a diagnostic and a prognostic factor, since it allows differentiation of astrocytomas and oligodendrogliomas and also because it is associated with a more benign prognosis (in case of lost ATRX activity) [54].

There are almost no data on the frequency of the *ATRX* mutation in SCA. A total of two cases have been reported describing such a mutation in grades II and III diffuse astrocytoma of the spinal cord [55, 56]. The summary data of the analysis of the two groups of patents (≤ 20 years and > 20 years) with high-grade spinal cord gliomas indicate an absence of this mutation in the younger group ($n = 5$) and its presence in 43% of older patients ($n = 7$) [57]. In addition, this mutation was also found in IDH-negative brain glioblastoma [57].

H3F3A. The *H3F3A* gene encodes the replication-independent histone H3.3, which participates in the structural organization of chromatin via active binding to transcription sites, as well as association with active and open chromatin [58]. Heterozygous mutations in the *H3F3A* gene are found in almost 80% of brainstem glioblastomas. Moreover, two mutually exclusive variants, namely substitution of lysine to methionine at position 27 (K27M) and substitution of glycine to arginine or valine at position 34 (G34R/V), are found in such cases [52, 59]. Both mutations are localized at positions close to the N terminus of the molecule, which undergoes a post-translational modification. Trimethylation of Lys27 is associated with decreased gene expression,

while acetylation activates transcription. In addition, the methylation of Lys27 is crucial for a proper functioning of the PRC2 complex involved in transcription inhibition and cell differentiation [60, 61]. The mutations abrogate these modifications and processes, which, apparently, can trigger the onset of glioma.

Certain mutations in *H3F3A* are found in tumors of specific localization with a specific level of expression of OLIG1, OLIG2, and FOXG1 transcription factors. Gliomas with different mutations in *H3F3A* are believed to have different cellular origins [52, 62]. The G34R/V mutation is mainly found in children diagnosed with intracranial non-midline glioblastomas [52, 59]; the frequency of this mutation is 20%–30% [63]. The K27M mutation is mainly found in malignant astrocytomas of the thalamus, and brainstem and the spinal cord are prevalent in adolescents and children [57, 64]. The K27M mutation is associated with high tumor aggressivity, even if it is classified histologically as low-grade astrocytoma [65]. However, according to some data, the prognosis of thalamic gliomas in adults carrying this mutation may not appear worse than that in patients without the aberration, which suggests heterogeneity of this molecular subgroup of diffuse gliomas [66].

The K27M mutation is often associated with mutations in *TP53* (thalamic gliomas) and chromosome 10 monosomy, while it is rarely diagnosed together with mutations in *BRAF* (V600E) and *ATRX* and never found together with mutations in *IDH1* and *EGFR* [64, 66, 67]. This incompatibility with *IDH1* is due to the fact that the mutation makes Lys27 methylation possible [62, 68]. Schwartzentruber et al. [52] demonstrated that the *ATRX* mutation is much more frequently associated with the G34R/V mutation than with the K27M mutation in *H3F3A*.

The K27M mutation in *H3F3A* in patients with spinal cord astrocytomas is associated with grade III and IV tumors. This mutation was detected in 61% of patients older than 20 years (n = 18) and in 54% of patients younger than 19 years (n = 24) diagnosed with grade III–IV SCA [57]. In another study, this mutation was found in 28% (n = 32) of patients with SCA but the malignancy grade of the astrocytomas with a confirmed mutation was not indicated [69]. Johnson et al. [36] revealed the K27M mutation in 77.8% of cases (n = 9) of spinal cord glioblastomas. Another study conducted in a cohort of 36 primary diffuse gliomas of the spinal cord showed approximately the same mutation frequency rate for grade III–IV gliomas in adults and children (52% and 54%; n = 11 and 19, respectively) [70]. Thus, this mutation is quite often associated with grade III–IV spinal cord gliomas. It should be noted that K27M is not present in other types of malignant tumors [71] and, therefore, may be pathognomonic for the primary spinal glioblastoma and may also serve as an indicator of the worst prognosis [64].

TP53. Protein P53 is a transcription factor that regulates the transcription of the thousands of genes involved in the cell cycle, cell differentiation, and apoptosis. Mutations in *TP53* are among the earliest genetic changes in tumor cells and are found in 60% of the precursor cells of low-grade astrocytomas [72]. These mutations are present in most secondary glioblastomas (65%), mainly in codons 248 and 273. In primary glioblastomas, mutations in various codons of *TP53* were found in 30% of patients [73].

Mutations in *TP53* provoke a more aggressive growth of grade I–II astrocytomas: i.e., they are considered an unfavorable prognostic factor [74]. As in the case of *ATRX*, the mutation in *TP53* is mutually exclusive with the 1p/19q codeletion typical of oligodendrogliomas. Detection of this mutation can serve as proof of a diagnosis of astrocytoma [75]. It is an interesting fact that, in contrast to intracranial glioblastomas, a *TP53* mutation in spinal cord glioblastomas is often detected in the absence of a *IDH1* mutation [14].

TP53 mutation is often found in grade III–IV SCA. For instance, Govindan et al. [76] revealed the mutation in five out of six glioblastomas, while Walker et al. [77] reported the presence of the mutation in 60% of diffuse astrocytomas. Similar data were obtained by Johnson et al. [36] for patients with high-grade spinal cord glioblastomas (66.7%). Overexpression of *P53* was diagnosed in 57% of patients over 20 years of age (n = 7) with grade III–IV spinal cord glioblastomas and in 40% of patients younger than 20 years of age (n = 5) [57].

PTEN. The *PTEN* gene encodes phosphatase PTEN and belongs to tumor suppressor genes. Phosphatase PTEN is involved in dephosphorylation of the membrane-bound phosphatidylserine PIP3 to PIP2, which regulates the PKB/AKT signaling pathway. In case of gene loss or its mutation, its function cannot be performed by other enzymes [78]. Impaired expression of *PTEN* results in constitutive activation of the PKB/AKT pathway, which, in turn, triggers a series of processes associated with the cell cycle, cell proliferation, migration, and angiogenesis. PTEN also regulates the mTOR signaling pathway, which controls the self-renewal and differentiation of tumor stem cells. Deletion in the *PTEN* gene increases the size of these cells and causes their proliferation rate to increase and the suppression of the apoptosis of neural progenitor cells [79]. Atypical migration of progenitor cells carrying a *PTEN* mutation can lead to cerebellar and hippocampal dysplasia, followed by gliomagenesis. However, additional mutations, for instance, mutations

in *TP53*, are required for the initiation of neoplastic changes [80]. Deletions in chromosome 10 in the region of *PTEN* are often found in tumors characterized by *EGFR* amplification [72]. However, mutations in this gene, on the contrary, are poorly associated with EGFR [81].

Inactivation of *PTEN* usually caused by an inactivating point mutation (12%) or deletion of the long arm of the 10q chromosome (32%) [82] occurs in various types of tumors, including astrocytomas. In the latter case, *PTEN* mutations are extremely rarely found in PA but are present in 18% of anaplastic astrocytomas and up to 40% of glioblastomas, mainly the primary ones [31, 82, 83]. Rare detection of *PTEN* mutations in grade I–II astrocytomas and secondary glioblastomas may be associated with methylation of the *PTEN* promoter, which is often found in low-grade gliomas and reduces PTEN protein production compared to the normal level [84]. Mutations in the *PTEN* gene are more common among older patients with anaplastic astrocytoma and young patients with glioblastoma [83]. Only sporadic reports of *PTEN* mutations in such a rare tumor as grades III and IV SCA are known [56].

From the prognostic point of view, a loss of the PTEN function is associated with higher tumor aggression and decreased survival of patients with anaplastic astrocytoma, whereas no correlations were found for glioblastoma [12].

EGFR. The *EGFR* gene encodes the epidermal growth factor receptor. EGFR is a transmembrane glycoprotein consisting of an extracellular ligand-binding domain, a hydrophobic transmembrane domain, and a cytoplasmic tyrosine kinase domain. Binding of a ligand by EGFR results in dimerization and autophosphorylation of the receptor, as well as phosphorylation of cell substrates, which triggers a cascade of intracellular receptors associated with cell division and proliferation.

Increased expression or amplification of the *EGFR* gene is characteristic of many tumors. In addition to overexpression and amplification, point mutations and structural rearrangements can also occur in the gene, thus altering the functional characteristics of its product. *EGFR* nucleotide sequences corresponding to its extracellular and intracellular domains hold certain positions that are most susceptible to mutagenesis [85]. Most *EGFR* mutations in gliomas, including EGFRvIII, affect the extracellular domain of the receptor, while being mainly associated with the intracellular domain in non-glioma tumors [86, 87]. About half of glioblastomas with *EGFR* amplification also contain deletions in exons 2–7. The product of EGFRvIII mutation is a constitutively active EGFR variant stimulating tumor angiogenesis in malignant gliomas [88]. As an activator of cell proliferation, EGFRvIII is expressed only by a specific fraction of glioblastoma cells, thus inducing proliferation not only of these cells, but also of the adjacent cells expressing wild-type EGFR [89].

Mutations in *EGFR* and *TP53* are mutually exclusive in glioblastomas [90]. As in the case of *PTEN* mutations, a mutation in *EGFR* is typical of primary glioblastomas; it is rare in secondary ones [91]. Overexpression of the gene was revealed in 60% of primary glioblastomas, while the remaining 40% carried the amplified gene. In addition, overexpression or amplification of *EGFR* was found in 33% of patients with anaplastic astrocytomas and in less than 10% of patients with oligodendrogliomas [85]. It is also known that changes caused by *EGFR* gene aberrations appear only in 3% of astrocytomas and glioblastomas carrying *IDH* mutations, while the frequency of such changes is much higher in the presence of wild-type IDH [35, 37].

SCA is a rare tumor. Thus, there is not enough data regarding the incidence of this marker to make any statistical inferences. Two cases of EGFR-positive anaplastic astrocytoma have been reported by Korean researchers [92, 93]. Another two studies mentioned EGFR-positive spinal cord glioblastomas. The marker was found in two out of six cases [76] and in three out of nine cases [56] in those studies, respectively.

Amplification and overexpression of *EGFR* is considered to be associated with a high degree of glioma malignancy, aneuploidy, and proliferative index, while a mutation in EGFRvIII is potentially associated with an aggressive disease course, refractoriness to therapy, and poor prognosis [94, 95]. Moreover, overexpression of *EGFR* significantly decreases the chances of survival of patients with anaplastic astrocytomas [96], which allows one to ascribe them to the subgroup with a poor prognosis [97].

Practical significance of the molecular markers associated with astrocytomas

To date, the histomorphological classification of tumors serves as the basis for predicting the course of oncological diseases. However, such a diagnosis based on visual evaluation criteria is to some extent subjective, sometimes leading to significant discrepancies in the evaluation of histological specimens. In addition, the clinical course of the disease in some cases is poorly correlated with the histomorphological classification, while tumors with a similar histological characterization may respond differently to the same therapy. In this regard, the interest in molecular markers as means for a more accurate disease classification and prognosis has increased in recent years.

A vast number of studies conducted over the last 10–15 years have significantly improved our under-

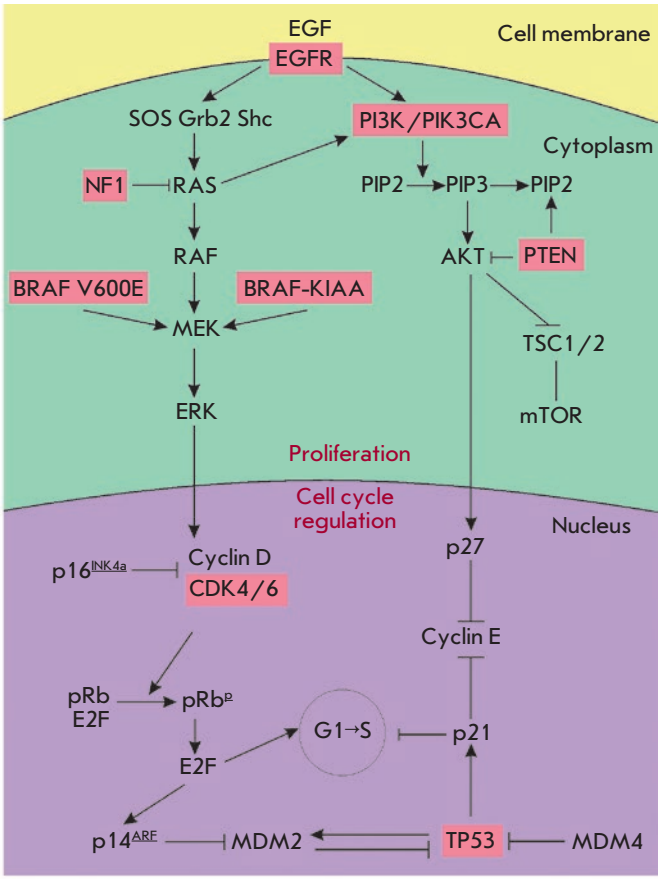

Fig. 3. Simplified scheme of the signaling pathways associated with the pathogenesis of glial tumors and the impact of the mutations associated with astrocytomas. The data are presented according to [99], with modifications

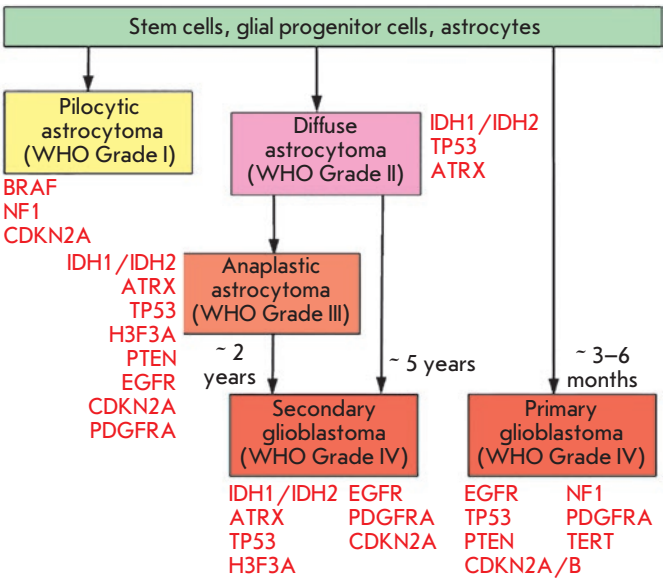

Fig. 4. The most common genetic changes associated with the development of astrocytomas of various degrees of malignancy. The data are adapted from [100], with modifications

standing of the mechanisms of the onset and progression of CNS glial tumors and revealed the key genes whose mutations or aberration can be considered potential prognostic and diagnostic factors (*Fig. 3*). In 2016, a series of molecular markers were included into the WHO Classification of CNS tumors. For instance, the *IDH* mutation test has become a part of the routine diagnosis and classification of gliomas [14].

Since the number of studies related to SCA-associated genetic changes is substantially lower than that of the studies devoted to brain astrocytomas, the current review considers markers of brain gliomas, including both the well-studied and those that are still under assessment for potential use. General information on the detection frequency of the 16 markers examined in various types of astrocytomas, their features, and prognostic value is presented in *Table*.

The information accumulated to date allows us to draw certain conclusions and make assumptions about the association of specific mutations with various types of astrocytomas (*Fig. 4*), a patient's age, other mutations, as well as a possible disease prognosis. For example:

– pilocytic astrocytomas mainly contain mutations in the *BRAF*, *NF1* and *CDKN2A* genes;

– mutations in *IDH1*, *ATRX* and *TP53* are mainly associated with primary glioblastomas and grade II–III astrocytomas (often found in combination with each other);

– mutations in *H3F3A* are mainly diagnosed in grades III–IV astrocytomas and, apparently, (in the case of a K27M mutation) are pathognomonic for the primary spinal glioblastomas;

– mutations in *EGFR* and *PTEN* are mostly associated with primary glioblastoma as well as anaplastic astrocytomas; and

– a mutation in *PDGFRA* is predominantly found in secondary but not primary glioblastomas.

The mutation V600E in *BRAF* (in children and adolescents) serves as a positive prognostic marker of grades I and II astrocytomas [98]. *H3F3A* K27M, *TP53*, *EGFR*, and *PTEN* are mutations that worsen the disease course and the overall prognosis.

Mutations in *IDH* are a crucial prognostic feature which allows one to divide diffuse infiltrative gliomas into three groups [99]. The most favorable prognosis is characteristic of the combination of mutant *IDH* (mutIDH) and the 1p/19q codeletion. The worst disease

Molecular markers associated with astrocytomas of the brain and the spinal cord

Gene/ mutation	Mutation frequency in astrocytomas				Annotation
	PA	DA	AA	GB (prim. and sec.)	
BRAF-KIAA1549	32%	Rare			It is more common for PA localized in the spinal cord and in the basilar region.
BRAF V600E	48%	Rare			It can be used for PA differentiation; it is most frequently found in supratentorial PA. It serves as a positive prognostic marker in children and young patients.
IDH1	-	>70%		70–80% (sec.) <5% (prim.)	*IDH1* and *IDH2* are mutually exclusive. mutIDH: positive prognostic marker wtIDH: more aggressive course. *IDH1*: possible application for exclusion of PA and GB1.
IDH2	-	<3%			
_TP53_	-	29% (increased expression)		65% (sec.) 30% (prim.)	More aggressive disease course. Mutually exclusive to the 1p/19q codeletion; can be potentially used for astrocytoma differentiation. **Revealed in 60%–67% of grades III–IV SCA.**
ATRX	+	60–70%		57% (sec.) 4% (prim.)	It rarely appears in the absence of mutations in *IDH* and *TP53*, it is mutually exclusive to 1p/19q codeletion. It can be used for differentiation of astrocytomas and 1p/19q codeletion. The prognosis is more favorable in case of a loss of th ATRX activity.
_H3F3A_ K27M		+		+ (50% in prim. spinal cord GB)	Mostly present in children. Midline tumors of the brain and the spinal cord. Never diagnosed together with *IDH1* and *EGFR*. Often found together with *TP53*. **Apparently, pathognomonic for primary GB of the spinal cord.**
H3F3A G34R/V				20–30%	Present in adolescents and young patients. More favorable prognosis. Non-midline intracranial glioblastomas. Often found together with the *ATRX*, *TP53*, and *PDGFRA* mutations.
EGFR	-	+	33%	100% (prim.) rare (sec.)	Typical for primary GB. Rarely found together with the mutation in *IDH*, mutually exclusive to *TP53* mutation. Associated with high malignancy and poor prognosis.
FGFR2	+	3.5%		2.5%	Mutually exclusive mutations in *IDH* and *EGFR*. The expression level decreases increasing the malignancy degree.
PDGFRA	-	3–69%	12–33%	31% (mainly sec.)	
PTEN	Extremely rare	Rare	18%	40% (mainly prim.)	More aggressive course in case of anaplastic astrocytomas.
_NF1_	15–20%	+	+	15–18% (prim.)	Is associated mainly with astrocytomas.
CDKN2A	+		+	+	

Note. Mutations found in astrocytomas of the brain and spinal cord are shown in bold. The symbols + and – stand for the presence or absence of a mutation in the specific type of astrocytoma; an empty cell means a lack of information. The presented data are based on information reviewed in the current paper.

course is characteristic of tumors carrying wild-type *IDH* (wtIDH). Such tumors are usually aggressive and similar to primary glioblastomas in their molecular characteristics (aberrations in *EGFR*, *PTEN*, *NF1*, *CDKN2A/B*). The third group, for which the prognosis turned out to be intermediate between the two, includes mutIDH in the absence of 1p/19q codeletion. In the overwhelming majority of cases, this variant is associated with mutations in *TP53* and *ATRX*. Regardless of the malignancy degree and histological characteristics of the tumor, the prognosis for this variant is always more favorable than that for wtIDH.

It should be noted that the molecular profiles of astrocytomas in children differ significantly from the adult variants and mainly contain mutations in such genes as *BRAF*, *H3F3A*, and *ATRX* [99].

To date, there is no information on any identification of markers such as *IDH1/2*, *H3F3A* G34R/V, and *FGFR2* in SCA. Pilocytic astrocytomas of the spinal cord were shown to be associated with mutations in the

BRAF, *CDKN2*, *NF1*, and *PTEN* genes, while malignant grades III–IV SCA variants are associated primarily with *H3F3A* K27M (mostly young patients and children), *TP53*, and *PTEN* [32]. The remaining mutations discussed in the current review have been reported mainly as sporadic cases and cannot be used to make any statistical inferences.

In addition to their prognostic and diagnostic values, biomarkers can also be used in the development of drugs for targeted therapy of astrocytomas. For example, partial efficacy of selective inhibitors of isocitrate dehydrogenase with the *IDH1* R132H mutation has been shown both *in vitro* and in glioma models [100]. Preliminary tests of the JNJ-42756493 drug *in vitro* and *in vivo* confirmed that growth of a tumor carrying recombinant *FGFR-TACC* was inhibited in two patients in whom the standard therapy had earlier been ineffective [101]. Some targeted drugs, such as MAb-425 and nimotuzumab (targeted against EGFR), as well as crenolanib and nilotinib (targeted against PDGFR), are already in phases II–III of clinical trials [102]. At the same time, it is necessary to understand that the drugs that have shown good results in the treatment of intracranial astrocytomas may turn out to be ineffective against SCA, due to the possible differences in their genetic profiles.

Currently, not all molecular markers associated with astrocytomas (especially with the even less common SCA type) show potential for clinical usage, taking into account their prognostic, diagnostic, or therapeutic value. In some cases, this is due to insufficient information on the detected genetic aberrations. Recently, retrospective studies of clinical tissue samples aimed at identifying target molecular markers have been carried out. Such studies allow researchers to cover up to several hundred samples and obtain statistically significant genetic landscapes of target tumor types. Further research in this direction can provide much better elucidation of the genetic and epigenetic changes that occurr in tumor cells, it can help identify new promising biomarkers, and develop innovative strategies for the diagnosis and treatment of astrocytomas. ●

This work was supported by RFBR (project № 18-29-01042).

REFERENCES

1. Samartzis D., Gillis C.C., Shih P., O'Toole J.E., Fessler R.G. // Global Spine J. 2015. V. 5. № 5. P. 425–435.
2. Kaprealian T. / Astrocytic Tumors of the Spinal Cord. In: Adult CNS Radiation Oncology. Principles and Practice // Eds Chang E., Brown P., Lo S., Sahgal A., Suh J. Cham: Springer, 2018. P. 129–145.
3. Zadnik P.L., Gokaslan Z.L., Burger P.C., Bettegowda C. // Nat. Rev. Neurol. 2013. V. 9. № 5. P. 257–266.
4. Mechtler L.L., Nandigam K. // Neurol. Clin. 2013. V. 31. P. 241–268.
5. Chamberlain M.C., Tredway T.L. // Curr. Neurol. Neurosci. Rep. 2011. V. 11. P. 320–328.
6. Duong L.M., McCarthy B.J., McLendon R.E., Dolecek T.A., Kruchko C., Douglas L.L., Ajani U.A. // Cancer. 2012. V. 118. P. 4220–4227.
7. Lonser R.R., Weil R.J., Wanebo J.E., DeVroom H.L., Oldfield E.H. // J. Neurosurg. 2003. V. 98. P. 106–116.
8. Chamberlain M.C., Tredway T.L. // Curr. Neurol. Neurosci. Rep. 2011. V. 11. P. 320–328.
9. Louis D.N., Ohgaki H., Wiestler O.D., Cavenee W.K., Burger P.C., Jouvet A., Scheithauer B.W., Kleihues P. // Acta Neuropathol. 2007. V. 114. P. 97–109.
10. Teng Y.D., Abd-El-Barr M., Wang L., Hajiali H., Wu L., Zafonte R.D. // Exp. Neurol. 2019. V. 311. P. 135–147.
11. Collins V.P., Jones D.T., Giannini C. // Acta Neuropathol. 2015. V. 129. № 6. P. 775–788.
12. Smith J.S., Jenkins R.B. // Front. Biosci. 2000. V. 5. P. 213–231.
13. Raco A., Esposito V., Lenzi J., Piccirilli M., Delfini R., Cantore G: // Neurosurgery. 2005. V. 56. P. 972–981.
14. Abd-El-Barr M.M., Huang K.T., Moses Z.B., Iorgulescu J.B., Chi J.H. // Neuro-Oncol. 2018. V. 20. № 6. P. 729–742.
15. Karsy M., Neil J.A., Guan J., Mark M.A., Colman H., Jensen R.L. // Neurosurg. Focus. 2015. V. 38. № 3. Article ID E4.
16. Harrop J.S., Ganju A., Groff M., Bilsky M. // Spine. 2009. V. 34(Suppl). P. 69–77.
17. Oghaki H., Kleihues P. // J. Neuropathol. Exp. Neurol. 2005. V. 64. № 6. P. 479–489.
18. Oghaki H. // Neuropathol. 2005. V. 25. № 1. P. 1–7.
19. Kanu O.O., Hughes B., Di C., Lin N., Fu J., Bigner D.D., Yan H., Adamson C. // Clin. Med. Oncol. 2009. V. 3. P. 39–52.
20. Jones T.S., Holland E.C. // Toxicol. Pathol. 2011. V. 39. № 1. P. 158–166.
21. Penman C.L., Faulkner C., Lowis S.P., Kurian K.M. // Front. Oncol. 2015. V. 5. Article ID 54.
22. Jacob K., Albrecht S., Sollier C., Faury D., Sader E., Montpetit A., Serre D., Hauser P., Garami M., Bognar L., et al. // Br. J. Cancer. 2009. V. 101. № 4. P. 722–733.
23. Jeuken J.W., Wesseling P. // J. Pathol. 2010. V. 222. P. 324–328.
24. Hawkins C., Walker E., Mohamed N., Zhang C., Jacob K., Shirinian M., Alon N., Kahn D., Fried I., Scheinemann K., et al. // Clin. Cancer Res. 2011. V. 17. P. 4790–4798.
25. Ida C.M., Lambert S.R., Rodriguez F.J., Voss J.S., McCann B.E., Seys A.R., Halling K.C., Collins V.P., Giannini C. // J. Neuropathol. Exp. Neurol. 2012. V. 71. P. 631–639.
26. Jones D.T., Hutter B., Jager N., Korshunov A., Kool M., Warnatz H.J., Zichner T., Lambert S.R., Ryzhova M., Quang D.A.K., et al. // Nat. Genet. 2013. V. 45. P. 927–932.
27. Jones D.T., Kocialkowski S., Liu L., Pearson D.M., Ichimura K., Collins V.P. // Oncogene. 2009. V. 28. P. 2119–2123.
28. Schindler G., Capper D., Meyer J. Janzarik W., Omran H., Herold-Mende C., Schmieder K., Wesseling P., Mawrin C., Hasselblatt M., et al. // Acta Neuropathol. 2011. V. 121. № 3. P. 397–405.

29. Badiali M., Gleize V., Paris S., Moi L., Elhouadani S., Arcella A., Morace R., Antonelli M., Buttarelli F.R., Figarella-Branger D., et al. // Brain Pathol. 2012. V. 22. P. 841–847.
30. Huillard E., Hashizume R., Phillips J.J., Griveau A., Ihrie R.A., Aoki Y., Nicolaides T., Perry A., Waldman T., McMahon M., et al. // Proc. Natl. Acad. Sci. USA. 2012. V. 109. P. 8710–8715.
31. Horbinski C., Nikiforova M.N., Hagenkord J.M., Hamilton R.L., Pollack I.F. // Neuro-Oncology. 2012. V. 14. P. 777–789.
32. Shankar G.M., Lelic N., Gill C.M., Thorner A.R., van Hummelen P., Wisoff J.H., Loeffler J.S., Brastianos P.K., Shin J.H., Borges L.F., et al. // Acta Neuropathol. 2016. V. 131. P. 147–150.
33. Horbinski C., Hamilton R.L., Nikiforov Y., Pollack I.F. // Acta Neuropathol. 2010. V. 119. № 5. P. 641–649.
34. Cancer Genome Atlas Research Network // Nature. 2008. V. 455. P. 1061–1068.
35. Parsons D.W., Jones S., Zhang X., Lin J.C.-H., Leary R.J., Angenendt P., Mankoo P., Carter H., Siu I.-M., Gallia G.L., et al. // Science. 2008. V. 321. № 5897. P. 1807–1812.
36. Johnson A., Severson E., Gay L., Vergilio J.A., Elvin J., Suh J., Daniel S., Covert M., Frampton G. M., Hsu S., et al. // Oncologist. 2017. V. 22. № 12. P. 1478–1490.
37. Yang H., Ye D., Guan K.L., Xiong Y. // Clin. Cancer Res. 2012. V. 18. P. 5562–5571.
38. Yan H., Parsons D.W., Jin G., McLendon R., Rasheed B.A., Yuan W., Kos I., Batinic-Haberle I., Jones S., Riggins G.J., et al. // N. Engl. J. Med. 2009. V. 360. №. 8. P. 765–773.
39. Huse J.T., Aldape K.D. // Clin. Cancer Res. 2014. V. 20. № 22. P. 5601–5611.
40. Dang L., White D.W., Gross S., Bennett B.D., Bittinger M.A., Driggers E.M., Fantin V.R., Jang H.G., Jin S., Keenan M.C., et al. // Nature. 2009. V. 462. № 7274. P. 739–744.
41. Noushmehr H., Weisenberger D.J., Diefes K., Phillips H.S., Pujara K., Berman B.P., Pan F., Pelloski C.E., Sulman E.P., Bhat K.P., et al. // Cancer Cell. 2010. V. 17. № 5. P. 510–522.
42. Lu C., Ward P.S., Kapoor G.S., Rohle D., Turcan S., Abdel-Wahab O., Edwards C.R., Khanin R., Figueroa M.E., Melnick A., et al. // Nature. 2012. V. 483. № 7390. P. 474–478.
43. Fu Y., Zheng S., Zheng Y., Huang R., An N., Liang A., Hu C. // Int. J. Biochem. Cell. Biol. 2012. V. 44. № 5. P. 770–775.
44. Watanabe T., Nobusawa S., Kleihues P., Ohgaki H. // Am. J. Pathol. 2009. V. 174. № 4. P. 1149–1153.
45. Ellezam B., Theeler B.J., Walbert T., Mammoser A.G., Horbinski C., Kleinschmidt-DeMasters B.K., Perry A., Puduvalli V., Fuller G.N., Bruner J.M., et al. // Acta Neuropathol. 2012. V. 124. № 3. P. 449–451.
46. Anderson M.D., Gilbert M.R. // J. Nat. Comp. Canc. Netw. 2014. V. 12. № 5. P. 665–672.
47. Jiao Y., Killela P.J., Reitman Z.J., Rasheed A.B., Heaphy C.M., de Wilde R.F., Rodriguez F.G., Rosemberg S., Oba-Shinjo S.M., Nagahashi M.S.K., et al. // Oncotarget. 2012. V. 3. P. 709–722.
48. Karsy M., Guan J., Cohen A.L., Jensen R.L. Colman H. // Curr. Neurol. Neurosci. Rep. 2017. V. 17. Article ID 19.
49. Kannan K., Inagaki A., Silber J., Gorovets D., Zhang J., Kastenhuber E.R., Hequy A., Petrini J.H., Chan T.A., Huse J.T. // Oncotarget. 2012. V. 3. P. 1194–1203.
50. Clynes D., Jelinska C., Xella B., Ayyub H., Scott C., Mitson M., Taylor S., Higgs D.R., Gibbons R.J. // Nat. Commun. 2015. V. 6. P. 1–11.
51. Clynes D., Gibbons R.J. // Curr. Opin. Genet. Dev. 2013. V. 23. P. 289–294.
52. Schwartzentruber J., Korshunov A., Liu X.-Y., Jones D.T.W., Pfaff E., Jacob K., Sturm D., Fontebasso A.M., Quang D.-A.K., Tonjes M., et al. // Nature. 2012. V. 482. P. 226–231.
53. Rodriguez F.J., Brosnan-Cashman J.A., Allen S.J., Vizcaino M.A., Giannini C., Camelo-Piragua S., Webb M., Matsushita M., Wadhwani N., Tabbarah A., et al. // Brain Path. 2019. V. 29. № 1. P. 126–140.
54. Wiestler B., Capper D., Holland-Letz T., Korshunov A., von Deimling A., Pfister S.M., Platten M., Weller M., Wick W. // Acta Neuropathol. 2013. V. 126. № 3. P. 443–451.
55. Takai K., Tanaka S., Sota T., Mukasa A., Komori T., Taniguchi M. // World Neurosurg. 2017. V. 108. P. 991.e13–991.e16.
56. Shows J., Marshall C., Perry A., Kleinschmidt-DeMasters B.K. // Brain Pathol. 2016. V. 26. № 1. P. 120–123.
57. Nagaishi M., Nobusawa S., Yokoo H., Sugiura Y., Tsuda K., Tanaka Y., Suzuki K., Hyodo A. // Brain Tumor Pathol. 2016. V. 33. P. 267–269.
58. Talbert P.B., Henikoff S. // Nat. Rev. Mol. Cell Biol. 2010. V. 11. P. 264–275.
59. Wu G., Broniscer A., McEachron T.A., Lu C., Paugh B.S., Becksfort J., Qu C., Ding L., Huether R., Parker M., et al. // Nat. Genet. 2012. V. 44. P. 251–253.
60. Caren H., Pollard S.M., Beck S. // Mol. Aspects Med. 2013. V. 34. P. 849–862.
61. Lewis P.W., Muller M.M., Koletsky M.S., Cordero F., Lin S., Banaszynski L.A., Garcia B.A., Muir T.W., Becher O.J., Allis C.D. // Science. 2013. V. 340. P. 857–861.
62. Sturm D., Witt H., Hovestadt V., Khuong-Quang D.A., Jones D.T.W., Konermann C., Pfaff E., Tonjes M., Sill M., Bender S., et al. // Cancer Cell. 2012. V. 22. P. 425–437.
63. Lee J., Solomon D.A., Tihan T. // J. Neurooncol. 2017. V. 132. P. 1–11.
64. Solomon D.A., Wood M.D., Tihan T., Bollen A.W., Gupta N., Phillips J.J., Perry A. // Brain Pathol. 2016. V. 26. P. 569–580.
65. Aihara K., Mukasa A., Gotoh K., Saito K., Nagae G., Tsuji S., Tatsuno K., Yamamoto S., Takayanagi S., Narita Y., et al. // Neuro-Oncol. 2014. V. 16. P. 140–146.
66. Feng J., Hao S., Pan C., Wang Y., Wu Z., Zhang J., Yan H., Zhang L., Wan H. // Hum. Pathol. 2015. V. 46. P. 1626–1632.
67. Nguyen A.T., Colin C., Nanni-Metellus I., Padovani L., Maurage C.A., Varlet P., Miguel C., Uro-Coste E., Godfraind C., Lechapt-Zalcman E., et al. // Neuropathol. Appl. Neurobiol. 2015. V. 41. P. 403–408.
68. Khuong-Quang D.A., Buczkowicz P., Rakopoulos P., Liu X.-Y., Fontebasso A.M., Bouffet E., Bartels U., Albrecht S., Schwartzentruber J., Letourneau L., et al. // Acta Neuropathol. 2012. V. 124. P. 439–447.
69. Tanaka S., Otani R., Hongo H., Matsuda H., Ikemura M., Nomura M., Takayanagi S., Nejo T., Takahashi S., Kitagawa Y., et al. // Neuro-Oncol. 2017. V. 19(suppl. 6). P. vi176.
70. Gessi M., Gielen G.H., Dreschmann V., Waha A., Pietsch T. // Acta Neuropathol. 2015. V. 130. P. 435–437.
71. Je E.M., Yoo N.J., Lee S.H. // Acta Pathol. Microbiol. Immunol. Scand, 2014. V. 122. № 1. P. 81–82.
72. Khani P., Nasri F., Chamani F.K., Saeidi F., Nahand J.S., Tabibkhooei A., Mirzaei H. // J. Neurochem. 2019. V. 148. № 2. P. 188–203.
73. Kanu O.O., Hughes B., Di C., Lin N., Fu J., Bigner D.D, Yan H., Adamson C. // Clin. Med. Oncol. 2009. V. 3. P. 39–52.
74. England B., Huang T., Karsy M. // Tumor Biol. 2013. V. 34. P. 2063–2074.
75. Lipp E.S., McLendon R.E. // Semin. Oncol. Nurs. 2018. V. 34. № 5. P. 430–442.

76. Govindan A., Chakraborti S., Mahadevan A., Chickabasavaiah Y.T., Santosh V., Shankar S.K. // Brain Tumor Pathol. 2011. V. 28. P. 297–303.
77. Walker C., Baborie A., Crooks D., Wilkins S., Jenkinson M.D. // Br. J. Radiol. 2011. V. 84. № S2. P. S90–S106.
78. Sami A., Karsy M. // Tumor Biol. 2013. V. 34. № 4. P. 1991–2002.
79. Groszer M., Erickson R., Scripture-Adams D.D., Lesche R., Trumpp A., Zack J.A., Kornblum H.I., Liu X., Wu H. // Science. 2001. V. 294. P. 2186–2189.
80. Marino S., Krimpenfort P., Leung C., van der Korput H.A., Trapman J., Camenisch I., Berns A., Brandner S. // Development. 2002. V. 129. P. 3513–3522.
81. Ohgaki H., Dessen P., Jourde B., Horstmann S., Nishikawa T., Di Patre P.L., Burkhard C., Schüler D., Probst-Hensch N.M., Maiorka P.C., et al. // Cancer Res. 2004. V. 64. P. 6892–6899.
82. Ohgaki H., Kleihues P. // Am. J. Pathol. 2007. V. 170. № 5. P. 1445–1453.
83. Smith J.S., Tachibana I., Passe S.M., Huntley B.K., Borell T J., Iturria N., O'Fallon J.R., Schaefer P.L., Scheithauer B.W., James C.D., et al. // J. Nat. Canc. Inst. 2001. V. 93. № 16. P. 1246–1256.
84. Wiencke J.K., Zheng S., Jelluma N., Tihan T., Vandenberg S., Tamgüney T., Baumber R., Parsons R., Lamborn K.R., Berger M.S., et al. // Neuro-Oncol. 2007. V. 9. P. 271–279.
85. Ekstrand A., James C., Cavenee W., Seliger B., Pettersson R.F., Collins V.P. // Canc. Res. 1991. V. 8. P. 2164–2172.
86. Janne P.A., Engelman J.A., Johnson B.E. // J. Clin. Oncol. 2005. V. 23. P. 3227–3234.
87. Lee J.C., Vivanco I., Beroukhim R., Huang J.H., Feng W.L., DeBiasi R.M., Yoshimoto K., King J.C., Nghiemphu P., Yuza Y., et al. // PLoS Med. 2006. V. 3. Article ID: e485.
88. Katanasaka Y., Kodera Y., Kitamura Y., Morimoto T., Tamura T., Koixumi F. // Mol. Cancer. 2013. V. 12. Article ID: 31.
89. Inda M.M., Bonavia R., Mukasa A., Narita Y., Sah D.W., Vandenberg S., Brennan C., Johns T.G., Bachoo R., Hadwiger P., et al. // Genes Dev. 2010. V. 24. P. 1731–1745.
90. McNamara M.G., Sahebjam S., Mason W.P. // Cancers (Basel). 2013. V. 5. № 3. P. 1103–1119.
91. Rasheed B.K., Wiltshire R.N., Bigner S.H., Bigner D.D. // Curr. Opin. Oncol. 1999. V. 11. P. 162–167.
92. Ryu S.J., Kim J.Y., Kim K.H., Park J.Y., Kuh S.U., Chin D.K., Kim L.S., Chi Y.E., Kim S. H. // Eur. Spine J. 2016. V. 25. P. 4067–4079.
93. Jeong S.M., Chung Y.G., Lee J.B., Shin I.Y. // J. Korean Neurosurg. Soc. 2010. V. 47. № 1. P. 68–70.
94. Shinojima N., Tada K., Shiraishi S., Kamiryo T., Kochi M., Nakamura H., Makino K., Saya H., Hirano H., Kuratsu J., et al. // Cancer Res. 2003. V. 63. P. 6962–6970.
95. Aldape K., Zadeh G., Mansouri S., Reifenberger G., von Deimling A. // Acta Neuropathol. 2015. V. 129. P. 829–848.
96. Wrensch M., Wiencke J., Wiemels J., Miike R., Patoka J., Moghadassi M., McMillan A., Kelsey K.T., Aldape K., Lamborn K.R., et al. // Cancer Res. 2006. V. 66. P. 4531–4541.
97. Batchelor T., Betensky R., Esposito J.M., Pham L.D., Dorfman M.V., Piscatelli N., Jhung D., Rhee D., Louis D.N. // Clin. Canser Res. 2004. V. 10. P. 228–233.
98. Aquilanti E., Miller J., Santagata S., Cahill D.P., Brastianos P.K. // Neuro-Oncol. 2018. V. 20(S7). P. 17–26.
99. Camelo-Piragua S., Kesari S. // Exp. Rev. Neurotherapeut. 2016. V. 16. № 9. P. 1055–1065.
100. Rohle D., Popovici-Muller J., Palaskas N., Turcan S., Grommes C., Campos C., Tsoi J., Clark O., Oldrini B., Komisopoulou E., et al. // Science. 2013. V. 340. P. 626–630.
101. Di Stefano A.L., Fucci A., Frattini V., Labussiere M., Mokhtari K., Zoppoli P., Marie Y., Bruno A., Boisselier B., Giry M., et al. // Clin. Cancer Res. 2015. V. 21. № 14. P. 3307–3317.
102. Liang S., Shen G. Molecular Targets of CNS Tumors. Rijeka: InTech Press, 2011. P. 325–342.

Targeted Drug Delivery in Lipid-like Nanocages and Extracellular Vesicles

A. V. Sokolov, N. N. Kostin, L. A. Ovchinnikova, Y. A. Lomakin, A. A. Kudriaeva*
M.M. Shemyakin and Yu.A. Ovchinnikov Institute of Bioorganic Chemistry, Russian Academy of Sciences, Miklukho-Maklaya Str. 16 /10, Moscow, 117997, Russia
*E-mail: anna.kudriaeva@gmail.com
Received January 15, 2019; in final form, May 15, 2019
DOI: 10.32607/20758251-2019-11-2-28-41

ABSTRACT **The possibility of targeted drug delivery to a specific tissue, organ, or cell has opened new promising avenues in treatment development. The technology of targeted delivery aims to create multifunctional carriers that are capable of long circulation in the patient's organism and possess low toxicity at the same time. The surface of modern synthetic carriers has high structural similarity to the cell membrane, which, when combined with additional modifications, also promotes the transfer of biological properties in order to penetrate physiological barriers effectively. Along with artificial nanocages, further efforts have recently been devoted to research into extracellular vesicles that could serve as natural drug delivery vehicles. This review provides a detailed description of targeted delivery systems that employ lipid and lipid-like nanocages, as well as extracellular vesicles with a high level of biocompatibility, highlighting genetically encoded drug delivery vehicles.**
KEYWORDS **Liposomes, polymeric carriers, extracellular vesicles, self-assembling vesicles, nanocages.**
ABBREVIATIONS **BG – bacterial ghosts; EVs – extracellular vesicles; HIV – human immunodeficiency virus; GEEV – genetically encoded extracellular vesicles; MHC – major histocompatibility complex; BBB – blood-brain barrier; DCs – dendritic cells; IL – interleukin; LPS – lipopolysaccharide; siRNA – small interfering RNA; MSCs – mesenchymal stem cells; PEG – polyethylene glycol; MPS – mononuclear phagocyte system; TNF – tumor necrosis factor; EAE – experimental autoimmune encephalomyelitis; EDTA – ethylenediaminetetraacetic acid.**

INTRODUCTION

In addition to small-molecular compounds, biopolymers, their fragments, peptides, proteins, oligonucleotides, RNA, or DNA are now being applied more often in creating therapeutics. In order to prevent the activity loss that is a result of external factors, new requirements continue to emerge to regulate both the production of drugs and their administration in a patient's organism. However, the main challenge in the implementation of potential therapies in clinical practice is the difficulty of delivering a drug to the target cells. Delivery without carriers, in turn, is hampered by premature drug degradation, as well as the low permeability of cell membranes. To date, both the development and optimization of new techniques for drug delivery are among the most widely investigated areas of nanobiomedicine.

The existing delivery systems could be divided into two groups: viral vectors (lentiviruses, adenoviruses, retroviruses [1]) and non-viral vectors (macro- and nanoparticles, polymeric particles) [2]. The rapid advances in nanotechnology expedite the creation of new drug delivery methods that exploit nanoparticles made from various materials and possess various surface characteristics, as well as physicochemical properties that meet the needs particular to a given task [3]. However, each type of nanoparticle has its own advantages and disadvantages that limit its application. The nanocages currently under development could serve as delivery vehicles for protein therapeutics [4], as well as DNA [5] and RNA [6]. Nanoparticles derived from natural polymers, such as phospholipids, polysaccharides, proteins, and peptides, are more effective thanks to their biocompatibility [7], as well as their lack of toxic degradation products [8], in comparison with those derived from synthetic polymers. The nano-sized pharmaceutical carriers currently applied in clinical practice possess many useful properties; namely, effective intracellular delivery and prolonged circulation in the bloodstream, reduced toxicity thanks to pref-

erential localization on a target site, improved pharmacokinetics and biodistribution of the therapeutic agent, as well as the capacity to release the drug under particular physiological conditions [9]. Besides, either natural extracellular vesicles or those previously artificially loaded with a drug are currently being actively studied for drug delivery [10]. Herein, we discuss in detail various aspects of lipid and lipid-like delivery vehicles, highlighting their application prospects for extracellular vesicles.

LIPID AND LIPID-LIKE DELIVERY VEHICLES

Liposomes and their derivatives are the first, the best-known and frequently applied drug delivery vehicles. In the last decade, many lipid and lipid-like vesicles, such as liposomes, niosomes, ethosomes, transfersomes, solid lipid nanospheres (SLNs), nanostructured lipid carriers, as well as lipid-polymer hybrid nanoparticles, have been developed and scrutinized during numerous investigations. A schematic representation of the aforementioned nanocarriers is provided in *Fig. 1*. Lipid nanocarriers mostly consist of physiological lipids meant to provide safe and efficient delivery, as well as increased bioavailability of therapeutic agents. These nanoparticles are nontoxic and degrade in the organism as endogenous lipids.

Liposomes

Liposomes are the most prominent delivery vehicles. They were described for the first time as early as 1965 [11]. A functioning scaffold that consists of a lipid bilayer provides not only high shape mobility, but also the capacity to mimic the biophysical properties of living cells.

Liposomes consist mostly of natural and synthetic phospho- and sphingolipids, more often phosphatidylcholine and phosphatidylethanolamine, the main structural elements of biological membranes. Other phospholipids, such as phosphatidylserine, phosphatidylglycerol, and phosphatidylinositol, could be used additionally to prepare liposomes [12]. These vesicles have a span of size of almost 3 orders: bilayer vesicles (unilamellar) that, in turn, could be divided into two groups: small unilamellar vesicles (SUVs, 25–50 nm) and large unilamellar vesicles (LUVs, >100 nm), as well as multilamellar vesicles (MLVs) with a size of 0.05–10 μm. The most straightforward approach to producing SUVs is sonication of a lipid dispersion, whereas MLVs could be produced via mixing of previously prepared SUVs with a drug solution, followed by lyophilization [13] or via hydration of a lipid film. To note, adding organic solvents during hydration increases the encapsulation effectiveness from 10% to 40% [14]. LUVs, in turn, are produced through reverse-phase evaporation [15] or detergent removal [16]. In addition to the size-based classification of liposomes, there is another class based on charge, depending on the lipids and phospholipids embedded in the liposome structure: namely, neutral liposomes (phosphatidylcholine and phosphatidylethanolamine), anionic liposomes (phosphatidylserine, phosphatidylglycerol, phosphatide acids, and phosphatidylinositol), and cationic liposomes (stearylamine and DC-cholesterol) [17–19].

The conventional "first-generation liposomes" based on phospholipids exhibit low stability and are prone to early degradation after administration in a patient's organism, which is a significant flaw, especially in delivering cytotoxic agents [20]. Chitosan, a natural hydrophilic biodegradable polymer with low toxicity, could be used to stabilize liposomes [21]. However, even stable liposomes without regards to both charge and size could be effectively engulfed by the cells of the mononuclear phagocyte system (MPS) localizing in the liver and the spleen. This phenomenon is actively exploited to treat the various disorders afflicting these organs. In order to enhance both circulation time and delivery to other tissues and organs, stealth liposomes have been created via a modification of the liposomal surface with an inert hydrophilic polymer (polyethylene glycol (PEG) [22,23]) and additional blockage of the interaction with plasma proteins [24,25] so that these vesicles become "invisible" to MPS. Super stealth liposomes (SSLs) also have been developed by anchoring PEG on several molecules of phosphoethanolamine through β-glutamic acid [26]. This composition, as well as elongation of the PEG chain, has been shown to increase liposomal stability, prolong biological half-life, and improve the biodistribution profile [26,27]. Recently, it has been demonstrated that delivering therapeutic agents via the transfer of nanoparticles on the erythrocyte surface could be extremely effective even in the case of short-term circulation [28].

In addition to increasing both drug stability and circulation time in the bloodstream, directed delivery to defined target cells is required in most cases. To solve such an issue, various modifications of liposomes have been developed: for instance, imbedding dioleoylphosphatidylethanolamine (DOPE) in the composition of cationic liposomes facilitates the effective delivery to dendritic cell (DC) progenitors [29], whereas mannosylation of liposomes increases their engulfment by DCs [30]. Modification of liposomes with the synthetic polypeptide DARPin that is specific to the tumor receptor HER2 facilitates effective delivery of nanoparticles to HER2-expressing cells [31]. At present, several targeted liposome-based

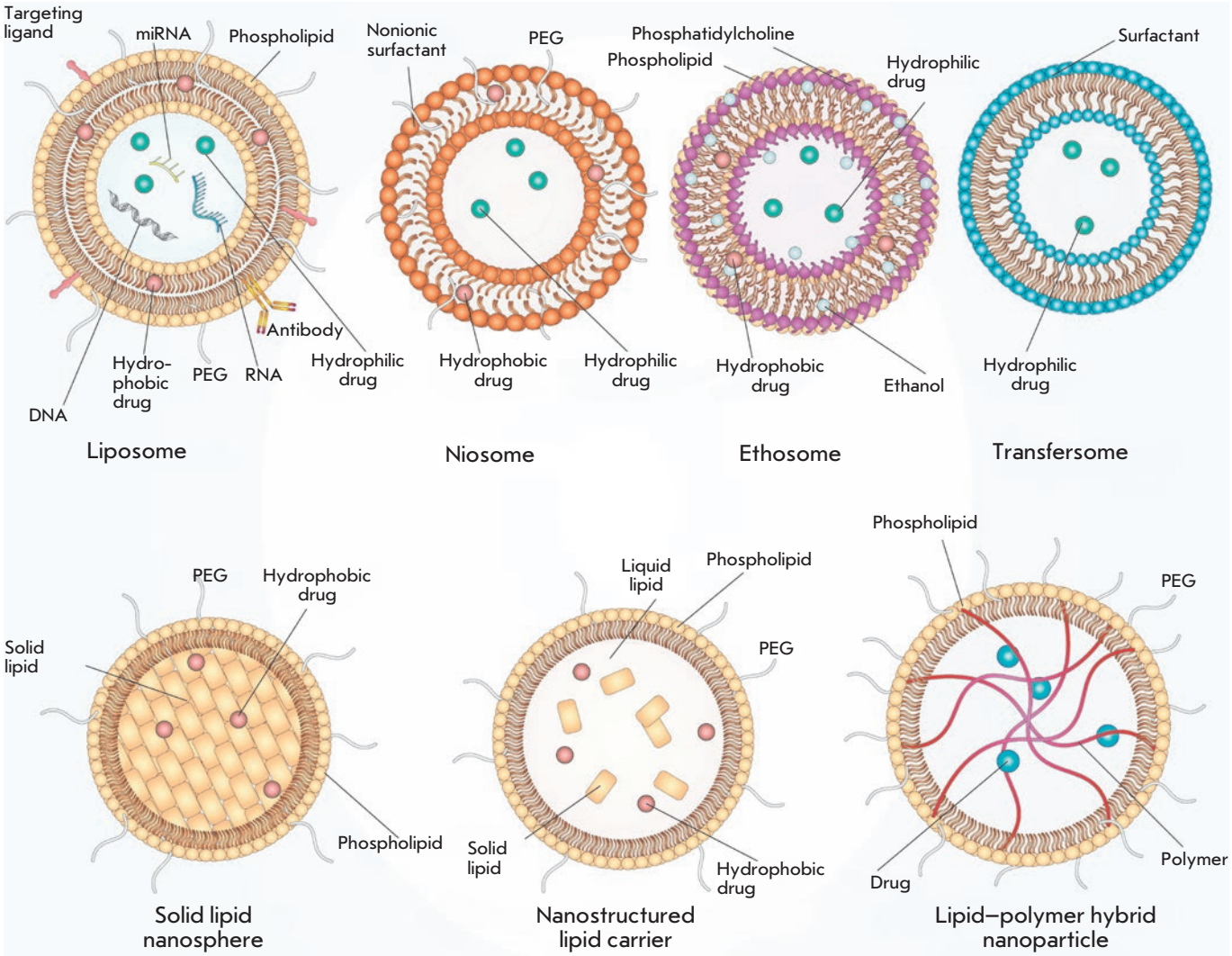

Fig. 1. The structure of lipid and lipid-like nanocarriers. Liposomes mostly consist of natural phospholipids, the main component of biological membranes. Niosomes consist of nonionic surfactant and cholesterol or its derivatives. Ethosomes represent lipid vesicles consisting of phospholipids and large quantities of ethanol. Transfersomes are elastic liposomes that are capable of deformation allowing them to penetrate deep into the skin. The cores of solid lipid nanospheres consist of a mixture of solid lipids. Nanostructured lipid carriers are composed of a mixture of both solid and liquid lipids. Lipid-polymer hybrid nanoparticles have a polymeric core, whereas the envelope is represented by a lipid bilayer

drugs are undergoing clinical evaluation. Among them, MCC-465 (PEG-modified liposomes containing doxorubicin and targeted via F(ab') dimers) [32], MM-302 (PEG-modified liposomes containing doxorubicin and are specific to HER2) [33], 2B3-101 (surface glutathione-carrying liposomes), and MBP-426 and SGT-53 (liposomes carrying transferrin and TfRscFv (anti-transferrin receptor single-chain antibody), respectively) seem to be the most promising [34, 35]. Nucleic acids, as well as small molecules, could be used for surface modification of liposomes in addition to conventional antibodies, their fragments, and peptides to increase selectivity [36]. Among the ligands for targeted delivery, aptamers are considered to be among the most promising candidates with unique features [37]. Thus, to date, liposomes are among the

most versatile approaches to delivery since they allow transferring multiple therapeutics, including antitumor and antimicrobial drugs, enzymes, vaccines, DNA, and RNA.

Many therapeutic agents encapsulated in liposomes are currently applied in clinical practice, and even more formulations are undergoing clinical trials [38]. The first liposomal carrier approved for clinical use in 1995 was the antitumor drug Doxil™/Caelyx™ [39]. Several other drugs, including Myocet™, DaunoXome™, Depocyt™, Marqibo™, Onivyde™, AmBisome™, DepoDur™, Visudyne™, Abelcet™ and Curosurf™, are used in cancer therapy as well.

Aside from antitumor therapy, liposomes are also being considered for the treatment of various autoimmune diseases, such as rheumatoid arthritis and multiple sclerosis (MS). For instance, Xemys is a mixture of the immunodominant peptides of the myelin basic protein (MBP), one of the major antigens during multiple sclerosis encapsulated within the mannosylated SUV. Full-length MBP, as well its fragments, has been considered as an effective therapy for autoimmune neurodegeneration for a long time [40]. It was shown that administration of particular MBP peptides encapsulated in liposomes suppress the development of experimental autoimmune encephalomyelitis (EAE) in model animals [41]. Currently, both phase I and phase II trials for Xemys have been successfully undertaken, and phase III has been approved [42]. Due to the modified liposomal surface with mannose residues, liposome-encapsulated MBP peptides are mostly engulfed by professional antigen-presenting cells (APCs)–DCs and macrophages–through their mannose receptors, CD206. An excessive presentation of MBP fragments on the MHC-II molecules on the surface of APCs is assumed to promote the induction of tolerance toward this protein, and hence reduce an autoimmune inflammation. Patients receiving Xemys showed decreased levels of monocyte chemoattractant protein 1 MCP-1/CCL2, the macrophage inflammatory protein (MIP-1/CCL4), as well as Interleukin-2 and Interleukin-7 [43]. The influence of several MBP peptides, namely, MBP46-62, 124-139 and 147-170, which are the drug components, on cytokine release and activation of immune cells has also been evaluated both in healthy donors and MS patients [44].

The ability of liposomes to foster targeted delivery of the antigen required for APC, and thus modulating the immune response, is being actively exploited in the development of antiviral and bacterial vaccines. To date, a number of drugs are at the stage of clinical trials as adjuvants for preventive and therapeutic vaccines against malaria, influenza, tuberculosis, the human immunodeficiency virus (HIV), and dengue [45], whereas the drugs Cervarix™, Inflexal™, and Epaxal™ are already commercially available liposomal vaccines against human papillomavirus (HPV), the influenza virus, and the hepatitis A virus, respectively [46].

Niosomes

Niosomes are 50- to 800-nm vesicles and consist of a nonionic surfactant bilayer often containing cholesterol and its derivatives [47]. The structure of niosomes allows encapsulating both the hydrophilic and hydrophobic drugs that are retained within the lumen and the bilayer, respectively. The properties of these vesicles could vary depending on their size, lamellarity, and the surface charge. As a delivery vehicle, niosomes offer several advantages in comparison with classic liposomes, such as increased biological half-life, ease of production and modification, high biocompatibility and reduced toxicity due to a nonionic nature, nonimmunogenicity, and biodegradability [48]. Furthermore, niosomes are almost undetectable to MPS. On the downside, they are not stable (albeit not as liposomes), tend to aggregate and could partially loose the encapsulated agent during delivery [49].

Despite a number of publications on both the formulation and application of niosomes, only a few drugs developed have moved to the clinical trial stage [47]. The majority of investigations demonstrated that encapsulation of drugs within niosomes offers several benefits, such as enhanced efficacy, a reduced number of side effects, as well as a convenient route of administration. Thus, niosomes are effective during intravenous, intramuscular, oral, intraocular, subcutaneous, pulmonary, intraperitoneal, and transdermal administration [50]. This type of vesicles is used to encapsulate various drugs, such as doxorubicin, insulin, ovalbumin, oligonucleotides, EGFP, hemagglutinin, DNA vaccines, interferon-α, etc. [51] Besides, niosomes are also employed for ocular administration of the drug Tacrolimus after corneal transplantation [52], for oral delivery of metformin [53], and in cosmetics manufacturing as well.

Ethosomes

Ethosomes, described for the first time in 1996, are a modification of classical liposomes and consist of phospholipids, ethanol (20–45%), and water [54]. Aside from ethanol, ethosomes could contain propylene glycol, as well as isopropanol. Depending on the preparation procedure, ethosomes could have a size ranging from several tenths of a nanometer to several microns. Both hydrophilic and hydrophobic molecules could

be encapsulated within ethosomes, and increasing the ethanol concentration in these vesicles facilitates the solubility of therapeutic agents and, therefore, enhances the embedding of these agents. Ethosomes are known to transcend classical liposomes in terms of transdermal delivery due to the negative ζ-potential. Moreover, ethanol leads to disorganization of lipids in the stratum corneum of the skin, thus significantly facilitating penetration of therapeutic particles into the deep dermal layers. Drug accumulation in the dermal layers results in prolonged release of therapeutic molecules from ethosomes, thus extending the curative effect [55]. The flaw of niosomes is that these vesicles could frequently induce allergic reactions to ethanol or other components [56]: so, they are exclusively limited to transdermal delivery. Furthermore, the flammability of ethanol dictates increased precaution when preparing, using, transporting, and storing these nanocontainers [57].

Transfersomes

Tranfersomes are vesicles containing phosphatidylcholine, surfactant, and ethanol. They are characterized by increased penetration through intercellular pores, which is achieved by adding membrane modifiers, sodium cholate, stearylamine, Span 60, Span 80, Tween 60 and Tween 80, the surfactants that destabilize lipid bilayers and increase the deformability of liposomal membranes [58]. Depending on the composition, when penetrating the skin layers, transformers either retain their structure intact or fuse with the cell membrane [59]. Due to their ability to easily change shape, they pass through pores 5–10 times smaller than their own diameter, thus ensuring a high level of penetration of therapeutics [60]. The efficiency of transformers as a delivery system was demonstrated for ibuprofen [61], terbinafine [62], and emodine [63].

In addition to the versatile lipid-like delivery systems listed above, a number of modifications have been developed for many specific purposes, including thermosensitive [64], magnetic [65], multifunctional "SMART" liposomes [66], and pharmacosomes, the amphiphilic phospholipid complexes of drug compounds [67].

Solid lipid nanospheres

An entirely new class of lipid particles that represents lipospheres or solid lipid nanospheres (SLNs) was developed in the early 1990s [68, 69]. In this type of vesicles, a solid lipid (most often neutral triglyceride) is used as a matrix to encapsulate the drug. It is also possible to use saturated fatty acids, while polar phospholipids are applied as lipophilic emulsifiers. Mono- and diglycerides are used much less frequently because of their polarity. SLNs can be obtained in various ways: by high-pressure homogenization, by the microemulsion method, and by precipitation of lipid particles during the evaporation of the solvent [70]. Compared to liposomes, SLNs are characterized by increased stability, the possibility of a controlled release, relatively easy and cheap methods of preparation [71], and the absence of toxicity in contrast to polymer vesicles [72]. Although SLNs possess many advantages compared to the existing delivery systems, they also have some limitations, such as low encapsulation effectiveness of hydrophilic drugs [18]. The likely reason for this is the low solubility of hydrophilic compounds both in the lipid bilayer and the matrix. Two approaches are used to improve the seizure of hydrophilic drugs, such as doxorubicin [73] and diminazene [74]. The first one employs oil-loaded SLNs, and the second one modifies the lipid matrix by incorporating amphiphilic compounds, phosphatidylcholine, polyglyceryl-3-diisostearate, and sorbitol, into it [75].

In addition, SLNs are characterized by uneven drug release [68, 76], and this disadvantage has not yet been resolved, which imposes rather significant restrictions on the use of SLNs since a high initial release rate can contribute to severe complications; for example, when delivering cytotoxic anticancer agents [68].

Nanostructured lipid carriers

Nanostructured lipid carriers NLCs are the second generation of SLNs and were developed in 1999 to address the issue of rapid release of a therapeutic agent that is common to the previous generation [77]. NLCs are lipid nanoparticles consisting of a solid lipid matrix and additionally containing a liquid lipid or oil. A mixture of solid and liquid lipids promotes uniform encapsulation of compounds and prevents their rapid diffusion [78, 79]. NLCs can be obtained via several approaches: high-pressure homogenization (the most frequently used method), by the microemulsion method, phase inversion, etc. The first preparations containing NLCs, cream NanoRepair Q10 ™ and serum NanoRepair Q10 ™ (Dr. Rimpler GmbH, Germany), were introduced into the cosmetics market in 2005. Currently, more than 30 cosmetics containing NLCs are marketed; however, there are no pharmaceutical preparations [80, 81].

Lipid-polymer hybrid nanoparticles

Finally, lipid-polymer hybrid nanoparticles (LPNs), which combine the characteristics of both polymer nanoparticles and liposomes, have been developed very recently. In this form of nanocontainers, the therapeu-

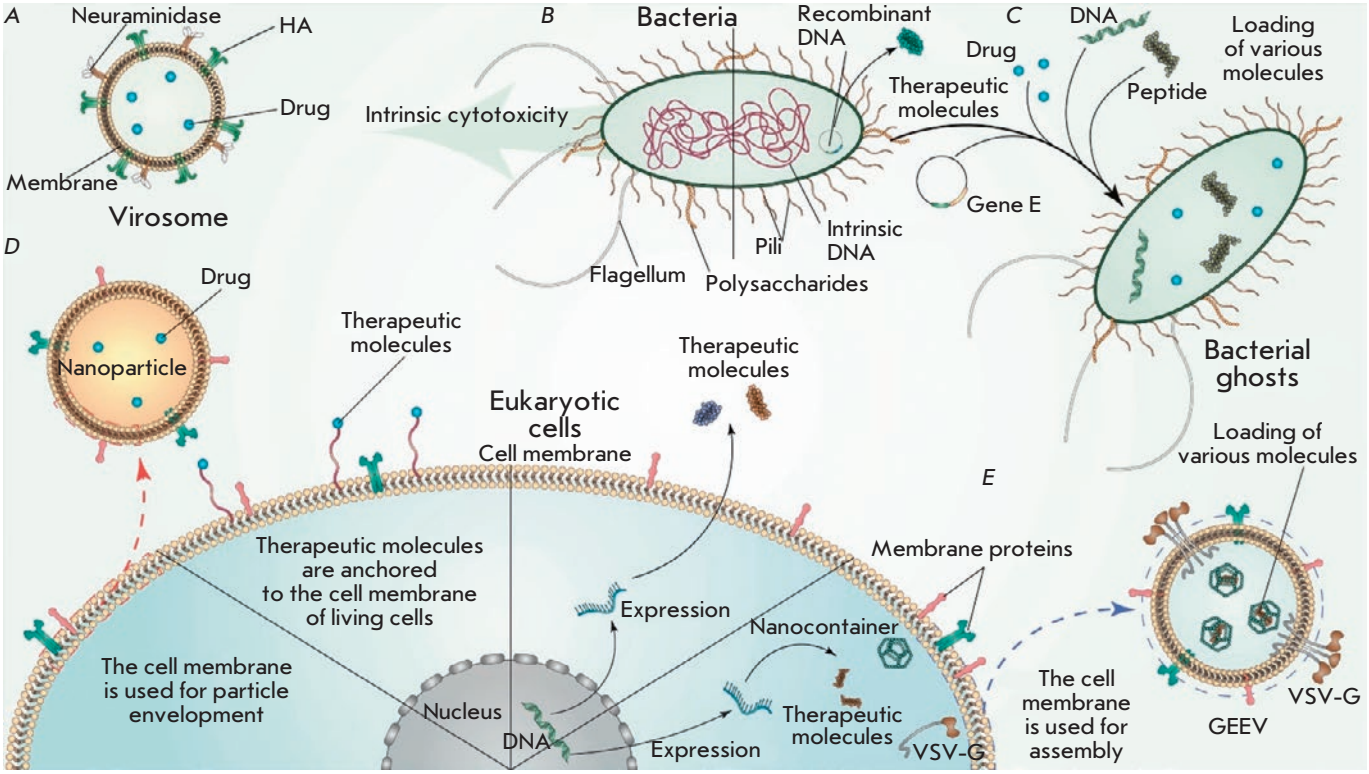

Fig. 2. Delivery systems based on natural membranes. Virosomes (**A**) are vesicles modified with viral proteins. Bacterial-based delivery vehicles (**B**) may possess their own cytotoxicity and can be genetically modified to secrete various molecules. By removing their cytoplasm content, bacterial ghosts are obtained and used to deliver not only plasmid DNA, but also low-molecular-weight drugs, peptides, and nucleic acids (**C**). Eukaryotic cells are used to encapsulate artificial nanoparticles (**D**), to carry ligands on their surface, to express therapeutic molecules, and also for the production of GEEVs (genetically encoded extracellular vesicles, **E**), which are also covered with the parent cell membrane. HA – hemagglutinin

tic drug is encapsulated in a polymer core surrounded by a lipid bilayer modified with PEG [82]. LPNs show high stability and are characterized by a uniform release of the loaded compound, whereas the lipid bilayer provides high biocompatibility [83]. Together, these factors ensure LPNs a great future as new effective drug carriers, but their therapeutic effect has not been fully proven so far.

EXTRACELLULAR VESICLES BASED ON NATURAL MEMBRANES

The delivery systems employing natural membranes are of particular interest. Their main advantages are high biocompatibility and carrier stability (*Fig. 2*). This approach has an enormous potential for creating intelligent delivery systems [84, 85], and it is assumed that they can be used for effective and easily controllable molecular-directed therapy. However, the likely disadvantages of these systems are their high production costs, possible purification challenges, and reduced storage stability.

Virosomes

Virosomes are vesicles containing viral glycoproteins, such as neuraminidase [86], influenza virus hemagglutinin [87], and hepatitis B virus protein L [88] in their phospholipid bilayer (*Fig. 2A*). Their presence imparts these carriers a number of positive properties, such as structural stability, delivery targeting, and contributes to receptor-mediated endocytosis and the subsequent release of its contents into the cytoplasm due to fusion with the lysosome membrane [89]. Virosomes can be used as carriers of therapeutic drugs [87, 90], act as an adjuvant, and be used as vaccines, some of which have already been approved for use in clinical practice [91, 92]. Due to the fact that pathogenic

viruses are used in the making of virosomes, uncertain safety and potentially strong *in vivo* immunogenicity are the main disadvantages of this kind of carriers. Currently, most virosome studies are focused on their application as vaccines and adjuvants for the treatment of cancer [93] and HIV [94].

Bacteria

From birth, many types of bacteria inhabit human organs, tissues and cavities. Through their transplantation or genetic modification, they can deliver various compounds (*Fig. 2B*). The examples include non-pathogenic bacteria like *Lactococcus lactis*, *Streptococcus gordonii*, etc. Recombinant lactic acid bacteria capable of delivering desired substances to human or animal mucous membranes are being actively studied [95, 96]. Other types of bacteria are used in the development of anticancer therapy and diagnosis. Such application is possible due to the ability of bacteria, such as Gram-positive anaerobes of the genus *Clostridia*, to penetrate, colonize, and accumulate in hypoxic and necrotic tumor tissues. In addition to their intrinsic cytotoxicity, their genetic modification confers them additional valuable properties, such as the regulated expression of various therapeutic and imaging agents [97, 98].

Bacterial ghosts

Bacterial ghosts (BGs) are the cell membrane-based carriers that are produced by expressing the bacteriophage lysis gene E in Gram-negative bacteria (*Fig. 2C*) [99]. Despite the fact that the so-called E-mediated lysis removes all of the cytoplasmic contents from the cell, including the genetic material, the cells retain bacterial surface antigenic elements, such as flagellum, fimbriae, and polysaccharides. The latter is the reason why BGs possess their own adjuvant activity, which makes them promising targets for vaccine development [100]. Additionally, BGs may be loaded with low-molecular-weight agents, peptides, and DNA. Various approaches have been developed to modify their inner surface for more accurate loading of these particles, including during their fermentation [101, 102].

Eukaryotic cells

Along with prokaryotic cells, the possibility of using eukaryotic cells, such as red blood cells, platelets, lymphocytes, macrophages, stem and dendritic cells (*Fig. 2D*) as carriers is being investigated [84, 103]. Among the different types of cells tested in this field, erythrocytes stand out in particular since they are the most common blood cells, lack genetic material, and possess a long bloodstream circulation time. Their internal volume can be used to load the agent, or drugs/particles/modifiers can be attached to the cell surface [104, 105]. The immune and stem cells can be used as carriers due to their tropism to inflammation foci and tumors and the ability to overcome the blood-brain barrier (BBB). In addition, stem cells can be transduced for *in situ* production of interferons and interleukins. It was shown that they are capable of absorbing silicon, polymeric and lipid nanoparticles without loss of viability [84, 106]. Macrophages can overcome the BBB and are actively used as nanoparticle carriers due to their natural ability to phagocytize particles and concentrate in the affected tissues, where they release the loaded substance over time. This approach is known as the "Trojan Horse approach" and was tested on gliomas [107], HIV-affected areas of a brain, and hypoxic solid tumors [84].

Genetically encoded extracellular vesicles

Recently, a new type of carriers has been developed: genetically encoded extracellular vesicles (GEEVs) (*Fig. 2E*). These GEEVs are based on a previously computationally designed self-assembling three-dimensional hollow protein dodecahedral framework composed of twenty KDPG-aldolase molecules [108]. The structural unit of these vesicles is a three-domain polypeptide. Each of these domains performs a function necessary for the assembly of GEEVs: the first one is the myristoylation signal, which anchors this structure to the membrane; the second one is the domain that forms the aforementioned three-dimensional protein framework; and the third one is the domain recruiting the endosomal sorting complex, ESCRT, which is responsible for membrane budding. The second important component of these vesicles, which confers them the ability to penetrate the target cells, is the membrane-anchored VSV-G protein. The latter is one of the vesicular stomatitis virus envelope proteins and is responsible for its endosome escape. When these structures are expressed in eukaryotic cells, vesicles with an average radius of 100 nm are formed; they are covered with a cell membrane and contain several of the aforementioned dodecahedrons [109]. These particles are able to load the required substances, such as low-molecular-weight compounds, RNA, peptides, proteins, and deliver them to other cells, while protecting them from degradation. In addition, the surface of GEEVs can be further modified with antibodies, receptors, or low-molecular-weight ligands for directed transport.

NATURAL EXTRACELLULAR VESICLES

Extracellular vesicles (EVs) are lipid spheres that are secreted by virtually any cell type. Being carriers of

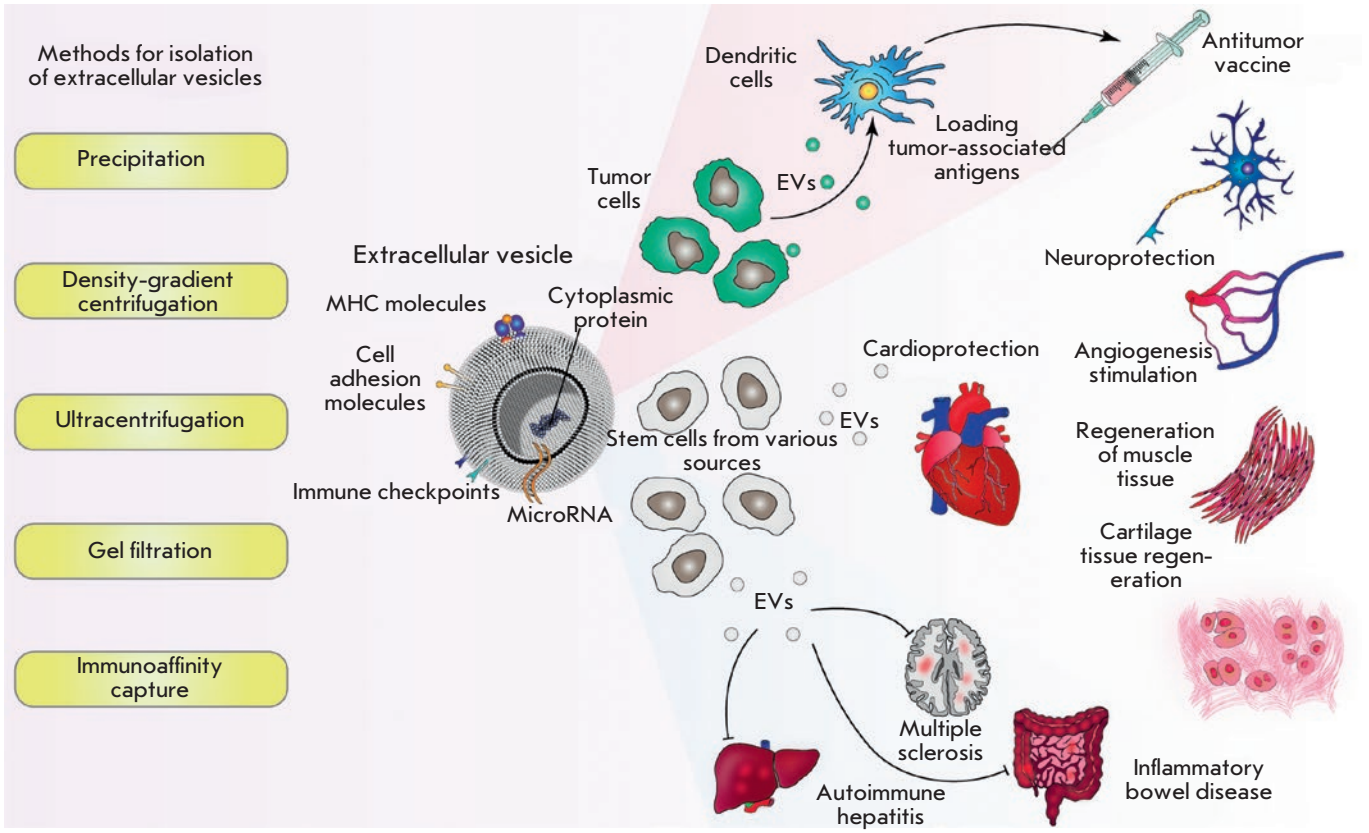

Fig. 3. Structure, isolation, and areas of application of extracellular vesicles. Extracellular vesicles (EVs) are lipid complexes secreted by many cells. Various bioactive molecules, such as micro RNA, immune checkpoints, cell adhesion molecules, and MHC, can be found on their surface and within their lumen. There are several techniques used to isolate and purify EVs (**left**). Tumor-derived vesicles could be applied to stimulate dendritic cells (DCs) in order to create DC-based cell vaccines. Natural EVs produced by stem cells possess multiple effects and could be applied both in regenerative medicine (for example, to induce regeneration and protect tissues and organs) and during autoimmune disorders of various etiologies and localization (**right**)

RNA, membrane and cytoplasmic proteins, lipids and carbohydrates, EVs mediate various functions in the body (for example, they participate in intercellular communication). Depending on the origin, they are divided into ectosomes (derived from neutrophils/monocytes), prostatosomes (extracted from seminal fluid), vexosomes (associated with the adenoviral vector), etc. Depending on the biogenesis mechanism, EVs are classified into exosomes, microvesicles, and apoptotic bodies [110]. The size of EVs also varies: for example, the size of exosomes lies in the range of 40–120 nm, whereas for microvesicles it may range from 50 to 1,000 nm [111].

Due to such properties as biocompatibility, non-immunogenicity (being obtained from a suitable cell type), as well as the ability to pass through the BBB, EVs represent a promising delivery vehicle for various molecules [112]. However, it was found that after intravenous injection of EVs into mice, only a small percentage of the vesicles penetrated the heart and brain and the largest amount was detected mostly in the spleen and liver [113]. It should be noted that EVs are predominantly negatively charged, which makes their pharmacokinetics similar to those of negatively charged liposomes [113]. In addition, the pharmacokinetics of EVs is highly dependent on the set of proteins and lipids on their surface. For example, it was found that phosphatidylserine on the surface of exosomes promotes their binding to cells expressing the T-cell immunoglobulin- and mucin-domain-containing molecule (Timd4), which in turn may indicate enhanced capture of such exosomes by macrophages known to express this receptor [114]. Changes in the composition of the surface proteins of

EVs also have an impact; for example, degradation of integrins-α6 and -β1 significantly reduced the accumulation of EV in the lungs of mice. At the same time, the physicochemical properties of EV, such as size and ζ-potential, remained intact [115]. Thus, EVs could selectively accumulate in tissues depending on the set of ligands on their surface, which makes them promising carriers for targeted delivery.

Currently, the methods used for isolation and purification of EVs are quite complex and require expensive equipment. The main purification methods are ultracentrifugation, density gradient centrifugation, ultrafiltration, precipitation, and gel filtration [116–119].

In addition to delivering defined therapeutic molecules, EVs from different cell types have a wide range of the properties required in clinical practice for the treatment of a wide variety of diseases, from ischemia and osteonecrosis to multiple sclerosis and cancer (*Fig. 3*).

Natural extracellular vesicles in modulating the immune response

Firstly, EVs could have a significant impact on the functioning of the immune system since they could both stimulate and suppress the immune response. For example, exosomes from DCs containing MHC molecules in a complex with an antigen could elicit an antigen-specific immune response [120]. Another interesting feature of DC-derived exosomes is that they can capture the ligands of Toll-like receptors and activate other dendritic cells, which could induce the immune response as well [121].

Immunosuppressive extracellular vesicles are also known. For example, BALB/c mice immunized with ovalbumin produced EVs that induced specific immune tolerance to ovalbumin in recipient mice [122]. Immunosuppressive EVs are potential therapeutic agents for various autoimmune and inflammatory diseases. For instance, vesicles derived from mesenchymal stem cells (MSCs) are able to suppress the proliferation of mononuclear cells obtained from a mouse with experimental autoimmune encephalomyelitis (EAE, a mouse model of multiple sclerosis) [123]. The immunomodulatory effects of extracellular vesicles have also been shown in models of the inflammatory bowel disease and autoimmune hepatitis [107, 108].

Tumor-derived EVs are promising candidates for creating anticancer vaccines due to their ability to transfer tumor antigens. For example, delivery of tumor-associated antigens to DCs was much more effective when using exosomes rather than a tumor lysate, and exosome-stimulated DCs showed more noticeable antitumor activity in a study with the mouse model of glioblastoma [124]. However, tumor EVs should be used with great caution: for example, apoptotic EVs from glioblastoma cells can induce resistance to therapy and a more aggressive behavior of neighboring tumor cells by transferring the components of the spliceosome [125].

Natural extracellular vesicles in regenerative medicine

EVs are endowed with great prospects for use in regenerative medicine and transplantation. To date, a large number of investigations have shown the direct pleiotropic regenerative effect of EVs on various organs and systems. For example, EVs could stimulate the growth of blood vessels, which can be applied in transplantation or in the case of ischemia, diabetic foot ulcers, and also prevent osteonecrosis [126–129]. Various studies have indicated that exosomes obtained from MSCs may contribute to the synthesis of collagen and the regeneration of both cartilage and muscle fibers [130–132].

The tissue-protective effect of EVs derived from stem cells has also been described. For example, exosomes from MSCs could enhance the survival of cardiomyocytes even during cyclic ischemia and reperfusion due to activation of the Wnt/β-catenin signaling cascade [133]. In a mouse model of myocardial infarction, it was shown that exosomes from embryonic stem cells improved the functioning of the heart muscle and also supported the survival of myocytes due to the presence of various microRNAs [78]. The neuroprotective effect of exosomes derived from different MSCs has also been demonstrated [134, 135]. Thus, EVs reduced gliosis initiated by inflammation of the brain when lipopolysaccharide (LPS) was injected into immature mice, reduced apoptosis of neurons, and also diminished the severity of structural defects in the white matter of the brain [134]. Moreover, mice exposed to EVs showed the best results in behavioral tests for spatial memory. The mechanism of this neuroprotective action, however, remains to be determined [134].

Natural EVs certainly have an enormous potential for therapeutic applications. However, due to their complex, often poorly studied mechanism of action, the likely heterogeneity of their composition, and due to unwanted immunosuppression in some cases, as well as activation of proliferative signaling pathways, these complexes should be used with extreme caution.

ARTIFICIALLY LOADED EXTRACELLULAR VESICLES

In addition to the aforementioned applications for EVs, these vesicles could also be loaded directly with various substances. The main benefit of using EVs as delivery vehicles comes from their natural origin,

which underlies the low immunogenicity of these nanocarriers. Additionally, EVs could be easily engulfed by target cells due to receptor-mediated interactions between the EV membrane and the cell [10].

Basically, there are two strategies for producing artificially loaded EVs: the first is to co-incubate EVs with therapeutic agents (often, small molecules) *in vitro*, whereas the second is to create a gene construct for subsequent transfection to establish cells to produce EVs loaded with the required cargo. Generally, small lipophilic molecules could be loaded in EVs via simple co-incubation. For instance, once incubated with exosomes in phosphate buffer for 5 min at room temperature, curcumin was effectively encapsulated within the vesicles. This formulation, in turn, outperformed free curcumin in terms of suppression of inflammation and reduced secretion of IL-6 and tumor necrosis factor alpha (TNF-a), and it was still able to penetrate the BBB. This method was also used to load chemotherapeutic agents, such as paclitaxel and doxorubicin, in EVs [137]. Exosomal preparations of both of these drugs were capable of penetrating through the BBB and were distributed within the brain in contrast to exosome-free formulations. Exosomes also increased the cytotoxicity of doxorubicin and paclitaxel. The possibility of reducing the therapeutic dose when using cytostatics for treating oncological diseases is undoubtedly an advantage of this dosage form, as it has not been possible to overcome such side effects as systemic inflammation and toxic effects on organ systems thus far [138].

Passive transport to exosomes is not always effective. To facilitate the loading of EVs, several techniques could be applied. Hence, vesicles and therapeutic agents are incubated in the presence of surfactants, such as saponin [139]. This compound forms a complex with the cholesterol present in the exosomal membrane, which facilitates its penetration by a therapeutic agent [140]. Electroporation is another approach to increasing the effectiveness of vesicle loading, and it showed up to 20% better loading results for doxorubicin. Electroporation is widely used for loading nucleic acids, such as miRNA and siRNA. A good example is exosomes containing siRNA to $KRAS^{G12D}$, a primary RAS mutation known to initiate pancreatic cancer [141]. The incubation of pancreatic cancer cells with these vesicles resulted in decreased levels of KRAS-G12D RNA, as well as increased survival of mice, inhibited tumor growth, and it diminished the rate of metastasis in comparison with the controls. Besides oncological diseases, vesicle-encapsulated miRNA could be applied to treat neurodegenerative diseases. Such complexes were shown to be effective *in vitro* in reducing the amounts of alpha-synuclein, a protein associated with Parkinson's disease [142]. Once intravenously administered, miRNA-loaded exosomes diminished the concentration of alpha-synuclein mRNA and the protein itself in the investigated areas of a mouse brain. Exosomes loaded with miRNA to beta-secretase (BACE1), a protein that generates the beta-amyloid fibrils associated with Alzheimer's disease, have also been created. Neural targeting was accomplished via a neuron-specific rabies virus glycoprotein (RVG) peptide fused with the exosomal membrane protein Lamp2. It allowed one to achieve a reduction of up to 62% of BACE1 protein expression; the mRNA synthesis was diminished up to 60% [112]. Even though electroporation is sufficiently effective in delivering nucleic acids within the vesicles, this technique has a significant flaw, since RNA could form aggregates during this procedure [143]. This issue, however, was less noticeable when EDTA was added, and special polymer electrodes and acid citrate buffer were used during electroporation.

Another, fundamentally different, strategy has been proposed to produce loaded vesicles. The feature of this approach is that donor cells are transfected with recombinant DNA (e.g., encoding miRNA) to secrete EVs containing the cargo desired during their biogenesis [144]. By using this approach, suppression of breast cancer xenograft growth was achieved via vesicles isolated from the culture media of transfected cells [145]. Transformation makes it possible to load EVs not only with nucleic acids, but also with proteins. In order to encapsulate the proteins within exosomes, they need to be modified with N-myristoylation tag and the domain binding to phosphatidylinositol 4,5-bisphosphate that ensure their anchoring to the exosomal membrane [146].

Thus, the application of both unmodified vesicles and ones additionally loaded with therapeutic agents for targeted drug delivery is at the top of the agenda in modern science.

CONCLUSION

The technology of creating and loading nanoparticles with therapeutic agents developed in the second half of the twentieth century remains, perhaps, one of the most promising drug delivery strategies to date. During the pioneer studies of lipid-like nanocontainers, most of the attention has been focused on increasing the stability, biocompatibility, and biodistribution of artificially created nanocarriers. Varying the lipid composition allows one to encapsulate both hydrophobic and hydrophilic compounds and thereby make it possible to tuck up the delivery route for almost any compound. The use of genetic structures with controlled expression [147], as well as simultaneous

loading of nanocontainers with substances acting differently, which can significantly increase the effectiveness of exposure, is also a promising direction [148]. Currently, the priority in drug development lies in improving delivery targeting. This issue can be solved both by modifying the already-known artificial nanocontainers and by studying the genetically encoded or natural extracellular vesicles discovered relatively recently. High biocompatibility and biodegradability confer them tremendous advantage over other synthetic nanoparticles. Although it remains difficult to assess their eventual future in pharmacy, mainly due to their relatively high cost, there is no doubt about the ability of EVs and GEEVs to effectively deliver drugs *in vivo*. Thus, it is safe to say that promising drugs based on vesicular transport for the treatment of severe and poorly treatable chronic, autoimmune and oncological diseases are expected to reach market within the next 10–20 years. ●

This work was supported by the Russian Science Foundation (grant No. 18-74-10079 "Self-assembling genetically encoded nanocages as an instrument to treat multiple sclerosis").

REFERENCES

1. Yin H., Kauffman K.J., Anderson D.G. // Nat. Rev. Drug Discov. 2017. V. 16. № 6. P. 387–399.
2. Ragelle H., Danhier F., Préat V., Langer R., Anderson D.G. // Expert Opin. Drug Deliv. 2017. V. 14. № 7. P. 851–864.
3. Kreuter J. // Int. J. Pharm. 2007. V. 331. № 1. P. 1–10.
4. Yu M., Wu J., Shi J., Farokhzad O.C. // J. Control. Release. 2016. V. 240. P. 24–37.
5. Shah M.A.A., Ali Z., Ahmad R., Qadri I., Fatima K., He N. // J. Nanosci. Nanotechnol. 2015. V. 15. № 1. P. 41–53.
6. Nikitenko N.A., Prassolov V.S. // Acta Naturae. 2013. V. 5. № 3. P. 35–53.
7. Liu Z., Jiao Y., Wang Y., Zhou C., Zhang Z. // Adv. Drug Deliv. Rev. 2008. V. 60. № 15. P. 1650–1662.
8. Sahin S., Selek H., Ponchel G., Ercan M.T., Sargon M., Hincal A.A., Kas H.S. // J. Control. Release. 2002. V. 82. № 2–3. P. 345–358.
9. Blanco E., Shen H., Ferrari M. // Nat. Biotechnol. 2015. V. 33. № 9. P. 941–951.
10. György B., Hung M.E., Breakefield X.O., Leonard J.N. // Annu. Rev. Pharmacol. Toxicol. 2014. V. 55. № 1. P. 439–464.
11. Bangham A.D. // Chem. Phys. Lipids. 1993. V. 64. № 1–3. P. 275–85.
12. Vemuri S., Rhodes C.. // Pharm. Acta Helv. 1995. V. 70. № 2. P. 95–111.
13. Kirby C., Gregoriadis G. // Nat. Biotechnol. 1984. V. 2. № 11. P. 979–984.
14. Gruner S.M., Lenk R.P., Janoff A.S., Ostro N.J. // Biochemistry. 1985. V. 24. № 12. P. 2833–2842.
15. Szoka F., Papahadjopoulos D. // Proc. Natl. Acad. Sci. U. S. A. 1978. V. 75. № 9. P. 4194–8.
16. Milsmann M.H., Schwendener R.A., Weder H.G. // Biochim. Biophys. Acta. 1978. V. 512. № 1. P. 147–55.
17. Miller C.R., Bondurant B., McLean S.D., McGovern K.A., O'Brien D.F. // Biochemistry. 1998. V. 37. № 37. P. 12875–12883.
18. Campbell R.B., Ying B., Kuesters G.M., Hemphill R. // J. Pharm. Sci. 2009. V. 98. № 2. P. 411–429.
19. Broekgaarden M., de Kroon A.I.P.M., van Gulik T.M., Heger M. // Curr. Med. Chem. 2014. V. 21. № 3. P. 377–91.
20. Lowe S.W., Ruley H.E., Jacks T., Housman D.E. // Cell. 1993. V. 74. № 6. P. 957–967.
21. Guo J., Ping Q., Jiang G., Huang L., Tong Y. // Int. J. Pharm. 2003. V. 260. № 2. P. 167–173.
22. Allen C., Dos Santos N., Gallagher R., Chiu G.N.C., Shu Y., Li W.M., Johnstone S.A., Janoff A.S., Mayer L.D., Webb M.S., et al. // Biosci. Rep. 2002. V. 22. № 2. P. 225–50.
23. Suk J.S., Xu Q., Kim N., Hanes J., Ensign L.M. // Adv. Drug Deliv. Rev. 2016. V. 99. P. 28–51.
24. Sharma A., Sharma U.S. // Int. J. Pharm. 1997. V. 154. № 2. P. 123–140.
25. Bergström K., Osterberg E., Holmberg K., Hoffman A.S., Schuman T.P., Kozlowski A., Harris J.H. // J. Biomater. Sci. Polym. Ed. 1994. V. 6. № 2. P. 123–32.
26. Pasut G., Paolino D., Celia C., Mero A., Joseph A.S., Wolfram J., Cosco D., Schiavon O., Shen H., Fresta M. // J. Control. Release. 2015. V. 199. P. 106–113.
27. Kabilova T., Shmendel E., Gladkikh D., Morozova N., Maslov M., Chernolovskaya E., Vlassov V., Zenkova M., Kabilova T., Shmendel E., et al. // Molecules. 2018. V. 23. № 12. P. 3101.
28. Zelepukin I. V., Yaremenko A. V., Shipunova V.O., Babenyshev A. V., Balalaeva I. V., Nikitin P.I., Deyev S.M., Nikitin M.P. // Nanoscale. 2019. V. 11. № 4. P. 1636–1646.
29. Markov O.O., Mironova N.L., Maslov M.A., Petukhov I.A., Morozova N.G., Vlassov V. V., Zenkova M.A. // J. Control. Release. 2012. V. 160. № 2. P. 200–210.
30. Markov O. V., Mironova N.L., Shmendel E. V., Serikov R.N., Morozova N.G., Maslov M.A., Vlassov V. V., Zenkova M.A. // J. Control. Release. 2015. V. 213. P. 45–56.
31. Deyev S., Proshkina G., Baryshnikova O., Ryabova A., Avishai G., Katrivas L., Giannini C., Levi-Kalisman Y., Kotlyar A. // Eur. J. Pharm. Biopharm. 2018. V. 130. P. 296–305.
32. Matsumura Y., Gotoh M., Muro K., Yamada Y., Shirao K., Shimada Y., Okuwa M., Matsumoto S., Miyata Y., Ohkura H., et al. // Ann. Oncol. Off. J. Eur. Soc. Med. Oncol. 2004. V. 15. № 3. P. 517–25.
33. Espelin C.W., Leonard S.C., Geretti E., Wickham T.J., Hendriks B.S. // Cancer Res. 2016. V. 76. № 6. P. 1517–1527.
34. Sankhala K.K., Mita A.C., Adinin R., Wood L., Beeram M., Bullock S., Yamagata N., Matsuno K., Fujisawa T., Phan A.T. // J. Clin. Oncol. 2009. V. 27. P. 2535–2535.
35. // clinicaltrials.gov. 2008. P. 2/1/2008-12/1/2013.
36. Torchilin V.P. In: Handbook of experimental pharmacology. // 2010. 3–53.
37. Zhou G., Wilson G., Hebbard L., Duan W., Liddle C., George J., Qiao L. // Oncotarget. 2016. V. 7. № 12. P. 13446–63.

38. Bobo D., Robinson K.J., Islam J., Thurecht K.J., Corrie S.R. // Pharm. Res. 2016. V. 33. № 10. P. 2373–2387.
39. Barenholz Y. (Chezy). // J. Control. Release. 2012. V. 160. № 2. P. 117–134.
40. Stepanov A., Lomakin Y., Gabibov A., Belogurov A. // Curr. Med. Chem. 2017. V. 24. № 17. P. 1761–1771.
41. Belogurov A.A., Stepanov A. V., Smirnov I. V., Melamed D., Bacon A., Mamedov A.E., Boitsov V.M., Sashchenko L.P., Ponomarenko N.A., Sharanova S.N., et al. // FASEB J. 2013. V. 27. № 1. P. 222–231.
42. Belogurov A., Zakharov K., Lomakin Y., Surkov K., Avtushenko S., Kruglyakov P., Smirnov I., Makshakov G., Lockshin C., Gregoriadis G., et al. // Neurotherapeutics. 2016. V. 13. № 4. P. 895–904.
43. Lomakin Y., Belogurov A., Glagoleva I., Stepanov A., Zakharov K., Okunola J., Smirnov I., Genkin D., Gabibov A. // Mediators Inflamm. 2016. V. 2016. P. 1–8.
44. Ivanova V. V., Khaiboullina S.F., Gomzikova M.O., Martynova E. V., Ferreira A.M., Garanina E.E., Sakhapov D.I., Lomakin Y.A., Khaibullin T.I., Granatov E. V., et al. // Front. Immunol. 2017. V. 8. P. 1335.
45. Bernasconi V., Norling K., Bally M., Höök F., Lycke N.Y. // J. Immunol. Res. 2016. V. 2016. P. 1–16.
46. Nisini R., Poerio N., Mariotti S., De Santis F., Fraziano M. // Front. Immunol. 2018. V. 9. P. 155.
47. Bartelds R., Nematollahi M.H., Pols T., Stuart M.C.A., Pardakhty A., Asadikaram G., Poolman B. // PLoS One. 2018. V. 13. № 4. P. e0194179.
48. Rajera R., Nagpal K., Singh S.K., Mishra D.N. // Biol. Pharm. Bull. 2011. V. 34. № 7. P. 945–53.
49. Kaur D., Kumar S. // J. Drug Deliv. Ther. 2018. V. 8. № 5. P. 35–43.
50. Moghassemi S., Hadjizadeh A. // J. Control. Release. 2014. V. 185. P. 22–36.
51. Shilpa S., Srinivasan B.P., Chauhan M. // Int. J. Drug Deliv. 2011. V. 3. № 1. P. 14–24.
52. Zeng W., Li Q., Wan T., Liu C., Pan W., Wu Z., Zhang G., Pan J., Qin M., Lin Y., et al. // Colloids Surfaces B Biointerfaces. 2016. V. 141. P. 28–35.
53. Marianecci C., Di Marzio L., Rinaldi F., Celia C., Paolino D., Alhaique F., Esposito S., Carafa M. // Adv. Colloid Interface Sci. 2014. V. 205. P. 187–206.
54. Touitou E. // US Pat. 5,716,638. 1996.
55. Yang L., Wu L., Wu D., Shi D., Wang T., Zhu X. // Int. J. Nanomedicine. 2017. V. 12. P. 3357–3364.
56. Bansal S., Prasad Kashyap C., Aggarwal G., Harikumar S. // IJRPC. 2012. V. 2. № 3. P. 704–713.
57. Sankar V., Ramesh S., Siram K. In: Alopecia. // InTech. 2018
58. Duangjit S., Opanasopit P., Rojanarata T., Ngawhirunpat T. // Adv. Mater. Res. 2011. V. 194–196. P. 537–540.
59. Chen J., Lu W.-L., Gu W., Lu S.-S., Chen Z.-P., Cai B.-C. // Expert Opin. Drug Deliv. 2013. V. 10. № 6. P. 845–856.
60. Gupta A., Aggarwal G., Singla S., Arora R. // Sci. Pharm. 2012. V. 80. № 4. P. 1061–80.
61. Irfan M., Verma S., Ram A. // Asian J. Pharm. Clin. Res. 2012. V. 5. № 3. P. 162–165.
62. Ghannoum M., Isham N., Herbert J., Henry W., Yurdakul S. // J. Clin. Microbiol. 2011. V. 49. № 5. P. 1716–20.
63. Lu K., Xie S., Han S., Zhang J., Chang X., Chao J., Huang Q., Yuan Q., Lin H., Xu L., et al. // J. Transl. Med. 2014. V. 12. № 1. P. 72.
64. May J.P., Li S.-D. // Expert Opin. Drug Deliv. 2013. V. 10. № 4. P. 511–527.
65. Nobuto H., Sugita T., Kubo T., Shimose S., Yasunaga Y., Murakami T., Ochi M. // Int. J. Cancer. 2004. V. 109. № 4. P. 627–635.
66. Sawant R.R., Torchilin V.P. // Soft Matter. 2010. V. 6. № 17. P. 4026.
67. Khulbe P. In: Novel Approaches for Drug Delivery. // 2017
68. Wong H.L., Bendayan R., Rauth A.M., Li Y., Wu X.Y. // Adv. Drug Deliv. Rev. 2007. V. 59. № 6. P. 491–504.
69. Mukherjee S., Ray S., Thakur R. // Indian J. Pharm. Sci. 2009. V. 71. № 4. P. 349.
70. Mehnert W., Mäder K. // Adv. Drug Deliv. Rev. 2001. V. 47. № 2–3. P. 165–96.
71. Wissing S.., Kayser O., Müller R.. // Adv. Drug Deliv. Rev. 2004. V. 56. № 9. P. 1257–1272.
72. Müller R.H., Mäder K., Gohla S. // Eur. J. Pharm. Biopharm. 2000. V. 50. № 1. P. 161–77.
73. Maheswaran A., Brindha P., Mullaicharam A.R., Masilamani K. // Int. J. Pharm. Sci. Rev. Res. 2013. V. 23. № 1. P. 295–301.
74. Olbrich C., Gessner A., Schröder W., Kayser O., Müller R.H. // J. Control. Release. 2004. V. 96. № 3. P. 425–435.
75. Dolatabadi J.E.N., Valizadeh H., Hamishehkar H. // Adv. Pharm. Bull. 2015. V. 5. № 2. P. 151–159.
76. zur Mühlen A., Schwarz C., Mehnert W. // Eur. J. Pharm. Biopharm. 1998. V. 45. № 2. P. 149–55.
77. Müller R.H., Radtke M., Wissing S.A. // Adv. Drug Deliv. Rev. 2002. V. 54. P. S131–S155.
78. Li Q., Cai T., Huang Y., Xia X., Cole S., Cai Y. // Nanomaterials. 2017. V. 7. № 6. P. 122.
79. Iqbal M.A., Md S., Sahni J.K., Baboota S., Dang S., Ali J. // J. Drug Target. 2012. V. 20. № 10. P. 813–830.
80. Khan S., Baboota S., Ali J., Khan S., Narang R., Narang J. // Int. J. Pharm. Investig. 2015. V. 5. № 4. P. 182.
81. Czajkowska-Kośnik A., Szekalska M., Winnicka K. // Pharmacol. Reports. 2019. V. 71. № 1. P. 156–166.
82. Hadinoto K., Sundaresan A., Cheow W.S. // Eur. J. Pharm. Biopharm. 2013. V. 85. № 3. P. 427–443.
83. Chan J.M., Zhang L., Yuet K.P., Liao G., Rhee J.-W., Langer R., Farokhzad O.C. // Biomaterials. 2009. V. 30. № 8. P. 1627–1634.
84. Yoo J.-W., Irvine D.J., Discher D.E., Mitragotri S. // Nat. Rev. Drug Discov. 2011. V. 10. № 7. P. 521–535.
85. Zhang P., Liu G., Chen X. // Nano Today. 2017. V. 13. P. 7–9.
86. Almeida J., Edwards D.C., Brand C., Heath T. // Lancet. 1975. V. 306. № 7941. P. 899–901.
87. de Jonge J., Leenhouts J.M., Holtrop M., Schoen P., Scherrer P., Cullis P.R., Wilschut J., Huckriede A. // Biochem. J. 2007. V. 405. № 1. P. 41–9.
88. Kuroda S., Liu Q., Jung J., Iijima M., Yoshimoto N., Niimi T., Maturana A., Shin S.H., Jeong S.-Y., Choi E.K., et al. // Int. J. Nanomedicine. 2015. V. 10. № 1. P. 4159.
89. Liu H., Tu Z., Feng F., Shi H., Chen K., Xu X. // Acta Pharm. 2015. V. 65. № 2. P. 105–116.
90. Mohammadzadeh Y., Rasouli N., Aref M.H.S., Tabib N.S.S., Abdoli A., Biglari P., Saleh M., Tabatabaeian M., Kheiri M.T., Jamali A. // Biotechnol. Lett. 2016. V. 38. № 8. P. 1321–1329.
91. Bovier P.A. // Expert Rev. Vaccines. 2008. V. 7. № 8. P. 1141–1150.
92. Blom R.A.M., Amacker M., van Dijk R.M., Moser C., Stumbles P.A., Blank F., von Garnier C. // Front. Immunol. 2017. V. 8. P. 359.
93. Kaneda Y. // Adv. Drug Deliv. Rev. 2012. V. 64. № 8. P. 730–738.

94. Leroux-Roels G., Maes C., Clement F., van Engelenburg F., van den Dobbelsteen M., Adler M., Amacker M., Lopalco L., Bomsel M., Chalifour A., et al. // PLoS One. 2013. V. 8. № 2. P. e55438.
95. Wang M., Gao Z., Zhang Y., Pan L. // Appl. Microbiol. Biotechnol. 2016. V. 100. № 13. P. 5691–5701.
96. Bron P.A., Kleerebezem M. // Front. Microbiol. 2018. V. 9. P. 1821.
97. Forbes N.S. // Nat. Rev. Cancer. 2010. V. 10. № 11. P. 785–94.
98. Hosseinidoust Z., Mostaghaci B., Yasa O., Park B.-W., Singh A.V., Sitti M. // Adv. Drug Deliv. Rev. 2016. V. 106. № Pt A. P. 27–44.
99. Langemann T., Koller V.J., Muhammad A., Kudela P., Mayr U.B., Lubitz W. // Bioeng. Bugs. 2010. V. 1. № 5. P. 326–36.
100. Lubitz P., Mayr U.B., Lubitz W. // Springer, New York, NY. 2009. 159–170.
101. Farjadian F., Moghoofei M., Mirkiani S., Ghasemi A., Rabiee N., Hadifar S., Beyzavi A., Karimi M., Hamblin M.R. // Biotechnol. Adv. 2018. V. 36. № 4. P. 968–985.
102. Kudela P., Koller V.J., Lubitz W. // Vaccine. 2010. V. 28. № 36. P. 5760–5767.
103. Chen Z., Hu Q., Gu Z. // Acc. Chem. Res. 2018. V. 51. № 3. P. 668–677.
104. Villa C.H., Anselmo A.C., Mitragotri S., Muzykantov V. // Adv. Drug Deliv. Rev. 2016. V. 106. № Pt A. P. 88–103.
105. Yan J., Yu J., Wang C., Gu Z. // Small Methods. 2017. V. 1. № 12. P. 1700270.
106. Stuckey D.W., Shah K. // Nat. Rev. Cancer. 2014. V. 14. № 10. P. 683–691.
107. Ngandeu Neubi G.M., Opoku-Damoah Y., Gu X., Han Y., Zhou J., Ding Y. // Biomater. Sci. 2018. V. 6. № 5. P. 958–973.
108. Hsia Y., Bale J.B., Gonen S., Shi D., Sheffler W., Fong K.K., Nattermann U., Xu C., Huang P.-S., Ravichandran R., et al. // Nature. 2016. V. 535. № 7610. P. 136–139.
109. Votteler J., Ogohara C., Yi S., Hsia Y., Nattermann U., Belnap D.M., King N.P., Sundquist W.I. // Nature. 2016. V. 540. № 7632. P. 292–295.
110. Gusachenko O.N., Zenkova M.A., Vlassov V. V. // Biochem. 2013. V. 78. № 1. P. 1–7.
111. EL Andaloussi S., Mäger I., Breakefield X.O., Wood M. J.A. // Nat. Rev. Drug Discov. 2013. V. 12. № 5. P. 347–357.
112. Loughmiller J., Klintworth G. // Nat. Biotechnol. 2011. V. 29. № 4. P. 306–309.
113. Lai C.P., Mardini O., Ericsson M., Prabhakar S., Maguire C., Chen J.W., Tannous B.A., Breakefield X.O. // ACS Nano. 2014. V. 8. № 1. P. 483–494.
114. Miyanishi M., Tada K., Koike M., Uchiyama Y., Kitamura T., Nagata S. // Nature. 2007. V. 450. № 7168. P. 435–439.
115. Charoenviriyakul C., Takahashi Y., Morishita M., Nishikawa M., Takakura Y. // Mol. Pharm. 2018. V. 15. № 3. P. 1073–1080.
116. Merchant M.L., Rood I.M., Deegens J.K.J., Klein J.B. // Nat. Rev. Nephrol. 2017. V. 13. № 12. P. 731–749.
117. Vaswani K., Koh Y.Q., Almughlliq F.B., Peiris H.N., Mitchell M.D. // Reprod. Biol. 2017. V. 17. № 4. P. 341–348.
118. Foers A.D., Chatfield S., Dagley L.F., Scicluna B.J., Webb A.I., Cheng L., Hill A.F., Wicks I.P., Pang K.C. // J. Extracell. Vesicles. 2018. V. 7. № 1. P. 1490145.
119. Lane R.E., Korbie D., Trau M., Hill M.M. // Methods Mol. Biol. 2017. V. 1660. P. 111–130.
120. Montecalvo A., Shufesky W.J., Stolz D.B., Sullivan M.G., Wang Z., Divito S.J., Papworth G.D., Watkins S.C., Robbins P.D., Larregina A.T., et al. // J. Immunol. 2008. V. 180. № 5. P. 3081–90.
121. Sobo-Vujanovic A., Munich S., Vujanovic N.L. // Cell. Immunol. 2014. V. 289. № 1–2. P. 119–127.
122. Östman S., Taube M., Telemo E. // Immunology. 2005. V. 116. № 4. P. 464–476.
123. Mokarizadeh A., Delirezh N., Morshedi A., Mosayebi G., Farshid A.-A., Mardani K. // Immunol. Lett. 2012. V. 147. № 1–2. P. 47–54.
124. Liu H., Chen L., Liu J., Meng H., Zhang R., Ma L., Wu L., Yu S., Shi F., Li Y., et al. // Cancer Lett. 2017. V. 411. P. 182–190.
125. Pavlyukov M.S., Yu H., Bastola S., Minata M., Shender V.O., Lee Y., Zhang S., Wang J., Komarova S., Wang J., et al. // Cancer Cell. 2018. V. 34. № 1. P. 119-135.e10.
126. Hu Y., Rao S.-S., Wang Z.-X., Cao J., Tan Y.-J., Luo J., Li H.-M., Zhang W.-S., Chen C.-Y., Xie H. // Theranostics. 2018. V. 8. № 1. P. 169–184.
127. Komaki M., Numata Y., Morioka C., Honda I., Tooi M., Yokoyama N., Ayame H., Iwasaki K., Taki A., Oshima N., et al. // Stem Cell Res. Ther. 2017. V. 8. № 1. P. 219.
128. Li X., Xie X., Lian W., Shi R., Han S., Zhang H., Lu L., Li M. // Exp. Mol. Med. 2018. V. 50. № 4. P. 29.
129. Liu X., Li Q., Niu X., Hu B., Chen S., Song W., Ding J., Zhang C., Wang Y. // Int. J. Biol. Sci. 2017. V. 13. № 2. P. 232–244.
130. Zhang J., Guan J., Niu X., Hu G., Guo S., Li Q., Xie Z., Zhang C., Wang Y. // J. Transl. Med. 2015. V. 13. № 1. P. 49.
131. Zhang S., Chu W.C., Lai R.C., Lim S.K., Hui J.H.P., Toh W.S. // Osteoarthr. Cartil. 2016. V. 24. № 12. P. 2135–2140.
132. Nakamura Y., Miyaki S., Ishitobi H., Matsuyama S., Nakasa T., Kamei N., Akimoto T., Higashi Y., Ochi M. // FEBS Lett. 2015. V. 589. № 11. P. 1257–1265.
133. Cui X., He Z., Liang Z., Chen Z., Wang H., Zhang J. // J. Cardiovasc. Pharmacol. 2017. V. 70. № 4. P. 225–231.
134. Drommelschmidt K., Serdar M., Bendix I., Herz J., Bertling F., Prager S., Keller M., Ludwig A.-K., Duhan V., Radtke S., et al. // Brain. Behav. Immun. 2017. V. 60. P. 220–232.
135. Liu W., Wang Y., Gong F., Rong Y., Luo Y., Tang P., Zhou Z., Zhou Z., Xu T., Jiang T., et al. // J. Neurotrauma. 2018. P. neu.2018.5835.
136. Zhuang X., Xiang X., Grizzle W., Sun D., Zhang S., Axtell R.C., Ju S., Mu J., Zhang L., Steinman L., et al. // Mol. Ther. 2011. V. 19. № 10. P. 1769–1779.
137. Yang T., Martin P., Fogarty B., Brown A., Schurman K., Phipps R., Yin V.P., Lockman P., Bai S. // Pharm. Res. 2015. V. 32. № 6. P. 2003–2014.
138. Wang L., Chen Q., Qi H., Wang C., Wang C., Zhang J., Dong L. // Cancer Res. 2016. V. 76. № 22. P. 6631–6642.
139. Fuhrmann G., Serio A., Mazo M., Nair R., Stevens M.M. // J. Control. Release. 2015. V. 205. P. 35–44.
140. Wassler M., Jonasson I., Persson R., Fries E. // Biochem. J. 2015. V. 247. № 2. P. 407–415.
141. Kamerkar S., Lebleu V.S., Sugimoto H., Yang S., Ruivo C.F., Melo S.A., Lee J.J., Kalluri R. // Nature. 2017. V. 546. № 7659. P. 498–503.
142. Cooper J.M., Wiklander P.B.O., Nordin J.Z., Al-Shawi R., Wood M.J., Vithlani M., Schapira A.H. V, Simons J.P., El-Andaloussi S., Alvarez-Erviti L. // Mov. Disord. 2014. V. 29. № 12. P. 1476–1485.
143. Kooijmans S.A.A., Stremersch S., Braeckmans K., De Smedt S.C., Hendrix A., Wood M.J.A., Schiffelers R.M., Raemdonck K., Vader P. // J. Control. Release. 2013. V. 172. № 1. P. 229–238.
144. Kosaka N., Iguchi H., Yoshioka Y., Takeshita F., Matsuki

Y., Ochiya T. // J. Biol. Chem. 2010. V. 285. № 23. P. 17442–17452.
145. Ohno S.I., Takanashi M., Sudo K., Ueda S., Ishikawa A., Matsuyama N., Fujita K., Mizutani T., Ohgi T., Ochiya T., et al. // Mol. Ther. 2013. V. 21. № 1. P. 185–191.
146. Shen B., Wu N., Yang M., Gould S.J. // J. Biol. Chem. 2011. V. 286. № 16. P. 14383–14395.
147. Glinka E.M., Edelweiss E.F., Sapozhnikov A.M., Deyev S.M. // Gene. 2006. V. 366. № 1. P. 97–103.
148. Guryev E.L., Volodina N.O., Shilyagina N.Y., Gudkov S. V, Balalaeva I. V, Volovetskiy A.B., Lyubeshkin A. V, Sen' A. V, Ermilov S.A., Vodeneev V.A., et al. // Proc. Natl. Acad. Sci. U. S. A. 2018. V. 115. № 39. P. 9690–9695.

Assessment of the Phenylketonuria (PKU)-Associated Mutation p.R155H Biochemical Manifestations by Mass Spectrometry-Based Blood Metabolite Profiling

O. A. Baturina[1], A. A. Chernonosov[1], V. V. Koval[1,2], I. V. Morozov[1,2]*
[1]Joint Center for genomic, proteomic and metabolomics studies, Institute of Chemical Biology and Fundamental Medicine SB RAS, Lavrentiev Ave. 8, Novosibirsk, 630090, Russia
[2]Department of Natural Sciences, Novosibirsk State University, Pirogova Str. 2, Novosibirsk, 630090, Russia
*E-mail: mor@niboch.nsc.ru
Received December 12, 2018; in final form, March 27, 2019
DOI: 10.32607/20758251-2019-11-2-42-46

ABSTRACT **Homozygous siblings with different treatment histories represent an excellent model to study both the phenotypic manifestation of mutations and the efficacy of therapy. We compared phenylketonuria (PKU) manifestations in two different gender siblings who were homozygous carriers of a rare phenylalanine hydroxylase (*PAH*) mutation, p.R155H, subjected to different treatments. PKU caused by mild mutations may be easily underdiagnosed if the diagnosis is based solely on the phenylalanine (Phe) blood concentration. One of the described patients is an example of this diagnostic error. For reducing diagnostic errors, we suggest the use of more elaborate methods in screening practice, in particular mass spectrometric analysis of blood metabolites, the efficiency of which is demonstrated in the present study.**
KEYWORDS **phenylketonuria, hyperphenylalaninemia, p.R155H, blood phenylalanine, blood carnitine, mass spectrometry, missense mutation.**
ABBREVIATIONS **PKU – phenylketonuria; PAH – phenylalanine hydroxylase; CNS – central nervous system; C0 – free carnitine; C2-C18 – acylcarnitines.**

INTRODUCTION

Type I phenylketonuria (classic) (PKU; MIM 261600) is an autosomal recessively inherited disease caused by a deficiency of phenylalanine hydroxylase (PAH; [EC 1.14.16.1]) activity [1, 2]. The deficiency of enzymatic activity is usually caused by mutations in the phenylalanine hydroxylase gene [1]. Incomplete conversion of phenylalanine to tyrosine due to deficient activity of PAH results in accumulation of phenylalanine and toxic products of alternative metabolic pathways, such as phenylpyruvate, vinyl acetate, phenyllactate, and phenylacetylglutamine, in tissues and biological fluids, which leads to the disease symptoms: dementia in particular. Common features of phenylketonuria also include a decreased concentration of tyrosine and a changed balance of amino acids in biological fluids. A widely used classification of PKU severity, which is based on the blood phenylalanine concentration, was proposed by C.R. Scriver and S. Kaufman [3]. According to N. Blau et al. [4], PKU is classified, depending on the blood phenylalanine concentration before the beginning of treatment, as a classic (severe) form at concentrations above 1,200 μmol, a moderate form at concentrations in a range of 900–1,200 μmol, a mild form at concentrations of 600–900 μmol, and hyperphenylalaninemia at concentrations of less than 600 μmol.

Neonatal biochemical screening is currently the most widely used procedure for early diagnosis of genetic diseases and prevention of their effects. The World Health Organization defined the social and economic prerequisites for including diseases in national neonatal

screening programs [5]. Currently, neonatal screening for PKU, as one of the most common genetic diseases (rate of 1 : 10,000 to 1 : 25,000 among Caucasians [6]), is performed in most countries. In the Russian Federation, this screening involves several measurements of the blood plasma phenylalanine level, the first of which is carried out on day 4 or 5 after birth. If an elevated level is detected, the measurement is repeated. However, the blood phenylalanine-based diagnostics may be unreliable, in particular at borderline levels. The accurate diagnosis requires more advanced methods, especially in the case of mutations with a relatively high residual PAH activity when the blood phenylalanine level increases slightly, remaining less than 500 μmol, which is not enough for an unambiguous diagnosis. Mass spectrometric analysis of blood metabolites can provide a more accurate diagnosis based on assessing the concentrations of not only phenylalanine, but also tyrosine and other amino acids, which, in particular, provides the phenylalanine to tyrosine ratio. The diagnosis based on metabolite levels should be confirmed by genetic analysis with identification of *PAH* gene mutations and their inheritance patterns by determining the nucleotide sequences of the appropriate loci.

Currently, the main and most widely used method for PKU correction is diet therapy [7, 8] aimed primarily at preventing damage to the central nervous system (CNS), which leads to the degradation of mental abilities. To achieve this goal, diet therapy should begin no later than a few weeks after birth. Being generally quite effective, this diet restricts the intake of animal-derived proteins, which may lead to decreased concentrations of free carnitine (C0) and acylcarnitines (C2–C18) and, correspondingly, to impaired metabolism and mitochondrial dysfunction in some patients [9].

In this study, we determined blood metabolite levels in the presence and absence of diet therapy in two siblings who were homozygous carriers of a PKU-associated mutation, p.R155H, of the *PAH* gene, using mass spectrometry of dried blood samples. Related homozygous patients with different histories of diet therapy may be considered as a unique model for studying both the phenotypic manifestation of the mutations and the efficacy of therapy.

EXPERIMENTAL

Both patients were children of the same parents. The girl (1), who was born in Russia in June 2009, was diagnosed with PKU upon neonatal biochemical screening; she received a diet with a limited content of phenylalanine from the second month of life. The boy (2), who was born in Uzbekistan in July 2001, was not diagnosed with PKU upon neonatal screening and did not receive diet therapy. Blood samples for mass spectrometric analysis were taken in 2010, approximately one year after the start of diet therapy for patient 1. Simultaneously, the physical development and CNS status of the patients were assessed, which did not reveal any serious abnormalities. The study was performed in accordance with the requirements of the Medical Ethics Committee of the Institute of Chemical Biology and Fundamental Medicine of the Siberian Branch of the Russian Academy of Sciences (ICBFM SB RAS).

Upon neonatal screening, blood samples were collected by paper filters (Perkin Elmer, Finland) and the blood phenylalanine concentration was determined using a Delfia/Victor counter and a reagent kit from the manufacturer (Wallac Oy, Finland). Genomic DNA was isolated from blood as previously described [10]. Mutations in the *PAH* gene were identified by both DNA strands Sanger sequencing of PCR amplification products from all exons and adjacent intron regions of the *PAH* gene using a BigDye Terminator v.3.1 Cycle Sequencing kit and an ABI 3130xl genetic analyzer (Applied Biosystems, USA) at the Genomics Core Facility of the ICBFM SB RAS. The nucleotide DNA sequences of both patients were identical and corresponded to the known *PAH* gene sequences, except for the p.R155H mutation. The parents' DNA sequences confirmed inheritance of the p.R155H mutation. Mass spectrometric analysis of phenylalanine, tyrosine, and acylcarnitine levels was performed using a standard procedure [11] at the Mass Spectrometry Core Facility of the ICBFM SB RAS. Samples and internal standards were prepared using an Amino Acids and Acylcarnitines kit #55000 for newborn screening (Chromsystems Instruments & Chemicals, Germany); samples were prepared according to the kit manufacturer's protocol. The analysis was performed using an Agilent 6410 QQQ tandem mass spectrometer equipped with an ESI ionization system, which was coupled to an Agilent 1200 liquid chromatography system (Agilent Technologies, USA). Quantitative analysis was carried out in the multiple reaction monitoring (MRM) mode, with a total analysis time of 2.5 min. The signal was acquired and analyzed using the MassHunter v.1.3 software.

RESULTS AND DISCUSSION

The point mutation p.R155H is a substitution of G for A in exon 5 of the *PAH* gene, which results in the replacement of arginine with histidine in the PAH catalytic domain. According to the data from http://www.biopku.org [12], the residual activity of the enzyme carrying the mutation remains rather high (approximately 44% of the initial activity). Therefore, the p.R155H mutation is considered to be associated with hyperphenylalaninemia with a relative genotype-phenotype correlation coefficient of 8 on the scale proposed

by Guldberg et al. [1]. This rare mutation was previously described only in one case in compound with the p.D143G mutation in a hyperphenylalaninemia patient [13]. We studied two siblings who were homozygous carriers of the p.R155H mutation, one of whom was subjected to diet therapy, while the other was untreated. Being homozygous mutation carriers, these patients provide a unique opportunity to directly study the phenotypic manifestation of the mutation, while significant differences in therapy may be used to assess its comparative efficacy.

The initial phenotypic manifestation of the p.R155H mutation in patients 1 and 2 was somewhat different, despite the same *PAH* locus genotype and common pedigree. The blood phenylalanine concentration in patient 1 upon neonatal screening was 1,100 μmol; the patient was diagnosed with moderate PKU, and diet therapy was prescribed. Patient 2 was not diagnosed with PKU upon neonatal screening, which was performed in the Republic of Uzbekistan, possibly due to different timing and standards of screening. In 2010, the blood phenylalanine concentration in patient 2 was 497 ± 13 μmol (*Table 1*), which corresponds to severe hyperphenylalaninemia. Therefore, if only the blood phenylalanine level is used as a criterion, it may be concluded that the p.R155H/p.R155H genotype can manifest itself as a fairly wide range of symptoms, from mild hyperphenylalaninemia to moderate PKU, depending on the other patient's biochemical features associated with gender, feeding in the neonatal period, etc. In this case, neonatal screening that is based on the blood phenylalanine level may miss the disease, as in the case of patient 2.

The effective use of mass spectrometry for accurate diagnosis of PKU, in particular at intermediate blood phenylalanine concentrations, was described in studies by Chace et al. [15, 16]. Instead of the phenylalanine concentration, they suggested using the phenylalanine

Table. Blood metabolite concentrations measured by mass spectrometry

Metabolite	Patient 1, μmol/L	Patient 2, μmol/L	**Median concentration in healthy children (5th–95th percentile), μmol/L**[14]
Phe	298 ± 10	497 ± 13	45 (32–64)
Tyr	43 ± 2	86 ± 2	84 (48–159)
Phe/Tyr	6.9 ± 0.3	5.8 ± 0.1	
Free carnitine (C0)	31.7 ± 0.4	44.0 ± 1.1	15.5 (9.2–26.4)
Acetylcarnitine (C2)	10.4 ± 0.7	11.9 ± 0.3	17.3 (10.1–29.4)
Propionylcarnitine (C3)	1.48 ± 0.04	2.68 ± 0.2	1.42 (.81–2.56)
Butyrylcarnitine (C4)	0.11 ± 0.02	0.15 ± 0.02	0.19 (0.12–0.30)
Isovalerylcarnitine (C5)	0.11 ± 0.01	0.11 ± 0.01	0.09 (0.06–0.17)
Hexanoylcarnitine (C6)	0.04 ± 0.01	0.09 ±0.002	0.05 (0.02–0.10)
Octanoylcarnitine (C8)	0.02 ± 0.002	0.06 ± 0.02	0.05 (0.03–0.08)
Decanoylcarnitine (C10)	0.02± 0.002	0.07 ±0.002	0.07 (0.04–0.13)
Dodecanoylcarnitine (C12)	0.03 ± 0.02	0.09 ±0.002	0.08 (0.04–0.19)
Tetradecanoylcarnitine (C14)	0.06 ± 0.003	0.07 ±0.002	0.18 (0.11–0.31)
Hexadecanoylcarnitine (C16)	0.56 ±0.02	0.53 ±0.02	2.93 (1.65–4.76)
Octadecanoylcarnitine (C18)	0.34 ±0.01	0.32 ± 0.01	0.86 (0.52–1.43)

Values are presented as mean ± SEM of 5 or 6 independent measurements.

to tyrosine concentration ratio as a more accurate and selective diagnostic criterion, because the changes in overall amino acid levels are corrected in this case. The phenylalanine to tyrosine concentration ratio in the blood normally ranges from 0.49 to 0.93, rising to 1.3–14.3 in PKU patients [15, 16]. We detected high values of this parameter, which clearly and unambiguously indicated PKU in both patient 1 (6.9 ± 0.3) and patient 2 (5.8 ± 0.1) (*Table 1*). At the same time, the patients' parents (heterozygous carriers of mutations) showed the ratio typical of healthy people: 0.9 ± 0.1 (mother) and 0.7 ± 0.02 (father).

We also determined blood carnitine levels in the patients (*Table*) and compared them with the data of 20 healthy children [17]. As previously shown, carnitine levels may be a helpful criterion in the identification of congenital metabolic disorders and the levels vary significantly in different metabolic disorders [18]. It was also noted that carnitine concentrations significantly decrease in the blood of PKU patients with a phenylalanine-restricted diet not supplemented with carnitines [19]. In our patients, total carnitine levels were slightly decreased (44.9 μmol in patient 1 and 55.2 μmol in patient 2) compared to the normal levels of 60–100 μmol [20]. Total acylcarnitine levels (13.2 μmol in patient 1 and 13.9 μmol in patient 2) fully corresponded to the normal values. We determined potential carnitine deficiency using the ratio of acylcarnitine and free carnitine concentrations. The values (0.42 in patient 1 and 0.33 in patient 2) were significantly below the upper limit of the normal value (0.6), which indicates sufficient levels of free carnitine, as well as the normal proportion of acylcarnitines. Therefore, acylcarnitine concentrations in our homozygous carriers of p.R155H were within their normal range; however, several studies [21, 22] have demonstrated that acylcarnitine concentrations in patients with classic PKU are significantly different from normal values.

CONCLUSION

We examined two homozygous siblings with the PKU-associated mutation p.R155H who had different treatment histories: one was subjected to diet therapy, and the other did not receive treatment. If the blood phenylalanine concentration is used as the only diagnostic criterion for PKU, the condition should be classified as hyperphenylalaninemia in one patient and as moderate PKU in the other. At the same time, the phenylalanine to tyrosine concentration ratio enabled a reliable diagnosis of PKU in both patients. Therefore, the blood phenylalanine level alone cannot be a reliable criterion for the diagnosis of PKU in all cases and should not be used as the sole diagnostic criterion. Our findings confirm the possibility of using the phenylalanine to tyrosine concentration ratio as a more accurate and reliable criterion for neonatal screening. We also demonstrated that mass spectrometric analysis may be used as the main method of neonatal screening for PKU.

The determined blood concentrations of free and acylcarnitines indicate that homozygous carriers of the p.R155H mutation probably do not experience significant limitations in energy metabolism in cells, in contrast to patients with classic or moderate PKU. ●

This study was conducted under Government contracts (No. 0309-2019-0020 and 0309-2019-0007).

REFERENCES

1. Guldberg P., Rey F., Zschocke J., Romano V., Francois B., Michiels L., Ullrich K., Hoffmann G.F., Burgard P., Schmidt H., et al. // Am. J. Hum. Genet. 1998. V. 63. P. 71–79.
2. DiLella A.G., Kwok S.C., Ledley F.D., Marvit J., Woo S.L. // Biochemistry. 1986. V. 25. P. 743–749.
3. Scriver C.R., Kaufman S., Woo S.L. // Annu. Rev. Genet. 1988. V. 22. P. 301–321.
4. Blau N., van Spronsen F.J., Levy H.L. // Lancet. 2010. V. 376. P. 1417–1427.
5. Order of the Ministry of Health and Social Development of the Russian Federation of March 22, 2006 No. 185 On mandatory newborn screening for hereditary diseases.
6. Williams R.A., Mamotte C.D., Burnett J.R. // Clin. Biochem. Rev. 2008. V. 29. P. 31–41.
7. Ahring K., Bélanger-Quintana A., Dokoupil K., Gokmen Ozel H., Lammardo A.M., MacDonald A. // Clin. Nutr. 2009. V. 28. P. 231–237.
8. Bushueva T.V. // Questions of Modern Pediatrics. 2010. V. 9. P. 157–162.
9. Mutze U., Beblo S., Kortz L., Matthies C., Koletzko B., Bruegel M., Rohde C., Thiery J., Kiess W., Ceglarek U. // PLoS One. 2012. V. 7. P. 1–9.
10. Baturina O.A., Tupikin A.E., Lukjanova T.V., Sosnitskaya S.V., Morozov I.V. // J. Med. Biochem. 2014. V. 33. P. 333–340.
11. Chace D.H., Kalas T., Naylor E.W. // Clin. Chem. 2003. V. 49. P. 1797–1817.
12. Databases of Pediatric Neurotransmitter Disorders (PND), including the locus-specific database of PAH variants and BIOPKU genotypes database [Internet]. Division of Metabolism University Children's Hospital Steinwiesstrasse 75 CH-8032 Zürich Switzerland [cited 2018 Sep 10]. Available from: http:www.biopku.org
13. Dobrowolski S.F., Pey A.L., Koch R., Levy H., Ellingson C.C., Naylor E.W., Martinez A. // J. Inherit. Metab. Dis. 2009. V. 32. P. 10–21.
14. Liu Q., Wu J., Shen W., Wei R., Jiang .J, Liang J., Chen M., Zhong M., Yin A. // J. Matern. Fetal Neonatal. Med. 2017. V. 30 (22). P. 2697–2704.
15. Chace D.H., Mlllington D.S., Terada N., Kahier S.G., Roe

C.R., Hofman L.F. // Clin. Chem. 1993. V. 39. P. 66–71.
16. Chace D.H., Sherwin J.E., Hillman S.L., Lorey F., Cunningham G.C. // Clin. Chem. 1998. V. 44. P. 2405–2409.
17. Leontieva I.V., Nikolaeva E.A., Alimina E.G., Zolkina I.V. // Practice Pediatrician. 2012. V. 10. P. 74–79.
18. Jones L.L., McDonald D.A., Borum P.R. // Prog. Lipid Res. 2010. V. 49 (1). P. 61–75.
19. Vilaseca M.A., Briones P., Ferrer I., Campistol J., Riverola A., Castillo P., Ramon F. // J. Inherit. Metab. Dis. 1993. V. 16 (1). P. 101–104.
20. Weigel C., Kiener C., Meier N., Schmid P., Rauh M., Rascher W., Knerr I. // Ann. Nutr. Metab. 2008. V. 53. P. 91–95.
21. Fischer G.M., Nemeti B., Farkas V., Debreceni B., Laszlo A., Schaffer Z., Somogyi C., Sandor A. // Biochim. Biophys. Acta. 2000. V. 150. P. 200–210.
22. Engel A.G., Rebouche C.J. // J. Inherit. Metab. Dis. 1984. V. 7 (Suppl. 1). P. 38–43.

"Green" Synthesis of Cytotoxic Silver Nanoparticles Based on Secondary Metabolites of *Lavandula Angustifolia* Mill.

M. M. Belova[1,≠], V. O. Shipunova[2,3,4,≠,*], P. A. Kotelnikova[2], A. V. Babenyshev[3], E. A. Rogozhin[2], M. Yu. Cherednichenko[1], S. M. Deyev[2,4,5]

[1]Russian State Agrarian University-Moscow Timiryazev Agricultural Academy, Timiryazevskaya Str. 49, Moscow, 127550, Russia

[2]Shemyakin-Ovchinnikov Institute of Bioorganic Chemistry of the Russian Academy of Sciences, GSP-7, Miklukho-Maklaya Str. 16/10, Moscow, 117997, Russia

[3]Moscow Institute of Physics & Technology, Kerchenskaya Str. 1 "A", Moscow, 117303, Russia

[4]National Research Nuclear University MEPhI (Moscow Engineering Physics Institute), Kashirskoe sh. 31, Moscow, 115409, Russia

[5]Sechenov First Moscow State Medical University, Trubetskaya Str., 8-2, Moscow, 119991, Russia

*E-mail: viktoriya.shipunova@phystech.edu

[≠]Equally contributed

Received February 07, 2019; in final form, May 06, 2019

DOI: 10.32607/20758251-2019-11-2-47-53

ABSTRACT **In this study, we used "green" synthesis to prepare silver nanoparticles (NPs) from aqueous plant and callus extracts of the narrow-leaved lavender *Lavandula angustifolia* Mill. 35.4 ± 1.6 nm and 56.4 ± 2.4 nm nanoparticles, colloidally stable in phosphate-buffered saline, were synthesized using the plant extract and the callus extract, respectively. NPs were characterized by spectrophotometry, dynamic light scattering, and scanning electron microscopy. We studied the dynamics of the nanoparticle synthesis and evaluated the cytotoxic properties of the plant extract-based NPs. Modification of NPs with bovine serum albumin demonstrated that blockage of the nanoparticle surface completely suppressed NP cytotoxic activity *in vitro*. The synthesized NPs possess localized surface plasmon resonance properties and are of small sizes, and their surface can be modified with protein molecules, which makes them promising agents for cancer theranostics.**

KEYWORDS **green synthesis, silver nanoparticles, secondary metabolites, lavender.**

ABBREVIATIONS **BSA – bovine serum albumin; SM – secondary metabolite; LSPR –localized surface plasmon resonance; NP – nanoparticle; MS – Murashige and Skoog medium; PEG – polyethylene glycol; TDZ – thidiazuron.**

INTRODUCTION

Modern bionanotechnologies help unlock broad prospects for the development of new generations of drugs that can be used to combat socially impactful diseases. Bionanotechnological means and methods enable the creation of various nanostructures that serve as effective tools for the therapy and diagnosis (theranostics) of various diseases, in particular cancers.

The development of theranostic methods is based on multifunctional agents combining diagnostic and therapeutic functions [1–5]. These agents include metallic nanoparticles (NPs) with localized surface plasmon resonance (LSPR) properties [6]. The high chemical surface activity of these nanoparticles allows one to modify them by targeting agents for delivery to target cells, while LSPR makes these nanoparticles suitable for both detection and selective hyperthermal destruction of cells [7, 8]. The "green" synthesis that implies an environmentally friendly production of particles without the use of aggressive toxic and expensive substances is an alternative, economically more profitable, and environmentally safe way to prepare nanostructures compared to traditional physicochemical methods for NP synthesis, which are often expensive, labor-intensive, and not environmentally friendly [9].

In the "green" synthesis, secondary plant metabolites (SMs) are widely used as reducing agents [10–12]. They are particularly promising in "green" synthesis thanks to their low cost of production, short-term synthesis, and biosafety. Also, *in vitro* cultivation of plants enables one to scale up the production of necessary substances, because these methods yield large amounts of standardized plant materials within a short time period and produce desired SMs all year round.

The development of a successful nano-agent for effective action on cancer cells relies on a number of parameters, such as size, composition, coating, other physicochemical properties, blood-circulation characteristics, etc. Biocompatibility is one of the most essential parameters affecting the fundamental possibility of using the drug *in vivo*. NPs produced by "green" synthesis often have higher biocompatibility thanks to the use of natural substances with the necessary biological activity (noble metals, SMs, proteins), which is successfully used for various *in vitro* and *in vivo* studies. These particles are considered as promising for theranostics [13, 14].

In this work, we used "green" synthesis to prepare silver NPs based on aqueous extracts of the narrow-leaved lavender (*Lavandula angustifolia* Mill). The dynamics of nanoparticle synthesis and NP cytotoxic properties before and after surface modification were studied *in vitro*.

EXPERIMENTAL

Introduction of the plant material into culture *in vitro*

Narrow-leaved lavender (*L. angustifolia* Mill., Munstead, Lamiaceae Mart.) seeds were sterilized with a 5% sodium hypochlorite solution for 10 min. After sterilization, the seeds were washed twice in sterile distilled water and placed in Petri dishes with a Murashige and Skoog (MS) hormone-free medium [15]. Control seeds were germinated in non-sterile conditions on filter paper moistened with distilled water. Seed germination capacity was evaluated on the 15th day according to GOST 30556-98 [16]. Three weeks after planting, the seedlings were replanted into containers with the MS medium for further development.

Clonal micropropagation

Plants with a height of 10 cm (4–6 nodes) were cut into cuttings (a node with internode parts) and propagated in two stages: planting in the MS medium supplemented with 0.5 mg/L thidiazuron (TDZ) to stimulate aerial part growth and then replanted in ¼ MS medium with addition of 0.2 mg/L α-naphthylacetic acid to induce rhizogenesis [17].

Callusogenesis induction

Stem explants were placed in the MS medium supplemented with 0.5 mg/L of 2,4-dichlorophenoxyacetic acid (2,4-D). Callusogenesis was induced using previously *in vitro* cultivated plants.

Preparation of aqueous extracts

Aqueous extracts were prepared from the aerial part of the aseptic plants and the callus. The plant material, frozen in liquid nitrogen, was homogenized in a mortar. After achieving room temperature, the homogenate was added with distilled water at a 1 : 3 ratio. The mixture was placed in a water bath and boiled for 30 min [18]; the extract was filtered and centrifuged at 20,000 g for 60 min; the supernatant was collected and used for the synthesis of nanoparticles.

Isolation of predominant fractions of the plant extract

The aqueous lavender extract was investigated using analytical chromatography. Chromatograms of the aqueous lavender plant and callus extracts were analyzed at three wavelengths (214, 280, and 320 nm). The fractions corresponding to the maximum peaks (denoted by numbers in *Fig. 5A*) where dried using a lyophilizer and dissolved in a RPMI-1640 medium supplemented with 10% fetal bovine serum and used to evaluate cytotoxicity.

Nanoparticle synthesis

Silver nanoparticles were prepared using "green" synthesis by mixing 50 μL of a silver nitrate solution in water (1 g/L) and 50 μL of either the lavender plant or callus extracts in a concentration range of 0.5% to 30%. During particle synthesis, absorption spectra at 350–800 nm were measured at four time points (30, 60, 150, and 240 min) using an Infinite M100 Pro plate reader (Tecan, Austria). The efficiency of NP synthesis was evaluated by the LSPR peak intensity. The surface plasmon resonance peak is considered to be a qualitative criterion for the presence of metallic NPs in a system [19, 20].

The morphology of the synthesized nanoparticles was investigated by scanning electron microscopy at an accelerating voltage of 10 kV on a MAIA3 Tescan microscope (Czech Republic).

Nanoparticle Modification

NPs were modified with bovine serum albumin (BSA) by sorption of the protein on the particle surface. The efficiency of NP modification was indirectly confirmed by measuring their hydrodynamic size. Particle size was determined by dynamic light scattering on a Zetasizer Nano ZS analyzer (Malvern Instruments, Ltd).

Analysis of cytotoxic properties

The cytotoxic properties of the plant extract, its predominant fractions, and extract-based NPs were analyzed before and after stabilization with BSA using a standard MTT test. The analysis was performed on cell lines of different origins: Chinese hamster ovary (CHO) cells, human breast adenocarcinoma (SK-BR-3), human ovarian adenocarcinoma (SKOV3-1ip), as well as on a SKOV-kat line transfected with the Katushka red fluorescent protein for intravital monitoring of malignant tumor development *in vivo* in model laboratory animals [21].

RESULTS AND DISCUSSION

Silver nanoparticles for biomedical applications were synthesized using an aqueous extract of the narrow-leaved lavender, which is an essential oil plant widely used in the food, cosmetics, and pharmaceutical industries. The use of lavender secondary metabolites (SMs) capable of reducing metal ions from their salts is a promising, environmentally safe way to create NPs with antibacterial and cytotoxic properties. A number of nanoparticles produced via reduction of metal ions possess surface plasmon resonance properties and, therefore, are capable of heating, which may be used in cancer theranostics for tissue hyperthermia.

Narrow-leaved lavender cell and tissue culture

During *in vitro* cultivation, narrow-leaved lavender seedlings were produced (*Fig. 1A*). Seed germination upon introduction into *in vitro* culture did not differ significantly from germination in the control sample and was 80.0 ± 19.6%, which indicated the efficiency of the chosen sterilization method.

Propagation of plants on the MS medium supplemented with 0.5 mg/L TDZ resulted in seedlings with a mean height of 6.4 ± 2.1 cm. There was multiple shoot growth, which is considered to be a good indicator of efficient increase in the plant vegetative mass. Also, 4% of the cuttings had spontaneous rhizogenesis; these plants did not need further replanting.

For rooting of the remaining plants, we used a medium with low macroelement contents, ¼ MS supplemented with 0.2 mg/L α-naphthylacetic acid; in this case, the rate of rhizogenesis was 90.7–93.3%. This stage of clonal micropropagation significantly increased the efficiency of root formation in previously produced plants.

The rate of callusogenesis in stem explants was 95–99%. The callus had a loose consistency and a light green hue (*Fig. 1B*). A callus with these properties may be further used to produce a plant cell suspension, which increases the yield of SMs in *in vitro* culture.

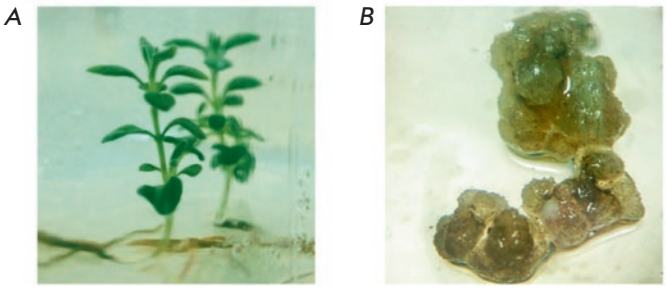

Fig. 1. Plants (A) and callus (B) of *Lavandula angustifolia* Mill., Munstead, produced in culture *in vitro*

Nanoparticle synthesis

Particles were produced by long-term incubation of a silver nitrate solution and lavender plant and callus extracts as described in the Experimental section. The efficiency of the synthesis of nanoparticles exhibiting a LSPR peak was quantitatively assessed by spectrophotometry, which enables identification of the LSPR peak and measurement of its intensity. The spectra of mixtures of the silver nitrate solution and lavender plant and callus extracts obtained at different time points (*Fig. 2*) demonstrate a monotonically increasing relationship between the NP sample absorbance at the LSPR peak wavelength and the extract concentration, as well as the silver salt and extract incubation time. The highest sample absorbance was observed for the synthesis using the plant extract (30%) at 240 min incubation and amounted to 0.82, which was 1.6-fold higher than a similar indicator for the callus extract (*Fig. 2*). Further, a 7.5% extract was used for NP synthesis, because a rather intense plasmon resonance peak was observed at this concentration, confirming the formation of nanostructures; also, silver salt excess was maintained in the solution.

Further, NP colloidal stability was studied. The particles showed aggregation and sedimentation stability in phosphate-buffered saline for a long time (monitoring duration was 3 months) without any surface modification, which is considered to be a good indicator for the chosen synthesis method. It should be noted that metal particles in most cases require additional treatment with various stabilizers (sodium citrate, proteins, PEG, and other polymers) to provide colloidal stability in buffer solutions. The synthesized NPs may be used for subsequent modification by biologically active molecules, in particular by polypeptides recognizing cancer cells (antibodies, scaffolds), which require long-term storage in saline solutions.

Processing of electron microscopy images yielded the mean size of nanoparticles: 35.4 ± 1.6 nm in synthe-

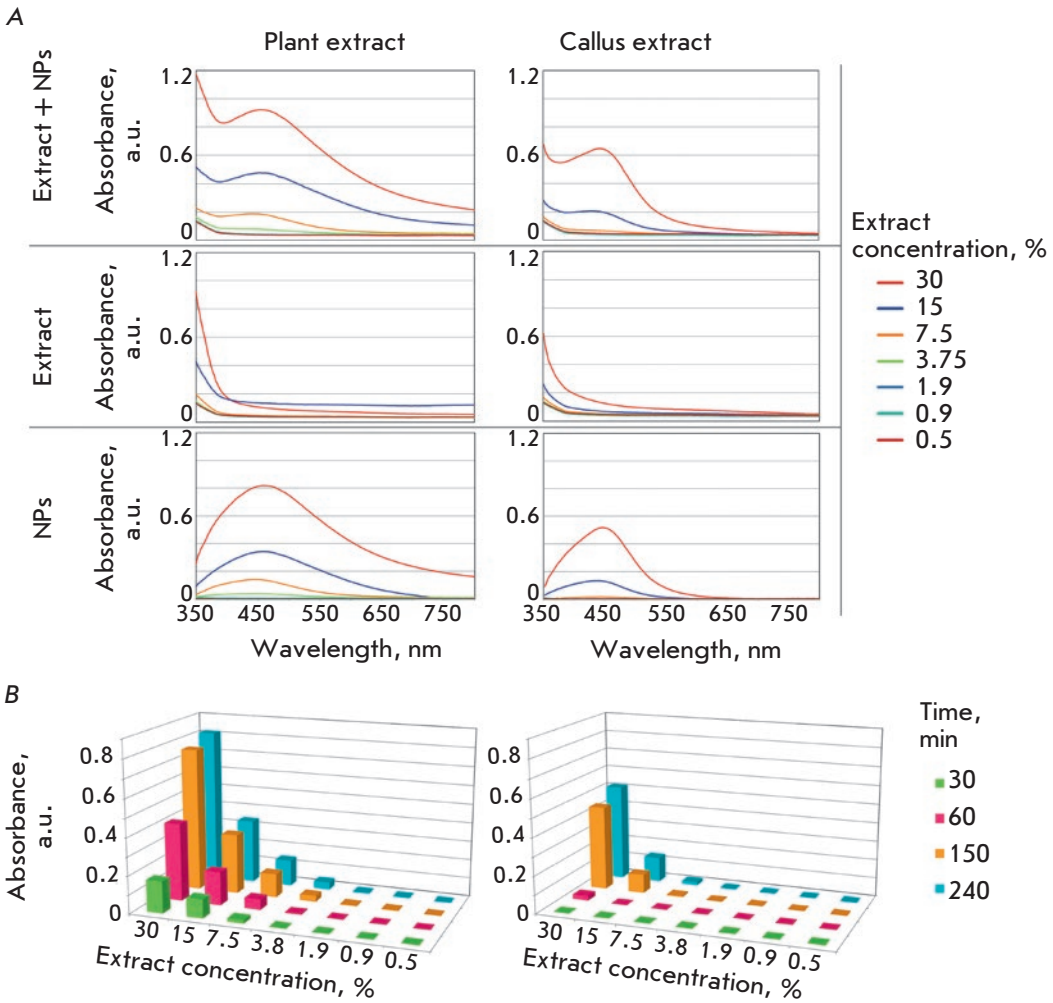

Fig. 2. Analysis of the nanoparticle synthesis efficiency. *A* – absorption spectra of an extract and nanoparticle mixture (top panels), an extract (middle panels), and nanoparticles (bottom panels) in a range of 350–800 nm, which were produced during 240 minute incubation of an aqueous silver nitrate solution (1 g/L) and plant (left panels) or callus (right panels) extracts at 0.5–30% concentrations (shown in colors). *B* – intensity of LSPR peaks during the synthesis of silver NPs, depending on the concentrations of plant (left panel) and callus (right panel) extracts and the time of incubation (shown in colors) of extracts and an aqueous silver nitrate solution (1 g/L)

sis with the plant extract and 56.4 ± 2.4 nm in synthesis with the callus extract (*Fig. 3B*). The NPs were mostly rounded, but some callus extract-based particles had a tetrahedron or a more complex polyhedron shape (*Fig. 3A*).

It should be noted that the size of the NPs used *in vivo* is of great importance, because it controls nanoparticle properties and affects their penetration through the blood-brain barrier [22–24].

Therefore, during the synthesis of nanoparticles, it is necessary to consider all the parameters controlling their size, as well as be capable of affecting these parameters to produce optimal size nanoparticles for successful penetration into the cell.

In further experiments, we used silver NPs produced using the plant extract, because they exceeded callus extract-based NPs in all aspects — they had a higher SPR peak intensity, a smaller size, and a more stable shape. Because application of nanoparticles for cancer theranostics purposes implies modification of their surface by various substances (antibodies, affibodies, etc.), which significantly affects the final hydrodynamic size, nanoparticles with a smaller mean diameter were chosen for the experiments.

Analysis of NP cytotoxic properties

To elucidate the prospects of synthesized NPs for various biomedical applications, in particular for cancer theranostics, we investigated the biocompatibility of these NPs in culture *in vitro*. A standard MTT test was used to study the effect of plant extract-based NPs and extract fractions that may affect the cytotoxicity of both the extract and the NPs.

According to the MTT test (*Fig. 4A*), synthesized unmodified nanoparticles were more cytotoxic against CHO and SK-BR-3 cell lines than they were against

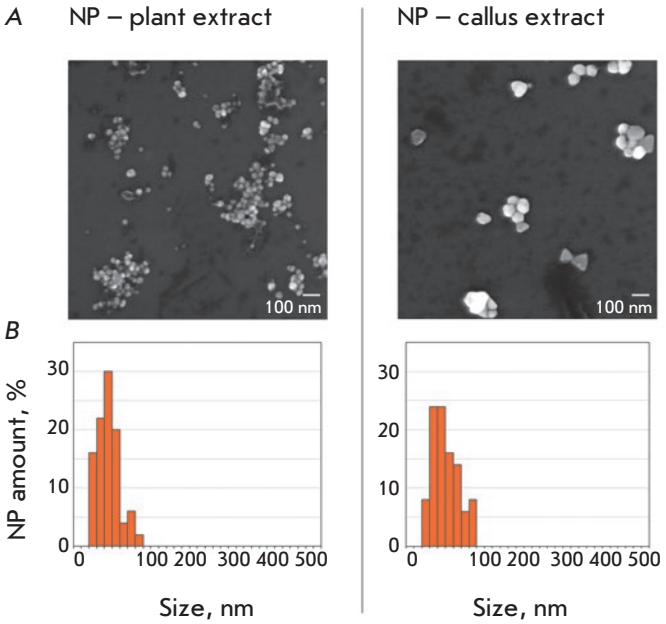

Fig. 3. Morphological analysis of silver nanoparticles. *A* – scanning electron microscopy microphotographs of nanoparticles at an accelerating voltage of 10 kV on a MAIA3 Tescan microscope (Czech Republic). *B* – NP size distribution histograms

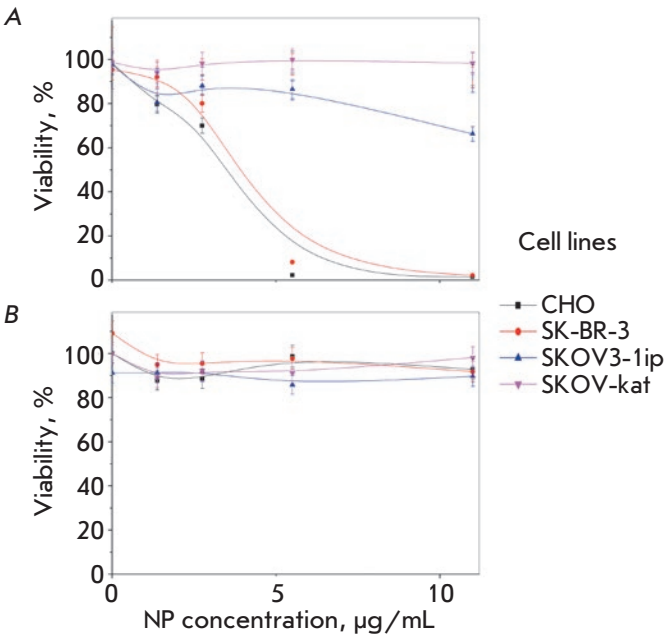

Fig. 4. Analysis of silver nanoparticle cytotoxicity by the MTT-test. Cell viability dependence (%) for CHO, SK-BR-3, SKOV3-1ip, and SKOV-kat lines (shown in colors) on the content of silver nanoparticles in the culture medium (μg/mL) before (*A*) and after (*B*) nanoparticle stabilization with bovine serum albumin (BSA)

SKOV3-1ip. Unmodified NPs did not affect the viability of SKOV-kat cells.

The effect of the plant extract and its main fractions isolated by analytical chromatography on CHO and SK-BR-3 cell lines was evaluated using the MTT test. The fractions corresponding to the highest absorbance peaks at λ = 280 nm (*Fig. 5A*) were isolated. Given the data presented in *Fig. 5A*, we supposed that the cytotoxicity of the produced NPs towards these cell lines was due to the presence of biologically active substances on the NP surface; namely, secondary metabolites from the plant extract used in their synthesis. To test this hypothesis, we analyzed the cytotoxic effect of both a 1% extract and its fractions, dried and dissolved in the growth medium. According to the MTT test (*Fig. 5B*), fractions 2 and 6 exhibited significantly greater cytotoxicity towards the SK-BR-3 line but had no effect on the viability of the CHO line. Fractions 3, 9, and 12 had the opposite effect. The highest cytotoxic effect on both cell lines was exerted by the extract itself, as well as by fractions 5, 7, 10, and 11, with the effect on the viability of the SK-BR-3 cell line being more pronounced. Therefore, we may suggest that the cytotoxic properties of the plant extract and, probably, the cytotoxic properties of NPs are determined mainly by fractions 5, 7, 10, and 11.

Because NPs exerted a cytotoxic effect on some cell lines, we suggest that blockage of the particle surface with a biocompatible protein may reduce this effect. Bovine serum albumin (BSA) not affecting cell viability was chosen as a blocking protein.

The diameter of the particles after stabilization with BSA increased by 71.9 nm, on average. According to the MTT test results in culture *in vitro*, the BSA-modified nanoparticles had no cytotoxic effect on all studied cell lines (*Fig. 4B*). These findings suggest that BSA shields the surface of NPs, thereby blocking their cytotoxicity.

CONCLUSION

Colloidally stable silver nanoparticles were produced by "green" synthesis using aqueous plant and callus extracts of the narrow-leaved lavender. We selected conditions for the synthesis of NPs stable in phosphate-buffered saline, which had a size of 35.4 ± 1.6 nm, optimal for application in cancer ther-

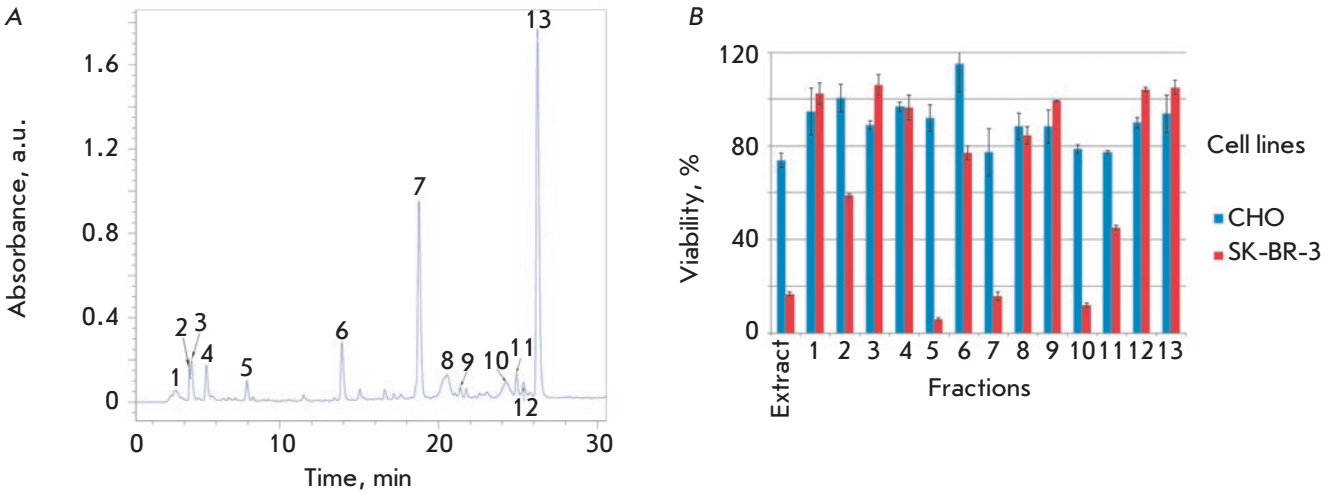

Fig. 5. Analysis of plant extract cytotoxicity. *A* – plant extract chromatogram (λ = 280 nm). Numbers denote the absorption peaks corresponding to the predominant fractions obtained from the extract. *B* – cytotoxicity analysis of the plant extract and its predominant fractions by the MTT-test. Dependence of the viability (%) of the CHO and SK-BR-3 cell lines (shown in colors) on the contents of the plant extract and its predominant fractions (1–13) in the medium

anostics. NPs were characterized by spectrophotometry, dynamic light scattering, and scanning electron microscopy. The cytotoxic properties of the plant extract-based particles were studied. Blockage of the NP surface with BSA was demonstrated to completely inhibit their cytotoxic effect *in vitro*. The produced NPs have a set of properties that predetermine the prospects of their use for the development of multifunctional agents combining diagnostic and therapeutic functions. ●

This study was supported by a grant of the Russian Science Foundation (project No. 19-14-00112) and the MEPhI Academic Excellence Project (Contract No. 02.a03.21.0005).

REFERENCES

1. Bazak R., Houri M., El Achy S., Kamel S., Refaat T. // J. Cancer Res. Clin. Oncol. 2015. V. 141. № 5. P. 769–784.
2. Guryev E.L., Volodina N.O., Shilyagina N.Y., Gudkov S.V., Balalaeva I.V., Volovetskiy A.B., Lyubeshkin A.V., Sen' A.V., Ermilov S.A., Vodeneev V.A., et al. // Proc. Natl. Acad. Sci. USA. 2018. V. 115. № 39. P. 9690–9695.
3. Nikitin M.P., Shipunova V.O., Deyev S.M., Nikitin P.I. // Nat. Nanotechnol. 2014. V. 9. P. 716–722.
4. Shipunova V.O., Zelepukin I.V., Stremovskiy O.A., Nikitin M.P., Care A., Sunna A., Zvyagin A.V., Deyev S.M. // ACS Appl. Mater. Interfaces. 2018. V. 10. № 20. P. 17437–17447.
5. Zelepukin I.V., Shipunova V.O., Mirkasymov A.B., Nikitin P.I., Nikitin M.P., Deyev S.M. // Acta Naturae. 2017. V. 9. № 14. P. 58–65.
6. Abramenko N.B., Demidova T.B., Abkhalimov E.V., Ershov B.G., Krysanov E.Yu., Kustov L.M. // J. Hazardous Materials. 2018. V. 347. P. 89–94.
7. Deyev S., Proshkina G., Ryabova A., Tavanti F., Menziani M.C., Eidelshtein G., Avishai G., Kotlyar A. // Bioconjugate Chem. 2017. V. 28. № 10. P. 2569–2574.
8. Tregubov A.A., Nikitin P.I., Nikitin M.P. // Chem. Rev. 2018. V. 118. № 20. P. 10294–10348.
9. Sharma V.K., Yngard R.A., Lin Y. //Adv. Colloid Interface Sci. 2009. V. 145. P. 83–96.
10. Ghosh S., Patil S., Ahire M., Kitture R., Gurav D.D., Jabgunde A.M., Kale S., Pardesi K., Shinde V., Bellare J. // J. Nanobiotechnol. 2012. V. 10. № 17. P. 1–10.
11. Harris A.T., Bali R. // J. Nanoparticle Res. 2008. V. 10. № 4. P. 691–695.
12. Rai M., Yadav A. // IET Nanobiotechnol. 2013. V. 7. № 3. P. 117–124.
13. Ovais M., Khalil A.T., Raza A., Khan M.A., Ahmad I., Islam N.U., Saravanan M., Ubaid M.F., Ali M., Shinwari Z.K. // Nanomedicine. 2016. V. 11. № 23. P. 3157–3177.
14. Soundarrajan C., Sankari A., Dhandapani P., Maruthamuthu S., Ravichandran S., Sozhan G., Palaniswamy N. // Bioprocess. Biosyst. Eng. 2012. V. 35. № 5. P. 827–833.
15. Murashige I., Skoog F. // Physiol. Plant. 1962. № 15. P. 473–497.

16. All Union State Standard 30556-98. Seeds of essential oil crops. Methods for determination of germination.
17. Gonçalves S., Romano A. // Biotechnol. Adv. 2012. V. 6. P. 1–9.
18. Makarov V.V., Makarova S.S., Love A.J. // Langmuir. 2012. V. 28. P. 1–5.
19. Sotnikov D.V., Zherdev A.V., Dzantiev B.B. Detection of intermolecular interactions based on surface plasmon resonance registration // Progress in Biological Chemistry (Moscow). 2015. V. 80. P. 1820–1832.
20. Vasileva P., Donkova B., Karadjova I., Dushkin C. // Colloids Surfaces A: Physicochem. Eng. Aspects. 2011. V. 382. P. 203–210.
21. Zdobnova T., Sokolova E., Stremovskiy O., Karpenko D., Telford W., Turchin I., Balalaeva I., Deyev S. // Oncotarget. 2015. V. 6. № 31. P. 30919–30928.
22. Kelf T.A., Sreenivasan V.K., Sun J., Kim E.J., Goldys E.M., Zvyagin A.V. // Nanotechnology. 2010. V. 21. № 28. P. 1–8.
23. Xin H., Sha X., Jiang X., Chen L., Law K., Gu J., Chen Y., Wang X., Fang X. // Biomaterials. 2012. V. 33. № 5. P. 1673–1681.
24. Zhou Y., Peng Z., Seven E.S., Leblanc R.M. // J. Controlled Release. 2018. V. 270. P. 290–303.

Septin Polymerization Slows Synaptic Vesicle Recycling in Motor Nerve Endings

P. N. Grigoryev, G. A. Khisamieva and A. L. Zefirov*
Kazan State Medical University, Butlerova Str. 49, Kazan, 420012, Russia
*E-mail: zefiroval@rambler.ru
Received December 3, 2018; in final form, March 14, 2019
DOI: 10.32607/20758251-2019-11-2-54-62

ABSTRACT **Septins are GTP-binding proteins recognized as a component of the cytoskeleton. Despite the fact that septins are highly expressed by neurons and can interact with the proteins that participate in synaptic vesicle exocytosis and endocytosis, the role of septins in synaptic transmission and the synaptic vesicle recycling mechanisms is poorly understood. In this study, neurotransmitter release and synaptic vesicle exocytosis and endocytosis were investigated by microelectrode intracellular recording of end-plate potentials and fluorescent confocal microscopy in mouse diaphragm motor nerve endings during septin polymerization induced by forchlorfenuron application. It was shown that forchlorfenuron application reduces neurotransmission during prolonged high-frequency (20 and 50 pulses/s) stimulation. Application of pairs of short high-frequency stimulation trains showed that forchlorfenuron slows the replenishment of the readily releasable pool. Forchlorfenuron enhanced FM 1-43 fluorescent dye loading by synaptic vesicle endocytosis but decreased dye unloading from the preliminarily stained nerve endings by synaptic vesicle exocytosis. It was concluded that the septin polymerization induced by forchlorfenuron application slows the rate of synaptic vesicle recycling in motor nerve endings due to the impairment of synaptic vesicle transport.**
KEYWORDS **motor nerve ending, neurotransmitter release, synaptic vesicle cycle, septins, forchlorfenuron.**
ABBREVIATIONS **EPP – end-plate potential; FCF – forchlorfenuron.**

INTRODUCTION

Neurotransmitters are secreted in a chemical synapse via exocytosis during the fusion between the membrane of a synaptic vesicle loaded with a neurotransmitter and the presynaptic membrane. This process takes place within specialized structures (active zones) upon opening of Ca^{2+} channels of the presynaptic membrane. A portion of the neurotransmitter released during exocytosis of an individual synaptic vesicle is known as a quantum. The reserve of synaptic vesicles is depleted during neurotransmitter release and replenished during endocytosis and vesicular transport. The presynaptic membrane gives rise to new vesicles, which are loaded with a neurotransmitter, delivered to the active zones, and again used in secretion (the recycling mechanism). A combination of exocytosis, endocytosis, and synaptic vesicle transport constitutes the synaptic vesicle cycle, an important presynaptic mechanism that ensures efficient long-term neurotransmitter release by a neuron. Synaptic vesicles in motor nerve endings are known to be functionally diverse and form several vesicle pools. The readily releasable pool consists of vesicles located in close proximity to the active zone. This pool is limited in size and depletes rather rapidly. It is efficiently replenished by synaptic vesicles from the recycling pool, which are formed from the presynaptic membrane via endocytosis (the short recycling pathway). Synaptic vesicles that constitute the large reserve pool and are formed on the surface of nerve terminal endosomes may be involved in secretion upon prolonged high-frequency neural activity (the long recycling pathway) [1–3]. The mechanisms regulating the presynaptic vesicle cycle and vesicular transport are of great interest to researchers. The cytoskeleton comprising several dynamically polarizing/depolarizing components (actin filaments, intermediate filaments, microtubules, and septins) can be one of these mechanisms.

Septins are the least-studied cytoskeletal component and belong to the recently discovered conserved family of GTP-binding proteins [4]. Septins are involved in cellular processes, such as cell division, reorganization of other cytoskeletal components, and intracellular transport. By acting as a specific barrier, septins can separate specialized membrane regions from each other [5]. Thirteen septin types (denoted as SEPT1–SEPT12, SEPT14) are known in mammals [6]. They bind to each other to form heterooligomeric

complexes that can be polymerized into more complex structures (filaments, rings, and networks). SEPT3, SEPT5–7, and SEPT11 have been identified in mature nerve terminals [7]; however, their functions have not been studied sufficiently. Hence, SEPT5 and SEPT7 are involved in axonal [7] and dendritic [8, 9] growth. SEPT5, SEPT6, and SEPT3 were found to colocalize with synaptic vesicles [7, 10, 11]. It has also been demonstrated that septins interact with a number of the proteins involved in exocytosis: Munc-18-1, synapsin II, VAMP2, synaptophysin, synaptotagmin 1, NSF, Hsc70, etc. It has been suggested that dynamic reorganization of septins is needed for synaptic vesicle exocytosis and neurotransmitter release [12–15]. Even less is known about the role played by septins in endocytosis and synaptic vesicle transport. The interaction of septins with the proteins taking part in endocytosis (clathrin, flotillin, and dynamin) [12, 16] and colocalization of septins and the cell membrane regions rich in phosphoinositol-4,5-bisphosphate, which are required for clathrin-dependent endocytosis [17, 18], imply that septins may be possibly involved in these processes.

Synaptic vesicle recycling upon stimulation of septin polymerization by forchlorfenuron (FCF) was evaluated by using a combination of the electrophysiological approach and confocal fluorescence microscopy. FCF selectively stimulates septin polymerization without affecting other cytoskeletal components (microtubules and actin filaments) and exhibits no cytotoxicity at concentrations up to 500 μM [19].

EXPERIMENTAL

Study object and solutions

Our experiments were performed using isolated neuromuscular specimens of mouse diaphragm. This study was conducted in compliance with the international guidelines for animal experiments. After isolation, the specimen was placed into a recording chamber and subjected to continuous perfusion using a solution for homeotherms with the following composition: NaCl, 125.0 mM; KCl, 2.5 mM; NaH_2PO_4, 1 mM; $CaCl_2$, 2 mM; $MgCl_2$, 1 mM; glucose, 11 mM; and $NaHCO_3$, 12 mM. The temperature and pH were maintained at a level of 24°C and 7.3–7.4, respectively. The perfusion solution was continuously saturated with carbogen (95%O_2/5%-CO_2). All the studies were performed only for the synapses located superficially. The motor nerve was stimulated with suprathreshold 0.2–0.3 ms rectangular pulses; the frequency of pulse trains was 0.2 pulses/s (low-frequency stimulation) or 20 and 50 pulses/s (high-frequency stimulation). Specimen contraction was suppressed using μ-conotoxin GIIIB (Peptide Institute, Inc, Japan) at a concentration of 1–2 μM. Septin polymerization was stimulated by adding forchlorfenuron (50 μM) to the perfusion solution for 40 min. All the substances except for μ-conotoxin GIIIB were purchased from Merch (Germany).

Electrophysiology

Single-quantum miniature end-plate potentials (MEPPs) spontaneously arising at rest and multi-quantum end-plate potentials (EPPs) arising in response to motor nerve stimulation were recorded using glass microelectrodes (tip diameter < 1 μm; resistance, 8–10 MΩ) filled with a 2.5 M KCl solution. A microelectrode was inserted into the muscle fiber close to the nerve ending under visual control. The resting membrane potential was controlled using a millivoltmeter. The experiments where changes in the resting membrane potential were > 5 mV were not taken into account. The signals were digitized using a La-2USB A-to-D card. Before applying high-frequency stimulation, 35–100 MEPPs and 7–10 EPPs under low-frequency stimulation were recorded. In order to analyze the number of quanta of the neurotransmitter released in response to each stimulus (the quantal content of EPPs), the amplitude of each recorded EPP and MEPP was normalized to a membrane potential level of -75 mV. The quantal content was calculated as a ratio between the EPP amplitude and the average MEPP amplitude, using correction for nonlinear summation [20, 21].

Fluorescence microscopy

Synaptic vesicle exocytosis and endocytosis were studied using a FM 1-43 fluorescent dye (SynaptoGreen C4, Merch) at a concentration of 6 μM. The dye reversibly binds to the presynaptic membrane and is entrapped by the newly emerging synaptic vesicles (is "loaded" into nerve endings) during endocytosis (after stimulation of exocytosis) [22, 23]. In this case, the bright fluorescence observed in the nerve ending demonstrated that the dye was captured by the synaptic vesicles that had undergone exocytosis and endocytosis [23]. Stimulation of exocytosis of pre-loaded vesicles caused the release ("unloading") of the dye from the nerve endings. Fluorescence was observed using a BX51W1 motorized microscope (Olympus, Germany) equipped with a DSU confocal scanning disc, a CoolLed pE-1 light-emitting diode lamp (CoolLed, UK), and an OrcaR2 CCD camera (Hamamatsu, Japan) connected to a PC using specialized Olympus Cell^P software. The optical equipment used to analyze the fluorescence of FM 1-43 consisted of a set of Olympus U-MNB2 light filters and an Olympus LUMPLFL60xw water immersion objective (1.0 NA). Fluorescence intensity was evaluated using the ImagePro software in arbitrary units (a.u.) as the average fluorescence of pixels in the image of a

nerve ending minus the background fluorescence. The background fluorescence was determined as the average fluorescence intensity in a square 50 pixels wide in the image region containing no nerve endings [24].

Statistical data analysis was performed using the Origin software (Origin Lab Corp.). The quantitative results of the study are shown as the mean ± standard error; n is the number of independent experiments. Statistical significance was estimated by ANOVA.

RESULTS

Neurotransmitter release during prolonged high-frequency stimulation in the presence of forchlorfenuron

It was established that a 40-min exposure to FCF caused no significant changes in the resting membrane potential of muscle fibers (-73.0 ± 2.8 mV, n = 20 and -71.7 ± 3.4, n = 20 in the control and test specimens; $p > 0.05$). Low-frequency stimulation resulted in a statistically insignificant reduction in the quantal content of EPPs (59.0 ± 5.8 quanta (n = 18) and 53.3 ± 4.7 quanta (n = 15) in the control and test specimens, respectively ($p > 0.05$)).

Prolonged (3-min) high-frequency stimulation of the control specimen at 20 pulses/s caused a three-phase reduction (depression) in the quantal content of EPP (*Fig. 1Aa*). An initial rapid decline down to 64.7 ± 4.1% (n = 9) of the baseline was observed during stimulation for 0.4 s. After a short plateau region lasting approximately 1.5–2 s, there was a second phase corresponding to a slow decline down to 54.2 ± 5.5% (n = 9) of the baseline by 15 s of stimulation. A further, even slower, decline reduced the quantal content of EPP down to 35.9 ± 6.5% (n = 9) of the baseline by 3 min of stimulation. Stimulation of the motor nerve at a higher frequency (50 pulses/s) for 2 min yielded similar three-phase dynamics of quantal content reduction, but depression of the neurotransmitter release was more pronounced (*Fig. 1Ba*). The initial rapid decline reaching 72.3 ± 3.0% (n = 9) of the baseline was no longer observed by approximately 0.16 s of stimulation. After the short plateau phase lasting 0.5–0.8 s, there followed a second reduction phase, which was characterized by

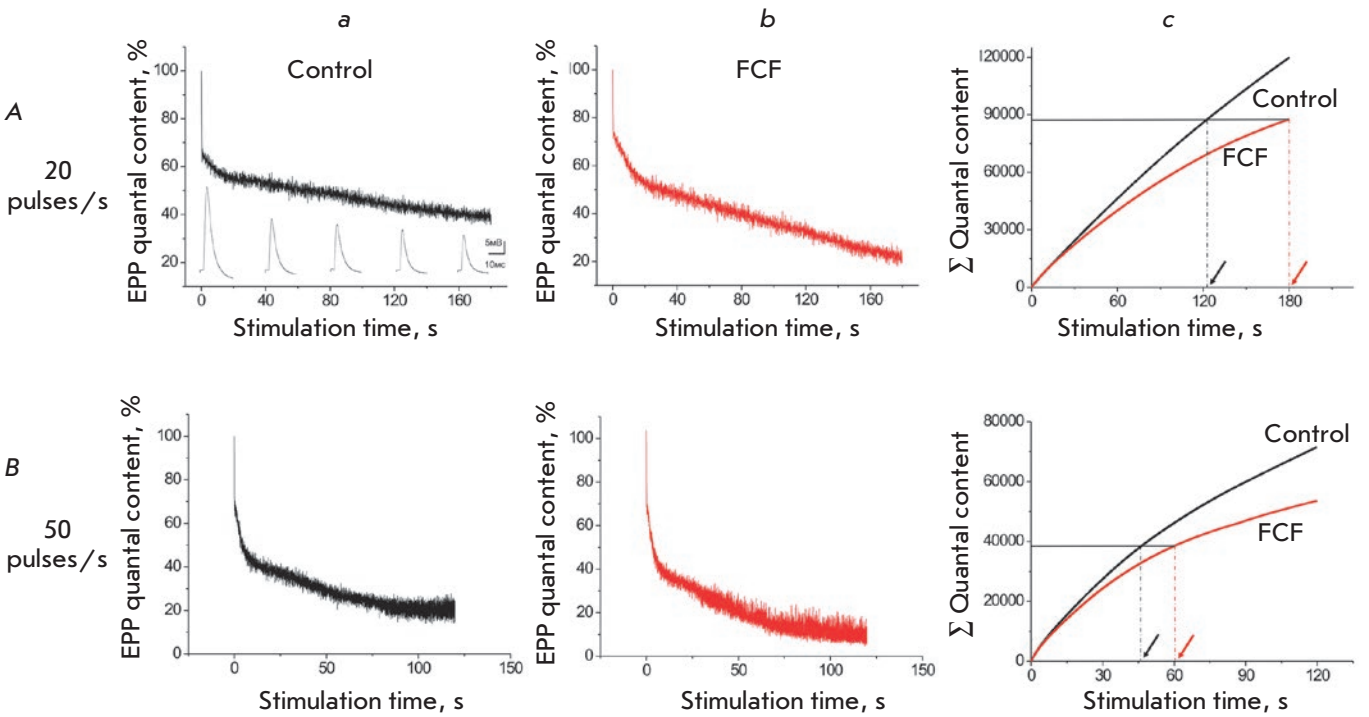

Fig. 1. Effect of forchlorfenuron on neurotransmitter release during high-frequency stimulation: *A* – the dynamics of EPP quantal content during prolonged high-frequency stimulation (20 pulses/s) in the control (a) and during FCF application (b). The initial quantal content was taken as 100 %. The averaged experimental data are presented (see the Results section). B – similar curves are shown for 50 pulses/s stimulation. *Ac* and *Bc* are the cumulative curves of released neurotransmitter quanta during high-frequency stimulation. Dotted lines indicate the stimulation time during which the same numbers of quanta are released in the control and during FCF application

slower decline kinetics. The third, even slower, phase started on the 5th second of stimulation. By the end of the 2nd minute of stimulation, the quantal content was at 22.7 ± 7.0% (n = 9) of the baseline.

No qualitative changes in the dynamics of decline in the quantal content of EPP were observed in the presence of FCF (there was a three-phase decline); however, the depression magnitude was deeper. During high-frequency stimulation (20 pulses/s, *Fig. 1Ab*), the quantal content of EPP decreased, down to 20.2 ± 6.8% (n = 7) of the baseline by the 3rd minute of stimulation. Upon stimulation at a frequency of 50 pulses/s, the decline in the quantal content of EPP was also more pronounced (*Fig. 1Bb*). By the end of the 2nd minute of stimulation, the quantal content in the test specimens had dropped down to 6.2 ± 3.6% (n = 9) of the baseline.

The cumulative curves showing the number of released neurotransmitter quanta revealed that the intensity of neurotransmitter release was statistically significantly reduced in the presence of FCF. Three-minute stimulation at a frequency of 20 pulses/s led to a release of 119,796 ± 8,161 quanta (n = 9) in the control specimens, while the neurotransmission after application of FCF was down by 27% (87,611 ± 9,025 quanta (n = 7), $p < 0.05$ (*Fig. 1Ac*). The two-minute stimulation at a frequency of 50 pulses/s resulted in a release of 71,505 ± 5,543 quanta (n = 9) in the control specimen; neurotransmission in the presence of FCF was lower by 25%: 53,553 ± 8,904 quanta (n = 9), $p < 0.05$ (*Fig. 1Bc*).

The deepened depression of neurotransmitter release upon high-frequency stimulation in the presence of FCF can be attributed to a suppression of mobilization (the replenishment rate of the readily releasable pool).

The replenishment rate of the readily releasable pool upon high-frequency stimulation in the presence of forchlorfenuron

In order to assess the replenishment rate of the readily releasable pool, we applied short (1 s) pulse trains at a frequency of 50 pulses/s, with different intervals between the trains (0.5, 3, and 60 s), to normal specimens and specimens in the presence of FCF [25]. In response to the first pulse train, the quantal content of EPP decreased abruptly during the first 6–8 pulses. Next, there followed a plateau (the quantal content remained at the same level) (*Figs. 2B,C*). Summation of the number of released quanta demonstrated that they were identical both in the control specimen and in the specimen exposed to FCF after the first pulse train (2,214 ± 192 (n = 12) and 2,205 ± 194 quanta (n = 12); $p > 0.05$). Therefore, the entire readily releasable pool (being ~1,700 quanta in mouse motor nerve terminals) was involved in secretion after the first pulse train [25, 26], while virtually not affecting the recycling pool (~ 80,000 quanta) [27]. A lower secretion level was observed for the second pulse train applied 0.5 and 3.0 s after the first one (*Figs. 2B,C*) because of the incomplete replenishment of the readily releasable pool. Thus, the total number of quanta released during the second pulse train in the control specimen and in the specimen exposed to FCF was 88.3 ± 1.0% (n = 12) and 83.9 ± 1.0% (n = 12), respectively, of the number of quanta released during the first pulse train ($p < 0.01$). When the interval between the pulse trains stood at 3 s, the number of quanta released was 93.0 ± 0.8% (n = 13) and 88.5 ± 1.2%, respectively (n = 13); $p < 0.01$. Therefore, neurotransmitter release in the specimen exposed to FCF was recovered much less efficiently than that in the control sample; the most significant changes were observed during the plateau phase (*Figs. 2B,C*). At high intervals between the pulse trains (60 s), secretion recovered completely: to 100.1 ± 1.0% (n = 12)) in the control specimens and 98.9 ± 0.7% (n = 12) in the specimens exposed to FCF. Taking into account that the average time of synaptic vesicle recycling in mouse motor nerve terminals is ~ 50 s [27], it is fair to assume that replenishment of the readily available pool during a short interval between pulse trains (0.5 and 3 s) occurs due to the recycling pool only, but not due to synaptic vesicle endocytosis. Therefore, application of FCF does not alter the readily releasable pool but slows its replenishment rate due to the recycling pool.

FM 1-43 loading into nerve terminals in the presence of forchlorfenuron

Aggravation of suppression of neurotransmitter release in response to prolonged high-frequency stimulation in the presence of forchlorfenuron (*Fig. 1*) can also be related to the disturbed synaptic vesicle endocytosis. We have attempted to test this assumption in experiments using the FM 1-43 fluorescent dye. It is known that the processes of synaptic vesicle endocytosis follow exocytosis at a 1 : 1 ratio. Therefore, special experimental conditions need to be created to evaluate endocytosis under which the levels of neurotransmitter release are identical in the control and test (FCF application) series and identical numbers of vesicles undergo exocytosis. An analysis of the cumulative curves of neurotransmitter release (*Fig. 1Ac*) demonstrated that the numbers of neurotransmitter quanta released in response to a 2- and 3-min stimulation of the control and test specimens at a frequency of 20 pulses/s were almost identical. These stimulation times were used to study FM 1-43 loading. If the endocytosis processes are not affected, one can expect the degree of dye loading and fluorescence intensity to be identical. However, the fluorescence intensity in the nerve terminals in

the presence of FCF was much higher than that in the control specimens: 71.6 ± 2.7 a.u. (n = 123) and 54.1 ± 2.3 a.u. (n = 123), respectively; $p < 0.01$ (*Fig. 3A*). Stimulation at a higher frequency (50 pulses/s) lasting 45 s in the control series and 1 min in the test series (the number of released quanta are also equal under these conditions (*Fig. 1Bc*)) resulted in a statistically higher fluorescence intensity in the specimens exposed to FCF (42.9 ± 2.1 a.u. ((n = 125)) compared to that in the control specimens (37.0 ± 1.7 a.u. (n = 125); $p < 0.05$) (*Fig. 3A*). Therefore, stimulation of septin polymerization by FCF increased the number of dye-loaded vesicles in the nerve terminal.

Unloading FM 1-43 from the nerve terminals in the presence of forchlorfenuron

In this experimental series, we evaluated the effect of FCF on synaptic vesicle exocytosis. At the first stage, all the specimens were loaded with FM 1-43. For this purpose, we applied a prolonged 3-min stimulation of the motor nerve at a frequency of 20 pulses/s in a solution containing FM 1-43 [28]. The control specimens were then perfused with a standard solution, while the test specimens were perfused with a solution containing FCF. Prolonged high-frequency stimulation was applied 40 min later (*Fig. 3B*). The fluorescence intensity of the nerve terminal decayed efficiently as

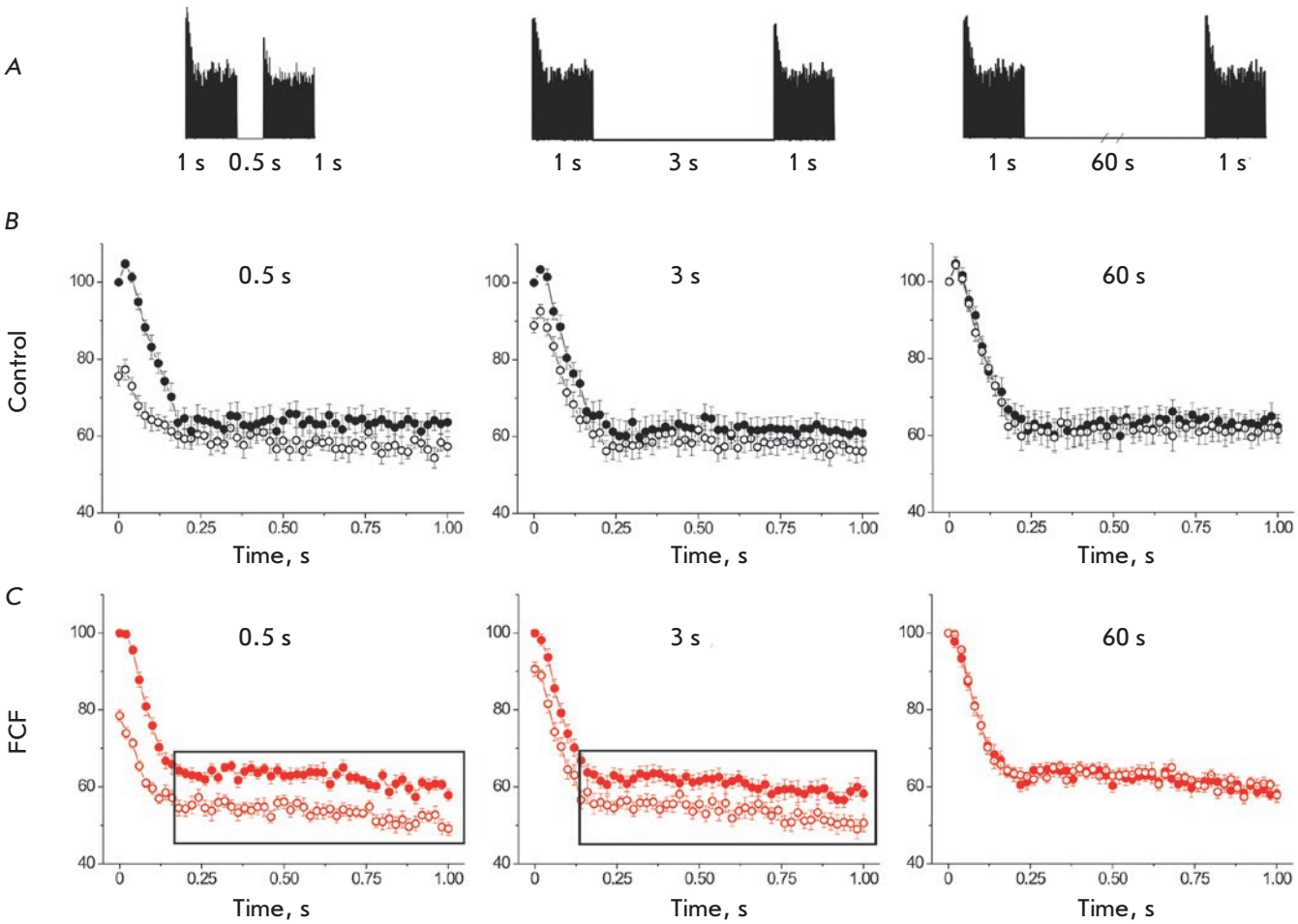

Fig. 2. Effect of forchlorfenuron on the replenishment of the readily releasable pool during high-frequency stimulation. *A* – The experimental scheme. Pairs of short (1 s) stimulation trains with a frequency of 50 Hz and a delay time of 0.5, 3 and 60 s between the first and the second train were given. *B* and *C* – The dynamics of neurotransmitter release during the first (dark circles) and the second (white circles) trains in the control and during FCF action. In each experiment, the value of the quantal content of the first EPP in the first train was taken as 100 %. It is noticeable that application of FCF leads to stronger depression of neurotransmitter release during the second stimulation train at delay times of 0.5 and 3 s than in the control experiments

the fluorescent dye was released, together with the neurotransmitter during synaptic vesicle exocytosis. It was found that the rate of dye unloading decreased in the specimens exposed to FCF. By the end of the 1st minute of stimulation at a frequency of 20 pulses/s, the fluorescence intensity in the control and test specimens had decreased to 78.9 ± 1.0 % (n = 8) and 77.3 ± 1.3% (n = 10) ($p > 0.05$) of the baseline, respectively; after a 10-min stimulation, it had decreased to 22.7 ± 2.2 % (n = 8) and 36.0 ± 3.5% (n = 10) ($p < 0.05$) of the baseline, respectively (*Fig. 3B*). After a 1-min stimulation at a frequency of 50 pulses/s, the fluorescence intensity in the control and test specimens was 63.2 ± 2.3 % (n = 11) and 68.2 ± 1.8% (n = 11) ($p > 0.05$) of the baseline, respectively. After a 10-min stimulation, it decreased to 28.3 ± 1.8% (n = 11) and 34.7 ± 2.3% (n = 11) ($p < 0.05$) of the baseline, respectively (*Fig. 3B*). One can observe that statistically significant differences between the control and test curves recorded during stimulation at frequencies of 20 and 50 pulses/s were observed only after 1.5–2.5 min of stimulation. The deceleration of dye unloading demonstrates that the transport rate of the vesicles of the recycling and possibly the reserve pools to the secretion sites in the active zones decreased after the exposure to FCF.

DISCUSSION

Like other cytoskeletal components, septins are present in the cell in the polymerized and depolymerized forms. Polymerized septins form near the cytoplasmic membrane [29]; therefore, one can expect them to be directly involved in the regulation of the processes of the synaptic vesicle cycle taking place near the presynaptic membrane. Application of forchlorfenuron is one of the most potent and convenient tools that can be used to study the septin function. The effects of FCF and other methods used to impair septin function (application of small interfering RNA and transgenic animals) were shown to be identical in studies focused on various cellular mechanisms [12; 30–34].

Septins in neurotransmitter release and synaptic vesicle exocytosis

The role played by septins in the regulation of exocytosis and neurotransmitter release is rather controversial. Thus, it had been assumed that SEPT8 facilitates exocytosis by separating the complex of vesicular proteins VAMP2/synaptophysin. These proteins further interact with SNAP25, and the SNARE complex assembly takes place [14]. Meanwhile, it was discovered that polymerized SEPT5 can form a physical barrier within the active zones, which hinders synaptic vesicle exocytosis and can affect the distance between a calcium channel and a synaptic vesicle [10]. Knockout mice unable to express SEPT4 exhibited lower levels of neurotransmitter release [35]. The disturbed function of the ubiquitously expressed septin variant SEPT2 revealed that exocytosis was altered [12]. Meanwhile, no significant alterations in neurotransmitter release were detected in mice unable to express SEPT5 and SEPT3 [36]. It was demonstrated that stimulation of septin polymerization by FCF reduces the intensities of synchronous, asynchronous, and spontaneous neurotransmitter release in mouse motor neurons [12]. We also detected that application of FCF causes a less pronounced but equivocal decrease in the quantal content. These differences are possibly related to the fact that different durations of exposure to FCF and non-identical extracellular calcium concentrations were used. It is known that higher concentrations or exposure durations potentiate the effect of forchlorfenuron [19]. We used an exposure duration of 40 min, while Tokhtaeva et al. [12] applied a longer exposure duration (1 h). This could be the reason why we observed a weaker effect of stimulation of septin polymerization on the function of SNARE proteins.

Septins and synaptic vesicle endocytosis

The intensity of fluorescent dye loading and fluorescence of nerve endings after exposure to FCF was much higher than that in the control specimens, while the intensities of neurotransmitter secretion were identical (and exocytosis was identical as well) (*Fig. 3A*). In other words, the number of stained vesicles per nerve ending was greater. These data could have been interpreted as enhancement of synaptic vesicle endocytosis. However, this conclusion can be drawn only if vesicles loaded with the dye were repeatedly engaged in neurotransmitter release at the same rate. An analysis of the curves of dye unloading (*Fig. 3B*) demonstrated that stimulation at frequencies of 20 and 50 pulses/s reduced the rate of release of the pre-loaded FM 1-43 fluorescent dye. This fact indicates that delivery of dye-loaded vesicles to the secretion sites has been slowed down rather than that endocytosis has been enhanced. Meanwhile, the divergence between the curves of unloading dynamics during the first several minutes of recording was not sufficiently significant to be able to independently cause a reduction in the number of released neurotransmitter quanta of 25–27% in the presence of FCF. Therefore, disruption of transport and recycling of the synaptic vesicles formed by endocytosis immediately during high-frequency stimulation can be regarded as another explanation to the reduction in the neurotransmitter release upon septin polymerization. This can also be supported by the revealed enhanced loading of the FM 1-43 fluorescent dye (*Fig. 3A*). Thus, in the control specimens, a vesicle

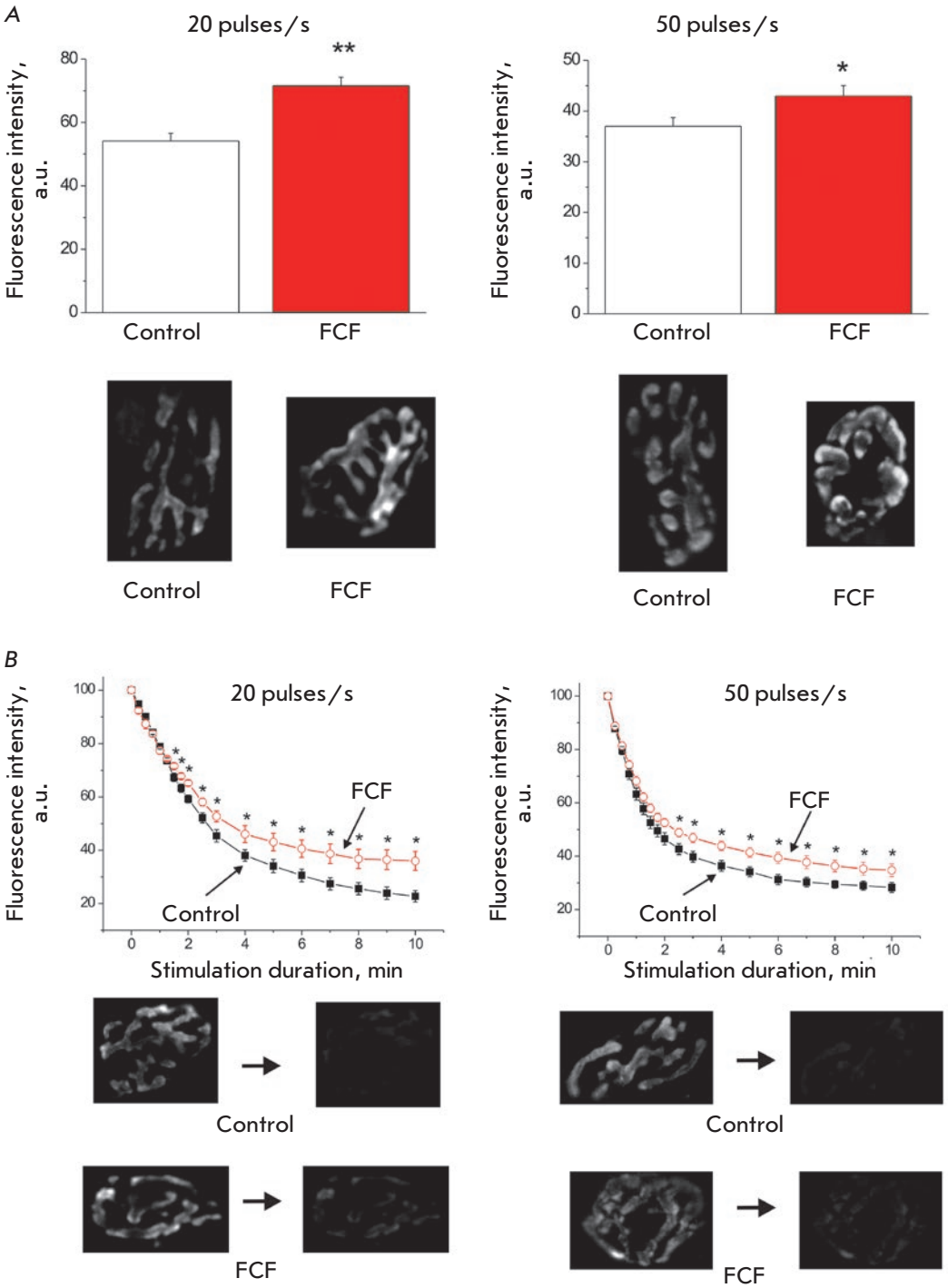

Fig. 3. Effect of forchlorfenuron on FM 1-43 loading and unloading during high-frequency stimulation. *A* – Fluorescence intensity of nerve endings loaded with FM 1-43 at high-frequency stimulation (20 and 50 pulses/s) in the control and during FCF application in case of equal neurotransmitter release (described in details in the Results section). The fluorescence images of nerve endings from individual experiments are shown below. *B* – The dynamics of fluorescence intensity decay (dye unloading) of preliminarily stained nerve endings in the control (black squares) and upon FCF action (white circles) during high-frequency stimulation (20 and 50 pulses/s). In each experiment, the initial nerve ending fluorescence was taken as 100 %. Fluorescence images of nerve endings from individual experiments before and at the end of stimulation are shown below

population is repeatedly involved in exocytosis and releases FM 1-43, along with the neurotransmitter, while the number of synaptic vesicles carrying the dye in a nerve ending becomes lower than the expected value after high-frequency stimulation. Exposure to FCF reduces the percentage of vesicles repeatedly involved in secretion because of the impaired transport of synaptic vesicles that newly emerges during endocytosis. As a result, the number of synaptic vesicles loaded with the fluorescent dye in the presence of FCF is higher than that in the control, which is the reason why the FM 1-43 fluorescence in the presence of FCF is brighter (*Fig. 3A*). Meanwhile, exposure to FCF can also impair the endocytosis mechanism and the entire process can

be slowed down. The histochemical data demonstrating that SEPT3 is substantially colocalized with dynamin indicate that septins can potentially be involved in synaptic vesicle endocytosis [37]. Other septins, SEPT5 and SEPT9, were also found to interact with dynamin [16].

Septins and synaptic vesicle transport

In the beginning of prolonged high-frequency stimulation, vesicles from the readily releasable and recycling pools take part in the neurotransmitter release. Later (after several dozen seconds), the newly emerging vesicles can be repeatedly involved in secretion. To ensure this, a new synaptic vesicle needs to form via endocytosis, be loaded with a neurotransmitter, get into the recycling pool, and subsequently replenish the readily releasable pool via mobilization. In other words, the vesicle transport route consists of two components: the recycling pool - readily releasable pool and the endocytosis - recycling pool. In all likelihood, septins ensure the functioning of both components. The electrophysiological data demonstrating a reduced replenishment rate of the readily releasable pool after high-frequency stimulation indicate that vesicle transport to the active zones is less efficient upon septin polymerization (*Fig. 2*). The data on enhanced loading and slowed-down unloading of FM 1-43 indicate that vesicle transport from the endocytosis sites is suppressed (*Figs. 3A,B*).

Involvement of septins in the functioning of the actomyosin motor can be considered a mechanism through which they participate in synaptic vesicle transport. It was established that septins can interact with actin [38] and nonmuscle myosin II [39], which take part in synaptic vesicle transport [40–42]. The ability of polymerized septins to form barriers impeding synaptic vesicle transport is one of the mechanisms that explain why the intracellular transport is impaired [5, 10].

CONCLUSIONS

Hence, our findings demonstrate that septins are involved in the processes of synaptic vesicle cycle and synaptic vesicles reuse in neurotransmitter release during prolonged high-frequency activity of a neuromuscular junction. ●

This work was supported by the Russian Foundation for Basic Research (grant no. 17-04-01870-a) and the Russian Science Foundation (grant no. 14-15-00847-P) (in the part of conducting the experimental modeling of disruption of synaptic vesicle recycling).

REFERENCES

1. Gan Q., Watanabe S. // Front. Cell Neurosci. 2018. V. 12. Article 171.
2. Zefirov A.L. // Ross Fiziol Zh Im I M Sechenova. 2007. V. 93. № 5. P. 544–562.
3. Rizzoli S.O., Betz W.J. // Nat. Rev. Neurosci. 2005. V. 6. № 1. P. 57–69.
4. Byers B., Goetsch L. // J. Cell. Biol. 1976. V. 69. P. 717–721.
5. Mostowy S., Cossart P. // Nat. Rev. Mol. Cell. Biol. 2012. V. 13. № 3. P. 183–194.
6. Hall P.A., Russell S.E. // J. Pathol. 2004. V. 204. P. 489–505.
7. Tsang C.W., Estey M.P., DiCiccio J.E., Xie H., Patterson D., Trimble W.S. // Biol. Chem. 2011. V. 392. № 8–9. P. 739–749.
8. Tada T., Simonetta A., Batterton M., Kinoshita M., Edbauer D., Sheng M. // Curr. Biol. 2007. V. 17. № 20. P. 1752–1758.
9. Xie Y., Vessey J.P., Konecna A., Dahm R., Macchi P., Kiebler M.A. // Curr. Biol. 2007. V. 17. № 20. P. 1746–1751.
10. Yang Y.M., Fedchyshyn M.J., Grande G., Aitoubah J., Tsang C.W., Xie H., Ackerley C. A., Trimble W.S., Wang L.Y. // Neuron. 2010. V. 67. P. 100–115.
11. Kinoshita A., Noda M., Kinoshita M. // J. Comp. Neurol. 2000. V. 428. № 2. P. 223–239.
12. Tokhtaeva E., Capri J., Marcus E.A., Whitelegge J.P., Khuzakhmetova V., Bukharaeva E., Deiss-Yehiely N., Dada L.A., Sachs G., Fernandez-Salas E., et al. // J. Biol. Chem. 2015. V. 290. № 9. P. 5280–5297.
13. Beites C.L., Campbell K.A., Trimble W.S. // Biochem. J. 2005. V. 385. Pt 2. P. 347–353.
14. Ito H., Atsuzawa K., Morishita R., Usuda N., Sudo K., Iwamoto I., Mizutani K., Katoh-Semba R., Nozawa Y., Asano T., Nagata K. // J. Neurochem. 2009. V. 108. № 4. P. 867–880.
15. Khuzakhmetova V., Nurullin L., Bukharaeva E. // BioNanoSci. 2016. V. 6. P. 249–251.
16. Maimaitiyiming M., Kobayashi Y., Kumanogoh H., Nakamura S., Morita M., Maekawa S. // Neurosci. Lett. 2013. V. 534. P. 322–326.
17. Zhang J., Kong C., Xie H., McPherson P.S., Grinstein S., Trimble W.S. // Curr. Biol. 1999. V. 9. P. 1458–1467.
18. Krauss M., Haucke V. // Rev. Physiol. Biochem. Pharmacol. 2011. V. 161. P. 45–66.
19. Hu Q., Nelson W.J., Spiliotis E.T. // J. Biol. Chem. 2008. V. 283. № 43. P. 29563–29571.
20. del Castillo J., Katz B. // J. Physiol. 1954. V. 124. P. 560–573.
21. McLachlan E.M., Martin A.R. // J. Physiol. 1981. V. 311. P. 307–324.
22. Betz W.J., Bewick G.S., Ridge R.M. // Neuron. 1992. V. 9. № 5. P. 805–813.
23. Zefirov A.L., Grigoryev P.N., Petrov A.M., Minlebaev M.G., Sitdikova G.F. // Tsitologiia. 2003. V. 45. № 12. P. 1163–1171.
24. Zefirov A.L., Abdrakhmanov M.M., Mukhamedyarov M.A., Grigoryev P.N. // Neuroscience. 2006. V. 143. № 4. P. 905–910.
25. Ruiz R., Cano R., Casanas J.J., Gaffield M.A., Betz W.J., Tabares L. // J. Neurosci. 2011. V. 31. № 6. P. 2000–2008.
26. Zefirov A.L. // Bull. Exp. Biol. Med. 1985. V. 98. № 5. P. 1462–1465.
27. Zefirov AL, Zakharov AV, Mukhametzianov RD, Petrov AM, Sitdikova GF. // Ross Fiziol Zh Im I M Sechenova. 2008. V. 94. № 2. P.129–141.
28. Grigoryev P.N., Zefirov A.L. // Acta Naturae. 2015. V. 7. № 3. P. 81–88.

29. Bridges A.A., Zhang H., Mehta S.B., Occhipinti P., Tani T., Gladfelter A.S. // Proc. Natl. Acad. Sci. USA. 2014. V. 111. № 6. P. 2146–2151.
30. Vagin O., Tokhtaeva E., Garay P. E., Souda P., Bassilian S., Whitelegge J.P., Lewis R., Sachs G., Wheeler L., Aoki R., et al. // J. Cell. Sci. 2014. V. 127. P. 3294–3308.
31. Wasik A.A., Polianskyte-Prause Z., Dong M.Q., Shaw A.S., Yates J.R. 3rd, Farquhar M. G., Lehtonen S. // Mol. Biol. Cell. 2012. V. 23. P. 3370–3379.
32. Ghossoub R., Hu Q., Failler M., Rouyez M.C., Spitzbarth B., Mostowy S., Wolfrum U., Saunier S., Cossart P., Jamesnelson W., et al. // J. Cell. Sci. 2013. V. 126. P. 2583–2594.
33. Kim S.K., Shindo A., Park T.J., Oh E.C., Ghosh S., Gray R.S., Lewis R.A., Johnson C.A., Attie-Bittach T., Katsanis N., et al. // Science. 2010. V. 329. P. 1337–1340.
34. Mostowy S., Danckaert A., Tham T.N., Machu C., Guadagnini S., Pizarro-Cerdá J., Cossart P. // J. Biol. Chem. 2009. V. 284. P. 11613–11621.
35. Ihara M., Yamasaki N., Hagiwara A., Tanigaki A., Kitano A., Hikawa R., Tomimoto H., Noda M., Takanashi M., Mori H., et al. // Neuron. 2007. V. 53. № 4. P. 519–533.
36. Tsang C.W., Fedchyshyn M., Harrison J., Xie H., Xue J., Robinson P.J., Wang L.Y., Trimble W.S. // Mol. Cell. Biol. 2008. V. 28. № 23. P. 7012–7029.
37. Xue J., Tsang C.W., Gai W.P., Malladi C.S., Trimble W.S., Rostas J.A., Robinson P.J. // J. Neurochem. 2004. V. 91. № 3. P. 579–590.
38. Kinoshita M., Field C.M., Coughlin M.L., Straight A.F., Mitchison T.J. // Dev. Cell. 2002. V. 3. № 6. P. 791–802.
39. Joo E., Surka M.C., Trimble W.S. // Dev. Cell. 2007. V. 13. № 5. P. 677–690.
40. Miki T., Malagon G., Pulido C., Llano I., Neher E., Marty A. // Neuron. 2016. V. 91. № 4. P. 808–823.
41. Grigoryev P.N., Zefirov A.L. // Dokl. Biol. Sci. 2016. V. 470. № 1. P. 217–219.
42. Hayashida M., Tanifuji S., Ma H., Murakami N., Mochida S. // J. Neurosci. 2015. V. 35. № 23. P. 8901–8913.

The Role of Recombinant Human Cyclophilin A in the Antitumor Immune Response

A. A. Kalinina[1], Yu. Yu. Silaeva[2], D. B. Kazansky[1], L. M. Khromykh[1*]
[1]Federal State Budgetary Institution «N.N. Blokhin National Medical Research Center of Oncology» of the Ministry of Health of the Russian Federation, Kashirskoye Sh. 24, Moscow, 115478, Russia
[2]Federal State Budget Institution of Sciences «Institute of Gene Biology» Russian Academy of Sciences, Vavilova Str. 34/5, Moscow, 119334, Russia
*E-mail: lkhromykh@list.ru
Received February 13, 2019; in final form, May 13, 2019
DOI: 10.32607/20758251-2019-11-2-63-67

ABSTRACT **Cyclophilin A (CypA) is a multifunctional protein that exhibits an isomerase activity and exists in the intracellular and secretory forms. Secretory CypA promotes regeneration of the hematopoietic and the immune systems of an organism by stimulating stem cell migration from the bone marrow. New approaches based on CypA are currently being developed for the treatment of limb ischemia, neutralization of the side effects of Cyclosporine A (CsA) therapy, etc. However, the role of CypA in the antitumor immune response is still unexplored. In this work, we used the model experimental system of lymphoma EL-4 rejection in B10.D2(R101) mice and showed that recombinant human CypA (rhCypA) stimulates the antitumor immune response via early recruitment of granulocytes to the tumor cell localization site and rapid accumulation of effector T-killers.**
KEYWORDS **Cyclophilin A, pro-inflammatory factor, antitumor immune response, transgenic mice, T-cell receptor.**
ABBREVIATIONS **CypA – Cyclophilin A; rhCypA – recombinant human CypA; TCR – T-cell receptor; MHC – major histocompatibility complex; PBS – phosphate buffered saline; i.p. – intraperitoneal injection; APCs – antigen-presenting cells; CD – cluster of differentiation.**

INTRODUCTION

Cyclophilin A (CypA) is a member of the peptidyl-prolyl isomerase family and exists in the intracellular and secretory forms. Cytosolic CypA is detected in all tissues and has multiple functions [1]. This protein takes part in signal transduction through the T-cell receptor (TCR) [1]. Being a ligand for Cyclosporine A, the protein mediates its immunosuppressive action [1].

Secretory CypA is a pro-inflammatory factor that attracts innate immunity cells (granulocytes, macrophages, and dendritic cells) to the inflammation site and mediates the pathogenesis of various diseases [1]. The protein acts as a chemoattractant for stem cells, immature granulocytes, and the progenitors of dendritic cells, T- and B-lymphocytes; and induces the migration of these cells from the bone marrow to peripheral organs [2]. In this regard, CypA takes part in regenerative processes. CypA regulates the action of other chemokines and the production of pro-inflammatory cytokines [3]. CypA was shown to induce the differentiation and maturation of dendritic cells, and to enhance antigen uptake and presentation by these cells [4]. Hence, CypA can modulate both the innate and the adaptive immunity. A vast body of experimental data suggests the application of CypA in the treatment of viral diseases and limb ischemia, for neutralizing the side effects of Cyclosporine A, etc.

However, the role of CypA in the induction and development of the antitumor immune response remains poorly understood to date. The aim of the present study was to determine the functions of CypA in the early stages of the antitumor immune response. Here, we studied the effect of recombinant human CypA (rhCypA) on the rejection of lymphoma EL-4 cells in B10.D2(R101) mice. The immunomodulatory effect of rhCypA was identified, aimed at stimulating both the innate and the adaptive immune system. As a result, accelerated *in vivo* elimination of lymphoma cells was observed under rhCypA treatment. Moreover, it was shown using the model of antitumor immune response

to lymphoma EL-4 in transgenic 1D1b mice [5] that rhCypA stimulates the accumulation of tumor-specific cytotoxic T cells.

MATERIALS AND METHODS

Mice

C57BL/6 ($K^bI\text{-}A^bD^b$) and B10.D2(R101) ($K^dI\text{-}A^dI\text{-}E^dD^b$) mice were obtained from the breeding facility of the N.N. Blokhin National Medical Research Center of Oncology (Moscow, Russia). The transgenic mouse line 1D1b was generated on the genetic background of the B10.D2(R101) line in the Laboratory of Regulatory Mechanisms in Immunity of the N.N. Blokhin National Medical Research Center of Oncology [5]. These transgenic mice are characterized by expression of the β-chain of the memory-cell TCR, specific to the molecule of the major histocompatibility complex (MHC) class I H-$2K^b$, in T cells. Female and male mice (16–18 g) were used in the experiments. The study groups consisted of 6–8 animals. All the experimental procedures were conducted in strict compliance with the protocols approved by the Ethics Committee on Animal Experimentation of the N.N. Blokhin National Medical Research Center of Oncology.

Production of rhCypA

The recombinant protein was isolated from the bacterial biomass of *E. coli* BL21(DE3)Gold transformed with the recombinant plasmid pETCYPopti that contained the full-length gene of human CypA [6]. RhCypA was used as a solution in Na-K phosphate buffered saline (PBS, pH 7.3) with purity above 95% according to electrophoresis data. The endotoxin content in the rhCypA samples was ≤ 0.038 ng per 1 mg of the protein according to the LAL test.

Immunization of mice

B10.D2(R101) and 1D1b mice were i.p. immunized with lymphoma EL-4 (K^bD^b) cells at doses of 3.0×10^5 and 1.0×10^6, respectively, in 500 μl PBS.

Mode of rhCypA administration

B10.D2(R101) mice were i.p. injected with 5 mg rhCypA/kg (100 μg/mouse) during 3 days post-immunization. The first protein injection was made 3 h post-implantation of EL-4 cells. 1D1b mice were subcutaneously dosed with 10 mg rhCypA/kg during 10 days post-immunization. Control mice received PBS as a placebo in a similar manner.

Cell isolation

B10.D2(R101) mice were euthanized by cervical dislocation on days 6, 9, and 12 post-immunization. The peritoneal cavities of mice were washed with 2 ml of ice-cold PBS to obtain the lavage. Splenocyte suspensions were prepared by isolating the murine spleens and homogenizing in a Potter tissue homogenizer in 3 ml of PBS. The 1D1b transgenic mice were euthanized on day 12 post-immunization; their splenocytes were isolated using a similar procedure. Erythrocytes were lysed in a lysis buffer (BD, USA). Cells were then washed in PBS and centrifuged (200 g, 5 min). Viable cells were counted in a Goryaev chamber after Trypan Blue-Eosin staining.

Antibodies

The following monoclonal antibodies were used for the analyses: anti-CD3ε – eFluor450 (clone 17A2) (eBioscience, USA); anti-CD8 – Pacific blue (clone 53-6.7) (BD Pharmingen, USA); anti-CD44 – APC (clone IM7) (eBioscience); anti-CD62L – APC-Cy7 (clone MEL-14) (eBioscience); anti-Vb6 – PE (clone RR4-7) (eBioscience); anti-Gr1 – APC (clone RB6-8C5) (BD Pharmingen); and anti-CD11b-PE – Cy7 (clone M1/70) (BD Pharmingen).

Flow cytometry analysis

The lavage and spleen cell samples ($1.0–5.0 \times 10^6$) were incubated with Fc block (clone 2.4G2, BD Pharmingen, USA) for 5 min at 4°C and stained with monoclonal antibodies for 40 min at 4°C. Cells were then washed with PBS by centrifugation (200 g, 5 min), followed by analysis on a FACS CantoII flow cytometer (BD, USA) using the FACSDiva 6.0. software. Dead cells were excluded from the analyses comprising staining with propidium iodide (BD, USA). In order to characterize cell subpopulations, $0.5–1.0 \times 10^6$ events were analyzed. The FlowJo 7.6. software (BD, USA) was used for further processing of the results.

Statistical analysis

Statistical data analysis was performed using the Student's t-test in Excel (Microsoft, USA). The differences were considered statistically significant at $p \leq 0.05$.

RESULTS

In this study, we used an allogenic system in which the EL-4 (K^bD^b) lymphoma cells were rejected in B10.D2(R101) ($K^dI\text{-}A^dI\text{-}E^dD^b$) mice because of the difference in a single MHC I class molecule (H2-K^b). It was shown that rhCypA administration results in complete EL-4 elimination by day 9 post-transplantation, whereas complete tumor rejection in the absence of rhCypA was observed on day 12 (*Fig. 1*).

The immune response to EL-4 was accompanied by granulocyte accumulation at the tumor cell localization site. The rhCypA induced intensive accumulation of

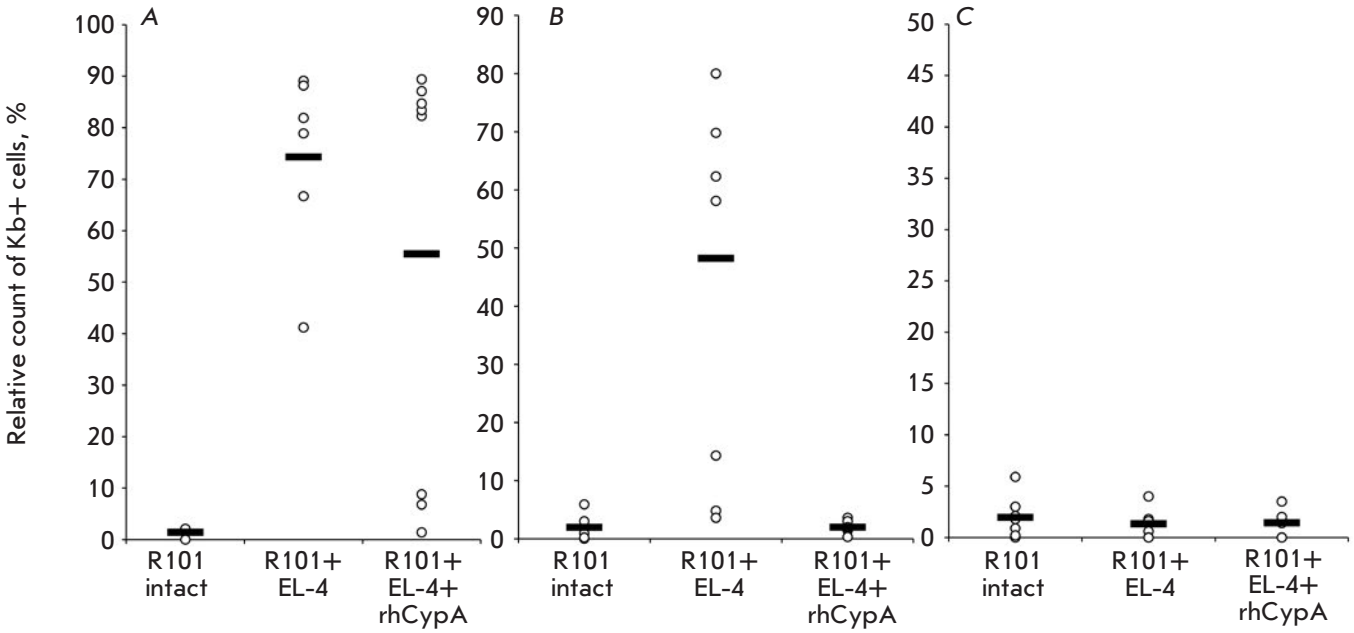

Fig. 1. The relative count of lymphoma EL-4 cells (Kb+, %) in the peritoneal cavity of B10.D2(R101) mice on days 6 (*A*), 9 (*B*) and 12 (*C*) post-immunization. Data obtained in three representative experiments are shown (M ± SD, n = 6–8). The relative count of Kb+ cells in the lavage of intact mice represents the level of unspecific binding of anti-Kb monoclonal antibodies

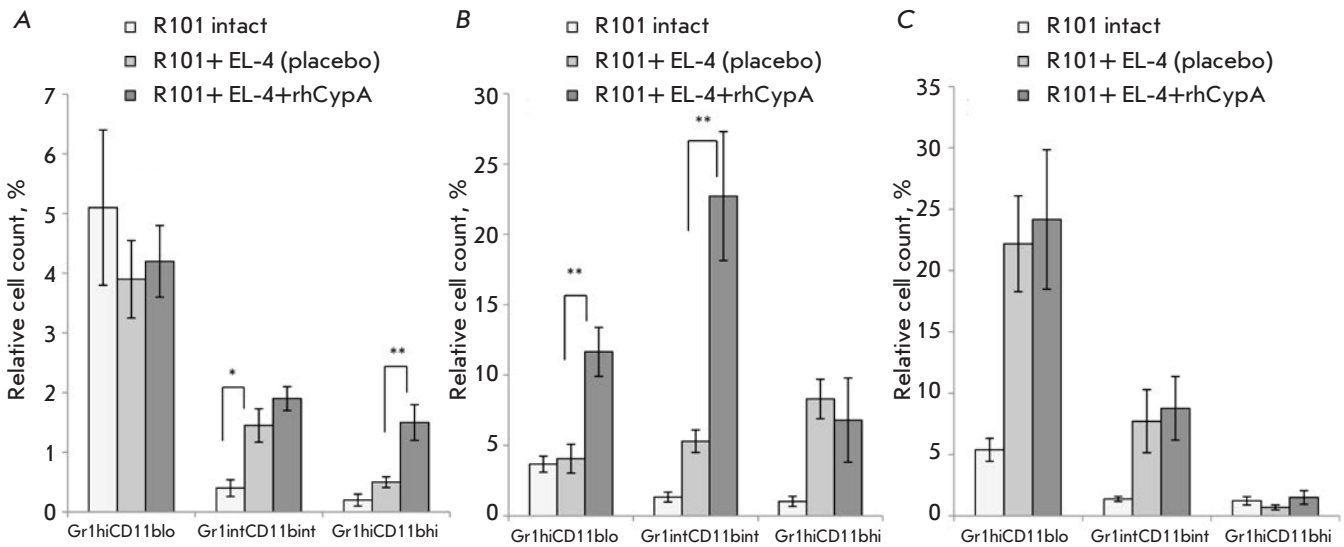

Fig. 2. Changes in the relative count (%) of immature neutrophils (Gr1hi CD11blo), promyelocytes and myelocytes (Gr1int CD11bint), and mature granulocytes (Gr1hi CD11hi) in the peritoneal cavity of B10.D2(R101) mice on days 6 (*A*), 9 (*B*), and 12 (*C*) post- immunization with lymphoma EL-4 cells. Data obtained in three representative experiments are shown (M ± SD, n = 6–8). *$p \leq 0.05$; **$p \leq 0.01$

mature granulocytes in the peritoneal lavage of mice on day 6 post-immunization: the relative count of these cells was threefold higher than that in the immunized control mice (*Fig. 2A*). On day 9 post-immunization, rhCypA stimulated recruitment of immature granulocytes (Grhi CD11blo) and promyelocytes and myelocytes (Grint CD11bint) in the peritoneal cavity of dosed mice. Cell counts in these subpopulations were

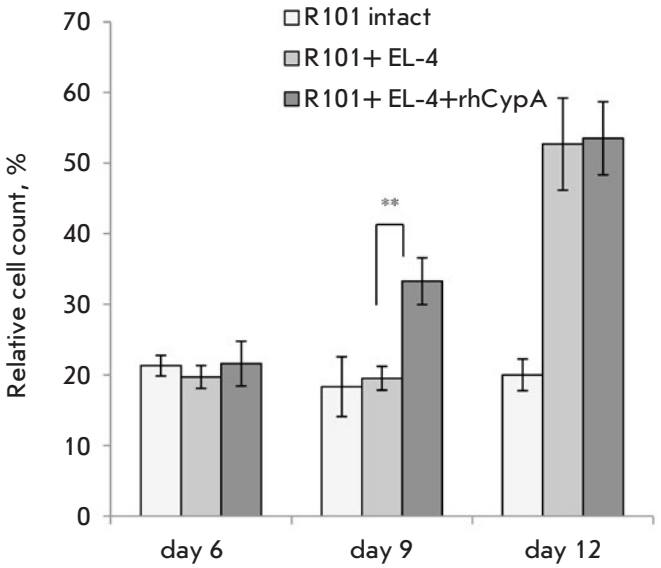

Fig. 3. The accumulation dynamics of effector CD8+ T-lymphocytes (CD62L-CD44+) in the spleen of B10.D2(R101) mice after immunization with lymphoma EL-4 cells. Data obtained in three representative experiments are shown (M ± SD, n = 6–8). $^{**}p \leq 0.01$

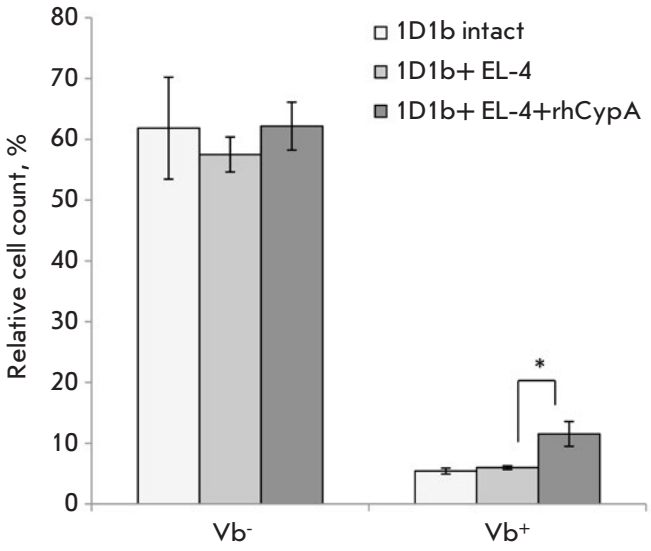

Fig. 4. The relative count (%) of effector CD8+ T-lymphocytes (CD62L-CD44+) with the endogenous TCR β-chains (**Vb6-**) or transgenic TCR β-chain (**Vb6+**) in the spleen of 1D1b transgenic mice on day 12 post-immunization. Data obtained in three representative experiments are shown (M ± SD, n = 6–8). $^{*}p \leq 0.05$

increased under rhCypA administration 2.5- and 4.5-fold, respectively, compared to the respective cell counts in immunized control mice (*Fig. 2B*).

Next, we evaluated the effects of rhCypA on quantitative and subpopulation changes in CD8+ T cells in tumor-bearing mice. The protein under study did not influence the dynamics of CD8+ T cell accumulation neither in the tumor localization site (as assessed by lavage analyses) nor at the systemic level (as assessed by splenocyte analyses; data are not shown). However, analyses of CD8+ T cell subsets of naive cells (CD62L+CD44-), central memory cells (CD62L+CD44+), and effectors (CD62L-CD44+) revealed that rhCypA induced enhanced accumulation (by 65% as compared to the placebo control) of effector cytotoxic T cells on day 9 post-transplantation of EL-4 tumor cells (data are not shown, *Fig. 3*). These data correlated well with the tumor rejection dynamics under rhCypA treatment (*Fig. 1*).

Therefore, it has been demonstrated that intraperitoneally injected rhCypA stimulated the antitumor immune response by inducing early recruitment of granulocytes to the tumor cell localization site and enhancing systemic accumulation of effector T-killers.

It was previously shown at our laboratory that transgenic 1D1b mice developed a significantly reduced pool of effector CD8+ T cells in response to EL-4 cells as compared to wild-type mice. Consequently, 1D1b mice could not reject this lymphoma [5, 7].

In this study, we evaluated the effects of rhCypA on the relative count of effector T cells expressing either endogenous TCR β-chains or the transgenic TCR β-chain as defined by anti-Vb6 antibody staining in 1D1b mice.

The *in vivo* experiments showed that rhCypA had no effect on the relative count of effector CD8+ T cells with endogenous TCR β-chains in 1D1b mice immunized with EL-4 cells (*Fig. 4*). Interestingly, administration of rhCypA significantly increased (2.0-fold as compared to the placebo control) the count of effector CD8+ T cells with the transgenic TCR β-chain (*Fig. 4*).

According to these data, we have assumed that rhCypA can modulate an antitumor immune response both in mice with the native TCR repertoire (B10.D2(R101)) and in transgenic 1D1b mice with the contracted TCR repertoire by inducing the accumulation of effector CD8+ T cells.

DISCUSSION

In this study, we evaluated the role of rhCypA in the development of the antitumor immune response to lymphoma EL-4 cells in B10.D2(R101) mice. It was shown that rhCypA stimulates granulocyte accumula-

tion at the tumor cell localization site and systemic accumulation of effector cytotoxic T cells, which results in rapid tumor elimination. It is well-known that tissue infiltration with neutrophils is the first phase of the immune response to infections and inflammation. These cells can take up an antigen and migrate to the draining lymph nodes and the spleen, where neutrophils come in contact with the antigen-presenting cells (APCs) and lymphocytes [8] or directly function as APCs [9], thus inducing the formation of the adaptive immune response. We have previously shown that neutrophils participate in the development of the immune response to allogenic tumor cells [10]. These cells could provide co-stimulatory signals (CD80 and CD86) and create the cytokine microenvironment (interleukin 12), which are both required for differentiation of cytotoxic T cells [10, 11]. It was shown in the present study that local processes in the peritoneal cavity taking place under rhCypA treatment correlate with the systemic immune response.

In 1D1b mice, the expression of the transgenic TCR β-chain in T cells both contracted the TCR repertoire and reduced the count of activated T cells [5]. The immune response to EL-4 in 1D1b transgenic mice was insufficient for complete tumor elimination and drove the immunoediting of EL-4 cells via the selection of less immunogenic tumor cell clones that killed transgenic mice within 60 days [7]. It was shown using this experimental model that rhCypA significantly stimulates the accumulation of tumor-specific cytotoxic T cells at the early phases of the immune response to lymphoma EL-4. These data allow one to assume that rhCypA can modulate the antitumor immune response both in mice with the native TCR repertoire and in those with the contracted TCR repertoire by inducing the accumulation of effector T-killers.

Hence, we have demonstrated that rhCypA has an immunostimulating effect, as it facilitates the development of the antitumor immune response by stimulating both innate and adaptive immunity. ●

REFERENCES

1. Nigro P., Pompilio G., Capogrossi M.C. // Cell Death Disease. 2013. V. 4. P. e888. doi: 10.1038/cddis.2013.410.
2. Khromykh L.M., Kulikova N.L., Anfalova T.V., Muranova T.A., Abramov V.M., Vasiliev A.M., Khlebnikov V.S., Kazansky D.B. // Cell Immunol. 2007. V. 249. № 1. P. 46–53.
3. Dawar F.U., Xiong Y., Khattak M.N.K., Li J., Lin L., Mei J. // J. Leukoc. Biol. 2017. V. 102. № 4. P. 989–992.
4. Bharadwaj U., Zhang R., Yang H., Doan D., Li M., Chen C., Yao Q. // J. Surgical Res. 2004. V. 121. № 2. P. 294.
5. Silaeva Yu.Yu., Kalinina A.A., Vagida M.S., Khromykh L.M., Deikin A.V., Ermolkevich T.G., Sadchikova E.R., Goldman I.L., Kazansky D.B. // Biochemisty. 2013. V. 78. № 5. 614–626.
6. Khromykh L.M., Kalinina A.A., Kozyr A.V., Kolesnikov A.V., Silaeva Yu.Yu., Kazansky D.B. Patent № 2603283. Russian Federation. 2015.
7. Silaeva Yu.Yu., Grinenko T.S., Vagida M.S., Kalinina A.A., Khromykh L.M., Kazansky D.B. // J. Immunotoxicol. 2014. V. 1. № 4. P. 393–399.
8. Mantovani A., Cassatella M.A., Costantini C., Jaillon S. // Nat Rev Immunol. 2011.V. 11. № 8. P. 519–523.
9. Takashima A., Yao Y. // J Leukoc Biol. 2015. V. 98. № 4. P. 489–496.
10. Maryukhnich E.V., Zvezdova E.S., Anfalova T.V., Khromykh L.M., Kazansky D.B. // Docl. Biol. Sci. 2007. V. 414. № 1. P. 242–245.
11. Pobezinskii L.A., Pobezinskaya E.L., Zvezdova E.S., Petrishchev V.N., Grinenko T.S., Baturina I.A., Anfalova T.V., Khromykh L.M., Vasil'eva T.V., Kazanskii D.B. // Dokl Biol Sci. 2005. V. 402. № 3. P. 224–229.

The Differential Anti-HIV Effect of a New Humic Substance-Derived Preparation in Diverse Cells of the Immune System

G.V. Kornilaeva[1], A.E. Siniavin[1,2]*, A. Schultz[3], A. Germann[3], C. Moog[4], H. von Briesen[3], A.S. Turgiev [1,5], E.V. Karamov[1]

[1]Gamaleya Center for Epidemiology and Microbiology. Gamaleya Str.1 8, Moscow, 123098, Russia

[2]Shemyakin-Ovchinnikov Institute of Bioorganic Chemistry, Miklukho-Maklaya Str. 16/10, Moscow GSP-7, 117997, Russia

[3]Fraunhofer Institut fuer Biomedizinische Technik (IBMT), Joseph-von-Fraunhofer-Weg 1, 66280 Sulzbach, Germany

[4]INSERM U1109, Fédération Hospitalo-Universitaire (FHU) OMICARE, Fédération de Médecine Translationnelle de Strasbourg (FMTS), Université de Strasbourg, 4 Rue Blaise Pascal, Strasbourg 67000, France

[5]Immunomica LLC, Novaya Basmannaya Str. 12, bldg. 2, ste. 103, Moscow, 107078, Russia

*E-mail: andreysi93@yandex.ru

Received March 03, 2019; in final form, April 15, 2019

DOI: 10.32607/20758251-2019-11-2-68-76

ABSTRACT **The anti-HIV activity of a new humic substance-derived preparation has been studied in individual pools of immune cells ($CD4^+$ T lymphocytes, macrophages, dendritic cells). Near-complete inhibition of the HIV infection (by more than 90%) was achieved by treating each of the abovementioned cell types with non-toxic concentrations of the preparation. The inhibitory effect demonstrates the possibility of preventing the depletion of a significant portion of functionally important immune cells. A comparative study of infection inhibition in individual cell pools has allowed us to reveal the differences in the preparation's effectiveness in each of the cell populations. A R5-tropic HIV-1 infection in macrophages exhibited maximum sensitivity to the preparation: 90% and 50% inhibition of the infection were observed in the presence of concentrations as low as 1.4 and 0.35 μg/ml, respectively. A 15- and 19-fold higher concentration was required to achieve the same extent of inhibition in dendritic cells infected with the same strain. The effectiveness of the drug in CD4 + T lymphocytes is quite comparable to its effectiveness in macrophages. The drug is universally effective for both the T- and M-tropic variants of HIV-1.**

KEYWORDS **humic derivative, suppression of HIV infection, CD4-positive T lymphocytes, macrophages, dendritic cells, T- and M-tropic HIV variants**

ABBREVIATIONS **HIV – human immunodeficiency virus; SBF-HS – solubilized butanol fraction of humic substances; HPLC – high-performance liquid chromatography; NMR – nuclear magnetic resonance; Mϕ – macrophages; DC – dendritic cells; PBMC – peripheral blood mononuclear cells; AZT – azidothymidine; CTL – cytotoxic lymphocytes.**

INTRODUCTION

Monocytes, macrophages, and dendritic cells, which constitute the cellular component of innate immunity and the first line of defense against pathogens [1–5], are the targets of HIV. The virus attacks the CD4-, CCR5-, and CXCR4-expressing cells present – depending on the invasion route – in the mucosa, blood, or lymphoid tissues. The transmission rate depends on both the expression level of the cellular surface receptors and the viral strain [6, 7]. A high viral production is commonly observed in CD4-positive T cells activated during acute infection [8]. Nevertheless, viral replication, in addition, takes place in quiescent CD4-positive memory cells, which also contain latently integrated or pre-integrated proviral DNA [9]. Cells harboring the viral genome represent a part of the infection reservoir that persists in the organism and may be retained for up to four years [9]. It is believed that quiescent

CD4-positive memory cells are the first to be infected, and that the viruses involved are predominantly of the R5 phenotype [10–12]. This may be due to intergin LFA-1 expression [13]. The increased ability of R5 viruses to replicate may also explain their prevalence during an acute or primary HIV infection [14].

The pathogenetic process of HIV infection also involves antigen-presenting cells, macrophages and dendritic cells [15–18] which possess virus-specific receptors and are capable of actively circulating in the blood and penetrating various lymphoid and non-lymphoid tissues. Dendritic cells are prototypical antigen-presenting cells with an extraordinary capacity for recognizing and processing antigens [19]. When immature, dendritic cells show increased ability to phagocytose, while their functional pattern changes upon maturation and they exhibit preferential cytokine-producing activity. Expression of CCR5 decreases in the course of maturation, whereas that of CXCR4 increases, which may lead to the infection of dendritic cells by viruses of both phenotypes [18]. In addition, Langerhans cells (epidermal dendritic cells) are capable of taking up HIV (without subsequent viral production) via a C-type lectin: langerin. Maturation is associated with a decrease in viral production, which may be 10 to 100 times lower in mature as compared to immature dendritic cells [20, 17]. Most researchers agree that dendritic cells are not active viral producers; rather, their major role (favored by a pronounced capacity for migration) is to traffic HIV from the entry sites to CD4-positive T cells, thus promoting fast virus dissemination throughout the organism. Macrophages are also amenable to HIV infection [21, 22]. Macrophage-tropic R5 viruses replicate in macrophages derived from peripheral blood mononuclear cells, as well as in CD4-positive lymphocytes [23]. Macrophages also vary in their ability to produce the virus. Viral production in infected macrophages is frequently of low intensity, and the virus is found sequestered in intracellular vacuoles. The reduced viral replication may be due to the intracellular mechanisms of nonspecific defense. R5 viruses usually exhibit no cytopathic effect, but some isolates – particularly those detected at late stages of the disease – propagate in macrophages to high titers and may induce cytopathic effects [24, 25]. In the majority of cases, the death of the infected macrophages is a result of necrosis. Of particular importance to the pathogenesis of the HIV infection is the ability of macrophages to serve as a viral reservoir that is resistant to antiretroviral therapies and cannot be recognized by the cytotoxic lymphocytes of the immune system (due to the absence of active viral reproduction and synthesis of virus-specific proteins, respectively).

On the whole, the literature data indicate that the permissiveness of immune cells to HIV largely depends on their stage of maturation/differentiation and functional polarization. Both the level of cytokine production and the receptor repertoire are known to be affected by those processes. The infection-induced exhaustion of the pool of HIV-sensitive immune cells ultimately jeopardizes the buildup of the immune response.

Studies of the major target cells involved in HIV pathogenesis (such as peripheral blood mononuclear cells, macrophages, and dendritic cells) constitute an invariable component of the current requirements that need to be met in designing the assessment of new antivirals. This approach allows one to determine (a) the efficacy of the compounds under study in each relevant cell population and (b) the probability of affecting the course of the pathogenetic process (and ultimately optimize the therapeutic regimen) by administering those compounds.

In this work, we report on studies of a new anti-HIV preparation, a solubilized butanol fraction of humic substances (SBF-HS). Mass spectrometry data and the results of an elemental analysis indicate that the fraction contains 52.7% (w/w) and 37.1% (w/w) carbon and oxygen, respectively, but considerably lower amounts of nitrogen (4.3% w/w) and sulfur (2.1% w/w) [26, 27]. It should be noted that an elemental analysis of humic substances isolated from the same source using the same isolation and fractionation methods yields reproducible results. High-performance liquid chromatography (HPLC) data demonstrate that the preparation is characterized by a high content of hydrophobic aromatic fragments (74%), which was confirmed by ^{13}C NMR. The hydrogen-to-carbon atomic ratio (H/C) is 0.8; the oxygen-to-carbon atomic ratio (O/C) is 0.53 [28–30].

It is known that humic substances form as a result of the decay of dead organisms and are among the vast reservoirs of organic carbon. SBF-HS is an ecologically sound and safe product exhibiting antitumor, antifungal, antibacterial, and antiviral activities. In addition, it stimulates hemopoiesis and acts as an immunomodulator, a powerful antioxidant, and an efficient hepatoprotector. SBF-HS stimulates cell-mediated immunity (particularly in inflammatory foci), accelerates the regeneration of wounds, burns, and ulcers of skin and mucosa, and lacks toxicity and allergenicity [31–33].

MATERIALS AND METHODS

SBF-HS

Lignin-containing solid waste resulting from the processing of vegetable feedstock was used as a starting

material for obtaining humic substances. The material was subjected to oxidative alkaline hydrolysis, followed by separation of the liquid phase, which was further acidified, and the resulting solid residue was isolated, washed, and dried. The intermediate product thus obtained was extracted with ethyl acetate. The resulting solid residue was extracted with *n*-butanol. In order to isolate and solubilize the biologically active fractions exerting antiviral effects, *n*-butanol was evaporated and the solid residue was purified by repeated precipitation from the alkaline solution (using concentrated hydrochloric acid). The fractions were standardized by the characteristic absorption bands in the infrared region (presence of specific absorption bands in the region 2–10 μm) and molar mass distribution (showing a maximum in the vicinity of 7,000 Da). The yield of the target product, the solubilized butanol fraction of humic substances (SBF-HS), approximated 40%.

Physicochemical methods for analyzing SBF-HS

Elemental analysis. Samples of the test compound were brought to complete dissolution by heating to 80–100°C in 2 ml of nitric acid, with a few drops of hydrogen peroxide added, for 3 hours. The solution was analyzed by atomic emission spectrometry with inductively coupled argon plasma (ICAP-9000; Thermo Jarrell Ash, USA).

GC-MS analysis. An accurately weighed sample of SBF-HS was adjusted to full air-dry weight and treated with 5 ml of toluene in an ultrasonic bath. The extracts were filtered, dried over anhydrous sodium sulfate, and evaporated in a nitrogen current. Some samples were methylated. An aliquot of the sample was analyzed by GC-MS on an equipment complex consisting of an HP5890A gas chromatograph, an HP5988A mass spectrometer, and an HP59970C data processing system (Hewlett-Packard, USA). The sample components were identified using the Wiley mass spectral library.

NMR spectroscopy was performed using a Bruker Avance 400 MHz NMR spectrometer.

Cell lines

CEM-SS, an immortalized line cloned from a human T4 lymphoblastoid cell line by adhesion using poly-L-lysine and characterized by increased ability of virus-induced syncytium formation and fusogenic activity, is widely used to study HIV and its inhibitors (NIH AIDS Reagent Program No. 776, USA). The cells were maintained in a RPMI-1640 medium (Sigma, USA) supplemented with 10% fetal calf serum (Sigma, USA) and 2 mM L-glutamine (Sigma, USA.).

Peripheral blood mononuclear cells (PBMCs) were isolated from the EDTA-anticoagulated blood of HIV-seronegative donors by Ficoll® Paque Plus (GE Healthcare Worldwide, USA) density gradient centrifugation. HIV was inoculated into mitogen-stimulated PBMC, which were obtained by culturing in the presence of 5 μg/ml phytohemagglutinin (PHA; Sigma, USA) for 3 to 4 days. The infected cells were maintained in a RPMI 1640 growth medium supplemented with 10% fetal calf serum, 100 μg/ml gentamicin, and 50 U/ml interleukin 2 (IL-2; Sigma, USA).

Human macrophages (Mϕ) were obtained by allowing the monocytes present in the PBMC suspension ($1–2 \times 10^6$ cells/ml) to adhere as a result of PBMC incubation at 37°C for 2 h; the adherent cells were further differentiated for 7–8 days in the presence of 0.2 μg/ml GM-CSF (Invitrogen, USA), and then added to the growth medium of the composition described above.

Dendritic cells (DCs) were obtained by culturing human monocytes in the presence of 20 ng/ml interleukin 4 (IL-4; Sigma, USA) for 7 days; the monocyte fraction was isolated from PBMC by the MACS (magnetic cell separation) technology, using human CD14 MicroBeads (Miltenyi Biotec, Germany). The antigen-presenting function of DCs was assessed according to the latter's ability to stimulate allogeneic proliferation of T cells.

The TZM-bl cell line (NIH AIDS Reagent Program No. 8129, USA) was obtained by genetic engineering of HeLa cells; it expresses CD4, CXCR4, and CCR5 and contains the Tat-dependent luciferase reporter gene under the regulatory control of HIV-1 LTR.

293T/17 human kidney epithelial cells were derived from the 293T cell line (ATCC® CRL-11268).

Env-pseudotyped virus production. Pseudoviruses were obtained according to the previously described method [34]. 293T/17 cells were seeded at a concentration of 2×10^6 per T-75 flask in a 20-ml DMEM growth medium. After 24 hrs, the cells were transfected with 4 μg of a HIV-1 *env* expression plasmid and 8 μg of an env-deficient HIV-1 backbone vector, pSG3ΔEnv, using the Fugene 6 transfection reagent (Promega, USA). After 4 h of incubation, the transfection medium was replaced with a fresh growth medium. Pseudovirus-containing culture supernatants were collected after 48 h and stored at -80°C. All plasmids were obtained from the international repository of the NIH AIDS Reagent Program.

TZM-bl assay. The neutralization analysis was performed using TZM-bl cells according to the Montefiori method [35], which is a modified version of the analysis by Wei et al. [36]. Fresh trypsinized cells were seeded in 96-well plates at a concentration of 1×10^4 cells/well

in 100 μl of a DMEM growth medium supplemented with 5 μg/ml DEAE-dextran. Various dilutions of the test compound were added to the cells and incubated for 45–90 min at 37°C. The cells were inoculated with 150,000 RLU (relative luminescent units) of the corresponding pseudovirus. After 48 h of incubation, the cells were washed with the medium and lysed, after which the amount of luciferase was determined in comparison with the virus control using a Victor X3 luminometer (Perkin Elmer). The 50% inhibitory concentration values were calculated using GraphPad Prism 6 by the log function (inhibitor), compared to the normalized response.

Viruses. The following HIV-1 strains were used to infect the cells:

HIV-1_{BRU}, reference strain of the X4 phenotype, actively replicating in T lymphoblastoid cells and sensitive to azidothymidine (AZT);

HIV-1_{AR216}, a clinical isolate of the X4 phenotype (obtained from an HIV-infected patient) adapted to T cell lines and highly resistant to AZT;

HIV-1_{Ba-L}, an M-tropic strain of the R5 phenotype;

HIV-1_{SF162}, an M-tropic strain of the R5 phenotype; and

HIV-1_{QH0}, an M-tropic strain of the R5 phenotype (isolated from an HIV-infected patient in Trinidad and Tobago).

To assess the biological activity, the median tissue culture infection dose ($TCID_{50}$) was determined for each viral stock by titration.

Assessment of cell viability

Cell viability was determined by the MTT assay based on the ability of live cells to convert the readily soluble yellow 3-(4,5-dimethylthiazol-2-yl)-2,5-diphenyltetrazolium bromide (MTT) into insoluble purple intracellular crystals of MTT-formazan. The conversion efficiency is indicative of the general level of dehydrogenase activity of the cells under study, which is to a certain extent directly proportional to the concentration of viable cells [37]. According to the generally accepted criteria, substances with CC_{50} ranging from 1 to 10 μg/ml are considered highly toxic; 11 to 20 μg/ml, toxic; 21 to 50 μg/ml, moderately toxic; and 51 to 100 μg/ml, slightly toxic. The substances with CC_{50} > 100 μg/ml are classified as non-toxic.

Studies of anti-HIV activity

To determine the antiviral activity, the cells were incubated at variable concentrations of SBF-HS (10, 1, 0.1, and 0.01 μg/ml) at 37°C in 96-well microtiter plates (Corning, USA) for 2 h. The virus was then inoculated at a multiplicity of infection of 100 $TCID_{50}$. Following the 24-h incubation, the unbound virus was removed by low-speed centrifugation and the cell pellet was re-suspended in a fresh portion of the growth medium. The microplates were monitored for 5 days; the cytopathic effect was assessed according to cell lysis and syncytium formation. The antiviral effect was evaluated according to the decrease in the production of HIV-1 core antigen, p24, which was measured by ELISA. The viral core antigen p24 is a highly conserved major protein universally adopted as a marker of HIV infection. The p24 level was measured using certified commercial test systems manufactured by Bio-Rad (USA) and Vector-Best (Russia).

Statistical analysis

Experimental data were obtained in three independent experiments, and the results were shown as the mean ± standard error of the mean (SEM). The significance of the differences between the samples was estimated using the Kolmagorov–Smirnov test and the one-way ANOVA test with Bonferroni adjustment (Origin Pro 2016G, OriginLab Corporation) for experiments with more than two subgroups. The half-maximal inhibitory concentration (IC_{50}) and 50% cytotoxic concentration (CC_{50}) were calculated based on the dose-effect curves using the Origin Pro 2016G and Sigma Plot 12.5 software. Differences were considered significant if the calculated p value was < 0.05.

RESULTS AND DISCUSSION

Characterization of the chemical composition of SBF-HS

Studies of the elemental composition of SBF-HS were performed in two repetitions. It was determined that SBF-HS is a polyelemental substance with a high content of P and Na (6,000 and 10,029 μg/ml, respectively). It is important to note that the test substance contained almost no heavy metals.

GC-MS analysis showed that fatty and resin acids were the most representative groups in the SBF-HS. Palmitic, oleic, and behenic acids were the predominant fatty acids (1.2 μg/g each). The contents of stearic, arachidic, and lignoceric acids in SBF-HS were lower (0.4 μg/g each). Among the resin acids, three components corresponding to the structural formula of $C_{20}H_{30}O_2$ (1.6 μg/g) were found in the analyzed sample. One of these components can be identified as abietic acid (0.6 μg/g). The other components were isomeric structures having this gross formula. The other two resin acids had the gross formula of $C_{20}H_{28}O_2$. The most characteristic peak in the mass chromatogram corresponded to levopimaric acid (18 μg/g).

We used NMR spectroscopy to compare data on the moiety composition of SBF-HS with the composition of humic acids in coal (*Table 1*). The content of carbonyl, carboxyl, and ester fragments in SBF-HS was similar to that of humic acids in coal. The content of phenolic groups in SBF-HS was slightly higher (11% versus 7–9%). The high C_{COO-H}/C_{COO-R} and C_{Ar-OH}/C_{Ar-OR} ratios were typical and represented the degree of hydrolysis of the structure. The high content of aromatic fragments was a typical feature of SBF-HS, while the aromatic portion of the structure was characterized by a large number of unsubstituted and O-substituted moieties.

Table 1. Moiety composition of SBF-HS

Moiety	Content, %C
$C_{C=O}$	3
C_{COO-H}	10
C_{COO-R}	2
C_{Ar-OH}	11
C_{Ar-OR}	7
C_{Ar-R}	21
C_{Ar-H}	27
$C_{O-Alk-O}$	0
C_{-CH-OH}	3
$C_{-CH2-OH}$	6
C_{CH3O}	15

Cytotoxicity of SBF-HS

In order to assess the cytotoxic effects, the cells were cultured in the presence of varied concentrations of SBF-HS for 3–4 days; the viability was then measured using the MTT assay.

Cytotoxicity studies in three independent experiments demonstrated that SBF-HS was non-toxic to both the CEM-SS cell line and the primary cells (PBMC) (*Table 2*). IC_{50} is the 50% inhibitory concentration (causing 50% suppression of the infection); CC_{50} is the 50% cytotoxic concentration (causing loss of viability in 50% of cells); SI is the selectivity index calculated as the ratio between CC_{50} and IC_{50}. The values are the means of three measurements, each performed in an independent experiment (antiviral activity was assessed together with toxicity).

Table 2. Antiviral activity, cytotoxicity, and selectivity index (SI) of SBF-HS in CEM-SS and primary CD4-positive T cells

Cell	Viral strain	Inhibition of HIV replication, μg/ml			Cytotoxicity CC_{50}, μg/ml	SI
		IC_{90}	IC_{50} ± SEM	R^2		
CEM-SS	$HIV\text{-}1_{BRU}$	5.4	0.8 ± 0.3	0.87	708	865
	$HIV\text{-}1_{AR216}$	26.0	4.6 ± 0.55	0.79		154
PBMC	$HIV\text{-}1_{BRU}$	5.3	0.9 ± 0.2	0.91	631	701
	$HIV\text{-}1_{AR216}$	11.5	1.04 ± 0.38	0.85		607

Antiviral activity of SBF-HS in continuous and primary CD4-positive T cells infected with AZT-sensitive or AZT-resistant HIV-1 strains

The data on the inhibition of the experimental HIV infection indicate that SBF-HS is able to efficiently suppress the infection induced by AZT-sensitive ($HIV\text{-}1_{BRU}$) and AZT-resistant ($HIV\text{-}1_{AR216}$) virus strains in both continuous and primary cells (*Table 2*). Of note, the concentrations required to achieve 50% suppression of the infection induced by the sensitive strain were almost identical in the continuous and primary cells (< 1 μg/ml).

The ability to suppress the infection induced by the AZT-resistant strain was cell-dependent: judging from the 50% inhibitory concentration (IC_{50}) values, SBF-HS was more efficient in PBMC than CEM-SS cells. The selectivity index (SI) characterizing the clinical promise of the preparation under study was comparably high in PBMC (600–800). This cellular model of an HIV infection is preferable to that based on the use of continuous cell lines. The main reason for the limited use of PBMC in experimental studies of the HIV infection is the lack of standardization and, as a consequence, the chance to encounter a donor with individual resistance to the HIV infection. In order to avoid the latter, we used a mixture of PBMCs isolated from three HIV-seronegative donors.

Antiviral activity of SBF-HS in PBMC, macrophages (Mϕ), and dendritic cells (DCs)

We further studied the antiviral activity of SBF-HS in PBMC, macrophages (Mϕ), and dendritic cells (DC) infected with the M-tropic HIV-1 strains $HIV\text{-}1_{Ba\text{-}L}$, $HIV\text{-}1_{SF162}$, and $HIV\text{-}1_{QH0}$ (*Table 3*).

Our studies made it possible to (a) differentially assess the efficacy of SBF-HS in distinct populations of immune cells and (b) generate data demonstrating that the activity of the preparation varies with the cell type.

The infection induced in Mϕ by the R5 strain $HIV\text{-}1_{Ba\text{-}L}$ exhibited maximum sensitivity to SBF-HS: 90% and 50% inhibition was observed in the presence of relatively low amounts of the preparation (*Table 3*), whereas 15- to 19-fold higher concentrations were required to achieve the same effect in DCs infected

Table 3. Inhibition of viral replication in TZM-bl, PBMC, Mϕ, and DCs infected with HIV-1_{SF162}, HIV-1_{QH0}, and HIV-1_{Ba-L}

Cells	Virus	Inhibitory concentration, μg/ml			
		IC_{90}	IC_{80}	IC_{50}	R^{2*}
PBMC	HIV-1_{SF162} HIV-1_{QH0}	5.8 60.0	3.0 20.0	0.9 ± 0.25 9.8 ± 2.9	0.89 0.72
Mϕ	HIV-1_{Ba-L}	1.4	0.9	0.3 5± 0.1	0.78
DC	HIV-1_{Ba-L}	21.0	12.0	6.8 ± 1.3	0.76
TZM-bl	SF162 pseudovirus QH0 pseudovirus	24.0 60.0	- -	5.0 ± 0.7 5.0 ± 1.2	0.85 0.87

*R^2 values were calculated for IC_{50}.

with the same strain. In PBMCs infected with the R5 strain HIV-1_{SF162}, 90% inhibition of the infection could be achieved at 6.0 μg/ml SBF-HS. As shown in *Table 1*, almost the same concentration of SBF-HS was sufficient to suppress an HIV infection induced by X4 strains. This observation emphasizes the universality of SBF-HS as an anti-HIV agent, against viruses of both phenotypes (R5 and X4). However, our studies demonstrated that there are HIV-1 strains that exhibit greater resistance to SBF-HS. For example, 10-fold higher concentrations are required to suppress the infection induced in PBMCs by HIV-1_{QH0}. The interstrain differences in the genome and pre-existing mutations resulting from the natural polymorphism of HIV-1 may be the likely reasons for the observed discrepancies in SBF-HS activity.

In spite of the differences in IC_{90} and IC_{50} observed between the studied virus–cell systems, 90% suppression of the infection by SBF-HS was achieved in all cases, which indicates that the preparation protected a considerable percentage of target cells attacked by HIV. Our observation that diverse populations of immune cells differed in the extent of HIV suppression regardless of the tropism and phenotype of the virus suggests that preparation bioavailability may be cell-type-dependent. The differences in infection inhibition in various subpopulations of immune cells, which are independent of the viral phenotype, probably indicate that there also are differences in the bioavailability of the preparation. The unequal penetration of drugs into various cells (tissues) is a fact well-known in the literature. This may result in an insufficient (suboptimal) concentration of the drug to inhibit the virus. Under incomplete suppression of virus replication, favorable conditions for the selective selection of resistant forms are established. This should be taken into account when performing preclinical studies of new drugs. Furthermore, more detailed studies into virus replication inhibitors using individual subpopulations of the immune cells involved in the pathogenesis of HIV are required.

Progressive diminution of subpopulations of immune cells, the hallmark of HIV infection, inevitably results in the deterioration of certain functions of the immune system, of which antigen presentation, stimulation of T cell proliferation, and regulation of antibody production by B cells are the most prominent. This is paralleled by a decrease in the turnover of immune cells. Although the mechanisms underlying the death of immune cells during an acute and chronic HIV infection have not been completely clarified, the data in the literature suggest that apoptosis, cytotoxic T lymphocytes, and the direct cytopathic effects of the virus are the likely factors involved. Our study demonstrates that SBF-HS makes it possible to achieve near-complete suppression of an HIV infection (by more than 90%); thus, a considerable portion of cells in diverse subpopulations will be rescued from depletion, thereby preserving the functionality of the immune system. Yet another important result of our study was the observation that SBF-HS exhibited maximum efficacy in suppressing an HIV infection in Mϕ. Mϕ, as well as memory T cells, serves as a reservoir of the virus, and this may be the main reason why complete eradication of HIV is impossible (and why lifelong administration of anti-HIV therapies is necessary). Some researchers believe that those cells may provide conditions favoring the selection of resistant strains.

Recent data indicate that Th17 cells producing interleukin 17 (IL-17) exhibit maximum susceptibility to the HIV infection and are, therefore, prone to rapid depletion [38]. IL-17 plays a key role in maintaining the intestinal mucosa impermeable [39]. Loss of IL-17 destroys the mucosal barrier and stimulates microbial translocation, which in turn causes HIV-associated immune hyperactivation [40–43]. Our recent understanding of the involvement of phenotypically distinct subpopulations of immune cells in HIV pathogenesis opens up opportunities hitherto unknown for assessing the anti-HIV potential of new compounds.

Table 4. Comparative efficiency assessment of six batches of SBF-HS in an experimental HIV infection CEM SS/HIV-1-Bru

SBF-HS batch No.	Cytotoxicity (CC_{50} ± SEM), μg/ml	Inhibitory concentration, μg/ml		SI
		IC_{90}	IC_{50}±SEM	
2660716	1100.0 ± 123	0.90	0.31 ± .012	3548
2640516	1251.0 ± 380	1.10	0.36 ± .001	3475
2690816	985.0 ± 210	0.95	0.34 ± .021	2897
2680716	1230.0 ± 138	1.00	0.38 ± .01	3242
2630416	1150.0 ± 226	0.95	0.35 ± .023	3285
2610316	1159.0 ± 195	0.94	0.31 ± 0.15	3738

Studying the reproducibility of HIV-infection inhibition by SBF-HS

Since stability is an important factor contributing to drug efficacy, we further studied whether the activity of SBF-HS differs between different batches of the preparation. Six batches were examined, and the activity was virtually the same in each case: the HIV infection was inhibited in a dose-dependent manner over the same range of concentrations and with a high SI in diverse virus–cell models HIV-1/Bru and TZM-bl–HIV pseudoviruses (*Tables 4, 5* and *Fig. 1*).

Pronounced suppression of single-cycle infection by SBF-HS was observed in three independent experiments where TZM-bl cells were infected with pseudoviruses differing in the origin of *env* sequences (which belonged to the A, B or C HIV subtype and two circulating HIV recombinants). Expression vectors for pseudovirus production were selected from the standard panel of HIV-1 reference strains (NIH AIDS Research and Reference Reagent Program; NIH ARRRP). As demonstrated in *Fig. 1*, the IC_{50} values for the pseudoviruses Q769.d22, WITO4160.33, CE1176_A3, 703357.c02, and BJOX002000.03.2 fall within the ranges 0.62–0.75, 0.49–0.55, 0.95–1.13, 0.91–0.98, and 0.99–1.19 μg/ml, respectively.

CONCLUSION

In conclusion, it is obvious that SBF-HS was capable of efficiently suppressing an experimental HIV-infection

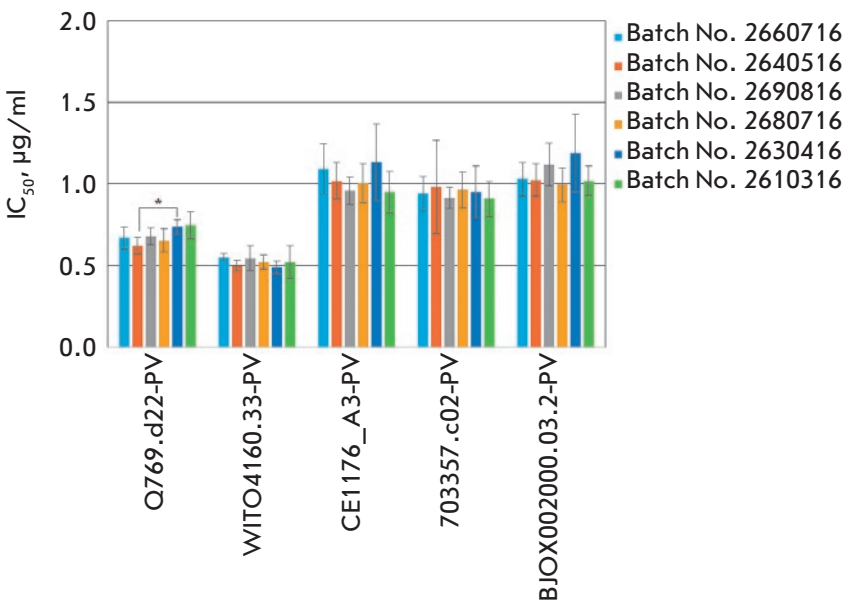

Fig. 1. Assessment of the efficacy of SBF-HS under conditions of single-cycle infection (TZM-bl cells and five HIV pseudoviruses). No statistical differences in the inhibition of pseudoviruses were observed between the tested batches of SBF-HS, except for the inhibition of the pseudovirus Q769.d22-PV between batches Nos. 2640516 and 2630416 (*) with $p < 0.05$

Table 5. Panel of the HIV-1 pseudoviruses used for infecting TZM-bl cells (single-cycle infection)

Virus	Origin (country)	Subtype	Infection stage	Transmission
Q769.d22-PV	Kenya	A	Acute/early	Sexual
WITO4160.33-PV	USA	B	II	Sexual
CE1176_A3-PV	Malawi	C	I/II transmitted founder virus	Sexual
703357.c02-PV	Thailand	CRF01_AE	I/II	Sexual
BJOX002000.03.2-PV	China/Beijing	CRF07_BC	I/II	IDU

and protecting cells from several distinct HIV subtypes and circulating recombinant forms. Assessment of the biological properties of six distinct batches of the preparation demonstrated that the fractionation technique used to obtain standardized preparations of SBF-HS was reliable.

Humic substances formed via the decay of dead organisms constitute one of the vast reservoirs of organic carbon. In 1988, during the International Humic Substances Society meeting, it was suggested that humic substances might offer significant promise as drugs for treating diverse diseases [44]. As of today, there is ample evidence of the rather unique properties of humic substances, which exhibit anti-inflammatory, wound-healing, antifungal, bactericidal, and even antineoplastic activities. In spite of those findings, it is not as if humic substances have become the subject of major scientific investigations. Only two companies (one in the United States and one in Russia) have so far succeeded in developing humic substance-based drugs and in completing all the requisite preclinical and clinical trials of their safety and efficacy [30]. This work supplements our knowledge base pertaining to the possible therapeutic utilities of humic substances, which are thereby extended to the treatment of an HIV infection. ●

This work was supported by the Russian Foundation for Basic Research (project No. ERA_Net RUS plus No. 16-54-76005).

REFERENCES

1. Geissmann F. // Nat. Immunol. 2007. № 8. P. 558–560.
2. Epelman S., Lavine K.J., Randolph G.J. // Immunity. 2014. № 41. P. 21–35.
3. Alvarez-Errico D., Vento-Tormo R., Sieweke M., Ballestar E. // Nat. Rev. Immunol. 2015. № 15. P. 7–17.
4. Wacleche V.S., Tremblay C., Routy J.-P., Ancuta P. // Viruses. 2018. V. 2. № 10. P. 65.
5. Stevenson M. // J. Neurovirol. 2015. № 21. P. 242–248.
6. Bagasra O., Hauptman S.P., Lischner H.W., Sachs M., Pomerantz R.J. // N. Engl. J. Med. 1992. № 326. P. 1385–1391.
7. Embretson J., Zupancic M., Ribas J., Burke A., Rack P., Tenner-Racz K., Haase A. // Nature. 1993. № 362. P. 359362.
8. Klatzmann D., Barre-Sinoussi F., Nugeyre T., Dauquet C., Vilmer E., Griscelli C., Brun-Vezinet F., Rouzioux C., Gluckman C., Chermann J.C. // Science. 1984. № 225. P. 59–62.
9. Siliciano J.D., Siliciano R.F. // J. Clin. Investig. 2000. № 106. P. 823–825.
10. Brenchley M., Hill B., Ambrozak D., Price A., Guenaga F., Casazza J., Kuruppu J., Yazdani J., Migueles S., Connors M., Roederer M., Couek D., Koup R.A. // J. Virol. 2004. № 78. P. 1160–1168.
11. Chun W., Chadwick K., Margolick J., Siliciano R.F. // J. Virol. 1997. № 71. P. 4436–4444.
12. Schnittman M., Lane H., Greenhouse J., Justement J., Baseler M., Fauci A. // Proc. Natl. Acad. Sci. USA. 1990. № 87. P. 6058–6062.
13. Tardif M.R., Tremblay M.J. // J. Virol. 2005. № 79. P. 13714–13724.
14. Schweighardt B., Roy A.-M., Meiklejohn A., Grace J., Moretto J., Heymann F. // J. Virol. 2004. № 78. P. 9164–9173.
15. Blauvelt A., Asada H., Saville M., Klaus-Kovtun V., Altman D., Yarchoan R., Katz S. // J. Clin. Investig. 1997. № 100. P. 2043–2053.
16. Dittmar M.T., Simmons G., Hibbitts S., O'Hare M., Louisirirotchanakul S., Beddows S., Weber J., Clapham P.R., Weiss R.A. // J. Virol. 1997. № 71. P. 8008–8013.
17. Granelli-Piperno A., Delgado E., Finkel V., Paxton W., Steinman R.M. // J. Virol. 1998. № 72. P. 2733–2737.
18. Zaitseva M., Blauvelt A., Lee S., Lapham C., Klaus-Kovtum V., Mostowski H., Manischewitz J., Golding H. // Nat. Med. 1997. № 3. P. 1369–1375.
19. Geissmann F., Manz M.G., Jung S., Sieweke M.H., Merad M., Ley K. // Science. 2010. № 327. P. 656–661.
20. Bakri Y., Schiffer C., Zennou V., Charneau P., Kahn E., Benjouad A., Gluckman J.C., Canque B. // J. Immunol. 2001. № 166. P. 3780–3788.
21. Grossman Z., Meier-Schellersheim M., Paul W.E., Picker L.J. // Nat. Med. 2006. № 12. P. 289–295.
22. Levy J.A. HIV and the pathogenesis of AIDS. Copiring. ASM Press, USA. 2010.
23. Gendelman H.E., Orenstein J.M., Baca L.M., Weiser B., Burger H., Kalter D.C., Meltzer M.S. // AIDS. 1989. № 3. P. 475–495.
24. Bergamini A., Dini L., Capozzi M., Ghibelli L., Placido R., Faggioli E., Salanitro A., Buonanno E., Cappannoli L., Ventura L., Cepparulo M., Falasca L., Rocchi G. // J. Infect. Dis. 1996. № 173. P. 1367–1378.
25. Kwa D., Vingerhoed J., Boeser B., Schuitemaker H. // J. Infect. Dis. 2003. № 187. P. 1397–1403.
26. Filov V.A., Reztsova V.V., Berkovich A.M. // Russian Journal for Biotherapeutics. 2002. V. 2. № 1 [in Russian].
27. Zhernov Y.V., Kremb S., Helfer M., Schindler M., Harir M., Mueller C., Hertkorn N., Avvakumova N.P., Konstantinov A.I., Brack-Werner R., Schmitt-Kopplin Ph., Perminova I.V. // N. J. Chem. 2017. № 41. P. 212–224.
28. Rice J. A., MacCarthy P. A. // Environ. Sci. Technol. 1990. № 24. P. 1875–1877.
29. Driver S.J., Perdue E.M. // Environ. Eng. Sci. 2015. V. 32. № 1. P. 66–70.
30. Grimalt J.O., Hermosín B., Inmaculada Y.G., Saiz-Jiménez C. // Sci. Total Environ. 1989. № 81. P. 421–428
31. Buzlama V.S., Berkovich A.M., Buzlama A.V. Materials of a satellite symposium ("Olipifat, a new Russian preparation") held by the Blokhin Oncology Research Center. 2002. Moscow [in Russian].
32. Nezhinskaya G.I., Gavrovskaya L.K., Berkovich A.M., Filov V.A. // Questions of Oncology. 2005. V. 51. № 5.
33. Kornilayeva G., Bercovich A., Pavlova T., Karamov E. // XV International AIDS Conf. 2004. 11–16 July, Bangkok, Thailand, abstract book. P. 167.
34. Scultz A., Koch S., Fuss M., Mazzotta A., Sarzotti-Kelsoe M., Ozaki D., Montefiori D., von Briesen H., Zimmermann H., Meyerhans A. // PLoS One. 2012. V. 7. № 12. P. 1–10.

35. Sarzotti-Kelsoe M., Bailer R.T., Turk E., Lin C.-L., Bilska M., Greene K.M., Gao H., Todd C.A., Ozaki D.A., Seaman M.S., et al. // J. Immunol. Methods. 2014. V. 409. P. 131–146.
36. Wei X., Decker J.M., Liu H., Zhang Z., Arani R.B., Kilby J.M., Saag M.S., Wu X., Shaw G.M., Kappes J.C.// Antimicrob. Agents. Chemoter. 2002. № 46. V. 6. P. 1896–1905.
37. Mossman T. // J. Immunol. Methods. 1993. № 65. P. 55–63.
38. Mitsuki Y.Y., Tuen M., Hioe C.E. // J. Leukoc. Biol. 2017. V. 101. № 1. P. 339–350.
39. Guglani L., Khader S.A. // Curr. Opin. HIV AIDS. 2010. № 5. P. 120–127.
40. Brenchley J.M., Price D.A., Schacker T.W., Asher T.E., Silvestri G., Rao S., Kazzaz Z., Bornstein E., Lambotte O., Altmann D., et al. // Nat. Med. 2006. № 12. P. 1365–1371.
41. Dandekar S., George M., Bäumler A.J. // Curr. Opin. HIV AIDS. 2010. № 5. P. 173–178.
42. Gordon S.N., Cervasi B., Odorizzi P., Silverman R., Aberra F., Ginsberg G., Estes J.D., Paiardini M., Frank I., Silvestri G. // J. Immunol. 2010. № 185. P. 5169–5179.
43. Vyboh K., Jenabian M.A., Mehraj V., Routy J.P. // J. Immunol. Res. 2015. № 6. P. 1–9.
44. Visser S.A. // Internat. Humic Substances Soc. Meet. Sevilla, Spain. 1988.

Studying the Possibilities of Using 2-Halogen-Substituted Acetamides As Acyl Donors in Penicillin Acylase-Catalyzed Reactions

N. V. Panin[1], M. V. Nikulin[1,2], E. S. Tiurin[2], V. V. Drobot[1,2], I. A. Morozova[1,2], V.K. Švedas[1*]
[1]Lomonosov Moscow State University, Belozersky Institute of Physicochemical Biology, Lenin Hills 1, bldg. 40, Moscow, 119991, Russia
[2]Lomonosov Moscow State University, Department of Chemistry, Lenin Hills 1, bldg. 3, Moscow, 119991, Russia
*E-mail: vytas@belozersky.msu.ru
Received March 23, 2018; in final form, April 26, 2018
DOI: 10.32607/20758251-2019-11-2-77-81

ABSTRACT **The possibility of using amides of halogen-substituted acetic acids as acyl donors in penicillin acylase-catalyzed reactions has been investigated, and the ability of this group of compounds to inactivate enzymes in the course of the catalytic conversion has been established. The strongest inactivating effect was demonstrated by iodoacetamide and bromoacetamide. However, the negative contribution of this side activity can be minimized by decreasing the temperature, when the rate of acyl donor conversion by penicillin acylases is still high enough, but the impact of enzyme inactivation becomes less significant. The catalytic activity of penicillin acylase from *Alcaligenes faecalis* in the conversion of 2-haloacetamides was significantly (5–8 times) higher than that of penicillin acylase from *Escherichia coli*.**
KEYWORDS **Penicillin acylases, substrate specificity, 2-haloacetamides, inactivation during the reaction**
ABBREVIATIONS **HPLC – high-performance liquid chromatography; NIPAB – 2-nitro-5-(phenylacetyl)amino-benzoic acid; PAA – phenylacetic acid.**

INTRODUCTION

Beta-lactam antibiotics are the most widely used antibacterial drugs of high clinical efficacy and low toxicity. The wide availability of the representatives of this antibiotic class is of great practical value, mainly due to the wide application of biocatalytic technologies in their production. However, the emerging resistance of pathogens to antibiotics limits the period of potency of the developed drugs and makes necessary a search for new derivatives. One of the key routes to creating more efficient semisynthetic analogues is to introduce novel N-acyl substituents covalently bound to the beta-lactam nucleus. The success of this process is directly related to the availability, efficiency, and ease of insertion of such N-acyl groups into the structure of the target compound. The ability of penicillin acylases to catalyze the effective acyl transfer (primarily of D-phenylglycine and *p*-hydroxy-D-phenylglycine residues from their amides and esters to the penicillin and cephalosporin nuclei) has played an important role in addressing the problem of antibiotic resistance. A detailed study of the complicated kinetics of enzymatic acyl transfer to external nucleophiles in aqueous media has revealed the major factors defining the efficiency of the process [1–3]. It allowed researchers to develop methods for the biocatalytic synthesis of ampicillin, amoxicillin, cephalexin, cefaclor, cefonicid, and cefprozil in an aqueous medium without using environmentally harmful organic solvents [4–11]. Further development of biocatalytic methods largely depends on the substrate specificity of the enzymes that are capable of catalyzing the transfer of other acyl groups to the nuclei of beta-lactam compounds. Thus, a combination of biocatalysis and click chemistry seems to be a promising direction, where enzyme-catalyzed synthesis of a beta-lactam compound with an N-acyl substituent containing an activated group is performed as the first step. This beta-lactam compound can then be used as a click-starting material to produce a variety of new derivatives. Synthesis of cefathiamidine, a popular antibiotic on the Chinese pharmaceutical market, can be an example to illustrate this approach. In this case, the

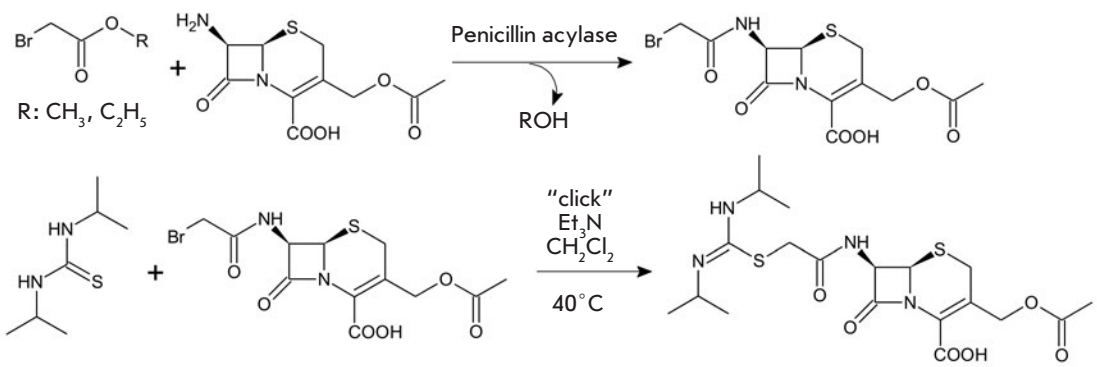

Fig. 1. Synthesis of antibiotic cefathiamidine from the activated N-bromoacetyl derivative of 7-aminocephalosporanic acid

activated N-acyl group is a residue of bromoacetic acid. Subsequent reaction of this group with *N*,*N*'-diisopropylthiourea yields the desired antibiotic (*Fig. 1*) [12, 13].

A sufficiently versatile method for obtaining a wide range of potential antibacterial drugs can be developed by varying the structure of the residue enzymatically inserted into the antibiotic core, the chemical nature of the activated groups, and the structure of the compound used at the click chemistry step.

One can expect the development of such an approach to be complicated by several factors: chemical modification (or even inactivation) of the enzyme due to interaction with activated groups of the initial substrates or final products, spontaneous destruction of the activated groups under the conditions of the biocatalytic reaction, and the necessity to search for suitable enzymes with the requested catalytic activity toward synthetic nonnatural substrates.

The goal of this work was to investigate the possibilities of using halogen-substituted acetic acid derivatives as potential acyl donors in the reactions catalyzed by penicillin acylases from *Escherichia coli* and *Alcaligenes faecalis*, as well as to study the dependence of their reactivity as substrates and ability to inactivate the enzymes on the nature of the activating group.

EXPERIMENTAL

Determination of enzyme activity with respect to 2-haloacetamides

A typical experiment was carried out as follows: 2-haloacetamide (200 μmol) was dissolved in 0.05 M phosphate buffer, thermostated at the desired temperature, and pH was adjusted to 7.5. The total volume of the reaction mixture was 800 μl; the substrate concentration was 0.25 M. The reaction was then started by adding an aliquot of the concentrated enzyme solution so that the concentration of active sites of penicillin acylase in the reaction mixture was 25 μM. The reaction was carried out in a thermostated cell; temperature and pH were maintained constant. Aliquots of 20 μl were sampled at regular intervals and mixed with 980 μl of a stock solution, which was a mixture of acetonitrile and distilled water at a 2:1 ratio (v/v). The samples were centrifuged for 5 min at 13,000 rpm in order to remove the precipitated protein and subjected to reverse phase HPLC analysis. Analysis conditions were as follows: flow rate, 0.7 ml/min; acetonitrile/water (25% acetonitrile v/v, 0.005 M phosphate buffer pH 3) used as an eluent; detection at 210 nm; Kromasil Eternity 5-C18 4.6×250 mm column; and sample volume, 20 μl. Chromatographic resolution R_s of the corresponding amide and acid exceeded 1.5 in all cases. The retention times of the components were as follows: chloroacetamide, 4.16 min; chloroacetic acid, 4.34 min; bromoacetamide, 4.27 min; bromoacetic acid, 4.73 min; iodoacetamide, 4.31 min; and iodoacetic acid, 5.92 min.

Studying the dependence between the conversion rate of the chromogenic substrate and the 2-chloroacetamide concentration

The inhibitory influence of chloroacetamide on the catalytic activity of penicillin acylase was studied using a CLARIOstar high-performance microplate reader (BMG LABTECH). A typical experiment was conducted using the following procedure: aliquots of a 1 mM chromogenic substrate, NIPAB solution, were added to the cells of a 96-well plate in order to create seven vertical columns with the NIPAB concentrations ranging from 0.01 to 0.3 mM, whereas the substrate concentrations in the horizontal rows were equal. Aliquots of a 700 mM inhibitor solution were then added to the cells along the horizontal rows in order to create eight rows of various inhibitor concentrations ranging from 0 to 400 mM, whereas the inhibitor concentrations in the columns were equal. The volume of the reaction mixture in each cell was adjusted to 216 μl by adding the required volume of 0.1 M potassium phosphate buffer (pH 7.5). Solutions of all the reagents were prepared in the same buffer. Reactions were started by adding

20 μl of the stock enzyme solution using a multichannel dispenser; the concentration of active sites of penicillin acylase in each cell was 10 nM. The temperature was maintained at 25°C. The enzyme activity was monitored as an accumulation of chromophore, *p*-nitro-*m*-carboxyaniline, at 400 nm in the Absorbance/PlateMode operating mode of increased accuracy (number of flashes per cell, 30; cycle time, 6 s; number of cycles, 74) with periodic mixing (500 rpm). To avoid random errors caused by the formation of local air bubbles, the absorption was measured in the statistical averaging mode (well scan function, spiral averaging). Stream regression data processing was carried out using the MARS Data Analysis software. The initial reaction rates were determined as the average value of the derivative within 10% of the NIPAB conversion. To determine the inhibition constant, the experimental data were analyzed in Dixon coordinates.

Studying penicillin acylase inactivation by 2-haloacetamides

The inactivation kinetics of penicillin acylase was studied using a CLARIOstar high-performance microplate reader (BMG LABTECH). A typical experiment was as follows: aliquots of a 1 M 2-haloacetamide solution were added to the cells of a 96-well plate in order to create eight rows with different 2-haloacetamide concentrations ranging from 0 to 470 mM, whereas the concentrations in all 12 columns were equal. The left half of the plate was used to study enzyme inactivation by 2-haloacetamide alone, while the right half was used to study the influence of phenylacetic acid (PAA), a highly specific competitive inhibitor of penicillin acylase, on this inactivation. The PAA concentration in all cells of the right half of the plate was 0.1 mM. The volume of the reaction mixture in each cell was adjusted to 196 μl by adding the required volume of 0.1 M potassium phosphate buffer (pH 7.5). Thus, six columns with an identical composition of reagents were created on the left part (without PAA) and on the right part (with PAA). The inactivation reaction was started simultaneously in the first and the seventh column by adding 20 μl of the enzyme stock solution, so that the concentration of the active sites of penicillin acylase in each cell was 10 nM. The aliquots of the enzyme stock solution were sequentially added to each following column using a multichannel dispenser after every 10 minutes of incubation. The temperature was maintained at 25°C. In order to determine the residual enzyme activity 50 min after the first incubation had been started, 24 μl of a 1 mM NIPAB solution was simultaneously added to all the cells. Thus, the concentration of the chromogenic substrate in each cell was 0.1 mM. The time of incubation of the enzyme in the first and seventh columns was 50 min; in the sixth and twelfth columns, 1 min. The residual activity of penicillin acylase was monitored as described above. Enzyme inactivation proceeded according to the first-order reaction kinetics; the corresponding inactivation constant was determined by analyzing the obtained experimental data.

The kinetics of inactivation of penicillin acylase by 2-haloacetamides was also studied using another technique. The enzyme solution (concentration of the active sites, 3 nM) was incubated with 100 mM 2-haloacetamide in 10 mM potassium phosphate buffer (pH 7.5) containing 0.1 M KCl at different temperatures (4, 15 and 25°C). Aliquots of the reaction mixture were sampled at regular intervals and added to a thermostated cuvette (25°C) containing a 0.1 mM NIPAB solution in 10 mM potassium phosphate buffer (pH 7.5) and 0.1 M KCl. The residual activity of the enzyme was monitored using a Shimadzu UV 1800 spectrophotometer at 400 nm.

RESULTS AND DISCUSSION

Selection of halogen-substituted acetic acid derivatives as potential substrates for research

The properties of a chemical compound, such as stability, solubility and usability, should be considered when choosing a substrate for an enzymatic reaction. It is especially important to bear in mind the preparative use of acyl donors. When selecting halogen-substituted acetamides for their study as potential substrates of penicillin acylases, the crucial factors were as follows: higher solubility and stability of amides compared to those of esters and, most importantly, the lachrymatory properties of the corresponding esters. Thus, vapors of ethyl bromoacetate are extremely irritating to the eye mucosa. This substance should be stored in a hermetically sealed vessel and operated with in an open vessel only in a well-functioning fume hood [14].

Studying the ability of 2-haloacetamides to bind in the active site of penicillin acylases

Potential substrates were studied for their ability to bind in the active site of penicillin acylase and thus inhibit its activity toward a chromogenic substrate. A typical example of the influence of 2-chloroacetamide on the catalytic activity of penicillin acylase from *Escherichia coli* is shown in *Fig. 2*. An analysis of the dependence between the conversion rate of NIPAB and the 2-chloroacetamide concentration showed that this compound is a competitive inhibitor with an inhibition constant of 0.12 ± 0.02 M (*Fig. 2*). It was observed that 2-haloacetamides possess lower affinity to the active site of penicillin acylases (by about four orders of magnitude) compared to that of specific substrates of this enzyme. Nevertheless, due to the high solubility of

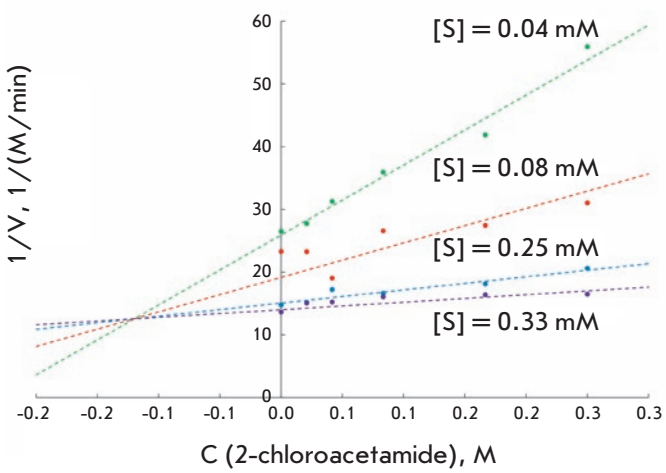

Fig. 2. Dependence between the initial rates of NIPAB hydrolysis catalyzed by penicillin acylase from *Escherichia coli* and concentration of the chromogenic substrate in the presence of various concentrations of 2-chloroacetamide. The experimental data are presented in Dixon coordinates. Experimental conditions: 25°C, 0.1 M potassium phosphate buffer (pH 7.5)

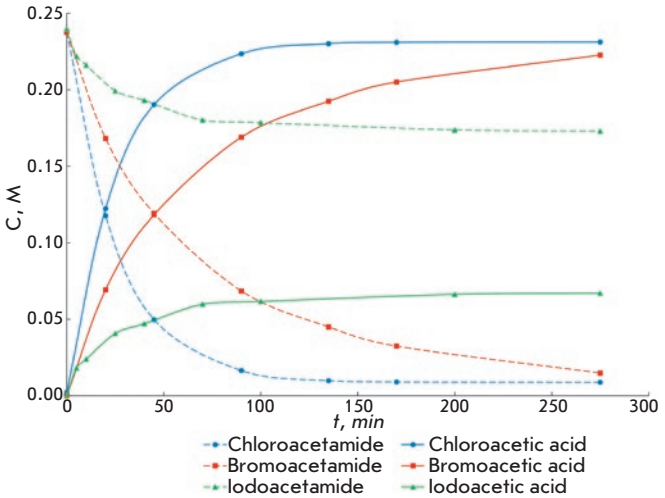

Fig. 3. Accumulation of the reaction products (solid curves) and consumption of the initial substrates (dashed curves) in the course of hydrolysis of 2-haloacetamides catalyzed by penicillin acylase from *Alcaligenes faecalis*. The reaction with chloroacetamide was carried out at 25°C; with bromo- and iodoacetamide, at 4°C. The experimental conditions are shown in the caption to *Table 2*

these substrates, it is possible to use their concentrated solutions and operate in the mode of maximum rate of enzymatic reaction.

Studying the reactivity of potential acyl donors

It was found that enzymatic hydrolysis of 2-haloacetamides is accompanied by inactivation of penicillin acylases. Inactivation especially prevailed in the case of hydrolysis of 2-iodoacetamide and 2-bromoacetamide. Inactivation of both enzymes was caused by binding of haloacetamides in the active site of penicillin acylases and was associated with their catalytic activity, since the addition of phenylacetic acid (a known competitive penicillin acylase inhibitor that binds in the active site) suppressed inactivation. Similar inactivation of penicillin acylase from *E.coli* in the course of a catalytic reaction was previously observed upon preparative enzymatic synthesis of D-phenylglycyl peptides [15]. Loss of enzyme activity upon conversion of the amides of halogen-substituted acetic acids proceeded according to first-order reaction kinetics; the corresponding inactivation rate constants are presented in *Table 1*.

Inactivation of penicillin acylase from *E.coli* by 2-iodoacetamide at an optimal pH of the enzyme and 25°C proceeded so rapidly that the substrate was hydrolyzed only to several percents. Enzyme inactivation in the presence of 2-bromoacetamide was slower, but it also prevented the use of this acyl donor in preparative synthesis under these conditions. We succeeded in slowing down the enzyme inactivation rate and suppressing the negative impact of this process on the catalytic conversion of acyl donors by reducing the temperature (*Fig. 3*). Thus, the loss of enzyme activity was decreased by more than an order of magnitude at 4°C upon hydrolysis 2-bromoacetamide, which makes it possible to use this compound as an acyl donor in reactions catalyzed by penicillin acylases under these conditions. It should also be noted that penicillin acylase from *Alcaligenes faecalis* was more active with respect to this group of substrates compared to the enzyme from *Escherichia coli* (see *Table 2*).

Table 1. The rate constants of inactivation of penicillin acylase from *Escherichia coli* upon enzyme interaction with 2-haloacetamides

Substrate	$k_{in} \cdot 10^4$, min^{-1}
Chloroacetamide	1.1 ± 0.1
Bromoacetamide	47 ± 2
Iodoacetamide	364 ± 34

*Experimental conditions: 25°C, 0.1 M potassium phosphate buffer (pH 7.5), 0.1 M 2-haloacetamide

Table 2. Specificity of penicillin acylases in 2-haloacetamides hydrolysis

Substrate \ Enzyme	Penicillin acylase from *E. coli*	Penicillin acylase from *A. faecalis*
	V, μM/s	
Chloroacetamide (25°C)	7.5 ± 1	63 ± 5
Bromoacetamide (4°C)	10.0 ± 1.3	58 ± 3
Iodoacetamide (4°C)	9.3 ± 1.3	45 ± 2

*Experimental conditions: 0.05 M potassium phosphate buffer (pH 7.5); the experiment with chloroacetamide was carried out at 25°C; with bromo- and iodoacetamide, at 4°C; the concentration of the active sites of penicillin acylase was 25 μM.

CONCLUSIONS

The ability of 2-halogen-substituted acetamides to inactivate penicillin acylases in the course of their conversion has been established by studying the possibility of using this group of compounds as acyl donors in biocatalytic acyl transfer reactions. The most efficient inactivation was observed upon conversion of iodoacetamide and bromoacetamide. However, the negative impact of this side activity can be minimized by lowering the temperature, when the catalytic activity of penicillin acylases with these acyl donors remains rather high and the role of enzyme inactivation in the overall process becomes insignificant. ●

This work was supported by the Russian Science Foundation (grant No. 17-74-10255).

REFERENCES

1. Svedas V.K., Margolin A.L., Borisov I.L., Berezin I.V. // Enzyme.Microb.Technol. 1980. V. 2. P. 313–317.
2. Gololobov M.Y., Borisov I.L., Svedas V.K. // J. Theor. Biol. 1989. V. 140. P. 193–104.
3. Youshko M.I., Švedas V.K. // Biochemistry (Moscow). 2000. V. 65. № 12. P. 1367–1375.
4. Gonçalves L.R.B., Sousa R.Jr., Fernandez-Lafuente R., Guisan J.M., Giordano R.L.C., Giordano R.C. // Biotechnol. Bioeng. 2002. V. 80. № 6. P. 622–631.
5. Youshko M.I., Švedas V.K. // Adv. Synth. Catal. 2002. V. 344. № 8. P. 894–898.
6. Youshko M.I., Van Langen L.M., De Vroom E., Van Rantwijk F., Sheldon R.A., Svedas V.K. // Biotechnol. Bioeng. 2002. V. 78. № 5. P. 589–593.
7. Youshko M.I., Moody H.M., Bukhanov A.L., Boosten W.H.J., Svedas V.K. // Biotechnol. Bioeng. 2004. V. 85. № 3. P. 323–329.
8. Zhang Y.-W., Wei D.-Z. // Preparative Biochemistry & Biotechnology. 2008. V. 38. P. 129–138.
9. Terreni M., Tchamkam J.G., Sarnataro U., Rocchietti S., Fernarndez-Lafuente R., Joser M. Guisan J.M. // Adv. Synth. Catal. 2005. V. 347. P. 121–128.
10. Feng S.-X, Liang S.-Z., Lou W.-Y. // Biocatal. Biotransform. 2008. V. 26. № 4. P. 321–332.
11. Susana M.S.A. Bernardino, Fernandes P., Fonseca L.P. // Biotechnol. Bioeng. 2010. V. 107. № 5. P. 753–762.
12. Wang H.L., Li L.W. // Chin. J. Mod. Appl. Pharm. 2010. V. 27. № 2. P. 126–127.
13. Zhang X.-L., Zong M.-H., Li N. // Bioresour. Bioprocess. 2016. V. 3. № 49. P. 1–8.
14. "Handbook of the chemist" V. 2. Leningrad-Moscow: Publishing House Khimia, 1964. P. 1024–1025.
15. Shcherbakova T.A., Korennykh A.V., van Langen L.M., Sheldon R.A., Švedas V.K. // J. Mol. Catal. B: Enzym. 2004. V. 31. P. 63–65.

The Profile of Post-translational Modifications of Histone H1 in Chromatin of Mouse Embryonic Stem Cells

T. Yu. Starkova[1*], T. O. Artamonova[2], V. V. Ermakova[1], E. V. Chikhirzhina[1], M. A. Khodorkovskii[2], A. N. Tomilin[1,3,*]

[1]Institute of Cytology of the Russian Academy of Sciences, Laboratory of Molecular Biology of Stem Cells, Tikhoretsky Ave. 4, St. Petersburg, 194064, Russia

[2]Peter the Great St.Petersburg Polytechnic University, Politekhnicheskaya Str. 29, St. Petersburg, 195251, Russia

[3]Saint Petersburg State University, 13B Universitetskaya Emb., St. Petersburg, 199034, Russia

*E-mail: t.starkova@incras.ru, a.tomilin@incras.ru

Received March 01, 2019; in final form, April 29, 2019

DOI: 10.32607/20758251-2019-11-2-82-91

ABSTRACT **Linker histone H1 is one of the main chromatin proteins which plays an important role in organizing eukaryotic DNA into a compact structure. There is data indicating that cell type-specific post-translational modifications of H1 modulate chromatin activity. Here, we compared histone H1 variants from NIH/3T3, mouse embryonic fibroblasts (MEFs), and mouse embryonic stem (ES) cells using matrix-assisted laser desorption/ionization Fourier transform ion cyclotron resonance mass spectrometry (MALDI-FT-ICR-MS). We found significant differences in the nature and positions of the post-translational modifications (PTMs) of H1.3-H1.5 variants in ES cells compared to differentiated cells. For instance, methylation of K75 in the H1.2-1.4 variants; methylation of K108, K148, K151, K152 K154, K155, K160, K161, K179, and K185 in H1.1, as well as of K168 in H1.2; phosphorylation of S129, T146, T149, S159, S163, and S180 in H1.1, T180 in H1.2, and T155 in H1.3 were identified exclusively in ES cells. The H1.0 and H1.2 variants in ES cells were characterized by an enhanced acetylation and overall reduced expression levels. Most of the acetylation sites of the H1.0 and H1.2 variants from ES cells were located within their C-terminal tails known to be involved in the stabilization of the condensed chromatin. These data may be used for further studies aimed at analyzing the functional role played by the revealed histone H1 PTMs in the self-renewal and differentiation of pluripotent stem cells.**

KEYWORDS **mouse embryonic stem cells, linker histone H1, post-translational modifications, 2-D electrophoresis, MALDI mass spectrometry.**

ABBREVIATIONS **MALDI-FT-ICR-MS – Fourier transform ion-cyclotron resonance mass spectrometry; PTM – post-translational modifications; ESC – embryonic stem cell; MEF – mouse embryonic fibroblast; AU-PAGE – acetic acid-urea polyacrylamide gel electrophoresis; SDS-PAGE – sodium dodecyl sulfate polyacrylamide gel electrophoresis; meK – lysine methylation; acK – lysine acetylation; pS/T – serine/threonine phosphorylation; MetO – methionine sulfoxide.**

INTRODUCTION

Chromatin architectural proteins include structural proteins, such as histone H1, which are devoid of enzymatic activity, bind nucleosomes without apparent DNA sequence specificity, and change the local and global architecture of chromatin [1–8]. Proteins belonging to the human and mouse histone H1 families include seven somatic subtypes (H1.0 through H1.5, and H1X), three testis-specific variants (H1t, H1T2m, and HILS1), and one variant restricted to oocytes (H1oo) [9–13]. The H1 variants have different evolutionary stability, euchromatin/heterochromatin distribution, and chromatin-binding affinity, which may be a result of post-translational modifications [14–17].

Over the past few decades, chromatin of ES cells and iPS cells has been the focus of extensive research because of the tremendous potential of these cells in biomedicine. Chromatin of these cells has some unique structural features that distinguish it from chromatin of differentiated cells [17–18]. In particular, heterochromatin of ES cells appears to be more relaxed due to a reduced expression of H1 proteins [19] and PTMs of nuclear proteins [18–20], leading to globally increased transcription. In this study, we compared PTMs of the

H1 variants from mouse–differentiated and ES cells. We report on novel ES cell-specific PTMs of H1 and discuss the potential impact of these PTMs on H1 functions and the structure of chromatin in ES cells.

MATERIALS AND METHODS

Ethics statement

All animal procedures were performed according to the Guidelines for the Humane Use of Laboratory Animals, with standards complying with those approved by the American Physiological Society. Mouse experiments were conducted strictly in agreement with the animal protection legislation acts of the Russian Federation and were approved by the Institute's Ethics Board as complying with the requirements for humane use of laboratory animals.

Mouse embryonic fibroblasts (MEFs) were isolated using animals after natural mating, which were sacrificed using the UK Home Office "Schedule 1" procedure requiring no specific ethical approval. The E14Tg2A cell culture was procured from BayGenomics. The NIH/3T3 cells were obtained from the Russian Cell Culture Collection (Institute of Cytology, St. Petersburg, Russia), where they were authenticated by STR DNA profiling analysis.

Mouse cell cultures

NIH/3T3 cells obtained from ATCC and mouse embryonic fibroblasts (MEFs) prepared from mid-gestation mouse embryos [21–22] were cultured in DMEM supplemented with 10% fetal bovine serum, L-glutamine, and 1% penicillin/streptomycin. Mouse ES cells (line E14Tg2A, BayGenomics) were cultured on gelatin-coated dishes in DMEM/F12 supplemented with 15% fetal bovine serum, 1% penicillin/streptomycin, L-glutamine, NEAA, and leukemia inhibitory factor (LIF). The cells were washed with PBS (pH 7.5), harvested with 0.05% trypsin (10 min at 37˚C), and collected by centrifugation at 2,000 g for 5 min. Pellets were frozen in liquid nitrogen and stored at -70˚C. To prepare the H1 samples for subsequent analysis, cells were collected from six plates (d = 10 cm).

Histone H1 variant extraction and separation

To preserve as much of the PTMs as possible, H1 proteins were extracted directly from frozen pellets, avoiding nucleus isolation, according to the previously described procedure [7]. The H1 variants were separated by 2-D electrophoresis as described previously [7–8].

Digestion and MALDI-FT-ICR-MS analysis

Following 2-D electrophoresis, gel fragments containing nuclear proteins were cut out, minced, and treated as described previously [7]. Biological samples were analyzed in two biological and two or three analytical replicates. The mass spectra were recorded and analyzed as described previously [7].

RESULTS

The objective of this study was to compare the PTMs of linker histones H1 from differentiated and pluripotent mouse stem cells. To separate the histone H1variants, we used a combination of AU-PAGE and SDS-PAGE, which is especially versatile for identifying charged acid-soluble proteins, including histones [7, 8, 23, 24]. *Figure 1* shows the results of 2-D electrophoretic separation of H1 from two types of differentiated cells (namely, spontaneously immortalized mouse embry-

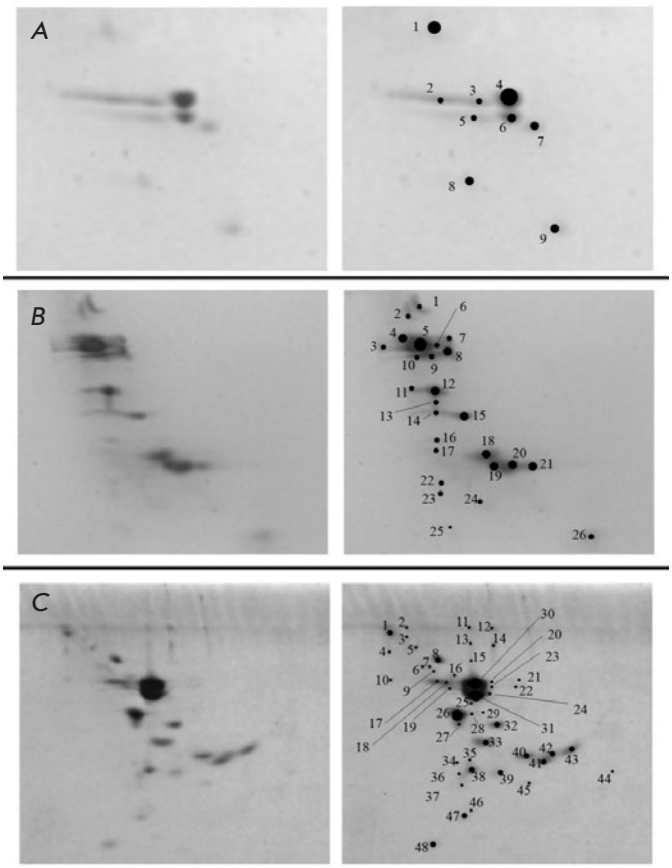

Fig. 1. Two-dimensional gel electrophoresis of H1-enriched extracts from NIH/3T3 cells (A), MEFs (B), and ES cells (C). H1 variants were identified in five fractions (marked 2–4, 6–7 in A), seven fractions (marked 4–10 in B), and eight fractions (marked 15–18, 20–21, 30–31 in C) for NIH/3T3, MEFs, and ES cells, respectively. The remaining fractions were attributed to the HMGB and HMGN of High-Mobility Group family proteins and other nuclear proteins (Table S1 [25])

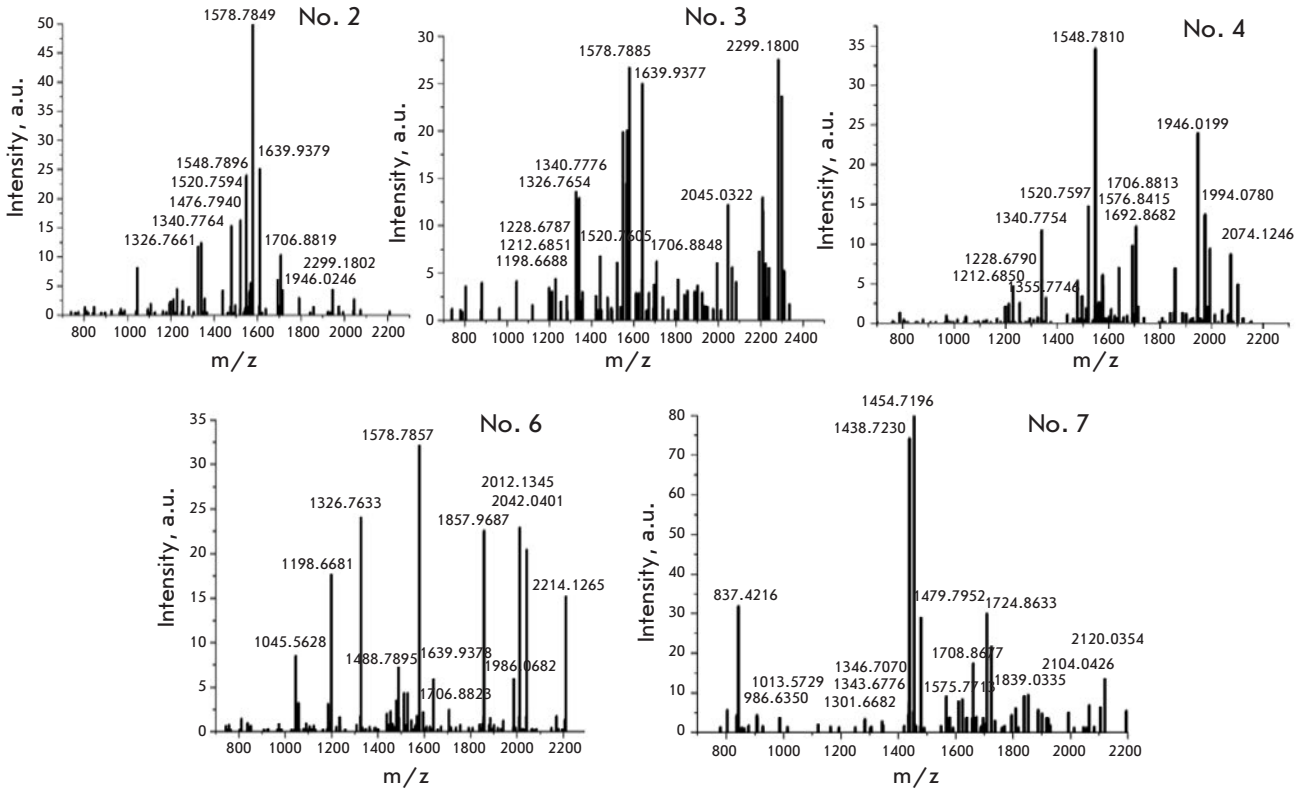

Fig. 2. Mass spectrum of the 2D NIH/3T3 H1 zones

onic fibroblasts (line NIH/3T3) and primary mouse embryonic fibroblasts (MEFs)) and from pluripotent stem cells (namely, mouse ES cells (line E14)). We identified H1 subtypes in NIH/3T3 cells (five fractions; *Fig. 1A*), MEFs (seven fractions; *Fig. 1B*), and ES cells (eight fractions; *Fig. 1C*). The remaining fractions were attributed to members of High Mobility Group family proteins and other nuclear proteins (*Table S1* [25]**)**. The results of the MS analysis of H1 are presented in *Table S2* [25] and *Figs. 2–4*.

Six H1 isoforms (H1.0, H1.1, H1.2, H1.3, H1.4, and H1.5) were detected and analyzed. We identified PTMs of H1 from NIH/3T3, MEFs, and ES cells (*Table*), which were represented by acetylation, methylation, and phosphorylation. The results are summarized in *Fig. 5,* which additionally includes the previously identified PTMs of H1 from mouse thymus [7]. The data for the H1.0 mouse thymus variant were missing, so we relied on the data obtained for MEFs and NIH/3T3 cells.

DISCUSSION

Methylation

H1 histones represent one of the main groups of nuclear proteins of chromatin that participate in the longitudinal compaction of replicated chromosome [24]. In chromatin of ES cells, there are 0.5 molecules of total H1 histone per nucleosome, which is twofold lower than in chromatin of differentiated cells [26]. Depletion of linker histone H1 in mice reduces chromatin compaction, global nucleosome spacing, and the overall levels of PTMs of some histones [26].

A comparative analysis of the H1 variants from NIH/3T3, MEFs, and ES cells revealed that the overall methylation of the H1.4 and H1.5 variants in ES cells was reduced compared to that in differentiated cells (*Fig. 5*). The identified methylation of H1 proteins in this region occurred at K34/K35, K63/65, and K73/75, depending on the H1 variant (*Table*).

Many of the PTMs, such as meK63/64 for the H1.2-H1.4 variants, meK47 for H1.3, meK97 for H1.2, meK117 for H1.2, and meK27 for H1.5, have been previously reported [7, 8, 10–12]. Methylation at these positions is thought to protect the ε-amino groups of lysines by increasing histone affinity to DNA and facilitating their transition to a locally repressed chromatin state [7, 8]. Importantly, we identified methylation at K75 for the H1.2-H1.4 variants exclusively in ES cells (*Fig. 5, Table S2* [25]). This PTM is located within the globular domain and may result in the protection of the ε-amino groups of the lysines in these cells.

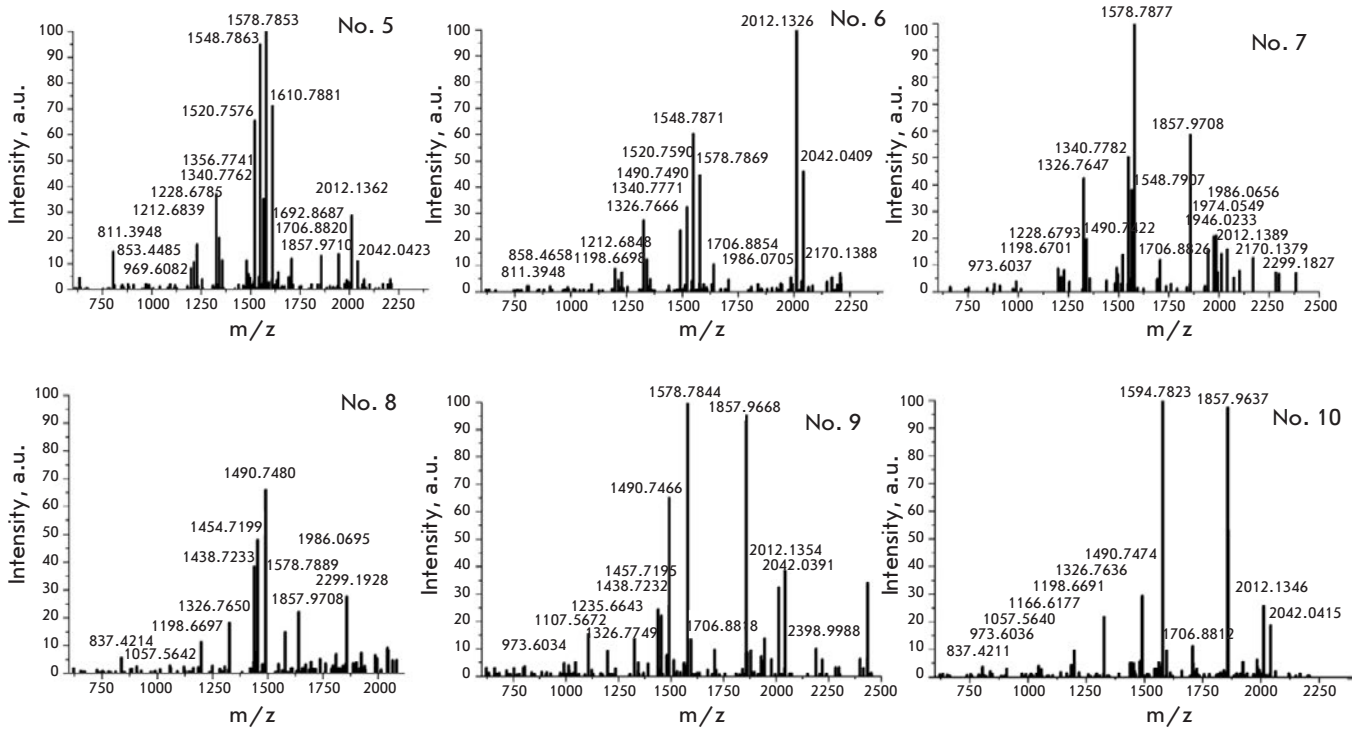

Fig. 3. Mass spectrum of the 2D MEFs H1 zones

Methylation of K108, K148, K151, K152 K154, K155, K160, K161, K179, and K185 in H1.1, as well as that of K168 in H1.2, has been identified exclusively in ES cells, whereas methylation of K202 and K204 in H1.4 may be limited to differentiated NIH3T3 cells and MEFs. Most of these PTMs are located within S/TPXK or (S/T) PXZ motifs near the phosphorylated serines and threonines of H1. The potential role of these modifications will be discussed in the Methyl/acetyl/phospho crosstalk section.

Acetylation

Our data demonstrated that the overall H1 acetylation level in ES cells had increased compared to that in differentiated cells (*Fig. 5*). As expected, we identified multiple acetylation sites in the N-terminal and globular domains of H1 (*Table*). In most cases, the exact biological role of these modifications remains unknown. One of the best studied acetylation sites is acK34-H1.4. The acK34-H1.4 is a hallmark of the promoters of the transcriptionally active gene and helps recruit the general transcription initiation complex TFIID to the promoters [27]. However, we have not identified this PTM in NIH/3T3, MEFs, and ES cells. We found methylation at this position of H1.4 in NIH/3T3 and MEFs but not in ES cells; the role of these modifications is not clear yet. Methylation protects the ε-amino groups of lysine, thus increasing histone affinity to DNA and facilitating the transition to a locally repressed chromatin state. Demethylation of K34-H1.4 in ES cells, on the other hand, may favor acetylation at this site and facilitate recruitment of the general transcription factor TFIID to the promoters.

AcK83 and acK87 of H1.1 and acK81 of H1.2 have been identified exclusively in ES cells. Reduction in the positive charge in this region due to acetylation of the amino group of lysine residues may destabilize H1-DNA interactions, resulting in the formation of a locally relaxed chromatin state.

The formation of open chromatin may also be facilitated by acetylation of lysine residues at the C-terminal regions of the H1.1-H1.3 variants. The reduced positive charge of the C-terminal domains of H1 proteins could weaken DNA/H1 interactions at the entry/exit regions of the core particle and prevent H1 interaction with regulatory chromatin proteins. Moreover, most of these C-terminal ES cell-specific acetylation and methylation sites of the H1.1-H1.3 variants are located within the S/TPXK or (S/T) PXZ motifs near the phosphorylated serines and threonines. Their potential biological role and the mechanism of regulation of H1-DNA interaction mediated by acetylation/methylation of lysins

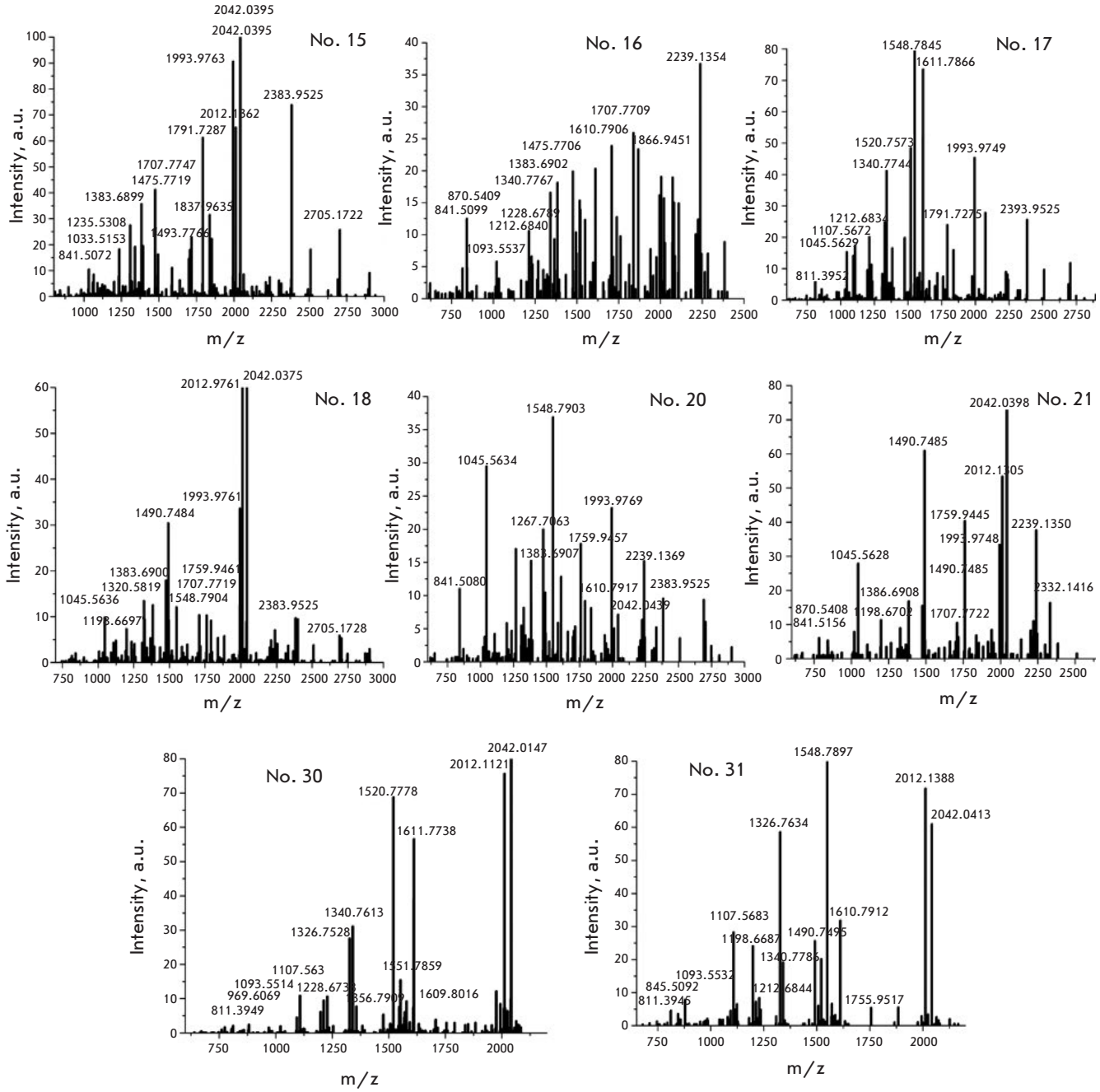

Fig. 4. Mass spectrum of the 2D ES H1 zones

within the S/TPXK or (S/T)PXZ motifs will be discussed in more detail in the Methyl/acetyl/phospho crosstalk section.

Phosphorylation

We identified several phosphorylation sites of H1: T24, S115, T120, and S123 of H1.1, S2, S41, T154, and T173 of H1.2 in both differentiated and ES cells. However, phosphorylation of S129, T146, T149, S159, S163, and S180 of H1.1; T180 of H1.2; and T155 of H1.3 were identified exclusively in ES cells, whereas S36 and S204 of H1.4 were not phosphorylated specifically in these cells (*Fig. 5*, *Table S2* [25]). The identified phosphorylation sites are located mainly in the C-terminal portions of H1 variants, and some of these are located within the methyl/acetyl-phospho motifs (S/T)PXK and (S/T)PXZ, which are phosphorylated during mitosis, resulting in the modulation of chromatin states (*Fig. 5*) [15,

Table. Potential modifications of the H1 histone variants from NIH/3T3, MEF, and ES cells identified by MALDI mass spectrometry. The modifications previously described in the literature are shown in bold

	H1 variant	modifications	Modification position
NIH/3T3	H1.0	Acetylation	**K12**, K132, K136, K137, K149
		Methylation	K139, K155, K156
		Phosphorylation	S135, T153
	H1.1	Acetylation	K17
		Methylation	K116, K121, K125
		Phosphorylation	S2, **S115**, T120
	H1.2	Acetylation	K17
		Methylation	**K46**, **K63**, K90, **K97**, **K117**, K121
		Phosphorylation	**S2**, S41, S89, T96, S113
	H1.3	Acetylation	K17
		Methylation	**K47**, **K64**
	H1.4	Acetylation	K17
		Methylation	**K34**, **K46**, **K63**, K195, K197, K200, **K202**, **K205**
		Phosphorylation	T18, S36, S41, T45
	H1.5	Acetylation	**K17**, K26, K12, K 180
		Methylation	**K27**, K31, K51, K62, **K63**, K74
		Phosphorylation	**S18**, T25, S40, S57, S111, T121, T132
MEFs	H1.0	Acetylation	**K12**, K180, K182, K184, K188
		Methylation	K14, K69, K73
		Phosphorylation	S66, T84, S185
	H1.1	Acetylation	**K17**, **K22**, K23, K29
		Methylation	**K35**, K116 , K121 , K125
		Phosphorylation	T24, **S115**, T120, S123
	H1.2	Acetylation	**K17**, K153, K156, K157, K159, K206, K210
		Methylation	K21, K22, **K46**, **K106**, **K117**, K121, **K148**
		Phosphorylation	**S2**, S41, **T154**, **T173**
	H1.3	Acetylation	K17
		Methylation	**K47**, **K64**
		Phosphorylation	T18
	H1.4	Acetylation	K17
		Methylation	**K34**, **K46**, **K63**, K195, K197, K200, **K202**, **K205**
		Phosphorylation	**S36**, **S41**, T45, **S204**
	H1.5	Acetylation	**K17**, K26, K143
		Methylation	**K27**, K31, **K45**, K62, K74, K134, K144, K147, K191, K193
		Phosphorylation	S111, T132, T149, S192
ES cells	H1.0	Acetylation	**K12**, K17, K20, K121, K122, K125, K127, K136, K137, K147, K148, K149, K155, K184, K188
	H1.1	Acetylation	**K17**, K83, **K87**, K133, K134, K136, K137, K144, K167, K168, K183
		Methylation	K108, K116, K148, K151, K152, K154, K155, K160, K161, K179, K185
		Phosphorylation	T24, S88, **S115**, T120, S123, S129, T146, T149, S159, S163, S180
	H1.2	Acetylation	**K17**, K81, **K122**, **K127**, K130, K149, K153, K156, K157, K172, K175, K176, K178
		Methylation	**K46**, **K63**, K75, K121, **K148**, **K168**
		Phosphorylation	**T154**, **S173**, T180
	H1.3	Acetylation	**K17**, K154, K157, K158
		Methylation	**K47**, **K64**, K75
		Phosphorylation	T155
	H1.4	Acetylation	K17
		Methylation	**K46**, **K63**, K75
	H1.5	Acetylation	K17
		Methylation	K45, K74

28–34]. It remains to be experimentally determined whether the observed phosphorylation at some sites and/or lack thereof at the other sites within H1 variants is functionally related to the maintenance of the pluripotent states of ES cells and/or the differentiation capacity of these cells.

Phosphorylation at S173 (H1.2) and S187 (H1.4) occurs during interphase and is necessary for chromatin relaxation and activation of transcription [15, 30–32]. Taking into account the fact that these serines lie within the methyl-phospho switch motifs, methylation of K172 of H1.2 in ES cells may promote phosphorylation of the adjacent S173. The pS173 may, in turn, promote acetylation of K172, leading to transcription activation.

Methyl/acetyl/phospho crosstalk

In addition to stand-alone PTMs of H1, we identified several conjoint PTMs, such as the following methylation/phosphorylation sites: meK148/pT149-H1.1 and meK179/pS180-H1.1 in ES cells, meK191/pS192-H1.5 in MEFs, which are located mainly in the C-terminal regions of the proteins (*Fig. 5*). Their structural organization resembles the methyl-phospho switch regions of core histones; one relevant example is the K9/S10 site in histone H3 [35–38]. The regulatory state of the K9/S10 site is characterized by a stable meK and dynamic phosphorylation of the S/T residue located next to K. Phosphorylation of S10 and S28 in H3 leads to acetylation at K9 and K27, respectively, resulting in transcription activation [39].

In addition, we also identified several other acetylation/phosphorylation sites, including acK17/pT18 in H1.4 and H1.5 from NIH/3T3 cells, acK17/pT18 in H1.3 from MEFs, acK23/pT24 in H1.1 from MEFs, acK184/pS185 in H1.0 from MEFs, acK153/pT154 in H1.2 from MEFs and ES cells, acK154/pT155-H1.3 from ES cells, and acK172/pS173 in H1.2 from ES cells. These acetylation/phosphorylation regions are characteristic of both ES and differentiated cells. Their structural organization resembles that of the methyl-phospho switch regions, with the only exception that methylation changes to acetylation. It is possible that the mechanisms of methyl/acethyl-phospho region regulation of H1 are similar to those discussed above for the methyl-phospho switch regions of core histones [40–41]. In this scenario, acetylation of the lysines within the K(S/T) motif may lead to transcription activation in a similar fashion. This hypothesis, however, requires further experimental validation.

Citrullination

Citrullination of H1.2 to H1.4 at R54 promotes acquisition and maintenance of the pluripotent cell state [42]. Mechanistically, it displaces H1 from chromatin, promoting an open chromatin state. Citrullination is the replacement of arginine with citrulline. This change leads to the displacement of the peak of ERSGVSLAALK peptide at 0.9844 m/z in the mass spectra. We observed a "displacement" peak of low intensity in the region of 1131.64 m/z, but the determination accuracy is expressed as 9.8 ppm. When analyzing the modifications, we did not take into account peaks higher than 3.0 ppm. Therefore, we cannot clearly establish whether citrullination takes place in our H1.2–H1.4 ES samples. Additional studies and MS/MS mass spectrometry are needed to verify this assumption.

Formylation

Formylation of H1 variants was revealed in H1.2 at the K63-K85 and K97 positions in mouse tissues but not in cell lines [43]. We did not identify H1 formylation sites in H1 variants from the cells. The biological role of formylation is unknown, but it has been suggested that a specific enzyme can catalyze formylation during demethylation of lysines by amine oxidase LSD1 [44].

Oxidation

We identified the oxidation site for methionine at the M31 position for H1.0 of NIH/3T3 and MEFs but not in ES cells (*Table 2S* [25]). Oxidation of methionine produces MetO (methionine sulfoxide) [45]. The positions of M residues in proteins often contribute to the formation of the hydrophobic bonds between their sulfur atoms and rings of the aromatic residues of tryptophan, phenylalanine, or tyrosine [46]. These hydrophobic sulfur-ring bonds ensure the structural stability of proteins, which is approximately equal to that of an ionic salt bridge [46]. The interaction with M establishes the optimal positioning needed to ensure antioxidant protection of aromatic amino acids. Oxidation of methionine to MetO destroys this hydrophobic bond and may destroy the normal protein 3D folding. Oxidized proteins are characterized by increased surface hydrophobicity [47], which correlates with the age-related increase in the MetO content [45]. The absence of oxidation sites of H1 in ES cells is consistent with the unlimited self-renewal potential of these cells.

CONCLUSIONS

In this study, we compared the PTMs of H1 from differentiated and pluripotent cells. We have shown that the total levels of methylation/acetylation of H1.3–H1.5 in ES cells are similar to those in differentiated cells; however, we have not found any significant differences between the nature and positions of the post-translational modifications in the H1.3-H1.5 proteins of ES and differentiated cells. In addition to re-

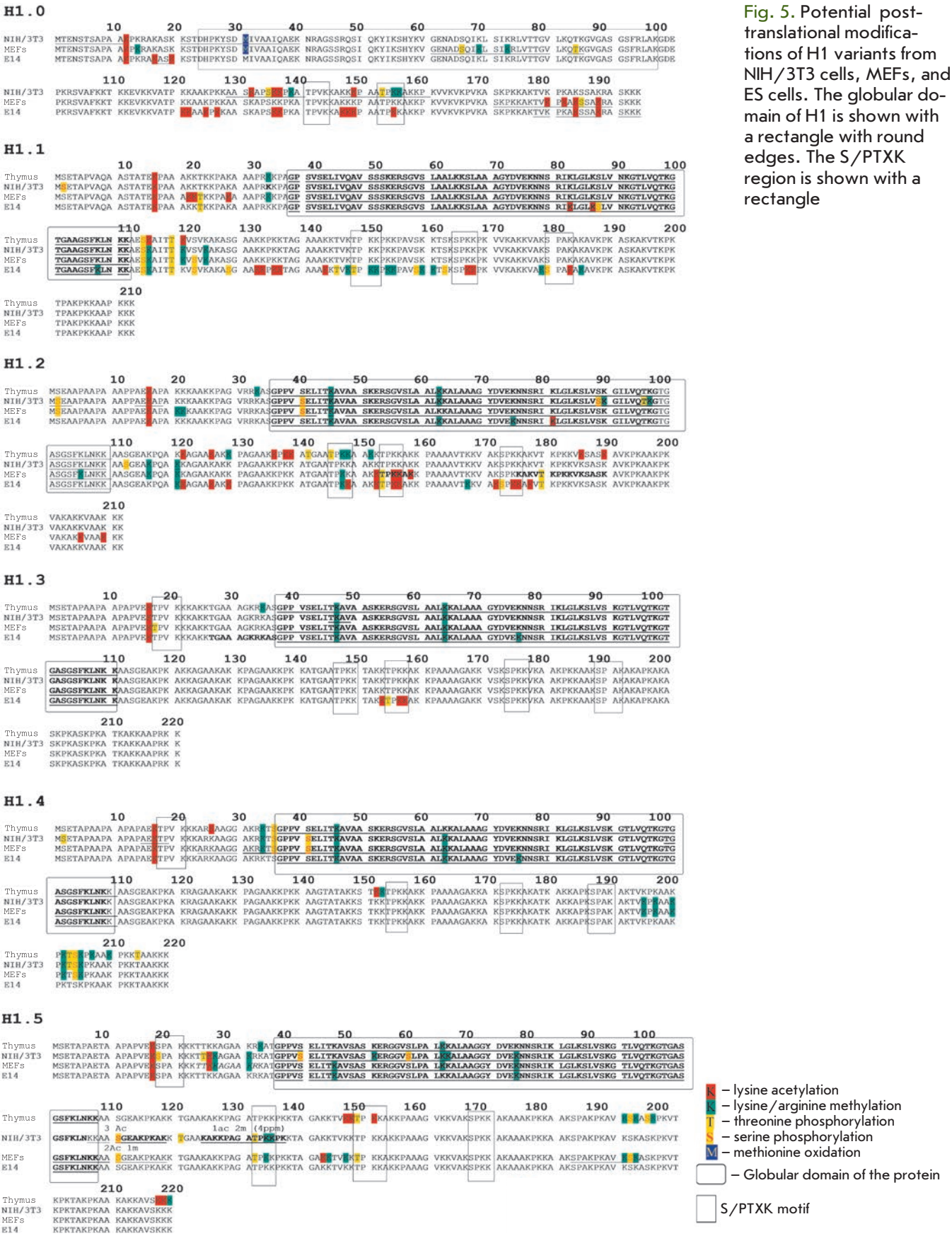

Fig. 5. Potential post-translational modifications of H1 variants from NIH/3T3 cells, MEFs, and ES cells. The globular domain of H1 is shown with a rectangle with round edges. The S/PTXK region is shown with a rectangle

duced H1.0 expression levels in pluripotent cells [20], we have demonstrated that H1.0 and H1.2 are also characterized by an increased acetylation in ES cells (*Fig. 5*). The majority of acetylation sites in H1.0 and H1.2 from ES cells are located within the C-terminal domains of the proteins, namely in the 97–121 and 145–169 regions. These regions are present within the two known sub-domains of the C-terminal tail, which are involved in the stabilization of condensed chromatin [20, 48]. Reduction of the positive charge of the N- and C-terminal regions of H1 proteins could weaken the H1–DNA interaction at the entry/exit regions of the core particle and prevent H1 interaction with regulatory chromatin proteins such as HMGN and HMGB1/2 [49–50]. It is known that HMGB1/2-proteins are able to displace histone H1, thus facilitating nucleosome remodeling and modulating the accessibility of nucleosomal DNA to transcription factors or other sequence-specific proteins [51]. Displacement of H1 from the nucleosome should lead to the formation of an open chromatin structure, which is characteristic of stem cell chromatin.

Thus, an open structure of chromatin in pluripotent stem cells can be effected both by a reduction of the total level of H1 expression and by the presence of post-translational modifications in H1 proteins (H1.0, H1.2), which lead to disruption of their binding to DNA and, as a consequence, to the formation of chromatin with a looser structure. The biological role of the currently best known H1 modifications is not clear yet. Further studies are required to identify the functional roles of PTMs and to elucidate their crosstalk. This knowledge will contribute to a deeper understanding of the molecular processes that underlie the chromatin function in pluripotent cells. ●

These studies were supported by the Russian Foundation for Basic Research (grant No. 18-04-01199). MALDI-mass spectrometry analysis of H1 proteins was carried out using the scientific equipment of the Center of Shared Usage ("The analytical center of nano- and biotechnologies of SPbSPU") with financial support from the Ministry of Education and Science of the Russian Federation.

REFERENCES

1. White A.E., Hieb A.R., Luger K. // Sci. Rep. 2016. V.6 № 19122. P.1-14.
2. Ausió J. // Bioessays. 2015. V.37. P. 46-51.
3. Crane-Robinson C. // Biochim Biophys Acta. 2016. V.1859. № 3. P. 431-435.
4. Song F., Chen P., Sun D., Wang M., Dong L., Liang D., Xu R.M., Zhu P., Li G. // Science. 2014. V. 344. № 6182. P. 376–380.
5. Zhou B.R, Jiang J, Feng H., Ghirlando R., Xiao T.S., Bai Y. // Mol Cell. 2015. V. 59. № 4. P. 628-638.
6. Chikhirzhina E., Starkova T., Polyanichko A. The Role of Linker Histones in Chromatin Structural Organization. 1. H1 Family Histones. Biophysics. 2018. Vol. 63, No. 6, pp. 858–865.
7. Starkova T.Y., Polyanichko A.M., Artamonova T.O. Khodorkovskii M.A., Kostyleva E.I., Chikhirzhina E.V., Tomilin A.N. // Physical Biology. 2017. V.14 P. 016005.
8. Kowalski A., Pałyga J. // Gel Electrophoresis – Principles and Basics. 2012. V.8. P. 117-136.
9. Parseghian M.H., Newcomb R.L., Hamkalo B.A. // J Cell Biochem. 2001. V. 83. P. 643-659.
10. Happel N., Doenecke D. // Gene. 2009. V. 431. P. 1-12.
11. Izzo A., Kamieniarz K., Schneider R. // Biol Chem. 2008. V. 389. P. 333-343.
12. Fyodorov D.V., Zhou B.R., Skoultchi A.I., Bai Y. // Nat. Rev. Mol. Cell. Biol. 2018. V. 19.P. 192-206.
13. Millán-Arino L., Izquierdo-Bouldstridge A., Jordan A. // Biochim Biophys Acta. 2016. V.1859. P. 510-519.
14. Khochbin S. // Gene. 2001. V. 271. P. 1–12.
15. Talasz H., Sapojnikova N., Helliger W., Lindner H., Puschendorf B. // J Biol Chem. 1998. V. 273. P. 32236–32243.
16. Ponte I., Vidal-Taboada J.M., Suau P. // Mol. Biol. Evol. 1998. V.15. P. 702–708.
17. Th'ng J.P., Sung .R, Ye M. et al, // J Biol Chem. 2005. V. 280. P.27809–17814.
18. Serrano L., Vazquez B.N., Tischfield J. // Experimental Biology and Medicine. 2013. V. 238. P. 259–270.
19. Meshorer E., Yellajoshula D., George E., Scambler P.J., Brown D.T., Misteli T. // Developmental Cell. 2006. V.10. № 1. P. 105–116.
20. Terme J.M., Sesé B., Millán-Ariño L. Mayor R., Izpisúa Belmonte J.C., Barrero M.J., Jordan A. // J Biol Chem. 2011. V. 286. P. 35347-35357.
21. Liskovykh M, Chuykin I, Ranjan A., Safina D., Popova E., Tolkunova E., Mosienko V., Minina J., Zhdanova N., Mullins J. et al. // PLoS ONE. 2011. V. 11. P. e27345.
22. Liskovykh M., Ponomartsev S, Popova E., Bader M., Kouprina N., Larionov V., Alenina N., Tomilin A. // Cell Cycle. 2015. V. 4. № 8. P. 1268-1273.
23. Goldknopf I.L., Busch H. // Physiol Chem Phys. 1975. V.7. P. 23-30.
24. Maresca T.J., Heald R. // Cell Cycle. 2006. V. 5. P. 589-591.
25. https://drive.google.com/open?id=15hmp5ku-JHzy3PX-W8vAtHk13jYt97Fty
26. Fan Y., Nikitina T., Zhao J., Fleury T.J., Bhattacharyya R., Bouhassira E.E., Stein A., Woodcock C.L., Skoultchi A.I. // Cell. 2005. V. 123. № 7. P. 1199-1212.
27. Kamieniarz K., Izzo A., Dundr M., Tropberger P, Ozretic L., Kirfel J., Scheer E., Tropel P., Wisniewski J.R., Tora L., et. all. // Genes Dev. 2012. V. 26. № 8. P. 797-802.
28. Dou Y., Gorovsky M.A. // Mol Cell. 2000. V.6. P. 225-231.
29. Chadee D.N., Taylor W.R., Hurta R.A., Allis D., Wright J., Davie J. // J Biol Chem. 1995. V. 270. P. 20098-20105.
30. Sarg B., Helliger W., Talasz H., Forg B., Lindner H. // J Biol Chem. 2006. V. 281. P.6573–6580.
31. Harshman S.W., Young N.L., Parthun M.R, Freitas M.A. // Nucl Acids Res. 2013. V. 41. №21. P. 9593-9609.
32. Liao R. ,Mizzen C.A. // Biochim Biophys Acta. 2016. V. 1859. P. 476-485.
33. Alexandrow M.G., Hamlin J.L. // JCB. 2005. V.168. P. 875-886.

34. Strunnikov A.V., Hogan E., Koshland D. // Genes Dev. 1995. V. 9. P. 587-599.
35. Daujat S., Zeissler U., Waldmann T., Happel N., Schneider R.// J Biol Chem. 2005. V. 280. P. 38090-38095.
36. Lachner M., Jenuwein T. // Curr Opin Cell Biol. 2002. V. 14. P. 286–298.
37. Li Y., Danzer J.R., Alvarez P. Belmont A.S., Wallrath L.L. // Development. 2003. V. 130. P. 1817–1824.
38. Ayyanathan K., Lechner M.S., Bell P., Maul G.G., Schultz D.C., Yamada Y., Tanaka K., Torigoe K., Rauscher F.J. III // Genes Dev. 2003. V. 17. №15. P. 1855–1869.
39. Rossetto D., Avvakumov N., Cote J. // Epigenetics. 2012. V. 10. P. 1098–1108.
40. Cheung P., Tanner K.G., Cheung W.L., Sassone-Corsi P., Denu J.M., Allis C.D. // Mol Cell. 2000. V.5. №6. P. 905- 915.
41. Chadee D.N., Hendzel M.J., Tylipski C.P. Allis C.D., Bazett-Jones D.P., Wright J.A., Davie J.R. // J Biol Chem. 1999. V. 274. P. 24914-24920.
42. Christophorou M.A., Castelo-Branco G., Halley-Stott R.P. Oliveira C.S., Loos R., Radzisheuskaya A., Mowen K.A., Bertone P., Silva J.C., Zernicka-Goetz M. et al, // Nature. 2014. V. 507. № 7490. P. 104–108.
43. Wisniewski J.R., Zougman A., Krüger S., Mann M. // Mol Cell Proteomics. 2007. V. 6. № 1. P. 72–87.
44. Shi Y., Lan F., Matson C., Mulligan P., Whetstine J.R., Cole P.A., Casero R.A., Shi Y.// Cell. 2004. V. 119. P. 941–953.
45. Kim G., Weiss S.J., Levine R.L. // Biochim Biophys Acta. 2014. V. 1840. P. 901-905.
46. Valley C.C., Cembran A., Perlmutter J.D. Lewis A.K., Labello N.P., Gao J., Sachs J.N. // J Biol Chem. 2012. V. 287. № 42. P. 34979–34991.
47. Chao C.C., Ma Y.S., Stadtman E.R. // Proc Natl Acad Sci USA. 1997. V. 94. P. 2969–2974.
48. Lu X., Hansen J.C. // J Biol Chem. 2004. V. 279. P. 8701-8707.
49. Roque A., Ponte I., Suau P. // Chromosoma. 2016. V. 1859. P. 510-519.
50. Murphy K.J., Cutter A.R., Fang H. et al, // NAR. 2017. V. 45 P. 9917–9930
51. Stros M. // Biochim Biophys Acta. 2010. V. 799. P. 101–113.

A New MicroRNA Cluster Involved in the Reprogramming to a Pluripotent State

V. V. Sherstyuk[1,2,3,4#], G. I. Davletshina[1,2#], Y. V. Vyatkin[3,5,6], D. N. Shtokalo[5,6,7], V. V. Vlasov[4], S. M. Zakian[1,2,3,4*]

[1]The Federal Research Center Institute of Cytology and Genetics SB RAS, Lavrentyeva Ave. 10, Novosibirsk, 630090, Russia

[2]E.Meshalkin National medical research center Ministry of Healthcare of the Russian Federation, Rechkunovskaya Str. 15, Novosibirsk, 630055, Russia

[3]Novosibirsk State University, Pirogova Str. 2, Novosibirsk, 630090, Russia

[4]Institute of Chemical Biology and Fundamental Medicine SB RAS, Lavrentyeva Ave. 8, Novosibirsk, 630090, Russia

[5]AcademGene LLC, Lavrentyeva Ave. 6, Novosibirsk, 630090, Russia

[6]St. Laurent Institute, New Boston St., 317, 01801, Woburn, MA, USA

[7]A.P.Ershov Institute of Informatics Systems SB RAS, Lavrentyeva Ave. 6, Novosibirsk, 630090, Russia

*E-mail: zakian@bionet.nsc.ru

#These authors contributed equally to the work

Received October 31, 2018; in final form, April 10, 2019

DOI: 10.32607/20758251-2019-11-2-92-97

ABSTRACT **Reprogramming of somatic cells to a pluripotent state is a complex, multistage process that is regulated by many factors. Among these factors, non-coding RNAs and microRNAs (miRNAs) have been intensively studied in recent years. MiRNAs play an important role in many processes, particularly in cell reprogramming. In this study, we investigated the reprogramming of rat fibroblasts with a deleted locus encoding a cluster comprising 14 miRNAs (from miR-743a to miR-465). The deletion of this locus was demonstrated to decrease significantly the efficiency of the cell reprogramming. In addition, the cells produced by the reprogramming differed from rat embryonic and induced pluripotent stem cells, which was an indication that reprogramming in these cells had not been completed. We suggest that this miRNA cluster or some of its members are involved in regulating the reprogramming of rat cells to a pluripotent state.**

KEYWORDS **microRNA, pluripotent stem cells, reprogramming, CRISPR/Cas9.**

ABBREVIATIONS **iPSC – induced pluripotent stem cell; miRNA – microRNA; ESC – embryonic stem cell; CRISPR – clustered regularly interspaced short palindromic repeat; PAM – protospacer adjacent motif; RT-PCR – reverse transcription polymerase chain reaction; AP – alkaline phosphatase.**

INTRODUCTION

Pluripotent stem cells are cells capable of differentiating into derivatives of all three germ layers. One of the ways to produce pluripotent stem cells is to reprogram somatic cells by overexpressing Oct4, Sox2, Klf4, and c-Myc pluripotency factors [1]. This process results in the so-called induced pluripotent cells (iPSCs) that are widely used for studying early developmental and differentiation processes and modeling hereditary diseases and are a promising source of the cellular derivatives used in regenerative medicine. The reprogramming mechanisms have been well studied, and the changes in gene expression, chromatin organization, and metabolism are known. In addition, this process involves microRNAs (miRNAs) that are a class of small non-coding RNAs, from 18 to 23 nucleotides in length, that participate in post-transcriptional regulation of gene expression. MiRNAs play an important role in the regulation of various processes, including organism development and cell differentiation. To date, many miRNAs expressed in human, mouse, and rat pluripotent stem cells are known. The most studied miRNAs involved in the reprogramming process belong to the miR-290-295 and miR-302-367 clusters and miR-200 family [2]. However, many other miRNAs are involved in cell reprogramming as well; their functions remain unknown. Earlier, we analyzed the expression of miRNAs in rat embryonic stem cells (ESCs), iPSCs, and

embryonic fibroblasts and identified a miRNA cluster on the X chromosome (from miR-743a to miR-465) which was characterized by an increased expression level in pluripotent cells compared to that in fibroblasts [3]. In addition, expression of some miRNAs in this cluster decreases during spontaneous differentiation of pluripotent cells. Our findings suggest that these miRNAs may be involved in the processes of self-renewal and pluripotent state maintenance in stem cells, as well as in their reprogramming. To investigate the involvement of these miRNAs in the reprogramming process, we obtained rat fibroblasts carrying a deletion of the genome region encoding the miRNAs under study. Deletion of this region disrupts reprogramming to a pluripotent state, which indicates involvement of this miRNA cluster or some of its members in the regulation of the reprogramming process.

EXPERIMENTAL

Guide RNAs flanking a target miRNA cluster were selected using the Benchling online platform (https://benchling.com/crispr). We chose the following protospacers: 5'-CTTAGTTAACAGATTAGGAC-3' (PAM-TGG) and 5'-TTGCTAGAGTAATACCAACT-3' (PAM-TGG). The oligonucleotides were inserted into the pX-458-2sgRNA vector at the BbsI and BsaI sites. The pX-458-2sgRNA vector was obtained by hydrolysis of the pX333 vector (Addgene Plasmid #64073) by XbaI and KpnI restriction endonucleases, isolation and purification of a 444 bp fragment, and insertion of the fragment into the pSpCas9(BB)-2A-GFP (PX458) vector (Addgene Plasmid #48138) hydrolyzed by XbaI and KpnI.

Rat fibroblasts were cultured at 37 °C and 5% CO_2 in a 1:1 mixture of DMEM and F12 (Lonza) media supplemented with 10% fetal bovine serum (Gibco, USA), GlutaMAX (Gibco), and a mixture of 100 U/mL penicillin and 100 μg/mL streptomycin (Gibco). To obtain the deletion, fibroblasts (4×10^5) of male rats were electroporated with the pX-458-2sgRNA plasmid (5 μg) containing cloned RNA guides using a Neon Transfection System device (Invitrogen, USA). On the next day, the cells were sorted using a S3e Cell Sorter (Bio-Rad, USA) and subcloned into 96-well plates. After 7–14 days, the wells were examined under a microscope and those containing several growth islands were discarded to exclude polyclonal lines. Monoclonal lines were propagated, and the DNA was isolated and analyzed by PCR and Sanger sequencing. Primer sequences are given in *Table 1*.

For reprogramming, fibroblasts (5×10^4) were transduced with two samples of lentiviruses encoding Oct4, Sox2, Klf4, and c-Myc pluripotency factors and the tetracycline transactivator. One hour before transduction, 4 μg/mL polybrene (Sigma-Aldrich, USA) was added to the medium. Lentivirus samples were prepared using TetO-FUW-OSKM (Addgene Plasmid #20321) and FUdeltaGW-rtTA (Addgene Plasmid #19780) vectors and vectors encoding viral packaging proteins, psPAX2 (Addgene Plasmid #12260) and pMD2.G (Addgene Plasmid #12259), according to a protocol described elsewhere [4]. The next day after transduction, 2 μg/mL doxycycline (Sigma-Aldrich) was added to the medium; on the fourth day, the fibroblasts were plated onto a layer of mitotically inactive mouse embryonic fibroblasts and cultured in a N2B27 medium consisting of a N2 (DMEM/F12 with addition of N2) (Gibco) and B27 (Neurobasal with addition of B27) (Gibco) mixture, GlutaMAX, a mixture of 100 U/mL penicillin and 100 μg/mL streptomycin, 0.1 mM 2-mercaptoethanol (Sigma-Aldrich), 1,000 U/mL mouse LIF (StemRD), 1 μM PD0325901 (StemRD), and 3 μM CHIR99021 (StemRD). Reprogramming was performed in triplicate. On days 10–14 of reprogramming, some colonies were partially mechanically plated into individual wells for propagation and further analysis; on day 20, they were stained for alkaline phosphatase (AP) according to a protocol described elsewhere [4].

Immunofluorescent staining was performed as described previously [4]. The following primary antibodies were used for the analysis: SSEA-1 (sc-21702, 1:25), Oct4 (sc-5279, 1:200), and Sox2 (sc-20088, 1:200) (Santa Cruz Biotechnology, USA). Anti-rabbit or anti-mouse immunoglobulin secondary antibodies conjugated with Alexa 488 and Alexa 568 fluorescent dyes (Life Technologies, USA) were used for imaging.

RNA was isolated using a TRIzol reagent (Invitrogen) according to the manufacturer's protocol. The reverse transcription reaction was performed using 500 ng RNA, reverse transcriptase M-MLV (Invitrogen), and Random Hexamer primers (Thermo Scientific, USA). The prepared cDNA was analyzed on a LightCycler480 device (Roche, Switzerland) using a BioMaster HS-qPCR SYBR Blue kit (Biolabmix, Russia). The amplification reaction was carried out under

Table 1. Primer sequences for the PCR analysis of cell lines with a deletion of the target locus

Primer	Sequence, 5'–3'
FL1	CATACCTCAGAAACGCAAAAC
FL2	AGTTAATATCGAAAAGCCACC
IN1	CAGAATATATGGCTTATTGGA
IN2	GTTTTATACATACGCACACC
IN3	TATAAGAATGAAAGACGCCAAAC

Table 2. Primer sequences for analyzing the expression of pluripotent state markers

Gene	Sequence, 5'–3'
endo-Oct4	CACACTCTACTCGGTCCCTT TGCTTTCAATTCCTCCCCA
endo-Sox2	TATCGAGATAAACATGGCAA CAGAATCAAAACCCAGCAA
endo-Klf4	TCCGATCTACATTTATGACC TTATTGCACATCTGAAACCAC
endo-c-Myc	TCAAAGCCTAACCTCACAA GCAGTTAACATTATGGCTGA
Nanog	TACCTCAGCCTCCAGCAGAT GCAATGGATGCTGGGATACT
Esrrb	GGCGTTCTTCAAGAGAACCA CCCACTTTGAGGCATTTCAT
Tdgf1	TTGGACTTGTTGCTGGGATA CGGAAGGCACAAGCTGGA
Tcl1a	CCGATTAAATATCTCACTCAC TCTCTTATTTCTTGGCATCT
Utf1	TTGCTCCCCAGTCTCTGAAT GAGAAACGGTTTGGTCGAAG
Dnmt3l	AAGACCCATGAAACCTTGAACC GTTGACTTCGTACCTGATGACC
Pecam1	TCCTAAGAGCAAAGAGCAAC TGGGCTTGTCTGTGAATGT
Dppa3	TGGGGAAATCTCTTCTAATTGCT CTTCTAAATCAAACTACCAGGCTT

the following conditions: 95˚C for 5 min; 40 cycles of 95˚C for 15 s and 60˚C for 1 min. Primer sequences are given in *Table 2*.

The search for potential targets was performed using the TargetSpy v1.1 [5], miRanda v3.3a [6], and TargetScan v7.0 [7] software. We selected only the target genes predicted by all three programs and having a reduced expression level in rat ESCs and iPSCs compared to that in fibroblasts. The mRNA expression data were obtained earlier [8].

RESULTS AND DISCUSSION

The studied miRNA cluster is localized in locus 37 of the X chromosome long arm and consists of 14 miRNAs: miR-743a, miR-743b, miR-742, miR-883, miR-471, miR-3551, miR-741, miR-463, miR-880, miR-878, miR-881, miR-871, miR-3580, and miR-465 (*Fig. 1A*). We tested the hypothesis on the involvement of this miRNA cluster in the reprogramming to a pluripotent state using knockout of these miRNAs, which was induced by deletion of a genome fragment encoding them. A deletion was created using the CRISPR/Cas9 system with two guide RNAs flanking the locus to be deleted. A total of 94 subcloned lines of male rat fibroblasts were generated; of these, seven lines carried a deletion of the target DNA locus (*Fig. 1B*). The presence of a deletion in the subclones was verified by PCR with flanking primers. In addition, a translocation of the deleted fragment was analyzed using nested primers (*Fig. 1C*). In some lines, the presence of a deletion was confirmed by Sanger sequencing (*Fig. 1D*).

Expression of exogenous pluripotency factors was simultaneously activated in fibroblast lines with a miRNA cluster deletion and in the control cell line. The latter was used for the generation of knockout lines and was electroporated with the pX-458-2sgRNA plasmid not encoding the guide RNAs. The efficiency of the reprogramming of miRNA knockout fibroblasts was significantly lower compared to that of the control line (*Fig. 2A*). During reprogramming, some colonies from both control and experimental wells were partially mechanically transferred for further analysis. The morphology of the cells produced in the control experiment corresponds to that of rat ESCs. These iPSC-like cells are successfully cultured, retain their morphology, and are positively stained for AP after terminating the expression of exogenous pluripotency factors (*Fig. 2B*). They express markers of a pluripotent state, which is confirmed by immunofluorescent staining and real-time RT-PCR (*Fig. 2C,D*).

The cells produced by reprogramming of fibroblasts with knockout of the miR-743a–miR-465 miRNA cluster have an epithelial morphology, which indicates that they have passed the initial reprogramming stage – the mesenchymal-epithelial transition. However, these cells, unlike the control line, form loose colonies. The reprogramming process is incomplete, and the cells die in the absence of doxycycline, which indicates their dependence on the expression of exogenous pluripotency factors. It is worth noting that the cells with knockout of the miR-743a–miR-465 cluster are positively stained for AP and SSEA-1, confirming passage of the initial stages of pluripotency reprogramming (*Fig. 2B,C*). These cells also express pluripotency markers, but their expression level is significantly lower than that in the control group of cells (*Fig. 2D*).

Targets of the studied miRNAs include genes of the TGF-β signaling pathway; its inhibition promotes reprogramming [9]. A significant proportion is represented by genes of the Wnt signaling pathway; its inhibition at early stages is necessary for a successful reprogramming of cells [10]. There are also known reprogramming inhibitors: Cdkn1a and Zeb1 [11, 12].

MiRNAs play an important role in the regulation of various processes, in particular in the reprogramming of cells to a pluripotent state. To date, only a small number of the miRNAs expressed in pluripotent cells and involved in the reprogramming process have been studied. The emergence of genome editing tools has

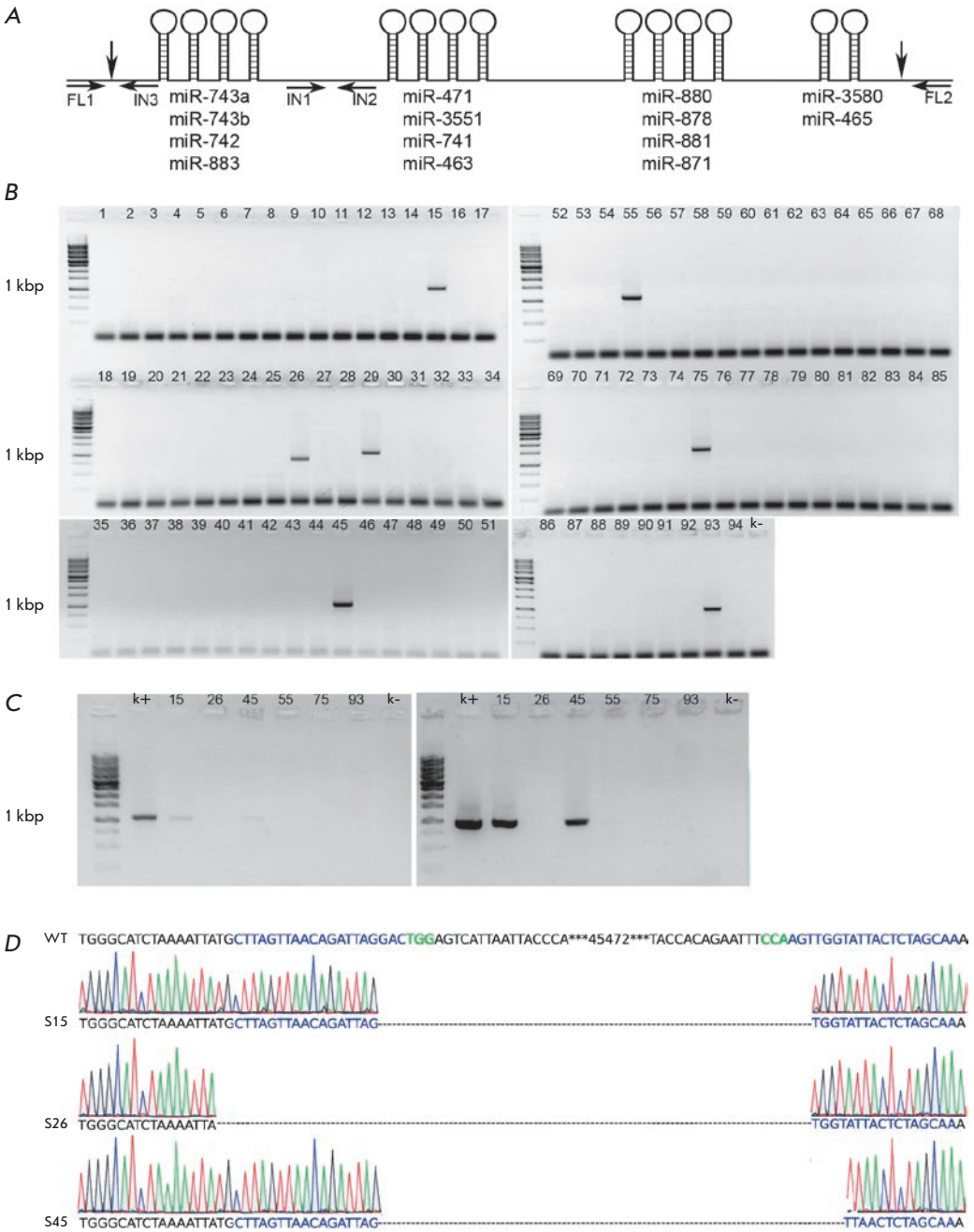

Fig. 1. *A* – schematic of the studied miRNA cluster. Horizontal arrows denote PCR primers; vertical arrows denote sites of double strand breaks. *B* – results of the PCR analysis for deletion in subclones. FL1 and FL2 primers were used. *C* – results of the PCR analysis for detection of polyclonal lines (left) and translocation (right) using FL1-IN3 and IN1-IN2 primer pairs, respectively. k+ and k– – positive and negative PCR controls. *D* – examples of Sanger sequencing of PCR products from cells carrying a deletion, using FL1 and FL2 primers. WT – wild type

greatly accelerated progress in the study of the functions of both protein-coding genes and non-coding RNAs. Unlike miRNA inhibitors, e.g., on the basis of LNA oligonucleotides, the CRISPR/Cas9 system provides more specific and permanent miRNA knockout. In addition, the use of CRISPR/Cas9 enables knockout of the entire miRNA cluster.

The investigated miRNA cluster is located near the protein-coding gene *Slitrk2*. Similar miRNA clusters have been found in other mammalian species, in particular in mice and humans [13]. These miRNA clusters in different species are supposed to have a common ancestor, but significant differences in the pre-miRNA and seed-region sequences indicate a rapid evolution of these miRNAs [13, 14]. A high expression level of these miRNA clusters was detected in mouse and human testes, and involvement of these miRNAs in the regulation of spermatogenesis in mice was shown by

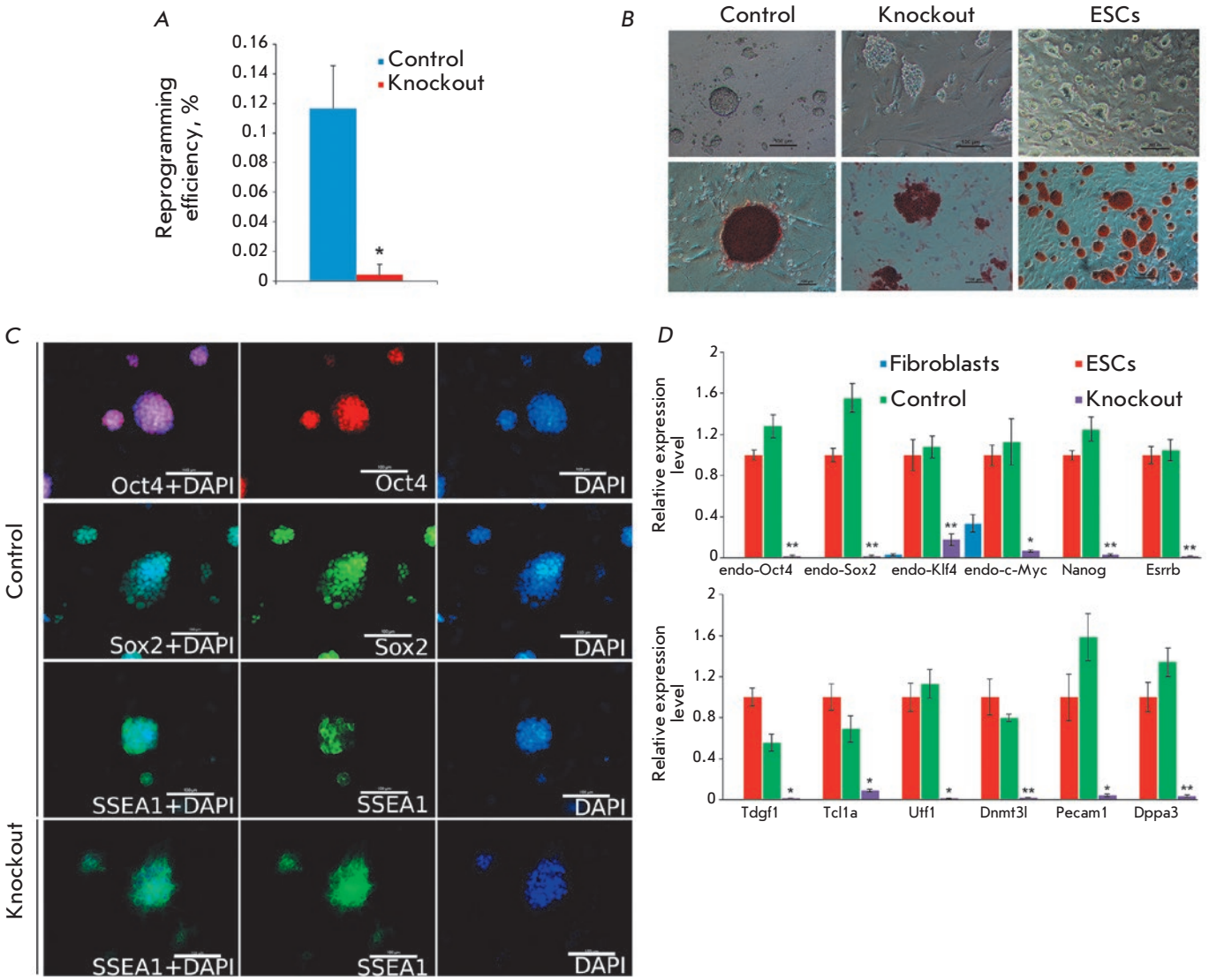

Fig. 2. *A* – efficiency of the reprogramming of control and knockout fibroblasts. The star denotes statistically significant differences, *$p < 0.05$, a Mann-Whitney U-test. *B* – representative images of colonies produced by reprogramming, as well as rat ESCs. Upper panel – phase-contrast, lower panel – staining for AP. *C* – immunofluorescence staining of colonies produced by reprogramming. Scale bar is 100 μm. *D* – RT-PCR analysis of pluripotency state markers. Stars denote statistically significant differences in gene expression between knockout and control cells, *$p < 0.05$, **$p < 0.005$, a Student's t-test

deletion of some of them [13–15]. The existence of common target genes for these mouse and human miRNAs was functionally confirmed, despite the differences in their nucleotide sequences [14]. It is also worth noting that miRNAs from this cluster are able to functionally compensate for their mutual absence [13]. Unlike mice, the expression level of some miRNAs in rats, in particular miR-741, is comparable in testes and pluripotent cells, which may indicate the species-specific features of pluripotent rat cells [3, 15]. However, a huge pool of potential target genes may comprise to common genes involved in the reprogramming process in different species. Therefore, this miRNA cluster may be involved in the reprogramming of not only rat cells, but this issue requires further study.

Disruption of the reprogramming process upon deletion of a DNA fragment containing a cluster of 14 miRNA (miR-743a through miR-465) suggests that all or some of them are involved in this process. It is worth noting that deletion of this large-sized fragment

might affect either unknown regulatory elements or non-annotated genes. In any case, our study may be considered as a first step in the investigation of this miRNA cluster during the reprogramming of cells to a pluripotent state. ●

The authors are grateful to E.V. Grigor'eva for assistance in experiments on reprogramming of rat cells as well as to A.A. Malakhova for help in cell sorting. The authors are also grateful to Andrea Ventura, Feng Zhang, Rudolf Jaenisch, Konrad Hochedlinger, and Didier Trono for the plasmids placed in the Addgene depository.
This study was supported by a grant of the Russian Science Foundation No. 16-14-10084.

REFERENCES

1. Takahashi K., Yamanaka S. // Cell. 2006. V. 126. № 4. P. 663–676.
2. Greve T.S., Judson R.L., Blelloch R. // Annu. Rev. Cell Dev. Biol. 2013. V. 29. P. 213–239.
3. Sherstyuk V.V., Medvedev S.P., Elisaphenko E.A., Vaskova E.A., Ri M.T., Vyatkin Y.V., Saik O.V., Shtokalo D.N., Pokushalov E.A., Zakian S.M. // Sci. Rep. 2017. V. 7. № 1. P. 2787.
4. Grigor'eva E.V., Shevchenko A.I., Medvedev S.P., Mazurok N.A., Zhelezova A.I., Zakian S.M. // Acta Naturae. 2015. V. 7. № 4. P. 56–69.
5. Sturm M., Hackenberg M., Langenberger D., Frishman D. // BMC Bioinformatics. 2010. V. 11. P. 292.
6. Betel D., Wilson M., Gabow A., Marks D.S., Sander C. // Nucl. Acids Res. 2008. V. 36. Database issue. P. D149–153.
7. Agarwal V., Bell G.W., Nam J.W., Bartel D.P. // Elife. 2015. V. 4. e05005.
8. Vaskova E.A., Medvedev S.P., Sorokina A.E., Nemudryy A.A., Elisaphenko E.A., Zakharova I.S., Shevchenko A.I., Kizilova E.A., Zhelezova A.I., Evshin I.S., et al. // Stem Cells Dev. 2015. V. 24. № 24. P. 2912–2924.
9. Ichida J.K., Blanchard J., Lam K., Son E.Y., Chung J.E., Egli D., Loh K.M., Carter A.C., Di Giorgio F.P., Koszka K., et al. // Cell Stem Cell. 2009. V. 5. № 5. P. 491–503.
10. Aulicino F., Theka I., Ombrato L., Lluis F., Cosma M.P. // Stem Cell Reports. 2014. V. 2. № 5. P. 707–720.
11. Brosh R., Assia-Alroy Y., Molchadsky A., Bornstein C., Dekel E., Madar S., Shetzer Y., Rivlin N., Goldfinger N., Sarig R., et al. // Cell Death Differ. 2013. V. 20. № 2. P. 312–320.
12. Samavarchi-Tehrani P., Golipour A., David L., Sung H.K., Beyer T.A, Datti A., Woltjen K., Nagy A., Wrana J.L. // Cell Stem Cell. 2010. V. 7. № 1. P. 64–77.
13. Zhang F., Zhang Y., Lv X., Xu B., Zhang H., Yan J., Li H., Wu L. // Mol. Biol. Evol. 2019. V. 36. № 4. P. 663–678.
14. Ramaiah M., Tan K., Plank T.M., Song H.W., Dumdie J.N., Jones S., Shum E.Y., Sheridan S.D., Peterson K.J., Gromoll J., et al. // EMBO Rep. 2019. V. 20. № 2. P. e46566.
15. Ota H., Ito-Matsuoka Y., Matsui Y. // PLoS One. 2019. V. 14. № 2. P. e0211739.

Bacteriophage MS2 As a Tool for Targeted Delivery in Solid Tumor Chemotherapy

E. F. Kolesanova[1*], M. V. Melnikova[1], T. N. Bolshakova[2], E. Yu. Rybalkina[3], I. G. Sivov[4]
[1] Institute of Biomedical Chemistry, Pogodinskaya Str. 10, bld. 8, Moscow, 119121, Russia
[2]N.F. Gamaleya Federal Research Center of Epidemiology and Microbiology, Gamalei Str. 18, Moscow, 123098, Russia
[3]Institute of Carcinogenesis, Federal National Medical Research Center of Oncology, Kashirskoe sh. 23, Moscow, 115478, Russia
[4]Biotechnologiya, Ltd., Efremova Str. 20, Moscow, 119048, Russia
*E-mail: ekaterina.kolesanova@ibmc.msk.ru
Received January 29, 2019; in final form, March 28, 2019
DOI: 10.32607/20758251-2019-11-2-98-101

ABSTRACT **Bacteriophage MS2 was employed for targeted delivery of an apoptosis-inducing agent, Tl^+, into a tumor tissue. The targeted delivery was ensured by iRGD peptide, a ligand of integrins presumably located on the surface of endotheliocytes of the tumor tissue neovasculature and certain tumor cells. The synthesized peptide was conjugated to MS2 capsid proteins. Tl^+ ions from $TlNO_3$ penetrated the phage particles and tightly bound to phage RNA. Peptide-modified MS2 preparations filled with Tl^+ caused cell death in two types of cultivated human breast cancer cells and effected necrosis of these tumor xenografts in mice. Neither peptide-conjugated bacteriophage MS2 without Tl^+ nor the phage filled with Tl^+ but without the peptide or the same phage with the non-conjugated peptide in solution produced such effects. The preparation exhibited no acute toxicity at a therapeutic dose.**

KEYWORDS **bacteriophage MS2, iRGD peptide, thallium (I) ions, targeted therapy, breast cancer.**

ABBREVIATIONS **BC – breast cancer; DMAI – dimethyl adipimidate; ED_{50} – effective dose (the dose that causes an effect equal to 50% of the maximal one); HPLC – high-performance liquid chromatography; LD_{50} – dose of a substance lethal to 50% tested animals; PFU – plaque-forming units; SDS – sodium dodecyl sulfate.**

INTRODUCTION

Recently, efforts by researchers involved in the development of anti-tumor drugs have focused on targeted therapeutic agents based both on novel and already-known cytostatic drugs [1]. The use of nanocontainers (liposomes, micelles, polymer nanoparticles, virus-like particles, and viruses) modified with specific ligands filled with a drug is considered the most efficient delivery method [2]. However, these innovative delivery methods do not solve the problem of cancer multidrug resistance, which has the potential to undermine all previous efforts to enhance drug efficacy [3].

It has been demonstrated that Tl^+ ions exhibit strong cytotoxic activity and inhibit the cancer drug resistance-associated protein that acts as an efflux pump [4]. Incorporation of Tl^+ into a "non-leaking" nanosized container equipped with a targeted delivery system could allow one to develop an efficient tool for tumor destruction, while the overall toxicity of Tl^+ can be significantly mitigated. In the 1980s, Tl^+ ions were successfully entrapped in cowpox virus particles [5]. The entrapment mechanism involved the formation of a strong conjugate between Tl^+ and viral RNA [6]. The bacteriophage MS2 selected as a nanocontainer can reproduce itself only in *Escherichia coli* cells that carry F-pili and are neither human symbionts nor pathogens [7]. The delivery direction was ensured via conjugation of phage capsid proteins and the $(Gly)_3$-iRGD peptide carrying the cycloSS-(CRGDKGPDC) (iRGD) moiety, which is responsible for binding to integrins that predominantly localize on the outer membranes of endothelial cells of the pathological neovasculature of solid tumors and on a number of tumor cells [8]. In this study, we experimentally tested the effectiveness of Tl^+-filled bacteriophage MS2 carrying a targeting peptide as a candidate antitumor agent.

EXPERIMENTAL

The procedure used to prepare bacteriophage MS2 was described earlier in [9]. The number of plaque-forming units (PFUs) per milliliter of the phage preparation was identified by agar overlay assay.

(Gly)3-iRGD peptide was prepared by automated solid-phase synthesis using 9-fluorenylmethoxycarbonyl amino acids (ChemPep, USA) on a 433A peptide synthesizer (Applied Biosystems) through the FastMoc method. The S–S bridge was formed by oxidation with I_2 [10]. The peptide was purified by reversed-phase HPLC (YMC-Triart C18 column, 21 × 250 mm, 10.0 μm, Switzerland; Agilent 1100 working station, Agilent, USA), elution by CH_3CN (BioSolve, Israel) concentration gradient in water containing 0.1% acetic acid. According to the data obtained by analytical reversed-phase HPLC (YMC-Triart C18 column, 2.1 × 50 mm, 2.0 μm, Agilent 1200 working station) with UV and mass-spectrometry detection, purity of the peptide preparation was ≥ 95%.

$(Gly)_3$-iRGD peptide was conjugated to bacteriophage MS2 capsid proteins using a homobifunctional reagent dimethyl adipimidate (DMAI, Sigma, USA) at a phage protein : peptide : DMAI molar ratio of 1 : 20 : 80, using the procedure described in [11]. The bacteriophage was separated from the excess reagents via precipitation with a 25% polyethylene glycol 6000 solution (Dia-M, Russia) containing 1 M NaCl. The precipitated bacteriophage was suspended in deionized water.

The bacteriophage was filled with Tl^+ using $TlNO_3$ (Sigma-Aldrich, USA). The peptide-conjugated bacteriophage MS2 (iRGD-MS2) (10^{11} PFUs) was incubated in 3 ml of a 0.5 μM $TlNO_3$ solution (5 h at 38°C), followed by precipitation according to the procedure described above and dialysis against phosphate buffered saline (0.14 M NaCl, 0.01 M sodium phosphate, pH 7.4).

The amounts of Tl^+ ions both inside and outside the virions (in the medium) were determined using the procedure described in [12]. A suspension of bacteriophage particles filled with Tl^+ was centrifuged for 10 min at 5,000 rpm to remove the thallium salt precipitate, diluted with 50 mM Tris-HCl buffer (pH 9.0) until a nominal concentration of 10^8 PFUs/ml, and denatured by heating with RNase in 0.05% SDS at +70°C for 30 min. Quenching of 1,3,6,8-pyrene tetrasulfonic acid fluorescence by Tl^+ ions was then recorded (excitation wavelength, 340 nm; emission wavelength, 465 nm) on an UV-1900 spectrofluorometer (BOC Sciences APP, USA). A calibration curve showing the dependence between the fluorescence quenching degree and [Tl^+] was used to calculate the content of Tl in the bacteriophage preparation. The Tl content in the buffer solution after dialysis was determined without pre-denaturation.

The cytotoxic effect of iRGD-MS2-Tl^+ on the cell cultures was studied using MCF-7 (hormone-dependent breast cancer) and MDA-MB-231 (hormone-independent breast cancer) cell lines. The cells were cultured in a serum-free medium (MSC1 Pan Biotech) and in the same medium supplemented with 5% fetal calf serum. The iRGD-MS2-Tl^+ preparation was added in 10-fold dilutions, starting with a concentration of 10^8 PFU/ml. The iRGD-MS2 preparation (the peptide-conjugated bacteriophage without Tl^+) was used as a control. Dead cells were counted after staining with Evans blue. The antitumor effect of the iRGD-MS2-Tl^+ preparation was tested in nude mice with MCF-7 or MDA-MB-231 cancer cell-derived xenografts. The mice were injected with 10^5–10^6 MCF-7 or MDA-MB-231 cells intradermally. Fourteen days later, the mice in the experimental groups received 200 μl of a suspension containing iRGD-MS2-Tl^+ at a dose corresponding to 10^8 PFU/kg intraperitoneally during 10 days (once per day). Mice in the control group were injected with iRGD-MS2, MS2-Tl^+, or MS2-Tl^+ + iRGD (2 μg/kg in solution) of the MS2 dosage equal to the iRGD-MS2-Tl^+ doses for experimental animals, and in the same volume of the solution. Each experimental and control group consisted of 11 animals. The necrotic activity of the preparation was determined as a ratio between the area of necrosis tissue and the total area of the tumor by analyzing digital images of histologic sections recorded using a ScanScope CS2 scanner 12 days after the last injection of bacteriophage preparations.

Acute toxicity of the iRGD-MS2-Tl^+ preparation was preliminarily studied on 10 female Wistar Kyoto (WKY) rats (weight, 200–250 g). The rats were housed under the conditions of 12-hour light and 12-hour dark cycle and given *ad libitum* access to a standard laboratory diet and water. The animals received a single intradermal injection of the preparation (10^8 PFU/animal, 500 μl). The state of the animals was monitored during three weeks post-injection.

Experiments on animals were carried out in compliance with the International Guidelines of the European Convention for the Protection of Vertebrate Animals used for Experimental and Other Scientific Purposes, and the principles of Good Laboratory Practice (GLP) approved by Degree no. 267 of the Ministry of Health of the Russian Federation dated June 19, 2003.

RESULTS AND DISCUSSION

MS2 preparations containing Tl^+ in the amount of 2.0×10^{-9} g-eq thallium per 10^8 PFUs were obtained by incubating the bacteriophage MS2 (both modified and unmodified with iRGD peptide) in the medium with $TlNO_3$. The Tl^+ content per PFU was 2.0×10^{-17} g-eq (~ 4 femtogram per PFU; i.e., 400 ng per 10^8 PFU). No Tl^+ ions were detected in the buffer solution used for dialysis of Th^+-filled bacteriophage, which indicates that Th^+ is tightly bound to phage RNA inside MS2 particles.

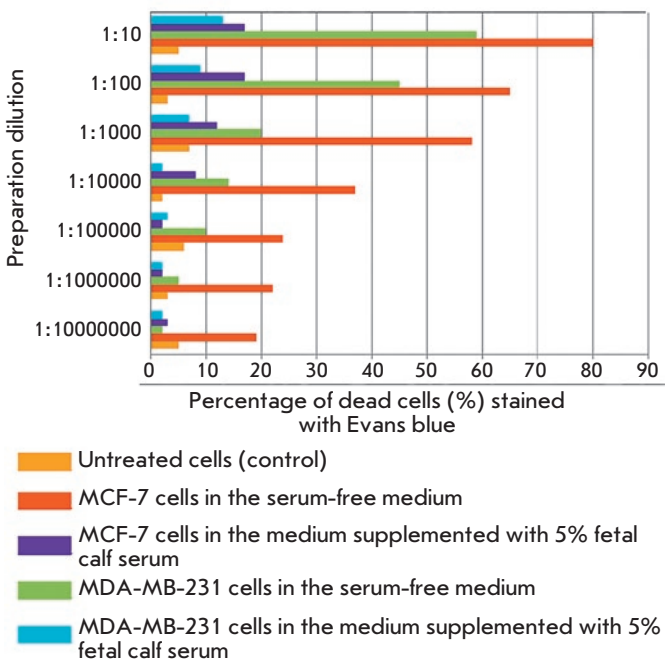

Fig. 1. The toxic effect of the iRGD-MS2-Tl^+ preparation on tumor cell cultures (cell death, %)

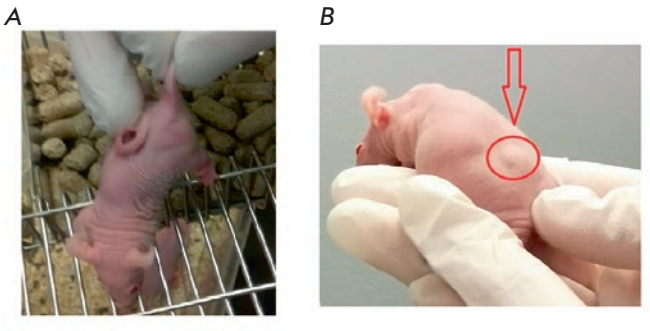

Fig. 2. MDA-MB-231 tumor in xenograft mice before (A) and after (B) treatment with a iRGD-MS2-Tl^+ preparation

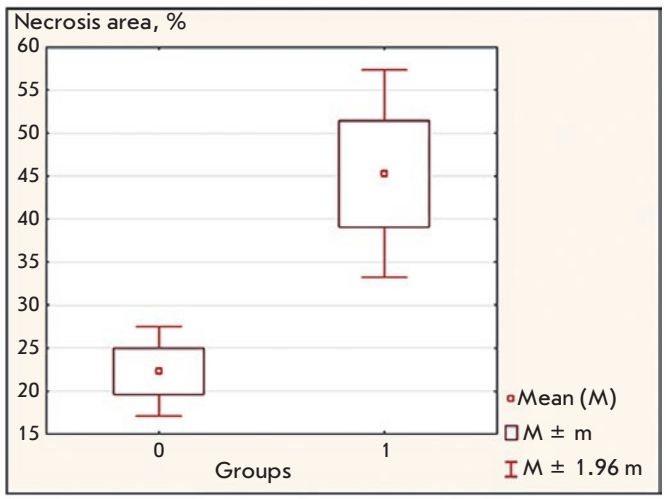

Fig. 3. Area of tumor tissue necrosis in mice xenograft of human BC. Group 1 – experimental animals that received a iRGD-MS2-Tl^+ preparation; group 0 – control animals that received iRGD-MS2, or MS2-Tl^+, or MS2-Tl^+ with a non-conjugated iRGD peptide (in a solution)

Figure 1 demonstrates that the iRGD-MS2-Tl^+ preparation had a cytotoxic effect on hormone-dependent and hormone-independent breast cancer cells in the serum-free medium. For hormone-dependent BC (MCF-7 cells), ED_{50} of the iRGD-MS2-Tl^+ preparation was slightly lower than 10^5 PFU/ml of the culture broth, while the cytotoxic effect of the preparation was statistically significant compared to the control specimen, up to a concentration of 10 PFU/ml. Hormone-independent breast cancer (MDA-MB-231) cells were more resistant to the preparation: for these cells, ED_{50} in a serum-free medium was 10^6–10^7 PFU/ml, while the cytotoxic effect of the preparation was statistically significant compared to the control specimen, up to a concentration of 10^4 PFU/ml. The cytotoxic activity of iRGD-MS2-Tl^+ was much weaker in the serum-containing medium, which may be an indication that serum components and iRGD-MS2-Tl^+ particles compete for penetration into the cells.

In mice with MCF-7 and MDA-MB-231 xenografts, the tumor volume was reduced 12 days following the injections of the iRGD-MS2-Tl^+ preparation compared to that in the control animals (*Fig. 2*). The necrotizing effect of iRGD-MS2-Tl^+ on the corresponding tumors was demonstrated histochemically. *Figure 3* shows that the iRGD-MS2-Tl^+ preparation was more efficient in causing tumor tissue necrosis ($p < 0.05$) than peptide-conjugated phage preparations without Tl^+ ions, Tl^+-filled phage preparations without the peptide, or Tl^+-filled phage preparations containing the non-conjugated peptide in the solution.

Evaluation of acute toxicity of the iRGD-MS2-Tl^+ preparation in Wistar Kyoto (WKY) rats demonstrated that a single-dose injection of iRGD-MS2-Tl^+ (10^8 PFU/animal; i.e., 1.6–2.0 μg Tl/kg) caused death in none of the animals after three weeks of follow-up. No noticeable changes in animal behavior were revealed. The total therapeutic dose of Tl^+ (4 μg/kg) was 5,000-fold lower than its LD_{50} (20 mg/kg).

CONCLUSIONS

Targeted delivery of ions of a toxic metal to a tumor neovasculature using phage display based on iRGD-MS2-Tl^+ particles causes efficient degradation of the entire tumor mass, while the risk of overall toxicity is significantly reduced. Therefore, it is reasonable to recommend conducting preclinical trials of iRGD-MS2-Tl^+ in order to develop a preparation which can potentially be further used to treat breast cancer. Since the iRGD peptide ligand interacts with a_vb_3 and a_vb_5 integrins on the surface of endothelial cells in the pathological vasculature [8], this drug may be efficient against other solid tumors characterized by intensive pathological neoangiogenesis.

This work was supported in part by Biotechnologiya, Ltd. The procedures for $(Gly)_3$-iRGD peptide synthesis and its conjugation to the bacteriophage MS2 were developed under the Program of Fundamental Research for State Academies of Sciences in 2013–2020. The peptide was synthesized using the equipment of the Core Facilities "Human Proteome" (Institute of Biomedical Chemistry). Animal experiments were conducted at the N.N. Petrov National Medical Research Center of Oncology of the Ministry of Health of the Russian Federation. The authors are grateful to A.A. Chistov (Institute of Biomedical Chemistry, Institute of Bioorganic Chemistry) for analyzing the iRGD peptide.

The materials in this article were used to obtain an RF Patent 2599462 "Method for Poly-signal Activation of Apoptosis of Malignant Solid Tumor Cells" and file a U.S. patent application (application no. 15/757,285 filed March 2, 2018) and a European patent application (PCT – WO 2017052419).

REFERENCES

1. Lee M.S., Dees E.C., Wang A.Z. // Oncology (Williston Park). 2017. V. 31. № 3. P. 198–208.
2. Fan Y., Moon J.J. // Vaccines. 2015. V. 3. № 3. P. 662–685.
3. Stavrovskaya A.A., Stromskaya T.P. // Biokhimiya. 2008. V. 73. № 5. P. 735–750.
4. Korotkov S.M., Brailovskaya I.V., Kormilitsyn B.N., Furaev V.V. // J. Biochem. Mol. Toxicol. 2014. V. 28. № 4. P. 149–156.
5. Zasukhina G.D., Vasilyeva I.M., Sdirkova N.I., Krasovsky G.N., Vasyukovich L.Ya., Kenesariev U.I., Butenko P.G. // Mutat. Res. 1983. V. 124. № 2. P. 163–173.
6. Ke A., Ding F., Batchelor J.D., Doudna J.A. // Structure. 2007. V. 15. № 1. P. 281–287.
7. Leclerc H., Edberg S., Pierzo V., Delattre J.M. // J. Appl. Microbiol. 2000. V. 88. № 1. P. 5–21.
8. Ruoslahti E. //Adv. Drug Deliv. Rev. 2017. V. 110–111. P. 3–12.
9. Knyazhev V.A., Sivov I.G., Sergienko V.I. // Moleculyarnaya genetika, mikrobiologiya i virusologiya. 2002. V. 20. № 2. P. 23–26.
10. Andreu D., Albericio F., Sole N.A., Munson M.C., Ferrer M., Barany G. // Methods Mol. Biol. 1994. V. 35. P. 91–169.
11. Synthetic peptides as antigens. / Eds van Regenmortel M.H.V., Muller S. Elsevier, 1999.
12. Donnelly D., Mihovilovic M., Gonzalez-Ros J.M., Ferragut J.A., Richman D., Martinez-Carrion M. // Proc. Natl. Acad. Sci. USA. 1984. V. 81. № 24. P. 7999–8003.

GENERAL RULES

Acta Naturae publishes experimental articles and reviews, as well as articles on topical issues, short reviews, and reports on the subjects of basic and applied life sciences and biotechnology.

The journal *Acta Naturae* is on the list of the leading periodicals of the Higher Attestation Commission of the Russian Ministry of Education and Science. The journal Acta Naturae is indexed in PubMed, Web of Science, Scopus and RCSI databases.

The editors of *Acta Naturae* ask of the authors that they follow certain guidelines listed below. Articles which fail to conform to these guidelines will be rejected without review. The editors will not consider articles whose results have already been published or are being considered by other publications.

The maximum length of a review, together with tables and references, cannot exceed 60,000 characters with spaces (approximately 30 pages, A4 format, 1.5 spacing, Times New Roman font, size 12) and cannot contain more than 16 figures.

Experimental articles should not exceed 30,000 symbols (approximately 15 pages in A4 format, including tables and references). They should contain no more than ten figures.

A short report must include the study's rationale, experimental material, and conclusions. A short report should not exceed 12,000 symbols (8 pages in A4 format including no more than 12 references). It should contain no more than four figures.

The manuscript and the accompanying documents should be sent to the Editorial Board in electronic form:
1) text in Word 2003 for Windows format;
2) the figures in TIFF format;
3) the text of the article and figures in one pdf file;
4) the article's title, the names and initials of the authors, the full name of the organizations, the abstract, keywords, abbreviations, figure captions, and Russian references should be translated to English;
5) the cover letter stating that the submitted manuscript has not been published elsewhere and is not under consideration for publication;
6) the license agreement (the agreement form can be downloaded from the website www.actanaturae.ru).

MANUSCRIPT FORMATTING

The manuscript should be formatted in the following manner:

- Article title. Bold font. The title should not be too long or too short and must be informative. The title should not exceed 100 characters. It should reflect the major result, the essence, and uniqueness of the work, names and initials of the authors.
- The corresponding author, who will also be working with the proofs, should be marked with a footnote *.
- Full name of the scientific organization and its departmental affiliation. If there are two or more scientific organizations involved, they should be linked by digital superscripts with the authors' names. Abstract. The structure of the abstract should be very clear and must reflect the following: it should introduce the reader to the main issue and describe the experimental approach, the possibility of practical use, and the possibility of further research in the field. The average length of an abstract is 20 lines (1,500 characters).
- Keywords (3 – 6). These should include the field of research, methods, experimental subject, and the specifics of the work. List of abbreviations.
- INTRODUCTION
- EXPERIMENTAL PROCEDURES
- RESULTS AND DISCUSSION
- CONCLUSION

  The organizations that funded the work should be listed at the end of this section with grant numbers in parenthesis.
- REFERENCES

  The in-text references should be in brackets, such as [1].

RECOMMENDATIONS ON THE TYPING AND FORMATTING OF THE TEXT

- We recommend the use of Microsoft Word 2003 for Windows text editing software.
- The Times New Roman font should be used. Standard font size is 12.
- The space between the lines is 1.5.
- Using more than one whole space between words is not recommended.
- We do not accept articles with automatic referencing; automatic word hyphenation; or automatic prohibition of hyphenation, listing, automatic indentation, etc.
- We recommend that tables be created using Word software options (Table → Insert Table) or MS Excel. Tables that were created manually (using lots of spaces without boxes) cannot be accepted.
- Initials and last names should always be separated by a whole space; for example, A. A. Ivanov.
- Throughout the text, all dates should appear in the "day.month.year" format, for example 02.05.1991, 26.12.1874, etc.
- There should be no periods after the title of the article, the authors' names, headings and subheadings, figure captions, units (s – second, g – gram, min – minute, h – hour, d – day, deg – degree).
- Periods should be used after footnotes (including those in tables), table comments, abstracts, and abbreviations (mon. – months, y. – years, m. temp. – melting temperature); however, they should not be used in subscripted indexes (T_m – melting temperature; $T_{p.t}$ – temperature of phase transition). One exception is mln – million, which should be used without a period.
- Decimal numbers should always contain a period and not a comma (0.25 and not 0,25).
- The hyphen ("-") is surrounded by two whole spaces, while the "minus," "interval," or "chemical bond" symbols do not require a space.
- The only symbol used for multiplication is "×"; the "×" symbol can only be used if it has a number to its

right. The "·" symbol is used for denoting complex compounds in chemical formulas and also noncovalent complexes (such as DNA·RNA, etc.).
- Formulas must use the letter of the Latin and Greek alphabets.
- Latin genera and species' names should be in italics, while the taxa of higher orders should be in regular font.
- Gene names (except for yeast genes) should be italicized, while names of proteins should be in regular font.
- Names of nucleotides (A, T, G, C, U), amino acids (Arg, Ile, Val, etc.), and phosphonucleotides (ATP, AMP, etc.) should be written with Latin letters in regular font.
- Numeration of bases in nucleic acids and amino acid residues should not be hyphenated (T34, Ala89).
- When choosing units of measurement, SI units are to be used.
- Molecular mass should be in Daltons (Da, KDa, MDa).
- The number of nucleotide pairs should be abbreviated (bp, kbp).
- The number of amino acids should be abbreviated to aa.
- Biochemical terms, such as the names of enzymes, should conform to IUPAC standards.
- The number of term and name abbreviations in the text should be kept to a minimum.
- Repeating the same data in the text, tables, and graphs is not allowed.

GUIDENESS FOR ILLUSTRATIONS

- Figures should be supplied in separate files. Only TIFF is accepted.
- Figures should have a resolution of no less than 300 dpi for color and half-tone images and no less than 500 dpi.
- Files should not have any additional layers.

REVIEW AND PREPARATION OF THE MANUSCRIPT FOR PRINT AND PUBLICATION

Articles are published on a first-come, first-served basis. The members of the editorial board have the right to recommend the expedited publishing of articles which are deemed to be a priority and have received good reviews.

Articles which have been received by the editorial board are assessed by the board members and then sent for external review, if needed. The choice of reviewers is up to the editorial board. The manuscript is sent on to reviewers who are experts in this field of research, and the editorial board makes its decisions based on the reviews of these experts. The article may be accepted as is, sent back for improvements, or rejected.

The editorial board can decide to reject an article if it does not conform to the guidelines set above.

The return of an article to the authors for improvement does not mean that the article has been accepted for publication. After the revised text has been received, a decision is made by the editorial board. The author must return the improved text, together with the responses to all comments. The date of acceptance is the day on which the final version of the article was received by the publisher.

A revised manuscript must be sent back to the publisher a week after the authors have received the comments; if not, the article is considered a resubmission.

E-mail is used at all the stages of communication between the author, editors, publishers, and reviewers, so it is of vital importance that the authors monitor the address that they list in the article and inform the publisher of any changes in due time.

After the layout for the relevant issue of the journal is ready, the publisher sends out PDF files to the authors for a final review.

Changes other than simple corrections in the text, figures, or tables are not allowed at the final review stage. If this is necessary, the issue is resolved by the editorial board.

FORMAT OF REFERENCES

The journal uses a numeric reference system, which means that references are denoted as numbers in the text (in brackets) which refer to the number in the reference list.

For books: the last name and initials of the author, full title of the book, location of publisher, publisher, year in which the work was published, and the volume or issue and the number of pages in the book.

For periodicals: the last name and initials of the author, title of the journal, year in which the work was published, volume, issue, first and last page of the article. Must specify the name of the first 10 authors. Ross M.T., Grafham D.V., Coffey A.J., Scherer S., McLay K., Muzny D., Platzer M., Howell G.R., Burrows C., Bird C.P., et al. // Nature. 2005. V. 434. № 7031. P. 325–337.

References to books which have Russian translations should be accompanied with references to the original material listing the required data.

References to doctoral thesis abstracts must include the last name and initials of the author, the title of the thesis, the location in which the work was performed, and the year of completion.

References to patents must include the last names and initials of the authors, the type of the patent document (the author's rights or patent), the patent number, the name of the country that issued the document, the international invention classification index, and the year of patent issue.

The list of references should be on a separate page. The tables should be on a separate page, and figure captions should also be on a separate page.

The following e-mail addresses can be used to contact the editorial staff: vera.knorre@gmail.com, actanaturae@gmail.com,
tel.: (495) 727-38-60, (495) 930-87-07

II ОБЪЕДИНЕННЫЙ НАУЧНЫЙ ФОРУМ

VI СЪЕЗД БИОХИМИКОВ РОССИИ
♦
IX РОССИЙСКИЙ СИМПОЗИУМ «БЕЛКИ И ПЕПТИДЫ»
ПОСВЯЩЕННЫЙ 60-ЛЕТИЮ ИБХ РАН
♦
VI СЪЕЗД ФИЗИОЛОГОВ СНГ

Сочи, Дагомыс — *1–6 октября 2019*

НАУЧНАЯ ТЕМАТИКА

СИМПОЗИУМ «ХИМИЯ И БИОЛОГИЯ НУКЛЕИНОВЫХ КИСЛОТ»
Руководители: Г.П. Георгиев, О.А. Донцова, А.Л. Коневега, М.П. Рубцова, П.В. Сергиев

IX РОССИЙСКИЙ СИМПОЗИУМ «БЕЛКИ И ПЕПТИДЫ»

Руководитель: В.Т. Иванов

- **Поиск, выделение и синтез новых природных пептидов и белков**
  Руководители: В.И. Цетлин, А.А. Василевский
- **Биологические функции и механизмы действия пептидов и белков**
  Руководители: С.М. Деев, А.А. Белогуров
- **Биоинженерия белков и пептидов**
  Руководители: А.Н. Федоров, Д.А. Долгих
- **Физико-химические методы исследования структуры пептидов и белков. Взаимосвязь «структура – функция»**
  Руководители: Р.Г. Ефремов, А.В. Финкельштейн
- **Химия и биология ферментов**
  Руководители: О.И. Лаврик, С.Н. Кочетков, И.В. Смирнов
- **Инновационные лекарственные средства на основе пептидов и белков**
  Руководители: Н.Ф. Мясоедов, Т.В. Овчинникова

СИМПОЗИУМ «ГЕНОМ. ПРОТЕОМ. МЕТАБОЛОМ»
Руководители: А.И. Арчаков, В.М. Говорун, А.В. Лисица, Е.Н. Ильина

СИМПОЗИУМ «ФУНКЦИОНАЛЬНАЯ ГЕНОМИКА»
Руководители: С.В. Разин, Е.С. Васецкий

СИМПОЗИУМ «БИОХИМИЧЕСКИЕ АСПЕКТЫ КЛЕТОЧНЫХ ТЕХНОЛОГИЙ»
Руководитель: М.А. Лагарькова, А.Н. Томилин

СИМПОЗИУМ «БИОИНЖЕНЕРИЯ: ФУНДАМЕНТАЛЬНЫЕ ОСНОВЫ И ПРИЛОЖЕНИЯ»
Руководители: В.О. Попов, А.С. Яненко

СИМПОЗИУМ «ОСНОВНЫЕ АСПЕКТЫ БИОХИМИИ»

- **Биология растений**
  Руководители: А.Н. Гречкин, Д.А. Лось
- **Гликобиология**
  Руководители: Н.В. Бовин, Т.А. Горшкова

СИМПОЗИУМ «БИОХИМИЯ И МОЛЕКУЛЯРНАЯ МЕДИЦИНА»
Руководители: А.М. Егоров, Н.Л. Клячко

СИМПОЗИУМ «МОЛЕКУЛЯРНЫЙ ИМИДЖИНГ»
Руководители: А.П. Савицкий, К.А. Лукьянов

ОРГАНИЗАТОРЫ ФОРУМА

- Российское биохимическое общество
- Союз физиологических обществ стран СНГ
- Союз аллергологов и иммунологов СНГ

WWW.RUSBIOCHEM.ORG
info@rusbiochem.org

ActaNaturae

Fluorescence of cells after staining with various proteins. The mean values for the three experiments ± mean error are given

Sample	Fluorescence intensity measured in the FL1 channel	
	SK-BR-3 cells	CHO cells
Unstained cells	3700 ± 400	3700 ± 900
+ β-LG-FITC	5700 ± 600	3300 ± 400
+ 4D5scFv-FITC	$2.7\times10^4 \pm 7\times10^3$	3200 ± 500
+ 4D5scFv-miniSOG	$2.3\times10^4 \pm 3\times10^3$	4600 ± 400
+ DARPin-miniSOG	$1.71\times10^4 \pm 1.6\times10^3$	3000 ± 400

Hence, it has been demonstrated that the targeted recombinant proteins 4D5scFv-miniSOG and DARPin-miniSOG are capable of highly specific binding to the HER2/neu receptor on the surface of human breast adenocarcinoma SK-BR-3 cells.

It was revealed that receptor-mediated internalization of proteins did not take place after the DARPin-miniSOG and 4D5scFv-miniSOG proteins were bound to the receptor on the surface of SK-BR-3 cells at +4°C. However, the receptor–protein complex undergoes internalization at +37°C, as evidenced by the reduction in the fluorescence intensity ΔMFI (the difference between the average fluorescence intensities of stained and unstained cells) (*Fig. 1*). The DARPin-miniSOG recombinant protein as part of its complex with the receptor is internalized faster than 4D5scFv-miniSOG, since ΔMFI for DARPin-miniSOG decreases twofold as compared to its baseline during the first 10 min, while ΔMFI for 4D5scFv-miniSOG is 40 min. These findings are consistent with the published data: 4D5scFv-miniSOG has a higher cytotoxicity than DARPin-miniSOG [5, 6], because 4D5scFv-miniSOG resides on the membrane for a longer time. Since necrosis is the predominant death mechanism of cells irradiated in the presence of these phototoxins, membrane damage makes a crucial contribution to the toxicity of targeted proteins. However, the decline in the fluorescence intensity of miniSOG can be indicative of reactions involving chromophore, which is also expected to affect its efficiency as a phototoxin.

In order to elucidate the reasons for the decline in the fluorescence intensity and toxicity of miniSOG-based proteins observed during their internalization, we evaluated the effect of various factors on the fluorescent properties of miniSOG. A hypothesis has been put forward that quenching of DARPin-miniSOG

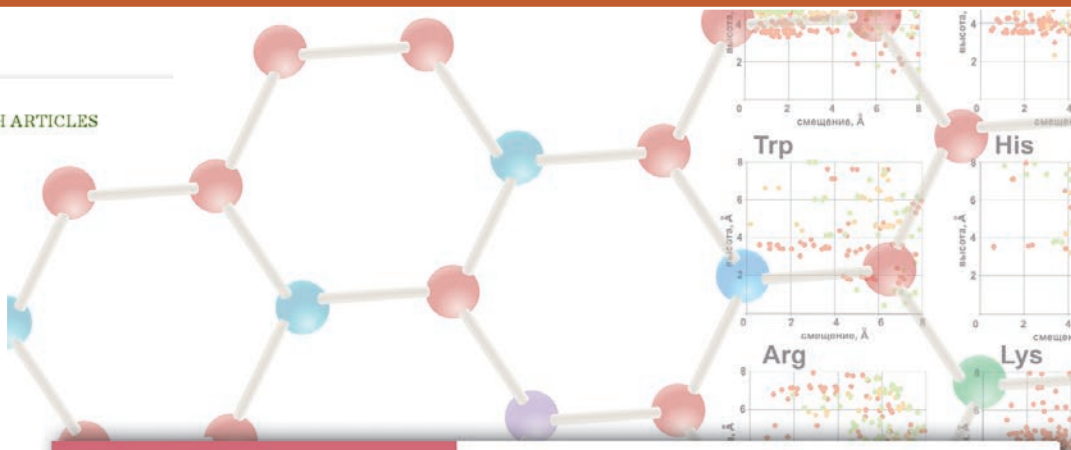

OCTOBER-DECEMBER 2018 VOL. 10 № 4 (39)
ISSN 2075-8251

ActaNaturae

The EIMB Hydrogel Microarray Technology: Thirty Years Later

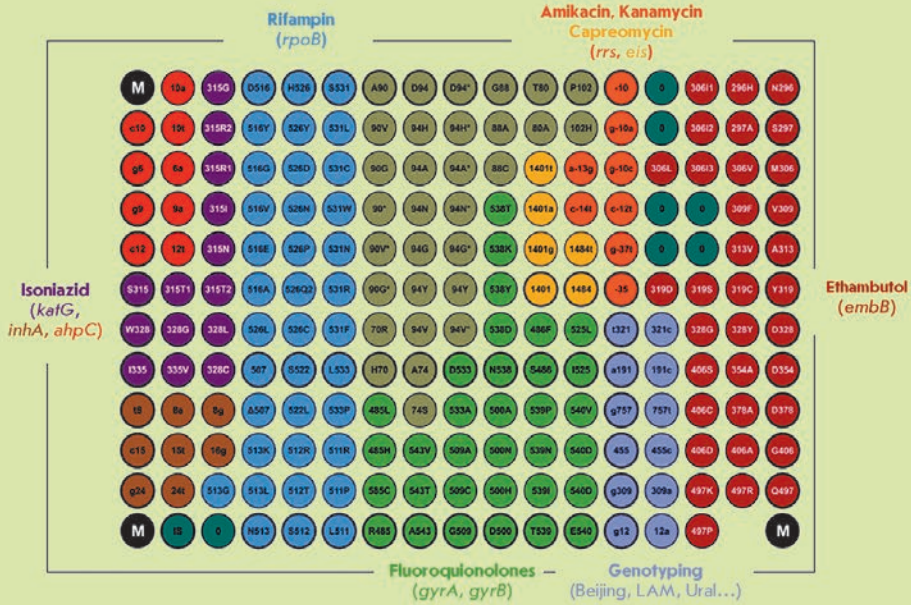

ActaNaturae

Journal "*Acta Naturae*" is a international journal on life sciences based in Moscow, Russia. Our goal is to present scientific work and discovery in molecular biology, biochemistry, biomedical disciplines and biotechnology. *Acta Naturae* is also a periodical for those who are curious in various aspects of biotechnological business, innovations in pharmaceutical areas, intellectual property protection and social consequences of scientific progress.

Being a totally unique publication in Russia, *Acta Naturae* will be useful to both representatives of fundamental research and experts in applied sciences.

Journal "*Acta Naturae*" is now available in open access in PubMed Central® and eLIBRARY.RU.

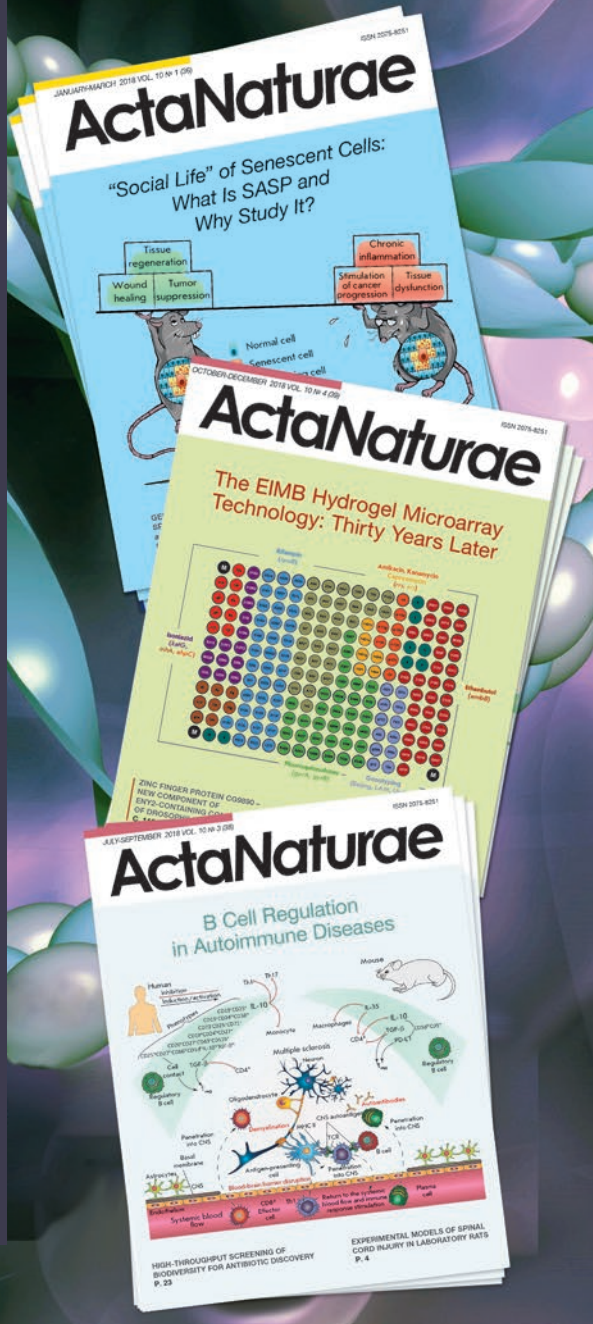

INFORMATION FOR AUTHORS:
if you want to publish in "Acta Naturae", please contact us: actanaturae@gmail.com